Instituto de Parasitología y Biomedicina López-Neyra (IPBLN)

Consejo Superior de Investigaciones Científicas (CSIC)

CONTROL OF NUCLEOTIDE HOMEOSTASIS AND GENOMIC INTEGRITY IN *TRYPANOSOMA BRUCEI*: ROLE OF HD NUCLEOTIDASES AND BASE EXCISION REPAIR

Universidad de Granada

Programa de doctorado en Bioquímica y Biología Molecular

Miriam Yagüe Capilla

Tesis Doctoral

Enero 2020

CONTROL OF NUCLEOTIDE HOMEOSTASIS AND GENOMIC INTEGRITY IN *TRYPANOSOMA BRUCEI*: ROLE OF HD NUCLEOTIDASES AND BASE EXCISION REPAIR

Memoria presentada por la Graduada
Miriam Yagüe Capilla para optar
al grado de Doctora en
Bioquímica y Biología Molecular

Granada, Enero de 2020

Miriam Yagüe Capilla

RESUMEN

Trypanosoma brucei es un parásito protozoario de la clase Kinetoplástida, agente causal de la tripanosomiasis humana africana (HAT) o comúnmente conocida como la "enfermedad del sueño". La transmisión está mediada por la picadura de la mosca tse-tsé (del género *Glossina*) y tanto parásito como vector se localizan mayoritariamente en el África subsahariana. Tras el desarrollo de numerosas iniciativas enfocadas al control de la enfermedad, el número de nuevos casos ha disminuido considerablemente, registrándose tan solo 977 casos en 2018 (WHO 2019). Sin embargo, a pesar de estos datos prometedores, los tratamientos disponibles siguen siendo escasos y muy tóxicos, y el desarrollo de resistencias constituye un inconveniente adicional (Buscher *et al.* 2017). Por esta razón, el descubrimiento de nuevos blancos de acción sigue siendo prioritario para mejorar la terapia contra la enfermedad. Por otra parte, *T. brucei* constituye un organismo modelo para el estudio de la biología de kinetoplástidos. La disponibilidad de sofisticadas herramientas de manipulación genética unido a la facilidad de cultivo y mantenimiento hacen de este organismo un paradigma para el estudio de la biología de organismos eucarióticos unicelulares.

En todos los organismos la preservación de la integridad genómica es esencial, y en concreto, el correcto mantenimiento de los niveles de los nucleótidos (dNTPs) posee un papel primordial. De hecho, desequilibrios en el "pool" de dNTPs da lugar a procesos que comprometen gravemente la viabilidad celular, como genotoxicidad, mutagénesis o tumorogénesis (Kohnken *et al.* 2015). De esta manera, los componentes del metabolismo de nucleótidos pueden suponer una fuente importante de dianas terapéuticas. Los dNTPs pueden ser sintetizados en la mayoría de organismos por dos rutas metabólicas, la vía de recuperación de nucleósidos pre-formados y la síntesis *de*

novo (Wang 2016). Mientras que *T. brucei* carece de las enzimas necesarias para sintetizar purinas *de novo*, es capaz de sintetizar los nucleótidos de pirimidina por ambas vías. A pesar de esta aparente redundancia metabólica para la generación de precursores pirimidínicos, ciertas enzimas implicadas en la biosíntesis del timidilato, como la dihidrofolato reductasa-timidilato sintasa (DHFR-TS), timidina kinasa (TK), desoxiuridina trifosfato hidrolasa (dUTPasa) o la citidina desaminasa (CDA), han demostrado ser esenciales para la viabilidad del parásito (Sienkiewicz *et al.* 2008; Castillo-Acosta *et al.* 2013; Leija *et al.* 2016; Valente *et al.* 2016). En concreto, líneas de *T. brucei* deficientes en TK no son viables y acumulan nucleósidos intracelulares tanto en ausencia como en presencia de un aporte exógeno de nucleósidos. Por otra parte, se ha demostrado que la fosforilación de la desoxiuridina (procedente de la desaminación de la desoxicitidina) via TK es un paso esencial en la síntesis de timidilato. Estas observaciones plantean la hipótesis de que *T. brucei* expresa nucleotidasas implicadas en la formación de nucleósidos intracelulares esenciales para la síntesis de timidilato. Por esta razón, el objetivo principal de esta tesis fue la identificación de dNTPasas en *T. brucei* que pudieran estar implicadas en este proceso.

En un esfuerzo por caracterizar nucleotidasas en el genoma de *T. brucei*, se han identificado dos nucleotidohidrolasas que contienen un dominio "histidine-aspartic acid" (HD) y que están relacionadas con la proteína humana "sterile alpha motif and HD domain-containing protein 1" (SAMHD1), que es una trifosfato desoxinucleósido hidrolasa (dNTPasa) que juega un papel esencial en la homeostasis de dNTPs/nucleósidos a lo largo del ciclo celular. Los dos parálogos identificados en *Trypanosoma* exhiben un dominio HD altamente conservado pero carecen del dominio SAM, así que se denominaron TbHD52 y TbHD82. En este trabajo, se ha evaluado el papel de estos ortólogos en viabilidad celular y control de la homeostasis de

nucleótidos. Ambas proteínas mostraron una localización diferencial, así como un diferente impacto sobre la proliferación celular. Mientras que TbHD82 era nuclear y prescindible, TbHD52 demostró ser una proteína mitocondrial esencial para la viabilidad, y células "knock-out" para la enzima son auxótrofas para timidina. La expansión del "pool" de dTMP en líneas deficientes en TbHD52, ya sea por suplementación del medio con nucleósidos de pirimidina o por la complementación con la enzima dCMP desaminasa humana, revierte el fenotipo deletéreo. Las observaciones obtenidas indican que TbHD52 tiene un papel central en la provisión de desoxinucleósidos pirimidínicos necesarios para la división celular. Asimismo, la ausencia de TbHD52 induce graves defectos en la progresión del ciclo celular, caracterizado por una parada en las fases S y G2/M y por la aparición de poblaciones aberrantes en cuanto al número y apariencia de núcleos y kinetoplastos. La cuantificación de dNTPs junto con un análisis metabolómico global de las líneas TbHD52-nulas puso de manifiesto profundas modificaciones en el perfil de precursores pirimidínicos, caracterizadas por una acusada acumulación de dCTP y derivados de citidina, así como una depleción significativa de dTTP y derivados de timidina. Estos resultados, junto con la intensa activación de foci nucleares de ɣH2A, un marcador temprano de daño en el DNA, sugieren que TbHD52 tiene un papel central en la homeostasis de dNTPs y en el abastecimiento de la desoxicitidina y timidina destinadas a la biosíntesis de timidilato.

Adicionalmente, a pesar de la estricta regulación de los niveles de dNTPs, en el DNA se producen constantemente lesiones derivadas del metabolismo endógeno o de agentes externos, los cuales pueden causar importantes daños como mutaciones o fragmentación (Chatterjee and Walker 2017). De hecho, durante el proceso de infección en el torrente sanguíneo, los parásitos están especialmente expuestos a estrés oxidativo

por la acción del sistema inmune. Para contrarrestar esta situación y preservar la integridad genómica, las células activan múltiples mecanismos de reparación, entre los cuales destaca la ruta de reparación de DNA por escisión de bases (BER). La enzima uracil-DNA glicosilasa (UNG), inicia la ruta de BER ante la presencia de uracilo en el DNA (Jacobs and Schar 2012). En este contexto, durante la respuesta inmune primaria, el óxido nítrico (NO) es liberado por los fagocitos, y en combinación con los radicales de oxígeno producen especies reactivas de nitrógeno que reaccionan con el DNA, generando roturas de cadena y bases modificadas (incluyendo desaminaciones de citosina), los cuales son sustratos para la UNG (Fang 1997). Estudios previos han demostrado la importancia de UNG para la virulencia de *T. brucei* (Castillo-Acosta *et al.* 2012b)*,* por lo que en esta tesis se ha profundizado en el daño en el DNA que se genera en respuesta al estrés oxidativo durante la interacción entre el patógeno y el huésped *in vivo*. Se ha analizado el contenido en uracilo y sitios abásicos en el DNA, así como la cantidad de foci de ɣH2A tanto *in vitro*, tras el tratamiento con donadores de NO, como *in vivo*, en parásitos aislados tras infección en modelos murinos. Los resultados ponen de manifiesto la aparición de daño genotóxico en *T. brucei* tras la exposición al NO *in vitro* y muestra que la ausencia de UNG genera mayores niveles de daño en el DNA. Por otra parte, los parásitos recuperados de ratones exhiben niveles más altos de roturas de cadenas de DNA, desaminación de bases y focos de reparación en comparación con las células cultivadas *in vitro,* y la ausencia de UNG conduce a un mayor daño del DNA también en infecciones animales. Estas observaciones sugieren que la respuesta inmune desarrollada por el huésped genera estrés oxidativo y daño en el DNA del parásito y enfatiza la importancia de BER en la protección contra el estrés genotóxico y oxidativo en *T. brucei*.

TABLE OF CONTENTS

ABBREVIATIONS

A

Ade. Adenine

Ado. Adenosine

ADP. Adenosine diphosphate

ADSL. Adenylosuccinate lyase

ADSS. Adenylosuccinate synthetase

AK. Adenosine kinase

AG. Aminoguanidine

AMP. Adenosine monophosphate

AMPD. Adenosine monophosphate deaminase

AMPK. 5' AMP-activated protein kinase

AP. Apurinic/apyrimidinic

APC. Antigen-presenting cells

APE. AP endonuclease

APRT. Adenine phosphoribosyl-transferase

ARP. Aldehyde reactive probe

ATM. Ataxia telangiectasia mutated

ATP. Adenosine triphosphate

ATR. Ataxia telangiectasia and Rad3-related protein

B

BER. Base excision repair

Ble. Phleomycin

Bp. Base pair

BSA. Bovine serum albumin

Bsd. Blasticidin

BSF. Bloodstream form

C

CDA. Cytidine deaminase

CDK. Cyclin-dependent kinase

CDP. Cytidine diphosphate

Chk1. Checkpoint kinase 1

CtIP. CtBP-interacting protein

CTP. Cytidine triphosphate

CTPS. Cytidine triphosphate synthetase

Cyd. Cytidine

Cyt. Cytosine

D

dAdo. Deoxyadenosine

dADP. Deoxyadenosine diphosphate

dAMP. Deoxyadenosine mono-phosphate

DAPI. 4′,6-diamidino-2-phenylindole

dATP. Deoxyadenosine triphosphate

DC. Dendritic cell

dCDP. Deoxycytidine diphosphate

DCTD. Deoxycytidine monophosphate deaminase

dCTP. Deoxycytidine triphosphate

dCyd. Deoxycytidine

DDR. DNA damage response

DETA-NO. Diethylenetriamine/nitric oxide adduct

dGDP. Deoxyguanosine diphosphate

dGMP. Deoxyguanosine mono-phosphate

dGTP. Deoxyguanosine triphosphate

dGuo. Deoxyguanosine

DHE. Dihydroethidium

DHFR-TS. Dihydrofolate reductase-thymidylate synthase

DIC. Differential interference contrast

DNA. Deoxyribonucleic acid

DNA-PK. DNA dependent protein kinase

dNTP. Deoxyribonucleotide

dNTPase. Deoxynucleoside triphosphohydrolase

Dox. Doxycycline

DSB. Double-strand breaks

dTDP. Deoxythymidine diphosphate

dThd. Deoxythymidine

dTMP. Deoxythymidine mono-phosphate

DTT. 1,4-Dithiothreitol

dTTP. Deoxythymidine triphosphate

dUDP. Deoxyuridine diphosphate

dUMP. Deoxyuridine monophosphate

dUrd. Deoxyuridine

dUTP. Deoxyuridine triphosphate

dUTPase. Deoxyuridine triphosphate nucleotidohydrolase

E

EC50. Half maximal effective concentration

EDTA. Ethylenediamine tetraacetic acid

EGTA. Ethyleneglycol tetraacetic acid

EndoV. Endonuclease V

eNOS. Endothelial nitric oxide synthase

ENT. Equilibrative nucleoside transporters

F

FACS. Fluorescence activated cell sorting

FBS. Fetal bovine serum

FDA. Food and drug administration

FITC. Fluorescein isothiocyanate

G

G-418. Geneticin

GDA. Guanine deaminase

GDP. Guanosine diphosphate

GSH. Glutathione

GMP. Guanosine monophosphate

GMPK. Guanosine monophosphate kinase

GMPR. Guanosine 5'-monophosphate oxidoreductase

GMPS. Guanosine 5'-monophosphate synthetase

GPI. Glycosylphosphatidylinositol

GTP. Guanosine triphosphate

Gua. Guanine

Guo. Guanosine

H

H2AX. H2A histone family member X

HAT. Human African trypanosomiasis

HD. Histidine-aspartic domain

HEPES. 4-(2-hydroxyethyl)-1-piperazineethanesulfonic acid

HGPRT. Hypoxanthine-guanine phosphoribosyltransferase

HIV. Human immunodeficiency virus

HR. Homologous recombination

Hyg. Hygromycin

Hyp. Hypoxanthine

I

IAGNH. Inosine-adenosine-guanosine-nucleoside hydrolase

IF. Immunofluorescence

IFNγ. Interferon gamma

Ig. Immunoglobulin

IL. Interleukin

IMP. Inosine monophosphate

IMPDH. Inosine 5'- monophosphate dehydrogenase

Ino. Inosine

iNOS. Inducible nitric oxide synthase

IPTG. Isopropyl-β-D-thiogalactopyranoside

K

Kan. Kanamycin

kDa. Kilodalton

kDNA. Kinetoplast DNA

KO. Knock-out

L

LB. Lysogeny broth

Lig3. DNA ligase-3

LPS. Lipopolysaccharide

M

MCP. Mitochondrial carrier proteins

5M-dCyd. 5-methyl-2′-deoxycytidine

MHC. Major histocompatibility complex

MMEJ. Microhomology-mediated end-joining

MMR. Mismatch repair

MOPS. 3-(N-morpholino) propane-sulfonic acid

mRNA. Messenger RNA

N

NDPK. Nucleoside diphosphate kinase

NER. Nucleotide excision repair

NHEJ. Non-homologous end-joining

NK. Natural killer

NMPK. Nucleoside monophosphate kinase

nNOS. Neuronal nitric oxide synthase

NO. Nitric oxide

NOS. Nitric oxide synthase

NTD. Neglected tropical diseases

O

OE. Overexpression

OGG1. 8-oxoguanine-DNA glycosylase

ONOO⁻. Peroxynitrite

ORF. Open reading frame

8-oxoG. 8-oxo-7,8-dihydro-deoxyguanine

P

PARP-1. Poly [ADP-ribose] polymerase 1

PBS. Phosphate-buffered saline

PCF. Procyclic form

PCR. Polymerase chain reaction

PFA. *p*-formaldehyde

PGE$_2$. Prostaglandin E$_2$

PI. Propidium iodide

Polβ. β-type DNA polymerase

PP2A. Serine/threonine protein phosphatase 2 A

PRTase. Phosphoribosyltransferase

Pur. Puromycin

PVDF. Polyvinylidene difluoride membrane

R

RNA. Ribonucleic acid

RNAi. RNA interference

RNR. Ribonucleotide reductase

RNS. Reactive nitrogen species

ROS. Reactive oxygen species

RT. Room temperature

RT-qPCR. Real-time quantitative polymerase chain reaction

S

SAM. Sterile alpha motif

SAMHD1. Sterile alpha motif and histidine-aspartate domain-containing protein 1

SB. Separating buffer

SD. Standard deviation

SDS. Sodium dodecyl sulfate

SIV. Simian immunodeficiency virus

SSB. Single-strand breaks

ssDNA. Single-stranded DNA

ssRNA. Single-stranded RNA

T

TAE. Tris-acetate-EDTA

TCA. Trichloroacetic acid

TDB. Trypanosome dilution buffer

TetR. Tetracycline inducible repressor

Th. T helper cell

TK. Thymidine kinase

TMPK. Thymidylate kinase

TNFα. Tumoral necrosis factor-α

TRYP1. Tryparedoxin peroxidase

T(SH)$_2$. Trypanothione

U

UDP. Uridine diphosphate

UMP. Uridine monophosphate

UMPK. Uridylate kinase

UNG. Uracil-DNA glycosylase

UPase. Uridine phosphorylase

UPRT. Uracil phosphoribosyl-transferase

Ura. Uracil

Urd. Uridine

UTP. Uridine triphosphate

UTR. Untranslated region

V

VSG. Variant Surface Glycoprotein

W

WB. Western blot

WHO. World health organization

X

Xan. Xanthine

Xao. Xanthosine

XMP. Xanthosine monophosphate

XRCC1. X-Ray Repair Cross Complementing 1

Z

ZPFM. Zimmerman postfusion medium

INTRODUCTION

A. INTRODUCTION

A.1. Human African Trypanosomiasis

A1.1. Etiology and epidemiology

The neglected tropical diseases (NTDs) encompass 20 different parasitic, viral and bacterial infections affecting more than one billion people worldwide. They present a diverse distribution across 149 tropical and sub-tropical countries located in Africa, Asia and America. Since they emerge as a relevant health threat and cause important economic losses in populations living in poverty, NTDs have gained increasing interest for the World Health Organization (WHO) (Akinsolu *et al.* 2019). In order to achieve control and elimination of the most devastating, the WHO defined 11 major NTDs, out of which *Leishmania*, *Trypanosoma cruzi* and *Trypanosoma brucei* are responsible for the afflictions of highest mortality. These kinetoplastid parasites cause leishmaniasis, Chagas' disease and African trypanosomiasis, respectively (Hotez *et al.* 2007).

Trypanosoma brucei is transmitted by the tsetse fly of the *Glossina* genus. Tsetse flies are found in sub-Saharan Africa though only certain species transmit the disease, and the mammalian host differs depending on the parasite subspecies. For instance, *T. b. brucei* only affects livestock, producing African animal trypanosomiasis, or nagana. On the other hand, the *T. brucei* subspecies *T. b. rhodesiense* and *T. b. gambiense* are the causative agents of Human african trypanosomiasis (HAT), commonly known as sleeping sickness. *T.b. gambiense* is prevalent in western and central Africa and causes the chronic form of the disease, whereas *T.b. rhodesiense* produces the acute pathology in eastern and southern Africa. Though *T.b. rhodesiense*

provokes a more severe form of the illness and is able to infect humans, animals are the main reservoir of the parasite. Hence, 95-97% of the reported cases correspond to *T.b. gambiense* (Fig. A1) (Franco *et al.* 2014; Kennedy and Rodgers 2019).
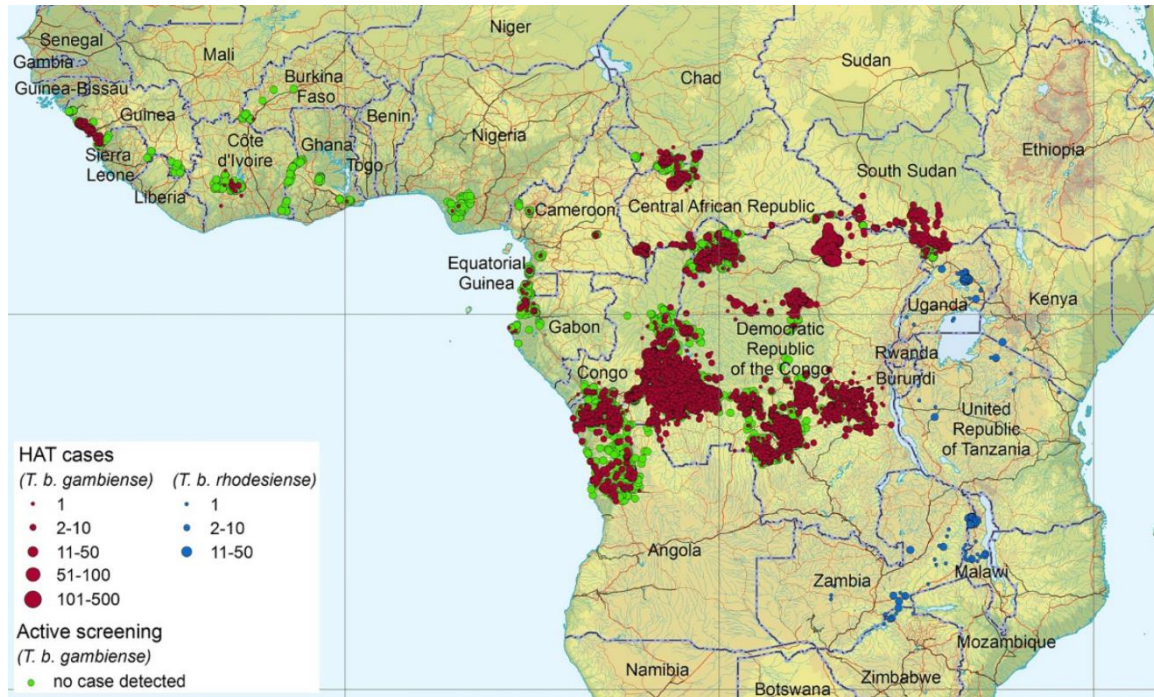
Figure A1. Distribution and number of reported cases for *T.b. gambiense* and *T.b. rhodesiense* human infection in the period of 2012-2016 (Franco *et al.* 2018). HAT is produced by two subspecies of the protozoan parasite *T. brucei*, which are mainly located across sub-saharian Africa. *T.b. rhodesiense* affects eastern and southern Africa, while *T.b. gambiense* has a higher prevalence of cases and is disseminated over western and central Africa.

A.1.2. Physiopathology of HAT and clinical treatment

Once the mammalian host is infected, HAT is composed of two sequential stages, named as hemo-lymphatic and meningo-encephalitic phases. In the early onset of the infection, trypanosomes disseminate through the lymphatic system giving rise to the hemo-lymphatic phase of the disease. Eventually, parasites cross the blood-brain barrier and invade the central nervous system; at this point the latter stage is diagnosed (Kennedy and Rodgers 2019).

Several treatments have been developed against HAT, which differ depending on the corresponding *T. brucei* subspecies (*T.b. gambiense* or *T.b. rhodesiense*) and the stage of the disease. For the early stage of trypanosomiasis, the drugs of choice are pentamidine and suramine, for *T.b. gambiense* and *T.b. rhodesiense* infection, respectively. Once the parasites reach the central nervous system, current treatments in use are melarsoprol and a combination of nifurtimox-eflornithine. Although melarsoprol is effective against both *T. brucei* subspecies, it is only employed to treat *T.b. rhodesiense*, since it has been demonstrated that the administration of nifurtimox and eflornithine in combination exhibit better efficacy in *T.b. gambiense* infections (Varikuti *et al.* 2018). Nevertheless, current treatments present severe problems with high toxicity and increasing parasite resistance. To overcome these pitfalls, intense research is under development with promising results, as treatments with benzoxaborole and fezinidazole are undergoing different clinical trials. Benzoxaborole has favorably completed stage I clinical trials, showing meningo-encephalitic cure in murine model (Jacobs *et al.* 2011; Steketee *et al.* 2018), whereas fexinidazol has already been successful in stage II/III clinical trials for *T.b. gambiense* infection (Mesu *et al.* 2018).

A.2. Biological characteristics of *T. brucei*

A.2.1. Cell architecture in *T. brucei*

T. brucei is a unicellular protozoan parasite that belongs to the *Trypanosomatida* order, Kinetoplastidia class. These organisms are characterized by the presence of a dense network of circular mitochondrial DNA (kDNA), termed kinetoplast, which gives name to the class. The cell shape is elongated and maintained by a highly polarized microtubule cytoskeleton, where the organelles are precisely positioned. *T. brucei* possesses several single-copy organelles, which includes the flagellar pocket, flagellum, kinetoplast, mitochondrion and nucleus, located between the posterior end and center of the cell (Fig. A2) (Matthews 2005).
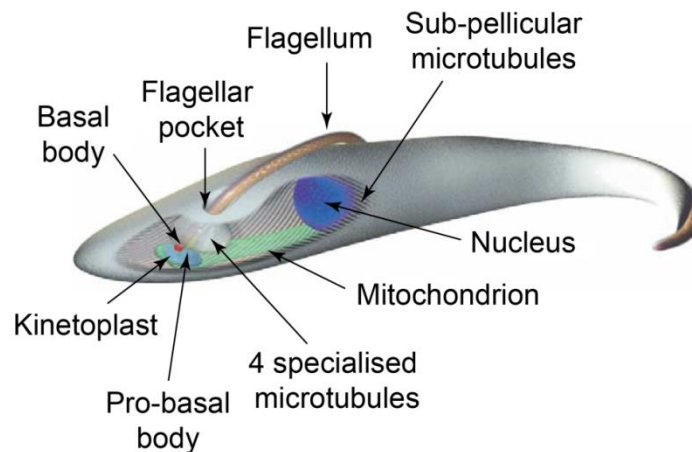
Figure A2. Cell structure of *T. brucei*. Schematic representation of the main organelles and structures present in *T. brucei* (McKean 2003).

The **flagellum** is essential for the motility of the parasite. It extends from the anterior pole throughout the external surface of the parasite until it reaches the flagellar pocket, in the posterior pole, where endo- and exocytosis take place (Overath and

Engstler 2004). Inside the flagellar pocket, the flagellum emerges from the basal body, where it connects to the kinetoplast.

Trypanosomes, unlike most eukaryotes, possess a single **mitochondrion,** which is also elongated and forms a network from the posterior to the anterior pole of the parasite. In bloodstream form (BSF) parasites, the mitochondrion is a narrow tubular structure and acristae, resembling a promitochondrion of anaerobic yeast. Most enzymes involved in oxidative phosphorylation are absent, since high concentrations of glucose in the bloodstream of the mammalian host enables glycolysis as a primary energy source. On the other hand, procyclic forms (PCF) trypanosomes are exposed to a glucose-poor environment inside the insect. Consequently, the mitochondrion is highly active and relies on oxidative phosphorylation for energy production (Priest and Hajduk 1994; Smith *et al.* 2017).

As previously mentioned, the mitochondrial genome is condensed in the **kinetoplast,** where DNA is organized in maxicircles and minicircles. Maxicircles are less abundant (about 50 copies/kinetoplast) and encode for mitochondrial genes as well as for two ribosomal ribonucleic acids (RNAs) and a ribosomal protein. In contrast, since mitochondrial messenger RNA (mRNA) undergoes intense RNA editing, the short guide RNAs required for this process are encoded in the minicircles (Goringer 2012).

A.2.2. Life cycle of the parasite

As in other parasites, the life cycle of *T. brucei* comprises several forms of differentiation between a vertebrate and an insect host. Thus, the infection begins when the tsetse fly, *Glossina* spp., injects the metacyclic trypomastigotes into a mammalian host during a bloodmeal. Inside the mammal, the parasite proliferates free in the

bloodstream, where it divides by binary fission (corresponding to the bloodstream long slender form) (Smith *et al.* 2017). Eventually, as the density of trypanosomes increases, the parasite differentiates to the non-proliferative short stumpy form, which is terminally cell cycle-arrested in G0/G1 phase of the cell cycle. This process is mediated by a quorum-sensing mechanism with the purpose of controlling the infection, thereby maintaining host survival and the probability of transmission (Silvester *et al.* 2017). After multiplication, the procyclic trypanosomes propagate to the salivary glands, where parasites are finally reprogrammed to quiescent metacyclic trypomastigotes. At this point, the life cycle re-starts after the inoculation of the trypanosomes into a new host (Fig. A3)(Smith *et al.* 2017).
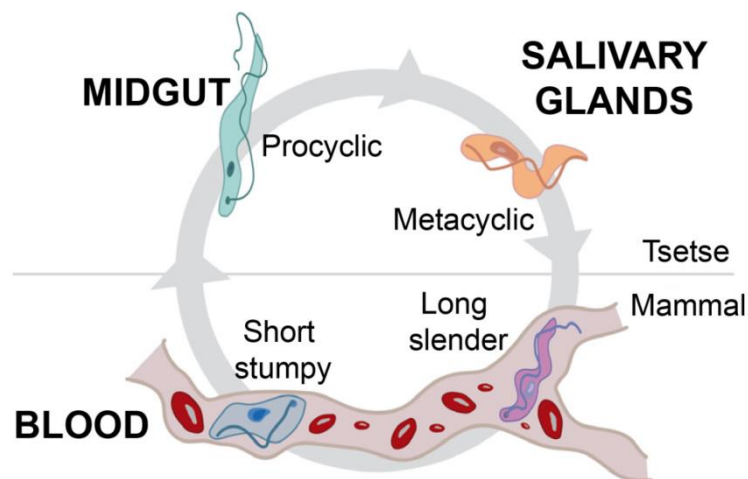
Figure A3. Life cycle of *T. brucei* in the mammalian host and insect vector. *T. brucei* is an extracellular protozoan parasite that completes its life cycle between an insect from the *Glossina* spp. (known as tsetse fly) and a mammal. Once the infected tsetse fly injects the parasites into the mammalian host, metacyclic trypomastigotes enter the lymphatic system and differentiate into diving long slender forms. Eventually, by a quorum-sensing mechanism, slender parasites transform into quiescent stumpy forms, which are cell cycle-arrested, until the tsetse fly bites the infected mammal. Inside the insect midgut, *T. brucei* turns into procyclic forms that will continue dividing. Once in the salivary glands, a new life cycle begins after differentiation to the metacyclic form and infection of a new host. Modified from Smith *et al.,* (2017).

A.2.3. Cell cycle division

As in most eukaryotic organisms, cell cycle in *T. brucei* consists of five phases: G0/G1, S, G2, M and cytokinesis (Fig. A4). However, cell division in trypanosomes presents certain peculiarities since it contains several single copy organelles and structures which must be duplicated and segregated in a precise order (McKean 2003).

G0/G1 phase. In the G0/G_1 phase, the earliest cytological event is the elongation and maturation of the pro-basal body and the nucleation of a new flagellum (McKean 2003; Hammarton 2007). After basal body duplication, a new Golgi appears *de novo*, partly synthesized from materials derived from the old Golgi (He *et al.* 2004).

S phase. During this stage deoxyribonucleic acid (DNA) is duplicated. The timing of nuclear and kinetoplast DNA division differs, so prior to the nuclear S phase (S_N phase), the kDNA initiates its replication (S_K phase). Furthermore, the S_K phase is much shorter than the S_N phase, and consequently kinetoplast segregation is also completed before the beginning of mitosis (McKean 2003).

G2 phase. In the G2 phase, basal bodies separate in a microtubule-mediated process (Robinson and Gull 1991) along with the kDNA, giving rise to a cell with a nucleus and two kinetoplasts (1N2K).

M phase. In *T. brucei*, mitosis presents unique features. First of all, the parasite lacks centrosomes, suggesting that the spindle assembly is mediated by chromatine-directed pathways (Tu *et al.* 2006). In addition to that, the mitotic spindle is assembled without the disruption of the nuclear envelope, so cells exhibit an enlarged nucleus corresponding to the 1N*2K population (Ogbadoyi *et al.* 2000). Besides, procyclic cells lack a mitosis to cytokinesis checkpoint, so mitosis disturbances may result in a cell with one nucleus and two kinetoplasts, and consequently asymmetric daughter cells. In

contrast, bloodstream form parasites undergo mitotic arrest, yet DNA is able to reentry G1 for another cycle and replication round (Tu and Wang 2005).

Cytokinesis. Cytokinesis in *T. brucei* is also unusual, since it does not rely on the classical actomyosin ring constriction (Hammarton 2007; Garcia-Salcedo *et al.* 2004). The site of furrow is determined by the flagellum attachment zone and is cleaved unidirectionally along the long axis from the anterior towards the posterior end of the cell. As a consequence, it separates both flagellums and, hence, gives as a result two daughter cells with identical structural and genetic content (Kohl *et al.* 2003; Zhou *et al.* 2014).
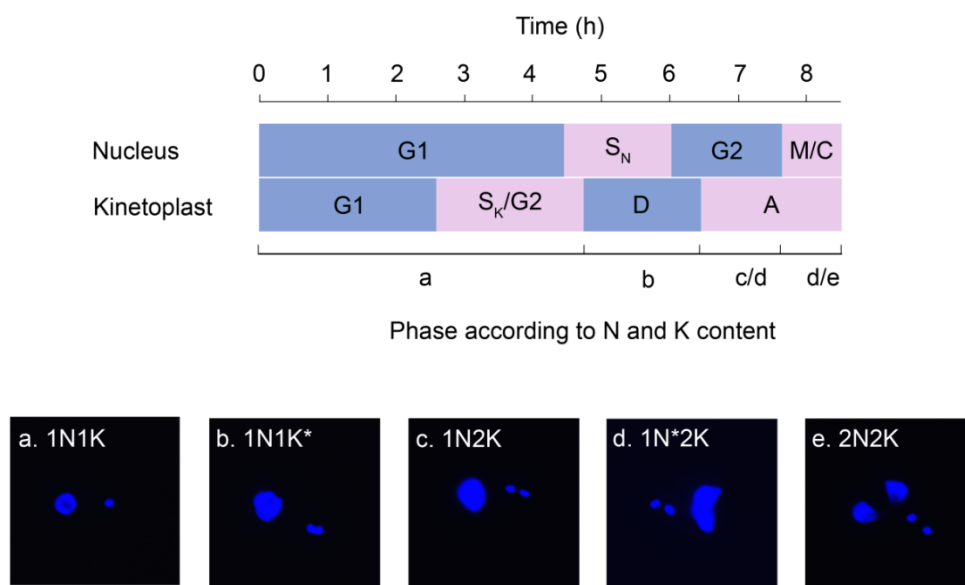
Figure A4. Cell cycle progression in *T. brucei*. The upper diagram describes the relative time course and the main phases (G1, S, G2, M and cytokinesis) discerning between nuclear and kinetoplast replication. S phase in the kinetoplast (S_K) is shorter and starts before nuclear DNA replication (S_N). Thus, kinetoplast division (D) and segregation (A) and nuclear mitosis (M) and cytokinesis (C) do not occur concurrently. Lower images show DAPI staining of the different trypanosome populations classified according to the number of nucleus (N) and kinetoplasts (K), where an asterisk indicates that the corresponding organelle is under segregation. Illustration adapted from (Benz *et al.* 2017).

A.2.4. Immune evasion: antibody clearance and antigenic variation

During mammalian infection the parasite proliferates in the bloodstream and is highly exposed to the immune system. For this reason, *T. brucei* has developed diverse strategies to escape host surveillance, such as antigenic variation and antibody clearance.

The trypanosomal membrane is covered by a monoclonal protective coat composed of the variant surface glycoprotein (VSG). This protein is anchored to the lipid membrane through the glycosylphosphatidylinositol (GPI) lipid anchor (Ferguson *et al.* 1988; Masterson *et al.* 1989), and its N- and C- terminal domains provide for antigenic diversity and membrane association, respectively (Schwede *et al.* 2011). Remarkably, VSGs present monoallelic expression (Borst 2002), so only one gene copy is expressed at a certain time in the parasite. Thus, though VSGs are extremely immunogenic, the parasite is able to evade immune clearance by switching the expressed VSG to another antigenically distinct variant, in a process termed as antigenic variation (Fig. A5)(Vickerman 1985).
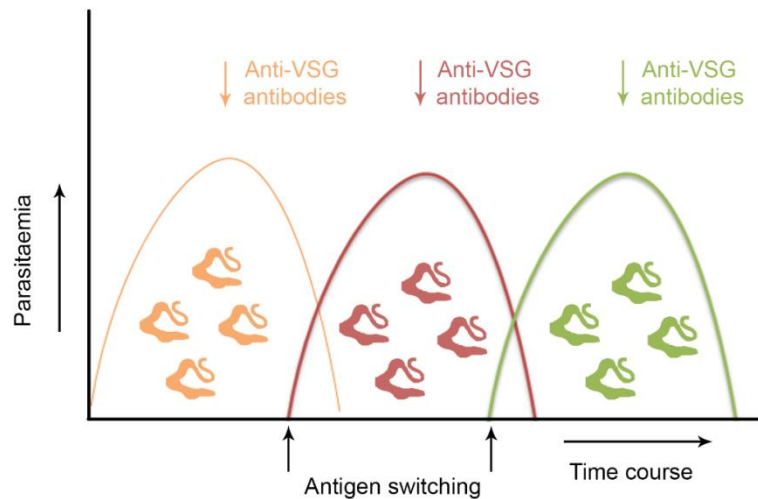
Figure A5. VSG expression and switching during *T. brucei* infection. Trypanosomes exhibit a highly immunogenic monoclonal VSG coat. During infection, the immune system generates specific antibodies against the expressed VSG, controlling the parasitaemia. However, through antigenic variation, parasites switch the VSG to another variant that delays recognition by the host immune system, causing the regression of the infection.

On the other hand, GPI-anchoring of VSGs also presents hydrodynamic fluidity, which contributes to another strategy of immune evasion. Once host-derived antibodies are bound to the cell surface, trypanosomes movement facilitates directional sorting of immunoglobulin-G (IgG)-VSG complexes along the plasma membrane. The IgG-VSG complex is rapidly sorted to the flagellar pocket, where it is endocytosed and antibody clearance occurs (Engstler *et al.* 2007).

A.3. Nucleotide biosynthesis in *T. brucei*

Deoxyribonucleotide triphosphate (dNTP) levels are strictly regulated in all organisms, since they play a pivotal role in DNA replication and repair. Indeed, perturbations in dNTP pools result in deleterious processes that notably compromise cell integrity, such as genotoxicity, mutagenesis or tumourogenesis (Kohnken *et al.* 2015). For this reason, enzymes involved in synthesis and degradation of dNTPs constitute valuable drug targets.

In most species, nucleotides can be synthesized by two metabolic routes, the *de novo* and the salvage pathway (Hassan and Coombs 1988) (O'Donovan and Neuhard 1970). However, most protozoan parasites including *T. brucei*, lack the *de novo* pathways for purine biosynthesis (Fish *et al.* 1982a; Fish *et al.* 1982b), so they are completely dependent on the salvage of preformed purine bases or nucleosides from the host organism to satisfy their purine demand. Nevertheless, though purine salvage enzymes resemble attractive targets for the design of inhibitors against protozoa, redundancy of purine transport and interconversion pathways difficult the development of inhibitors, as only guanosine 5'-monophosphate synthase (GMPS)-null parasites exhibited impaired virulence and growth (Li *et al.*). In contrast, several enzymes of pyrimidine metabolism in *T. brucei* demonstrated to be essential for the parasite, such as thymidine kinase (TK) (Leija *et al.* 2016; Valente *et al.* 2016), dihydrofolate reductase-thymidylate synthase (DHFR-TS) (Sienkiewicz *et al.* 2008), deoxyuridine triphosphate nucleotihydrolase (dUTPase) (Castillo-Acosta *et al.* 2013) or cytidine deaminase (CDA) (Leija *et al.* 2016). Hence, enzymes involved in pyrimidine biosynthesis may constitute promising drug targets.

A.3.1. Nucleotide transporters for salvage biosynthesis

Unlike mammalian cells, which take up nucleosides by membrane diffusion, trypanosomes have distinct active transporters that discriminate purines and pyrimidines.

In order to overcome the need for purines salvage from the host, trypanosomes have developed very efficient and redundant purine transporters, expressing a wide variety of equilibrative nucleoside transporters (ENTs). In *T. brucei*, transporters have been classified as P1 and P2-type, which are high-affinity adenosine transporters and mediate uptake of most purine nucleosides, and H-type transporters, involved in transport of purine nucleobases (Fig. A6). Additionally, two novel transporters with extreme selectivity and not included in the ENT family have been reported, XHT1 and ADET1, which are specific for hypoxanthine and adenine, respectively (Campagnaro *et al.* 2018).

P1-type transporters exhibit broad specificity for purine nucleosides and are encoded by multiple genes of the TbNT family (Sanchez *et al.* 2002). This family includes TbNT2 transporters (NT2-NT7), a tandem repeat of six genes that have shown affinity for adenosine (Ado), inosine (Ino) and guanosine (Guo), and with some exceptions (NT5-NT7) certain affinity for hypoxanthine (Hyp) (Sanchez *et al.* 2002). Apart from these genes, more recently, TbNT9 and TbNT10 were also included in this group. They both uptake the aforementioned nucleosides, and TbNT9 additionally mediates Hyp incorporation (Al-Salabi *et al.* 2007). In general, P1-type transporters are expressed both in BSF and PCF trypanosomes (James and Born 1980; Sanchez *et al.* 1999), although it has been reported that TbNT10 is exclusively present in the non-dividing short-stumpy form of the parasite (Sanchez *et al.* 2004). On the other hand, the P2-type transporter displays high affinity for aminopurines, so it only

transports adenine (Ade) and Ado (Carter and Fairlamb 1993). Besides, it is only expressed in BSF parasites.

H-transporters are considered high-affinity carriers for Hyp, yet they mediate transport of all purine nucleobases. Four main transporters have been identified in this class, which are TbH1 and TbH4 in PCFs (de Koning and Jarvis 1997a; Burchmore *et al.* 2003; Henriques *et al.* 2003) and TbH2 and TbH3 in BSFs (de Koning and Jarvis 1997b). TbH4 presents additional high and low affinity for Guo and Ino, respectively. Additionally, two more purine nucleobase transporters have been identified, TbNT11 and TbNT12 with limited specificity. Thus, TbNT12 is only involved in uptake of Ade and TbNT11 is not able to mediate guanine (Gua) incorporation (Ortiz *et al.* 2009).

In contrast, transport of pyrimidine nucleosides (with the exception of uracil) is accomplished with low efficiency. PCF trypanosomes possess two carriers for uridine and uracil transport (TbU1 and TbU2) and a cytosine transporter (TbC1). TbU1 is able to uptake uracil (Ura) as well as uridine (Urd), though its efficiency for the nucleobase transport is >40-fold higher than for the corresponding nucleoside (Gudin *et al.* 2006). On the other hand, TbU2 only translocates Urd. Finally, the C1 transporter presents high affinity for cytosine (Cyt) (de Koning and Jarvis 1998; Gudin *et al.* 2006). Likewise, BSF parasites express a highly efficient uracil transporter, TbU3, which also enables Urd, deoxyuridine (dUrd) and thymidine (dThd) uptake, yet at very high concentrations. Transport of dThd is also mediated by TbT1, however, it presents extremely low affinity and translocation efficiency with this nucleoside (Fig. A6) (Ali *et al.* 2013a).
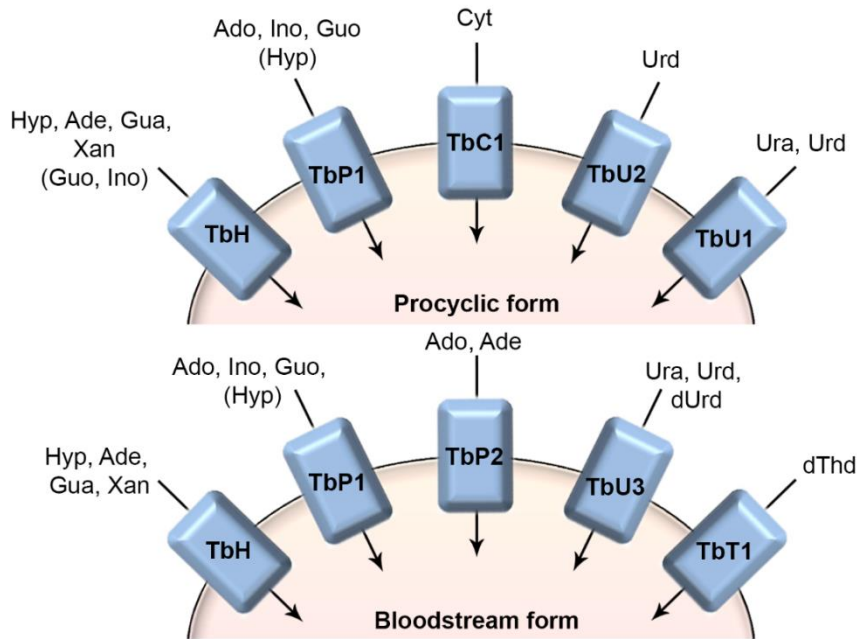
Figure A6. Schematic representation of nucleoside transporters in *T. brucei* procyclic and bloodstream forms. Trypanosomes display specific transporters for purine (TbH and TbP1-2) and pyrimidine (TbU1-3, TbC1 and TbT1) nucleosides, which also differ according to the life cycle of the parasite. Purines uptake is mediated by a wide range of transporters, divided in three general categories: H, P1 and P2-type. Nucleobases in general are transported by TbH transporters. TbP1 is a broad substrate nucleoside transporter present in all life cycle forms of the parasite, but TbP2 is absent in PCF cells. Though less efficient, pyrimidine transporters characterized to date are TbU1, TbU2 and TbC1 in PCFs and TbT1 and TbU3 in BSFs. Nucleoside abbreviations in the figure correspond to: Hyp (Hypoxanthine), Ado (Adenosine), Ino (Inosine), Guo (Guanosine), Ade (Adenine), Ura (Uracil), Urd (Uridine), dUrd (2'-deoxyuridine) and dThd (Thymidine).

A.3.2. Purine metabolism in parasitic protozoa

As aforementioned, *T. brucei* lacks the enzymes involved in *de novo* purine biosynthesis, so it completely relies on the salvage pathways to obtain the required purine content to survive (Fish *et al.* 1982a; Fish *et al.* 1982b). For this reason, in addition to expressing very efficient purine transporters (James and Born 1980), trypanosomatids have enzymes that enable AMP, IMP, XMP and GMP interconversion (Hassan and Coombs 1988). Hence, they only require salvage of a single purine

nucleoside from the host, such as Ado or Hyp, to satisfy their purine requirements.

The enzymes involved in purine salvage are nucleoside hydrolases/phosphorylases, purine phosphoribosyltransferases and kinases (Fig. A7). Purine salvage implies a two-step process for the generation of the monophosphate. First of all, the nucleoside is cleaved to the corresponding base by the action of inosine-adenosine-guanosine-nucleoside hydrolase (IAGNH, EC 3.2.2.1). Thereby Ado, Guo, Ino and xanthosine (Xao) generate Ade, Gua, Hyp and xanthine (Xan), respectively (Parkin 1996). Consecutively, a phosphoribosyltransferase (PRTase) catalyzes the transfer of ribose 5'-phosphate to the base, generating the corresponding nucleoside monophosphate. *T. brucei* encodes two different PRTases, hypoxanthine-guanine phosphoribosyltransferase (HGPRT, EC 2.4.2.8) and adenine phosphoribosyltransferase (APRT, EC 2.4.2.7). The substrate for HGPRT can be either Hyp, Xan or Gua (Teran *et al.* 2016; Dolezelova *et al.* 2018), whereas APRT only catalyzes the phosphoribosyl incorporation into Ade (Luscher *et al.* 2014). On the other hand, the cleavage-dependent pathway is not the only way to salvage Ade, since *T. brucei* expresses two putative adenosine kinases (AK, EC 2.7.1.20) that directly generate AMP. TbAK also displays a certain phosphorylation activity towards deoxyadenosine (dAdo) and Ino, yet the catalytic efficiency was several orders of magnitude lower compared to Ado (Vodnala *et al.* 2008). In contrast, no activity has been reported that salvages deoxyguanosine (dGuo).

Figure A7. Purine salvage in *T. brucei*. *T. brucei* is able to synthesize all purines from a unique purine precursor. A nucleotide hydrolase (IAGNH) cleaves the base, which can be converted to the corresponding monophosphate by a PRTase (HGPRT or APRT). Through the action of AK, adenosine can also directly give rise to AMP. Several enzymes enable the generation of the the remaining purine monophosphates. Finally, both ADP and GDP can produce the corresponding ribonucleotide or deoxyribonucleotide via NDK and RNR. Enzyme abbreviations in the figure correspond to: inosine-adenosine-guanosine-nucleoside hydrolase (IAGNH), hypoxanthine-guanine phosphoribosyltransferase (HGPRT), adenine phosphoribosyltransferase (APRT), adenosine kinase (AK), 5' AMP-activated protein kinase (AMPK), adenosine monophosphate deaminase (AMPD), adenylosuccinate synthetase (ADSS), adenylosuccinate lyase (ADSL), inosine-5'-monophosphate dehydrogenase (IMPDH), guanosine 5'-monophosphate synthetase (GMPS), guanosine 5'-monophosphate oxidoreductase (GMPR), guanosine 5'-monophosphate kinase (GMPK), guanine deaminase (GDA), nucleoside diphosphate kinase (NDPK), ribonucleotide reductase (RNR).

All monophosphates can be generated by the action of several enzymes. AMP is deaminated to IMP via adenosine monophosphate deaminase (AMPD, EC 3.5.4.6), which may generate XMP by the action of inosine 5'- monophosphate dehydrogenase (IMPDH, EC 1.1.1.205) and consecutively produces GMP via the guanosine 5'-monophoshate synthetase (GMPS, EC 6.3.5.2). IMP can also be originated from GMP through the action of guanosine monophosphate oxidoreductase (GMPR, EC 1.7.1.7). 5' AMP-activated protein kinase (AMPK, EC 2.7.4.3) and guanosine monophosphate kinase (GMPK, EC 2.7.4.8) phosphorylate AMP and GMP,

respectively, to the corresponding ADP and GDP. Finally, ADP and GDP can be either phosphorylated to GTP and ATP, respectively, by nucleoside diphosphate kinase (NDPK, EC 2.7.4.6), or reduced to dGDP and dADP by ribonucleotide reductase (RNR, EC 1.17.4.1) for the biosynthesis of the corresponding deoxyribonucleoside triphosphate via NDPK (Fig. A7) (Berriman *et al.* 2005).

A.3.3. Pyrimidine metabolism in *T. brucei*

In contrast to purine nucleotides, *Trypanosoma* possesses the machinery needed for *de novo* biosynthesis and pyrimidine salvage. Both pathways converge in UMP formation, which can enter different routes for dCTP or dTTP biosynthesis. On one hand, UMP is generated through synthesis *de novo* (Hammond and Gutteridge 1982) or uracil salvage, since uracil phosphoribosyltransferase (UPRT, EC 2.4.2.9) can transfer a phosphoribosyl moiety to the uracil. On the other hand, uracil-derived nucleosides and deoxynucleosides can be broken down to uracil through the action of the uridine phosphorylase (UPase, EC 2.4.2.3) Theoretically, parasites can also obtain dUrd from uracil since UPase and UPRT are reversible (Fig. A8). The enzymes involved in subsequent steps perform non-redundant activities, so many of them have been demonstrated to be essential for parasite survival. While enzymes involved in the *de novo* pathway have been demonstrated to be dispensable for viability *in vitro*, knock-out parasites exhibited defects in virulence, suggesting that pyrimidine salvage *in vivo* is not enough to counteract defects in *de novo* biosynthesis (Ong *et al.* 2013; Ali *et al.* 2013b).

For dCTP formation, UMP is phosphorylated to UTP via uridylate kinase (UMPK, EC 2.7.4.14) and NDPK. UTP latter generates CTP through the action of cytidine triphosphate synthetase (CTPS, EC 6.3.4.2) (Hofer *et al.* 2001). Indeed,

whereas *T. brucei* can salvage cytosine-derived nucleosides and deoxynucleosides, a cytidine kinase is absent in trypanosomal genome, requiring CTP as a metabolic intermediary for dCTP biosynthesis. At a later stage, NDPK is able to provide CDP for its reduction to dCDP via RNR, which is finally phosphorylated to dCTP again by the action of NDPK (Fig. A8).

Conversely, dTTP biosynthesis can be provided by the *de novo* pathway or dThd and deoxycytidine (dCyd) salvage. For the salvage pathway, *T. brucei* is endowed with a thymidine kinase (TK, EC 2.7.1.21) that catalyzes phosphorylation of dThd and dUrd to dTMP and deoxyuridine monophosphate dUMP, respectively (Leija *et al.* 2016; Valente *et al.* 2016). In the first case, dTMP is subsequently phosphorylated to dTTP via thymidylate kinase (TMPK, EC 2.7.4.9) and NDPK. On the other hand, dUrd can be directly salvaged or generated from dCyd deamination by cytidine deaminase (CDA, EC 3.5.4.5) (Leija *et al.* 2016). In mammals, dUMP can be also generated through deamination of dCMP via deoxycytidine monophosphate deaminase (DCTD), yet this enzyme is absent in *T. brucei*. Subsequently, dUMP is methylated to dTMP through the action of a bifunctional dihydrofolate reductase-thymidylate synthase (DHFR-TS, EC 2.1.1.45) enzyme (Fig. A8). Interestingly, it has been reported that DHFR-TS (Sienkiewicz *et al.* 2008), CDA (Leija *et al.* 2016) and TK (Valente *et al.* 2016; Leija *et al.* 2016) are all essential for *T. brucei*. DHFR-TS and CDA-null parasites could only be rescued by dThd supplementation (Sienkiewicz *et al.* 2008), in the first case, or the addition of dThd or dUrd in the medium, in the latter case. Besides, uracil supplementation was unable to restore cell viability, indicating that UPase activity is not enough to sustain thymidylate biosynthesis (Leija *et al.* 2016). Additionally, TK deficiency could not be compensated by any nucleobases or nucleosides (Valente *et al.* 2016; Leija *et al.* 2016), suggesting that its activity is

independent of extracellular salvage and that a pool of intracellular-derived dThd and dUrd are essential for the parasite. Indeed, TK is responsible for phosphorylation of dUrd to dUMP, the substrate of dTMP, and has an important role in *de novo* thymidylate biosynthesis.
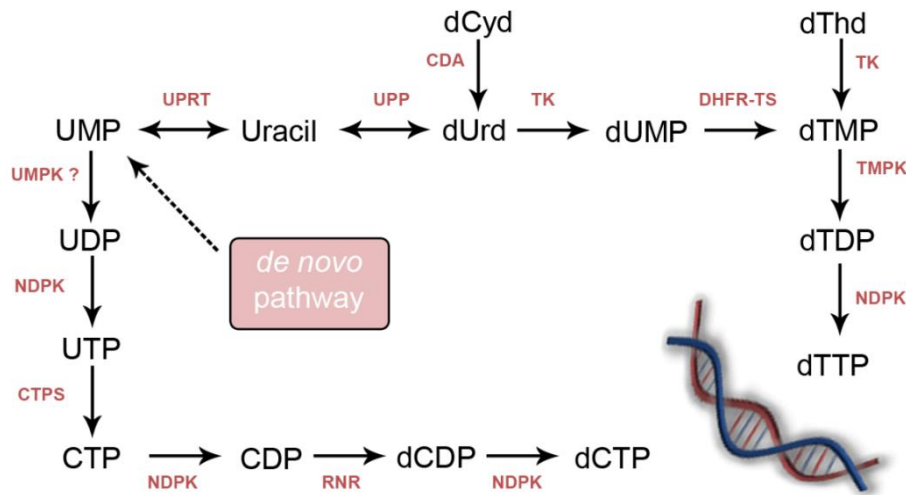
Figure A8. Metabolic pathways involved in the synthesis of pyrimidine nucleotides in *T. brucei*. Trypanosomatids are able to perform both *de novo* and salvage biosynthesis of pyrimidine nucleotides. UMP plays a central role in both pathways, as it can be produced by *de novo* synthesis or from salvage of dUrd and uracil via UPRT and UPase, and is an intermediate for both dCTP and dTTP biosynthesis. dCTP biosynthesis involves the action of NDPK, CTPS, RNR and presumably UMPK. dCyd salvage leads to dUrd formation via CDA. TK is able to phosphorylate both dUrd and dThd to dUMP and dTMP, respectively. dUMP is subsequently methylated to dTMP by DHFR-TS, which is finally phosphorylated to dTTP through the action of TMPK and NDPK. Enzyme abbreviations in the figure: uracil phosphoribosyltransferase (UPRT), uridine phosphorylase (UPase), cytidine deaminase (CDA), thymidine kinase (TK), dihydrofolate reductase-thymidylate synthase (DHFR-TS), thymidylate kinase (TMPK), nucleoside-diphosphate kinase (NDPK), uridylate kinase (UMPK), cytidine triphosphate synthetase (CTPS) and ribonucleotide reductase (RNR).

The observations regarding the role of TK suggest that *T. brucei* encodes nucleotidases that convert deoxypyrimidine nucleotides to their corresponding nucleosides. The exact enzymes involved in modulating intracellular deoxynucleoside pools in *T. brucei* remain to be established.

A.3.4. Human SAM and HD domain-containing protein 1 (SAMHD1)

While little is known about nucleotidases involved in deoxynucleoside production in *T. brucei*, in human cells a central player in dNTP homeostasis is the sterile alpha motif and histidine-aspartate domain-containing protein 1 (SAMHD1). This protein was initially described as an interferon ɣ (IFNɣ)-induced protein from the immune system (Li *et al.* 2000), with an important role in the restriction against the human immunodeficiency virus (HIV) (Lahouassa *et al.* 2013). More recently, it was described as a deoxynucleoside triphosphohydrolase (dNTPase), as it degrades all dNTPs into their corresponding deoxynucleosides and inorganic triphosphate (Goldstone *et al.* 2011), emerging as a crucial enzyme involved in the control of the dNTP pools.

Apart from the sterile alpha motif (SAM) and the histidine-aspartic (HD) domain, SAMHD1 presents at the N-terminus, at residues 11-14, a nuclear localization signal sequence, corresponding to KRPR (Brandariz-Nunez *et al.* 2012). The SAM domain is apparently involved in protein-protein and protein-RNA interactions (Kim and Bowie 2003; Qiao and Bowie 2005), whereas the HD domain corresponds to the catalytic core of the protein (Aravind and Koonin 1998). The assembly of the active enzyme requires a conformational change to a homo-tetramer allosterically regulated by dNTPs (Yan *et al.* 2013). Each subunit contains a catalytic site, where the dNTP substrate is bound in coordination with a Zn^{2+} ion, and two allosteric sites (primary and secondary) that accommodate GTP or dGTP residues and an additional dNTP, altogether coordinated by a Mg^{2+} ion (Fig. A9).
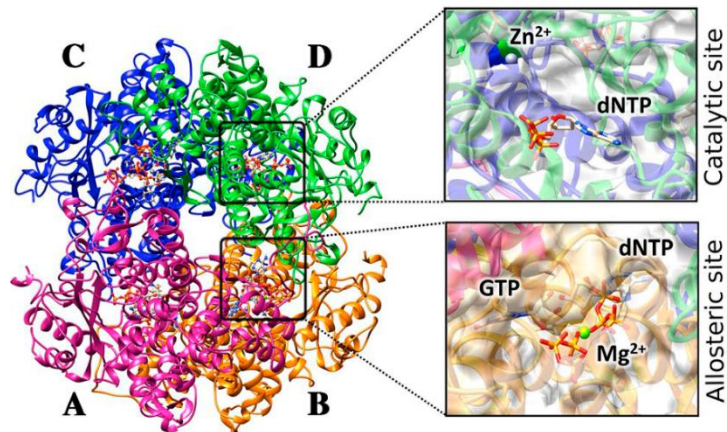
Figure A9. Structural representation of the HsSAMHD1 tetramer. Individual monomers are named from A to D and coloured differently. Each subunit contains a catalytic and an allosteric site. The catalytic site accommodates the dNTP substrate and requires the coordination by a Zn^{2+} ion, whereas the allosteric site contains GTP and an additional dNTP as cofactors in coordination with a Mg^{2+} ion (Cardamone *et al.* 2017).

The conformational change includes the following steps. First of all, GTP or dGTP bind to the primary allosteric site, inducing the dimer formation. Though both GTP and dGTP can potentially accommodate in the primary allosteric site, it probably occurs by GTP binding, as it presents a 1000-fold higher concentration in the cell compared to dGTP (Gavegnano *et al.* 2012). Meanwhile in the dimer, the C-terminal region blocks the catalytic site, hindering access to the substrate. Only once the allosteric dNTP is placed at the secondary allosteric site, tetramerization is induced and the conformational change moves the C-terminal region, consequently allowing substrate entry to the catalytic site (Zhu *et al.* 2015) (Fig. A10). As pyrimidine nucleotides can form more hydrogen bonds than purines, dCTP/dTTP binding is favored at the catalytic site (dCTP>dTTP/dGTP>dATP). This is opposed to the allosteric site, where purines, and specifically dATP, display higher affinity (dATP>dGTP>dTTP>dCTP) (Ji *et al.* 2014).
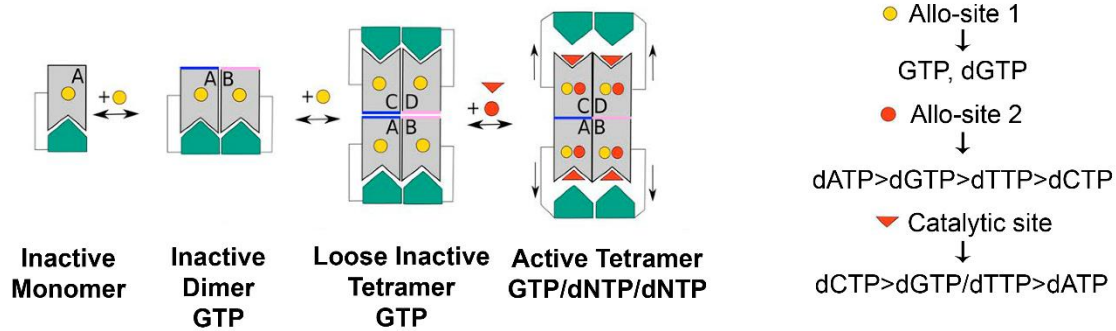
Figure A10. Scheme illustrating conformational changes to the final active SAMHD1 tetramer. First, GTP (or dGTP) attaches to the primary allosteric site (Allo-site 1), enabling the inactive dimer. Nevertheless, tetramerization is impeded until an additional dNTP binds to the secondary allosteric site (Allo-site 2). At this point, the C-terminal region moves and dNTP substrates can finally access the catalytic site of the active protein. Modified from Cardamone *et al*., (2017).

Apart from its dNTPase function, it has also been reported that the C-terminal region of SAMHD1 (residues 583-626) is involved in exonuclease activity on single-stranded RNA (ssRNA) and single-stranded DNA (ssDNA) (Beloglazova *et al.* 2013; Ryoo *et al.* 2014) by phosphorolytic cleavage of the phosphodiester moiety (Ryoo *et al.* 2016). Nucleic acid binding would prevent tetramerization, so this function would take place in the monomer and dimer state of the protein. Hence, the mechanism proposed to determine SAMHD1 activity is based on its oligomerization state (Seamon *et al.* 2015).

Due to its dNTPase activity, SAMHD1 may interfere with the maintenance of satisfactory dNTP levels required for replication and thus must be strictly regulated throughout the cell cycle. Indeed, it has been demonstrated that disturbances in its activity influence cell cycle progression (Franzolin *et al.* 2013). During simian immunodeficiency virus (SIV) or HIV-2 infection, the virion associated Vpx protein mediates SAMHD1 proteosomal degradation via E3 ubiquitin ligase (Ahn *et al.* 2012) (Hofmann *et al.* 2012). Nevertheless, in the absence of Vpx, corresponding to physiological conditions, SAMHD1 levels are not directly regulated via proteosomal

degradation (Tramentozzi *et al.* 2018), so its catalytic activity is predominantly controlled by post-translational modifications. One of the main mechanisms described to date is the phosphorylation at Thr592 by cyclin-dependent kinase 1 (CDK1) and CDK2 (Cribier *et al.* 2013; Welbourn *et al.* 2013), as it causes tetramer dissociation into the inactive monomer and dimer. Thr592 is positioned in a negatively charged region and upon phosphorylation generates repulsive interactions that inhibit tetramerization, and hence, dNTPase activity (Arnold *et al.* 2015; Tang *et al.* 2015). For this reason, as cyclin A2 is highly expressed during the S phase, it leads to SAMHD1 inactivation, whilst after mitotic exit, the serine/threonine protein phosphatase 2 A (PP2A) removes the Thr592 phosphate and restores SAMHD1 activity (Schott *et al.* 2018) (Fig. A11). Thus, this approach enables the regulation of SAMHD1 dNTPase function during the cell cycle.

Additionally, SAMHD1 has been associated with DNA repair processes. It has been reported that upon DNA damage, SAMHD1 binds to ssDNA/RNA and recruits the CtBP-interacting protein (CtIP) in order to promote homologous recombination (Daddacha *et al.* 2017). Furthermore, it has been suggested that SAMHD1 additionally prevents the release of ssDNA from stalled forks and subsequent aberrant activation of downstream signaling effectors (Coquel *et al.* 2018).
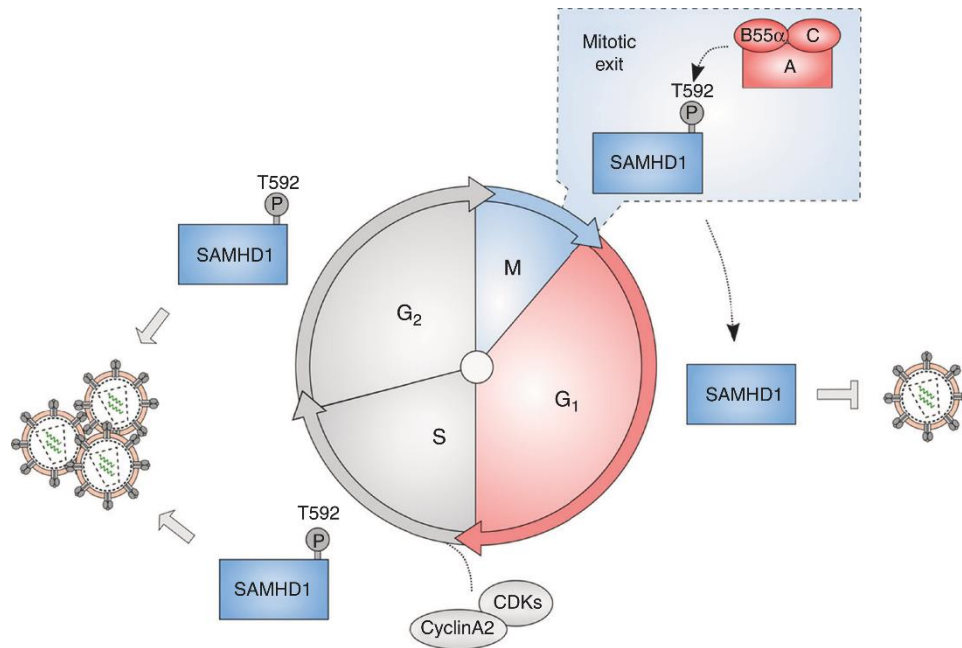
Figure A11. Regulation of SAMHD1 activity through the cell cycle by phosphorylation. At the S stage, cyclin A2 binds to the CDK, which mediates Thr592 phosphorylation of SAMHD1. In consequence, tetramerization and its dNTPase activity are inhibited until mitosis. After mitotic exit, PP2A-B55 holoenzyme dephosphorylates SAMHD1 and reestablishes its activity. Thus, SAMHD1 is highly functional in the G1 phase of the cell cycle (Schott *et al.* 2018).

A.4. DNA damage and repair

The DNA encodes the genetic information of every organism, so accurate replication and maintenance of genomic stability is essential for survival. However, since diverse processes can lead to DNA damage and alter this information, cells harbour very sophisticated mechanisms in order to circumvent or repair those potential lesions into DNA.

A.4.1. DNA damage and genome instability

DNA damage comprises any alteration in DNA that affects its content or that produces defects in transcription or replication, and may occur under the influence of exogenous and endogenous factors (Martin 2008; Chatterjee and Walker 2017). Exogenous factors include several types of chemical and physical agents, such as ionizing radiation or alkylating and oxidizing compounds, whereas the endogenous factors involve lesions produced by physiological cell metabolism. Indeed, the main source of DNA damage is endogenous (De Bont and van Larebeke 2004), and comprises the hydrolytic and oxidative action of free radical by-products, such as reactive oxygen and nitrosative species, replication errors and spontaneous base mismatches, deaminations, adducts and deletions (Chatterjee and Walker 2017).

Base deamination, both spontaneous and enzymatically-mediated, is the major source of mutagenesis, yet it also contributes to physiological processes, such as somatic hypermutation for antibody production (Blanc and Davidson 2010; Chandra *et al.* 2015) or genome variability in order to generate beneficial shifts to survive (Friedberg 2005). Under these circumstances, deamination of cytosine, adenine, guanine, and 5-methyl-cytosine produces uracil, hypoxanthine, xanthine and thymine, respectively. On the other hand, base deletions cause apurinic/apyrimidinic (AP) sites, single-strand breaks (SSB) and double-strand breaks (DSB). In this context, although DSBs are less frequent than other lesions, they have a profound impact on DNA stability, as they participate in recombination events (Khanna and Jackson 2001).

In order to maintain genomic integrity, the cell triggers a process named DNA damage response (DDR) (Harper and Elledge 2007). DDR involves the detection of the injury and its subsequent repair, which is determined by the type of lesion caused (Fig. A12). *T. brucei* exhibits differential expression of the repair machinery according

to the life cycle stage. Thus, parasites exposed to the immune response in the BSF show rapid DNA replication and upregulated DNA repair (Vieira-da-Rocha *et al.* 2018). *T. brucei* presents multiple DDR pathways that are classified as follows:

Direct repair. The action of an enzyme directly reverses a punctual lesion, without requiring DNA re-synthesis. This process embraces three pathways, such as alkylation reversal, photoreactivation and oxidative damage repair (Passos-Silva *et al.* 2010).

Base excision repair (BER). BER is the predominant pathway responsible for the repair of individual modifications that do not cause defects on the conformational structure. These lesions derive from a single base deamination, oxidation and alkylation, and DNA glycosylases initiate the process by the lesion removal. This pathway will be described in detail in the following subsection.

Nucleotide excision repair (NER). NER is the main pathway to repair bulky lesions that alter the tridimensional DNA conformation, such as pyrimidine dimers or DNA alkylation with larger alkyl group (Scharer 2013). Most enzymes involved in eukaryotic NER are present in trypanosomatids (Aslett *et al.* 2010).

Homologous recombination (HR). HR repairs DSBs through the exchange of the content between two DNA strands flanked by homologue sequences (Costes and Lambert 2012). In kinetoplastids most of the proteins involved in HR have been identified, and not only are very important for DSB repair, but also for antigenic variation. VSG switching in *T. brucei* primarily occurs via HR that mediates the locus-directed movement between the VSG present in the expression site and a VSG gene from a silent site (McCulloch and Barry 1999; Glover *et al.* 2013).

Non-homologous end-joining (NHEJ). NHEJ mediates DSBs repair through the direct ligation of the two DNA ends. *T. brucei* lacks some of the core proteins to perform this process, suggesting that NHEJ does not occur in this organism. In contrast, an alternative NHEJ pathway, microhomology-mediated end-joining (MMEJ), has been identified in *T. brucei* (Conway *et al.* 2002; Burton *et al.* 2007; Glover *et al.* 2008; Glover *et al.* 2011), which could play an important role in VSG switching (Glover *et al.* 2011).

Mismatch repair (MMR). MMR corrects replication errors that result in mispaired bases or modifications, such as methylation and oxidation, induced by genotoxic agents (Marinus 2012). Trypanosomatids encode all the enzymes required for a functional MMR (Bell *et al.* 2004). In addition, MMR also exerts a regulatory role in HR in *T. brucei* (Bell and McCulloch 2003).
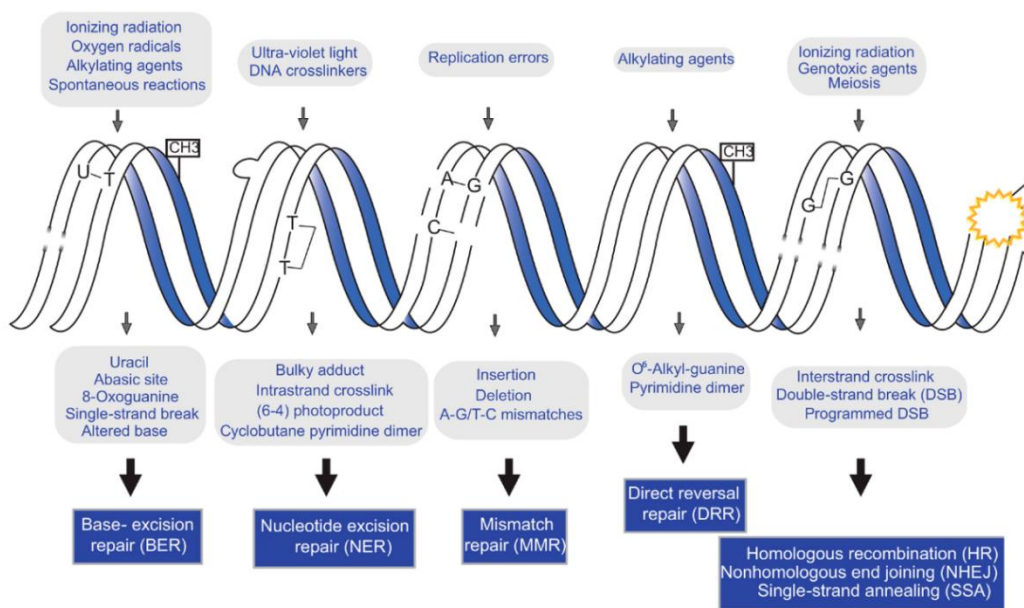
Figure A12. Schematic description of DNA lesions and the corresponding repair pathway. DNA is subjected to a variety of modifications by endogenous and exogenous agents. Alterations in DNA composition or structure activates the DDR, which, according to the lesion, triggers a specific repair mechanism. This diagram illustrates some representative damaging agents, the kind of lesions that each one produces and, depending on the type of modification, which repair pathway is activated (Genois *et al.* 2014).

Another important element in the DDR is the DNA damage detection and signaling to activate the corresponding repair pathway. This mechanism requires the recruitment of ataxia telangiectasia mutated (ATM), ataxia telangiectasia and Rad3-related protein (ATR) and DNA dependent protein kinases (DNA-PK), which will further phosphorylate downstream molecules that propagate the signaling cascade. This pathway is currently being applied to detect foci of DNA damage, since one important intermediate is the protein H2A histone family member X (H2AX), which is phosphorylated at Ser139 by ATM once DSBs are detected (Rothkamm *et al.* 2015). ɣH2AX then recruits to the damaged region additional proteins involved in signaling or the repair pathway. Hence, ɣH2AX serves as a biomarker of early damage, as foci can be assessed by immunofluorescence and flow cytometry (Kuo and Yang 2008). A H2A variant has been identified in *T. brucei* that is phosphorylated in Thr130 in response to DSBs (Glover and Horn 2012), so this useful technique to detect DNA damage can also be exploited in trypanosomal studies.

A.4.2. DNA repair via base excision repair

BER pathway is initiated through the recognition of the aberrant residue by a DNA glycosylase. It then cleaves the sugar-phosphate backbone and removes the modified base, creating an AP site. A wide variety of glycosylases exist, as they are specific to the damaged base. To date, only two distinct glycosylases have been identified in *T. brucei*, the uracil-DNA glycosylase (UNG) (Castillo-Acosta *et al.* 2012b) and the 8-oxoguanine-DNA glycosylase (OGG1) (Furtado *et al.* 2012), which remove uracil and 8-oxo-7,8-dihydro-deoxyguanine (8-oxoG), respectively. DNA glycosylases can also be classified as monofunctional or bifunctional, if they present

only glycosylase activity or an additional AP lyase activity, respectively. In the case of monofunctional glycosylases, the AP site is further recognized by the AP endonuclease (APE), which hydrolyzes the 5' phosphodiester bond of the AP site and creates a single-stranded DNA gap with a 3'-hydroxyl end and a 5'-deoxyribose phosphate end. Hereafter, a β-type DNA polymerase (Polβ) removes the 5'-deoxyribose phosphate group and incorporates the appropriate nucleotide. Finally, a DNA ligase catalyzes the formation of a phosphodiester bond and restores the integrity of the helix by sealing the nick (Fig. A13) (Robertson *et al.* 2009).
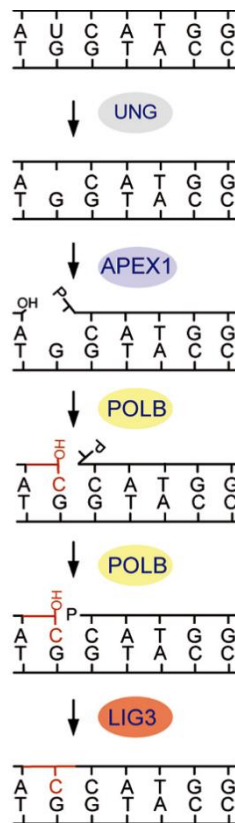
Figure A13. Illustrative representation of uracil repair by short-patch BER pathway. Concisely, monofunctional UNG detects uracil in DNA and catalyzes its excision, creating an AP site. Consecutively, the APE1 endonuclease hydrolyzes the 5' phosphodiester bond and generates a SSB. The Polβ fills the gap with the correct nucleotide and finally the nick in DNA is sealed by the action of Lig3. Enzyme abbreviations in the figure correspond to: uracil-DNA glycosylase (UNG), apurinic/apyrimidinic endonuclease 1 (APE1), DNA polymerase β (Polβ) and DNA ligase 3 (Lig3) (Robertson *et al.* 2009).

The gap-filling and ligation steps can occur by two different subpathways, a short-patch and a long-patch. In the short-patch, the single modified nucleotide is replaced through the action of Polβ and DNA ligase-3 (Lig3), coordinated by X-Ray Repair Cross Complementing 1 (XRCC1) (Kubota *et al.* 1996). In contrast, in the long-patch from 2 to 13 nucleotides are substituted via replicative DNA polymerases δ and ε, and require additional proteins to replace the newly-synthesized DNA chain (Frosina *et al.* 1996).

In trypanosomatids, most of the BER enzymes have been characterized, though no homologues for Lig3 and XRCC1 from the short-patch mechanism appear to be present. Nonetheless, some evidences suggest that both uracil and 8oxoG are repaired by the short-patch pathway (Akbari *et al.* 2007).

A.4.3. Role of uracil-DNA glycosylase (UNG) in DNA repair

UNGs are monofunctional glycosylases from the family I of the UDG enzymes that remove uracil from DNA. Uracil is a non-canonical base, but it may be misincorporated in the place of dTTP during DNA replication (Schormann *et al.* 2014). In this case, although uracil misincorporation is not a mutagenic event *per se*, further AP sites generated by UNG cleavage behave as a mutagenic lesion (Sedwick *et al.* 1986) (Guillet *et al.* 2006). In fact, dUTP accumulation in *T. brucei* subjected to dUTPase deletion induces an overall hypermutator effect (Castillo-Acosta *et al.* 2012a). Uracil can also appear in DNA after cytosine deamination, which generates an U:G mismatch. This mismatch is highly mutagenic if unrepaired, because adenine is incorporated opposite to uracil during replication, giving rise to T:A transitions

(Krokan *et al.* 2002). Therefore, uracil repair is a critical process in the maintenance of genomic integrity.

In mammals, uracil can be removed by at least three additional DNA glycosylases, SMUG1, TDG and MBD4 (Sousa *et al.* 2007), which are absent in trypanosomatids. Studies performed in several models reported that, although UNG is not essential for cell proliferation, deficient cells exhibit important defects, such as a hypermutator phenotype or development of tumourogenesis (Duncan and Weiss 1982; Chatterjee and Singh 2001; Nilsen *et al.* 2003; Alsoe *et al.* 2017). UNG exhibits additional functions, for instance, it is involved in somatic hypermutation for antibody maturation as well as in class switch recombination for the production of a wide antibody repertoire (Rada *et al.* 2002; Imai *et al.* 2003). In these processes UNG recognizes the U:G mismatch coming from a controlled enzymatic cytosine deamination performed by a cytidine deaminase activity that belongs to the APOBEC/AID family enzymes (Kavli *et al.* 2007). UNG is also relevant for other pathways, regardless its catalytic activity. For instance, it forms a complex that is essential for the replication of vaccinia virus (De Silva and Moss 2003), and it has also been reported that UNG is recruited to the integrase recombination complex by Vpr in HIV-1 (Selig *et al.* 1997). In addition to this, UNG has also been detected in damaged DNA foci in association with γH2AX (Zeitlin *et al.* 2011).

In *T. brucei,* previous studies showed that UNG is not essential for cell proliferation. Nevertheless, in agreement with data reported in other organisms, UNG knock-out parasites showed higher DNA fragmentation, hypersensibility to antifolates and oxidative agents, as well as a hypermutator phenotype. Interestingly, UNG-deficient parasites exhibited lower virulence in the murine model of the disease (Castillo-Acosta *et al.* 2012b). Altogether, these observations suggest that UNG has a key role in the

protection against the lesions produced by oxidative stress and that parasites with impaired BER pathway are specially sensitive to oxidative agents, such as nitric oxide, which is an important element of the immune response.

A.5. Effects of oxidative stress on DNA

As already described, *T. brucei* triggers important evading mechanisms to escape the antibody-mediated immune response, as antigenic variation. Nevertheless, it is also subjected to additional components of the immune system aimed at controlling parasitaemia. Indeed, several harmful molecules are released, which especially produce oxidative stress. Since DNA is one of the major targets of oxidative agents, it is thereby vulnerable to processes that compromise its integrity, such as mutagenesis, strand breaks and recombination.

A.5.1. Immune response towards trypanosomal infection

The front line of host defence is accomplished by the innate immunity, which is involved in the immediate nonspecific elimination of the pathogen and activation of subsequent adaptive immunity. This system is composed of several cellular effectors, such as granulocytes, macrophages, dendritic cells (DCs), mast cells and natural killer (NK) cells, soluble factors and physical barriers like epithelia of skin, gastrointestinal, respiratory or genitourinary tracts (Douglas and McDonald 2019). At a later stage, the adaptive immunity is activated, which is a specific response that relies on the activity of B and T lymphocytes (Dranoff 2004) (Fig. A14).
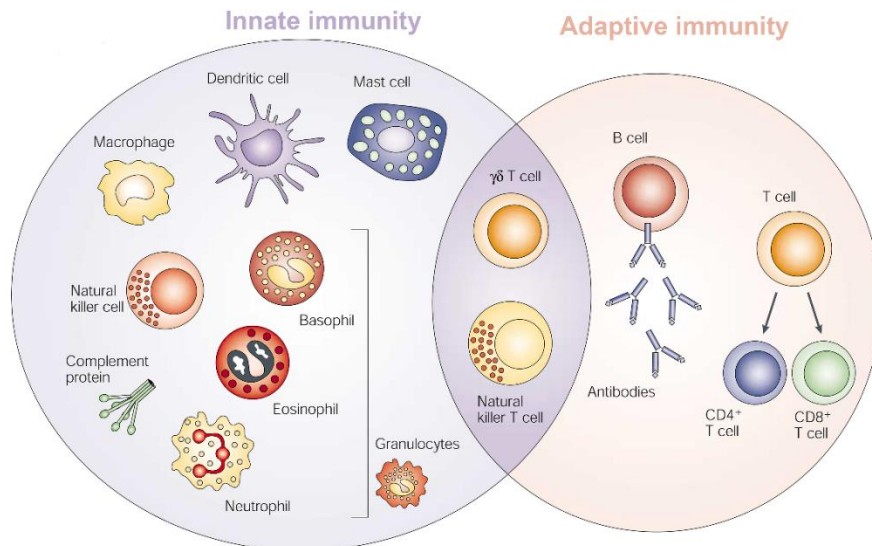
Figure A14. Components of innate and adaptive immunity. The innate response is triggered immediately against the infection and is composed of soluble factors (as the complement protein) and several type of cells, such as macrophages, natural killer cells, dendritic cells, mast cells and granulocytes. In contrast, the more specific adaptive immunity is developed later and is mainly performed by B and T lymphocytes. Natural killer T cells and γδT cells are lymphocytes belong to both kind of responses (Dranoff 2004).

At the beginning of the infection, diverse trypanosomal molecules are identified by membrane pattern recognition receptors on myeloid cells, such as macrophages and DCs, resulting in cellular activation (Kumar *et al.* 2011) and subsequent pathogen elimination. In the first instance, macrophages generate oxidizing agents, such as reactive nitrogen species (RNS) and reactive oxygen species (ROS), which are intrinsically trypanocidals. In addition, macrophages and other antigen-presenting cells (APCs) produce a highly polarized T helper-1 (Th1) proinflammatory cytokine response that releases IFN-γ, tumoral necrosis factor-α (TNF-α), nitric oxide (NO), interleukin-6 (IL-6) as well as a IL-1 and IL-12 (Mansfield and Paulnock 2005; Ponte-Sucre 2016) (Fig. A15).
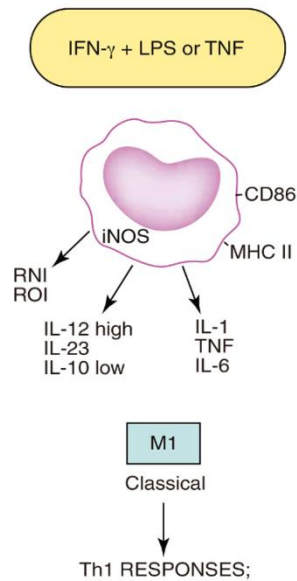
Figure A15. Macrophage activation and development of Th1 response. In the classical Th1 response, macrophages are activated by interferon-ɣ (IFN-ɣ) in addition to lipopolysaccharide (LPS) or tumor necrosis factor (TNF), producing proinflammatory cytokines and oxidative species, such as reactive nitrogen and oxidative species. Modified from Martinez, F.O. and Gordon, S. (2014).

Concomitantly, trypanosomal VSGs induce macrophage-derived TNF-α and IL-1 overproduction (Magez *et al.* 1998), which promote activation, proliferation and differentiation of B cells, leading to antibody production (Roldan *et al.* 1992; Silva-Barrios *et al.* 2018). DCs also have a pivotal role in the adaptive immune response, as they detect VSGs and consequently enhance major histocompatibility complex (MHC) and co-estimulatory molecules. This mechanism leads to T cell proliferation and differentiation, as well as IL-12 production (Kalinski *et al.* 1999; Dos-Santos *et al.* 2016).

In addition to evading strategies, trypanosomes are able to counteract the immune response through the induction of CD45-dependent T-cell death and memory B-cells apoptosis, thus affecting to the functionality of host lymphocytes (Antoine-Moussiaux *et al.* 2009; Bockstal *et al.* 2011). This process is known as exhaustion

(Rodrigues *et al.* 2014), and it has been suggested that is caused by the dense coat of VSGs (Silva-Barrios *et al.* 2018).

A.5.2. Nitric oxide and oxidative stress

One of the major oxidizing compounds released by macrophages is NO. This molecule has an unpaired electron that can rapidly react with a wide variety of molecules, as hemoproteins, thiol groups or oxygen and superoxide radicals. In addition to its role as a defense mechanism, it also acts as a cellular messenger. It exerts many physiological effects through cysteine S-nytrosylation and tyrosine nitration (Stamler *et al.* 1997; Hess *et al.* 2005). Thus, NO *per se* is not toxic, yet it gives rise to several molecules, referred as RNS, which subsequently generate an important cytotoxic response.

NO is produced by three isoforms of nitric oxide synthase (NOS), such as neuronal NOS (nNOS), endothelial NOS (eNOS) and inducible NOS (iNOS). These enzymes use L-arginine and oxygen as substrate, as well as a series of cofactors (Forstermann and Sessa 2012). Whereas nNOS and eNOS are constantly releasing low amounts of NO that perform signalling functions, iNOS is only activated in the macrophages in the presence of proinflammatory cytokine stimulus, such as IL-1b, IFNɣ, TNFα, IL-17 or IL-6, producing large amounts of NO, approximately 1000-fold higher than constitutive forms (Arzumanian *et al.* 2003). L-arginine is also a substrate of the arginase enzyme, which is expressed in macrophages and increased during infection (Gobert *et al.* 2000). Therefore, NO levels will depend on arginase and iNOS activities.

As aforementioned, NO is a very reactive molecule that in presence of oxygen can give rise to several NO-derivatives, where peroxynitrite (ONOO⁻) has a powerful and important oxidant character (Pacher *et al.* 2007) (Fig. A16). RNS can oxidize and nitrate DNA, and may cause SSBs through the attack on the sugar-phosphate backbone. The nitrosation of primary amines on DNA bases gives rise to deamination of several bases, such as adenine, cytosine, 5-methylcytosine, and guanine, producing hypoxanthine, uracil, thymine and xanthine respectively. Besides, RNS may also cause AP sites through base depurination, which subsequently may generate SSBs in DNA through the action of endonucleases. Indeed, ONOO⁻ can directly react with the nucleotidic sugar moiety, leading to DNA fragmentation. Thereby, RNS are important agents that are involved in deleterious processes, such as mutagenesis and fragmentation of DNA (Burney *et al.* 1999). In order to gain insight into the effects produced by RNS, the use of inhibitors is a powerful tool. In this context, aminoguanidine (AG) is a hydrazine that selectively inhibits the iNOS. It is structurally similar to L-arginine, so it competes with the substrate of iNOS for the active site (Corbett and McDaniel 1996; Bryk and Wolff 1998).

Figure A16. Nitric oxide synthesis in the macrophage and further peroxynitrite formation. The inducible nitric oxide synthase (iNOS) is activated by a wide variety of cytokines in the macrophages, leading to the generation of nitric oxide (NO). Concurrently, oxygen (O_2) is also produced during respiration. Both O_2 and NO can react, what generates a strong oxidant, the peroxynitrite (ONOO⁻). Modified from Pacher *et al*., (2007).

OBJECTIVES

B. OBJECTIVES

The preservation of genomic integrity is essential to ensure viability and proliferation of all organisms. In this context, the correct maintenance of dNTP pools plays a key role, as alterations in the nucleotide levels give rise to processes that seriously compromise cell integrity, such as genotoxicity, mutagenesis or tumourogenesis. Hence, both synthesis and degradation of nucleotides are strictly regulated by several enzymes.

Indeed, while *T. brucei* is able to perform pyrimidine biosynthesis both by the salvage and *de novo* pathways, previous studies have shown the essentiality of enzymes involved in thymidylate biosynthesis, such as DHFR-TS, TK or CDA. Interestingly, the essential character of TK together with the accumulation of deoxynucleosides in TK depleted cells clearly indicated that *T. brucei* encodes nucleotidases that provide a source of deoxynucleosides and that these enzymes must have an essential role in modulating intracellular pools. However, to date, dNTPases clearly involved in this pathway in *T. brucei* have not been characterized. Since in humans SAMHD1 appears to be the most relevant dNTPase controlling dNTP homeostasis, the first aim of this research was the identification of HsSAMHD1 orthologues in *T. brucei,* as well as the evaluation of their role in cell viability and homeostasis of pyrimidine dNTPs. To this purpose, the following specific objectives were proposed:

1. Identify potential HsSAMHD1 orthologues in *T. brucei* with a predicted dNTPase activity and determine their intracellular localization.
2. Evaluate the role of HsSAMHD1 orthologues in cell viability and cell cycle progression.

3. Establish the role of the identified dNTPases in the supply of pyrimidine and purine nucleosides.

4. Analyze the contribution of dNTPases to pyrimidine and thymidylate biosynthesis.

5. Determine the impact of perturbations in dNTP hydrolysis on genomic integrity.

DNA lesions can derive from polymerase action during replication or external agents that modify DNA bases, which can lead to severe damage, such as mutations, DNA breaks or AP sites. In the case of *T. brucei*, during infection parasites are especially exposed to an intense oxidative stress as a result of the response of the immune system. In order to counteract this situation and sustain genomic integrity, cells trigger multiple repair mechanisms. Previous studies conducted in the lab have already demonstrated the importance of UNG for *T. brucei* infectivity, as UNG-deficient parasites showed reduced virulence. Thus, a second general aim of this thesis was to analyze the occurrence of oxidative stress and the activation of DNA repair pathways during host-pathogen interactions *in vivo*. The following specific objectives were proposed:

1. Evaluate the impact of oxidative stress on DNA integrity in *T. brucei* BSFs exposed to genotoxic compounds *in vitro*.

2. Analyze the consequences on parasites of the potential oxidative stress that arises upon murine infection and the activation of a DNA damage response.

3. Determine the relevance of UNG and the BER pathway in counteracting DNA damage produced by oxidative stress.

MATERIALS AND

METHODS

C. MATERIALS AND METHODS

C.1. Materials

C.1.1. Trypanosomal cell lines

In this thesis, the protozoan parasite *T. brucei brucei* has been used as model organism, which is responsible for African Trypanosomiasis in animals, also known as nagana. Experiments have been performed in both the BSF and PCF of *T. brucei* trypomastigotes.

Information regarding the parental BSF and PCF cell lines coming from *T. brucei brucei* 427:

Parental cell line	Form	Selectable marker	Reference
Tb S16	BSF	G-418	(Wirtz *et al.* 1999)
Tb 449	PCF	Ble	(Biebinger *et al.* 1997)

Table C1. Description of the parental cell lines of *T. brucei* bloodstream and procyclic forms and culture conditions.

Briefly, *Tb* S16 BSF parasites harbor the T7 RNA polymerase as well as the tetracycline inducible repressor (TetR) gene, whereas *Tb* 449 PCF parasites only harbour the TetR in their genome.

All the transfectants used or produced were originated from *Tb* S16 and *Tb* 449 parental lines:

Mutant cell line	Form	Selectable marker	Description	Reference
TbHD82-OE	BSF	Pur [1]	Inducible ectopic TbHD82 ORF	This thesis
	PCF	Pur [1]	Inducible ectopic TbHD82 ORF	This thesis
TbHD82-myc OE	PCF	Pur [1]	Inducible ectopic TbHD82-myc fusion protein	This thesis
TbHD52-OE	PCF	Pur [1]	Inducible ectopic TbHD52 ORF	This thesis
TbHD52-myc OE	PCF	Pur [1]	Inducible ectopic TbHD52-myc fusion protein	This thesis
TbHD82-RNAi	BSF	Hyg [1]	RNA interference of TbHD82 ORF	This thesis
TbHD82-dKO	BSF	Bsd, Hyg	TbHD82 Knockout	This thesis
TbHD52-RNAi	BSF	Hyg [1]	RNA interference of TbHD52 ORF	This thesis
TbHD52-dKO	BSF	Bsd, Hyg	TbHD52 Knockout	This thesis
	PCF	Bsd, Hyg	TbHD52 Knockout	This thesis
TbHD52-dKO/OE	BSF	Bsd, Hyg, Pur [1]	HD52 Knockout + inducible ectopic TbHD52 ORF	This thesis
	PCF	Bsd, Hyg, Pur [1]	HD52 Knockout + inducible ectopic TbHD52 ORF	This thesis
TbHD52-dKO/TbCDA	BSF	Bsd, Hyg, Pur [1]	TbHD52 Knockout + inducible ectopic TbCDA ORF	This thesis
TbHD52-dKO/HsDCTD	BSF	Bsd, Hyg, Pur [1]	TbHD52 Knockout + inducible ectopic HsDCTD ORF	This thesis
TbUNG-KO	BSF	Bsd, Hyg	UNG Knockout	(Castillo-Acosta *et al.* 2012b)
TbUNG-KO/OE	BSF	Bsd, Hyg, Pur [1]	UNG Knockout + inducible ectopic TbUNG ORF	(Castillo-Acosta *et al.* 2012b)

Table C2. Description of the transgenic cell lines derived from parental *T. brucei* BSFs and PCFs and culture conditions

---

[1] Indicates that the addition of 1 μg/ml Dox to the culture media induces either the expression of the ectopic copy or the interference RNA, depending on the genetic background of the cell line.

C.1.2. Bacterial strains

The following *Escherichia coli* strains were employed in the thesis:

BL21(DE3) (Phillips *et al.* 1984). F⁻ *dcm, ompT, hsdS* ($r_B^- m_B^-$) *gal* λ (DE3). Used for protein expression.

XL1-Blue (Bullock WO 1987). *Rec A1, end A1, gyr A96, thi-1, hdsR17, supE44, relA1, lac* [F' *proAB lacI^q ZΔM15 Tn10* (Tet^r)]. Used for gene cloning.

C.1.3. Culture media

C.1.3.1. Bacteria culture media

Agar LB (*Lysogeny broth*). LB media, 15 g/l bacto-agar

LB. 10 g/l tryptone, 5 g/l yeast extract, 5 g/l NaCl

For bacterial selection, the culture media was supplemented with 100 μg/ml ampicillin or 50 μg/ml kanamycin, for XL1-Blue or BL21(DE3), respectively.

C.1.3.2. Parasite culture media

The culture media used for maintenance and culture of the parasites were HMI-9 and SDM-79 for BSF and PCF trypanosomes, respectively. Prior to use, the culture media was supplemented with 10% inactivated-fetal bovine serum (FBS) (GIBCO) plus corresponding antibiotics.

The information regarding the composition of the culture media was obtained from the research resources provided by the Rockefeller University

(http://tryps.rockefeller.edu/trypsru2_culture_media_compositions.html), and is listed below:

Components (mg/l approximate values)		HMI-9	SDM-79
Salts, etc	Bathocuproine disulfonate · Na$_2$	28	
	CaCl$_2$	165	180
	Deoxy-D-ribose		0.10
	D-ribose		0.10
	Fe(NO$_3$)$_3$ · 9 H$_2$O		0.14
	Glucosamine · HCl		50
	Glucose	4.5	1.9
	Hemin		7.5
	HEPES	5.96	8
	KCl	330	360
	KNO$_3$	0.076	
	Mercaptoethanol	15	
	MgSO$_4$	98	
	MgSO$_4$ · 7 H$_2$O		180
	MOPS		5
	NaCl	4.5	6.12
	NaHCO$_3$	3.02	3.98
	NaH$_2$PO$_4$ · H$_2$O	125	126
	Na$_2$SeO$_3$ · 5 H$_2$O	0.017	
	Phenol Red	15	11
L-aminoacids	Alanine	25	210
	Arginine · HCl	84	215
	Asparagine	25	8
	Aspartic acid	30	14

	Cysteine	182	0.02
	Cystine	91	29
	Glutamic acid	75	24
	Glutamine	584	320
	Glycine	30	15
	Histidine · HCl · H_2O	42	38
	Hydroxyproline		2
	Isoleucine	105	46
	Leucine	105	54
	Lysine ·HCl	146	72
	Methionine	30	85
	Phenylalanine	66	111
	Proline	40	615
	Serine	42	71
	Taurine		160
	Threonine	95	394
	Tryptophan	16	10
	Tyrosine	104	150
	Valine	94	42
	Ascorbic acid		0.010
	B12	0.013	
	Biotin	0.013	0.20
	Calciferol		0.020
Vitamins, etc	Choline chloride	4.0	0.80
	D-Ca pantothenate	4.0	0.70
	DL-alpha-tocopherol-Na_2PO_4		0.0020
	Folic Acid	4.0	4.7
	i-Inositol	7.2	1.41

	L-glutathione (reduced)		0.010
	Menadione		0.0020
	Niacin		0.0050
	Niacinamide	4.0	0.705
	p-aminobenzoic acid		2.01
	Pyridoxal ·HCl	4.0	0.705
	Pyridoxine ·HCl		0.0050
	Riboflavin	0.40	0.072
	Thiamine ·HCl	4.0	0.702
	Vitamin A acetate		0.028
Organic acids	Acetate ·Na		10
	Pyruvate ·Na	114	100
Purines, etc	Adenine $SO_4 \cdot 2\ H_2O$		2.0
	Adenosine		10.0
	$AMP \cdot H_2O$		0.04
	$ATP \cdot Na_2 \cdot 3\ H_2O$		0.20
	Guanine $\cdot$ HCl $\cdot 2H_2O$		0.06
	Guanosine		10.0
	Hypoxanthine	136	0.06
	Thymidine [2]	80	
	Thymine		0.06
	Uracil		0.06
	Xanthine ·Na		0.06
Lipids	Cholesterol		0.04
	Tween80		4.00

Table C3. Components of the HMI-9 and SDM-79 culture media

---

[2] Thymidine was excluded from HMI-9 medium in the case of pyrimidine-free medium preparation

C.1.4. Buffers and solutions

All the buffers were prepared with Milli-Q distilled water.

General buffers	
Lysis buffer	0.2 M Tris-HCl pH 8.0, 0.1 M EDTA
PBS 1X	137 mM NaCl, 2.7 mM KCl, 1.8 mM KH_2PO_4, 10 mM Na_2HPO_4, pH 7.4
PBS-250	250 mM NaCl, 2.7 mM KCl, 1.8 mM KH_2PO_4, 10 mM Na_2HPO_4, pH 7.4
PBS-500	500 mM NaCl, 2.7 mM KCl, 1.8 mM KH_2PO_4, 10 mM Na_2HPO_4, pH 7.4
SB-Glucose	44 mM NaCl, 57 mM Na_2HPO_4, 3 mM NaH_2PO_4, 10 mM glucose, pH 8.0
TAE	40 mM Tris, 20 mM acetic acid, 1 mM EDTA
TDB-Glucose	80 mM NaCl, 5 mM KCl, 20 mM Na_2HPO_4, 1 mM $MgSO_4$, 20 mM glucose, pH 7.4
Transfection buffers	
Cytomix	2 mM EGTA, 120 mM KCl, 0.15 mM $CaCl_2$, 10 mM K_2HPO_4/KH_2PO_4, 25 mM HEPES, 5 mM $MgCl_2 \cdot 6\,H_2O$, 0.5% Glucose, 100 µg/ml BSA (defatted), 1 mM Hypoxanthine, pH 7.6
ZPFM	132 mM NaCl, 8 mM KCl, 8 mM Na_2HPO_4, 1.5 mM $Mg(CH_3COO)_2$, 90 µM $Ca(CH_3COO)_2$, pH 7.0
Protein purification buffers	
Elution buffer	20 mM sodium phosphate (NaH_2PO_4/Na_2HPO_4), 0.5 M imidazole, 8 M urea, 0.5 M NaCl, pH 7.4 + protease inhibitor cocktail (Roche)
Lysis and binding buffer	20 mM sodium phosphate (NaH_2PO_4/Na_2HPO_4), 20 mM imidazole, 8 M urea, 0.5 M NaCl, pH 7.4 + protease inhibitor cocktail (Roche)
Wash buffer	20 mM sodium phosphate (NaH_2PO_4/Na_2HPO_4), 50 mM imidazole, 8 M urea, 0.5 M NaCl, pH 7.4 + protease inhibitor cocktail (Roche)
Antibody purification buffers	
Blocking buffer	100 mM ethanolamine-HCl, pH 8.0
Coupling buffer	50 mM HEPES, pH 7.5
Elution buffer	100 mM Glycine, pH 2.5
dNTP measurement buffers	
DNA Polymerase buffer	25 mM Tris-HCl pH 7.8, 1 mM DTT
dUTPase buffer	34 mM Tris-HCl, 5 mM $MgCl_2$, pH 7.8
Precipitation buffer	8.9 mM Tris-HCl, 0.65 N TCA
Buffers for protein studies	
Running buffer	250 mM Tris, 1.92 M glycine, 1% SDS
Sample buffer	67.5 mM Tris–HCl pH 6.8, 3% SDS, 10% glycerol, 5% β-mercaptoethanol
Stripping buffer	150 mM NaCl, 10 mM Tris-HCl, pH 2.3
Transfer buffer	25 mM Tris base, 186 mM glycine, 20% v/v methanol
Urea-cracking buffer	6 M urea, 10 mM Na_2HPO_4, 1% β-mercaptoethanol, pH 7.0

Table C4. Description of the components used to prepare the buffers for the different studies

C.1.5. Compounds

C.1.5.1. Nucleosides and nucleobases

The nucleosides and nucleobases used in this thesis are listed below, which were dissolved, filtered with 0.22 µm filters and stored at -20ºC until used.

Name	Abbreviation	Reference	Stock concentration	Solvent
5-Methyl-deoxycytidine	5M-dCyd	Santa Cruz Biotechnology	100 mM	H_2O
Adenosine	Ado	Sigma-Aldrich	50 mM	0.1 M NaOH
Deoxyadenosine	dAdo	Sigma-Aldrich	100 mM	H_2O
Deoxycytidine	dCyd	Sigma-Aldrich	100 mM	H_2O
Deoxyguanosine	dGuo	Sigma-Aldrich	50 mM	0.1 M NaOH
Deoxythymidine	dThd	Sigma-Aldrich	100 mM	H_2O
Deoxyuridine	dUrd	Sigma-Aldrich	100 mM	H_2O
Guanosine	Guo	Sigma-Aldrich	100 mM	0.1 M NaOH
Uracil	Ura	Sigma-Aldrich	100 mM	H_2O

Table C5. Description of the nucleosides and nucleobases used in the studies

C.1.5.2. Drugs

The drugs used for selection and culture of transgenic cell lines in this thesis are listed below. Thus, they were dissolved in milli-Q distilled water and filtered with 0.22 µm filter prior to use.

Name	Abbreviation	Reference	Selected organism	Final concentration of use
Ampicillin	Amp	Roche	*E. coli*	100 µg/ml
Blasticidin	Bsd	Gibco	*T. brucei*	5 µg/ml for BSF 10 µg/ml for PCF
Doxycycline	Dox	Sigma-Aldrich	*T. brucei*	1 µg/ml
Geneticin	G-418	Gibco	*T. brucei*	2.5 µg/ml for BSF
Hygromicin	Hyg	Sigma-Aldrich	*T. brucei*	5 µg/ml for BSF 50 µg/ml for PCF

Kanamycin	Kan	Sigma-Aldrich	*E. Coli*	50 µg/ml
Phleomycin	Ble	Sigma-Aldrich	*T. brucei*	0.5 µg/ml for PCF
Puromycin	Pur	Sigma-Aldrich	*T. brucei*	0.1 µg/ml for BSF 1 µg/ml for PCF

Table C6. Information regarding the antibiotics used during the thesis

C.1.5.3. Antibodies

Name	Primary/Secondary	Organism	Reference	Dilution for WB	Dilution for IF
Anti-*Tb*dUTPase	Primary	Rabbit	(Castillo-Acosta *et al.* 2008)	1:75,000	-
Anti-*Tb*TK	Primary	Rabbit	(Valente *et al.* 2016)	1:10,000	-
Anti-*Tb*ɣH2A	Primary	Rabbit	(Glover and Horn 2012)	-	1:100
Anti-c-myc	Primary	Mouse	Sigma-Aldrich	-	1:500
Anti-β-tubuline	Primary	Mouse	Sigma-Aldrich	1:10,000	-
Anti-*Tb*HD82	Primary	Rabbit	This thesis	1:10,000	1:100
Anti-*Tb*HD52	Primary	Rabbit	This thesis	1:10,000	1:500
Anti-*Tb*UNG	Primary	Rabbit	(Castillo-Acosta *et al.* 2012b)	1:50,000	-
Anti-*Tb*CDA	Primary	Rabbit	(Moro-Bulnes *et al.* 2019)	1:500	-
Anti-*Hs*DCTD	Primary	Mouse	Santa Cruz Biotechnology	1:1,000	-
Anti-Rabbit IgG, HRP Conjugate	Secondary	Goat	Promega	1:5,000	-
Anti-Mouse IgG, HRP Conjugate	Secondary	Goat	Promega	1:3,000	-
Anti-Rabbit IgG, Alexa Fluor® 488 Conjugate	Secondary	Goat	Sigma-Aldrich	-	1:100
Anti-Mouse IgG, Alexa Fluor® 488 Conjugate	Secondary	Goat	Sigma-Aldrich	-	1:500

Table C7. List of antibodies used in this thesis for western blot (WB) and immunofluorescence (IF) studies

C1.5.4. Other compounds

Aminoguanidine. *Aminoguanidine hemisulfate salt* (Sigma Aldrich).

DAPI. *ProLong Gold antifade reagent* (Invitrogen).

DETA-NO. *Diethylenetriamine/nitric oxide adduct* (Sigma Aldrich).

DHE. *Dihydroethidium* (Sigma-Aldrich).

MitoTracker. *MitoTracker Red CMX Ros* (Invitrogen).

Propidium iodide. *Propidium iodide solution* (Sigma-Aldrich).

C.1.6. Oligonucleotides

All the oligonucleotides used in this thesis were synthesized by the Genomics and Oligonucleotide Synthesis facilities of the Instituto de Parasitología y Biomedicina "López-Neyra".

Name	Sequence (5'-3')	Restriction site	Use
AE41	GAGTTTAACATGTTCTCGTCC	-	sequencing
AE42	CCTTCTCTTCTTTTGGGTTCGCTC	-	sequencing
Bsd3-5	TCAGAGATGGGGATGCTGTT GATTGTAGC	-	Check dKO cell lines
Bsd5-3	GCTACAATCAACAGCAT CCCCATCTCTGA	-	Check dKO cell lines
Pol dATP	AAATAAATAAATAAATAAATG GCGGTGGAGGCGG	-	dATP template for dNTP quantification
P255	CCGCCTCCACCGCC	-	Polymerase primer for dNTP quantification
P256	TTTGTTTGTTTGTTTGTTTGGGCG GTGGAGGCGG	-	dCTP template for dNTP quantification
P257	TTTATTTATTTATTTATTTA GGCG GTGGAGGCGG	-	dTTP template for dNTP quantification
P258	TTTCTTTCTTTCTTTCTTT CGGCG GTGGAGGCGG	-	dGTP template for dNTP quantification
SP6V	ATTTAGGTGACACTATAGAATA	-	sequencing
TbMyo1	GGATTGGCTGGAGAAGAATACA	-	Uracil determination
TbMyo2	GAGTGACGCCAATGCTATCT	-	Uracil determination
T7V	TAATACGACTCACTATA	-	sequencing

VCA33	GCGCGATTGCTGATCCC CATGTGTATCAC	-	Check dKO cell lines
VCA34	GTGATACACATGGGG ATCAGCAATCGCGC	-	Check dKO cell lines
VCA147	GCGCTAGCATGGAAG GGGAACTTGCCTTC	NheI	5' of TbHD82 ORF for expression
VCA148	GCGGATCCTTAGCG GCTGCGTTTATTTCC	BamHI	3' of TbHD82 ORF for *TbHD82*-OE generation and expression
VCA149	GCGCTAGCATGAGAA ATGGAATTATCTGTCG	NheI/BfaI	5' of TbHD52 ORF for *TbHD52*-cmyc generation and expression
VCA150	GCGGATCCTTATGG AGTATTGTAGAAG	BamHI	3' of TbHD52 ORF for *TbHD52*-OE generation and expression
VCA151	GCGGATCCAAGCTTC AAATTCGTCGAC TGCTGAAG	BamHI// HindIII	5'end for *TbHD82*-RNAi generation
VCA152	AACGGGCCCACCAAT AGGTTGGAATCGAG	ApaI	3'end for *TbHD82*-RNAi generation
VCA153	GCGGATCCAAGCTTC AAAATGTCGCA AACCATTG	BamHI// HindIII	5'end for *TbHD52*-RNAi generation
VCA154	AACGGGCCCACGGGA AAGGATAAAGCGAT	ApaI	3'end for *TbHD52*-RNAi generation
VCA171	CGCGGCCGCAACTGAGAG GGTGATTGGCG	NotI	5' end of TbHD82 5'UTR for *TbHD82*-dKO generation
VCA172	GCCTCGAGTCGTGTGATT TGCTAACGC	XhoI	3' end of TbHD82 5'UTR for *TbHD82*-dKO generation
VCA173	GCAGGCCTGTGCGCATGT ACGTTGTAGC	StuI	5' end of TbHD82 3' for *TbHD82*-dKO generation
VCA174	GGCTAGCGCGGC CGCCTATCGTCCAA GTGTTTCTA	NheI/NotI	3' end of TbHD82 3'UTR for *TbHD82*-dKO generation
VCA175	CATACTCGGTAGCAAA CCAGCAGCTCCCG	-	5' end of Tb427.6.2890 to check *TbHD82*-dKO cell line

VCA176	CACAACCTACACC GTCCATTGGCACATC	-	3' end of Tb427.6.2910 to check *TbHD82*-dKO cell line
VCA177	GCATTAATATGGAA GGGGAACTTGCCTTC	AseI	5' of TbHD82 ORF for *TbHD82*-OE and TbHD82-cmyc generation
VCA178c	GCGATATCGCGGCT GCGTTTATTTCCCGC	EcoRV	3' of TbHD82 ORF without STOP codon for *TbHD82*-cmyc generation
VCA180	GCGTTAACTGGAGTATTG TAGAAGGGGAG	HpaI	3' of TbHD52 ORF without STOP codon for *TbHD52*-cmyc generation
VCA191	GCCTAGATGAGAAAT GGAATTATCTGTCG	BfaI	5' of TbHD52 ORF for *TbHD52*-OE and TbHD52-cmyc generation
VCA202	CGCGGCCGCTGCAGG AACCGTGACTGGTAC	NotI	5' end of TbHD52 5'UTR for *TbHD52*-dKO generation
VCA203	GCCTCGAGGTCTGTTTAT GGACATTACGGAG	XhoI	3' end of TbHD52 5'UTR for *TbHD52*-dKO generation
VCA204	GCAGGCCTGTTCCACGCA AACTTTTTGG	StuI	5' end of TbHD52 3' for *TbHD52*-dKO generation
VCA205	GGCTAGCGCGGCCGC CAAAGGAAAAGGTGGTCCGTG	NheI/NotI	3' end of TbHD52 3'UTR for *TbHD52*-dKO generation
VCA206	GACGTGGCCATCCGT GAAGGAGCACTGC	-	5' end of Tb427.7.4820 to check *TbHD82*-dKO cell line
VCA207	CATGCTGTAATTCTGTGA GCCCTCGCTG	-	3' end of Tb427.7.4800 to check *TbHD82*-dKO cell line

Table C8. List of oligonucleotides employed in this work

C.1.7. Plasmids

Name	Vector	Size (bp)	Insert	Marker in *E. coli*	Marker in *T. brucei*	Use
pGRV23b +DCTD	pGRV23b [3]	5975	HsDCTD ORF	Amp	Pur	Generation of *TbHD52*-dKO/HsDCTD cell line
pGRV165	pGEM-T [4]	5226	TbHD82 ORF	Amp	-	Expression of TbHD82 with His-tag
pGRV166	pGEM-T [4]	4395	TbHD52 ORF	Amp	-	Expression of TbHD52 with His-tag
pGRV167	pET28a [5]	7550	TbHD82 ORF	Kan	-	Expression of TbHD82 with His-tag
pGRV168	pET28a [5]	6719	TbHD52 ORF	Kan	-	Expression of TbHD52 with His-tag
pGRV169	pGR19 [6]	7290	TbHD82 fragment	Amp	Hyg	Generation of *TbHD82*-RNAi cell line
pGRV170	pGRV19 [6]	7808	TbHD82 fragment	Amp	Hyg	Generation of *TbHD82*-RNAi cell line
pGRV171	pGR19 [6]	7376	TbHD52 fragment	Amp	Hyg	Generation of *TbHD52*-RNAi cell line
pGRV172	pGRV171	7980	TbHD52 fragment	Amp	Hyg	Generation of *TbHD52*-RNAi cell line
pGRV185	pGEM-T [4]	3514	TbHD82 5'UTR	Amp	-	Generation of *TbHD82*-dKO cell line
pGRV186	pGEM-T [4]	3365	TbHD82 3'UTR	Amp	-	Generation of *TbHD82*-dKO cell line
pGRV187	pHD887 [7]	4730	TbHD82 5'UTR, Bsd^R	Amp	-	Generation of *TbHD82*-dKO cell line
pGRV188	pHD887 [7]	4814	TbHD82 5'UTR, Bsd^R, 3'UTR	Amp	Bsd	Generation of *TbHD82*-dKO cell line
pGRV189	pGRV188	5397	TbHD82 5'UTR, Hyg^R, 3'UTR	Amp	Hyg	Generation of *TbHD82*-dKO cell line
pGRV190a	pGEM-T [4]	5226	TbHD82 ORF	Amp	-	Overexpression of TbHD82

pGRV190	pGRV23b [3]	7640	TbHD82 ORF	Amp	Pur	Overexpression of TbHD82
pGRV191a	pGEM-T [4]	5223	TbHD82 ORF without STOP codon	Amp	Pur	Expression of TbHD82 fused to cmyc
pGRV191	pGRV33 [8]	7682	TbHD82 ORF without STOP codon	Amp	Pur	Expression of TbHD82 fused to cmyc
pGRV192	pGRV23b [3]	5978	TbCDA ORF	Amp	Pur	Generation of *TbHD52*-dKO/TbCDA cell line
pGRV194a	pGEM-T [4]	4392	TbHD52 ORF without STOP codon	Amp	Pur	Expression of TbHD52 fused to cmyc
pGRV194	pGRV33 [8]	6851	TbHD52 ORF without STOP codon	Amp	Pur	Expression of TbHD52 fused to cmyc
pGRV197a	pGEM-T [4]	4393	TbHD52 ORF	Amp	Pur	Overexpression of TbHD52
pGRV197	pGRV23b [3]	6808	TbHD52 ORF	Amp	Pur	Overexpression of TbHD52
pGRV213a	pGEM-T [4]	3417	TbHD52 5'UTR	Amp	-	Generation of *TbHD52*-dKO cell line
pGRV214a	pGEM-T [4]	3240	TbHD52 3'UTR	Amp	-	Generation of *TbHD52*-dKO cell line
pGRV215	pHD887 [7]	4633	TbHD52 5'UTR, Bsd^R	Amp	Bsd	Generation of *TbHD52*-dKO cell line
pGRV216	pHD887 [7]	4592	TbHD52 5'UTR, Bsd^R, 3'UTR	Amp	Bsd	Generation of *TbHD52*-dKO cell line
pGRV217	pGRV216	5426	TbHD82 5'UTR, Hyg^R, 3'UTR	Amp	Hyg	Generation of *TbHD52*-dKO cell line

Table C9. List and principal components of the plasmids used in this thesis.

---

[3] (Castillo-Acosta *et al.* 2012b)
[4] Purchased from Promega
[5] Purchased from Novagen
[6] Kindly provided by Christine Clayton (Clayton *et al.* 2005)
[7] Kindly provided by Christine Clayton (Helfert *et al.* 2001)
[8] (Castillo-Acosta *et al.* 2012b)

C.1.8. Software and databases

C.1.8.1. Software

- *Adobe Photoshop*® *CS3* (version 10.0).

- *Biorender* ® *2019.*

- BLAST+® (Basic Local Alignment Search Tool, version 4) (Camacho *et al.* 2009).

- *CaryWin UV Software.*

- *Cell-R IX-81 Software.*

- *EndNote X2.*

- *FIJI/ImageJ* (version 1.4.3.67) (Schindelin *et al.* 2012).

- *FlowJo* (version 7.6).

- *Gene Construction kit*® version 1.03.1.

- *GraphPad Prism 8 Software.*

- *Huygens Essential software* (version 3.3).

- *IBM SPSS*® *Statistics* (versión 25).

- *Imaris software.*

-INTERPRO (Interpro protein sequence analysis & classification, version 11.0) (Mitchell *et al.* 2019).

-*JACOP ImageJ plugin* (Just Another Colocalization Plugin, version 2.1.1) (Bolte and Cordelieres 2006).

- *Jalview Desktop.*

- *Microsoft Office 2007 and 2010 (Microsoft Word, Microsoft Excel y Microsoft Power Point).*

- *Mozilla Firefox.*

- *Oligonucleotide Properties Calculator*, Northwestern University Medical School.

-PANTHER$^®$ (Protein ANalysis THrough Evolutionary Relationships, version 14.1) (Mi *et al.* 2019).

-SMART (Simple Modular Architecture Research Tool, version 8.0) (Letunic and Bork 2018).

C.1.8.2. Databases

- *EMBL-EBI* (http://www.ebi.ac.uk/).

- *KEGG Pathway Maps* (http://www.genome.jp/kegg/kegg3a.html/).

- *NCBI* (https://www.ncbi.nlm.nih.gov/).

- *PDB (Protein Data Bank)* (http://www.rcsb.org/pdb/home/home.do/).

- *TriTrypDB* (http://tritrypdb.org/tritrypdb/).

- *TrypTag* (http://tryptag.org/).

- *UniProt (Universal Protein Resource)* (http://www.uniprot.org/).

C.1.9. Statistical analysis

The Student's t-test was used for comparison of sets of data, based on the mean and standard deviation (S.D.) of at least three independent experiments. Variances of normally distributed data were analyzed with two-way ANOVA and Dunnett's *post-hoc* tests. Kolmogorov-Smirnov and Shapiro-Wilk tests were applied to verify data normality, and equality of variances was analyzed with Levene's test. If one of those tests failed, Welch's two-sample t-test was used. Statistics were calculated with either *GraphPad Prism* software or *IBM SPSS$^®$ Statistic*, and a *p* value ≤0.05 was considered statistically significant.

C.2. Methods

C.2.1. Trypanosome culture

C.2.1.1. Maintenance of trypanosomes and growth studies

The studies and generation of transgenic cell lines were performed in the *T. brucei* single-marker BSF and PCF. The BSF trypanosomes were cultured in HMI-9 supplemented with 10% (v/v) FBS at 37ºC and 5% CO_2, whereas PCF parasites were maintained in SDM-79 supplemented with 10% (v/v) FBS at 28ºC with no air exchange. The maintenance, as well as evaluation of cell proliferation, were accomplished with trypanosomes in logarithmic phase, so the cultures were generally diluted at $2 \cdot 10^5$ parasites/ml or $5 \cdot 10^3$ parasites/ml, for PCF or BSF parasites, respectively, in fresh media every 48 hours. Cell density was determined by counting trypanosomes with a Z2 Coulter Counter® (Beckman).

For the assays performed under dThd deprivation, the cultures were previously washed three times with HMI-9 pyrimidine-free media to remove any pre-existing dThd content.

C.2.1.2. Stable transfection of T. brucei by electroporation

Efficient transfection in *T. brucei* can be accomplished by the integration of a linearized-plasmid into the rDNA spacer region, which is non-subjected to transcription. Another frequent strategy is the recombination of a DNA sequence in the trypanosomal genome. Briefly, both approaches first required *E. coli* XL1-Blue strains transformation with the target plasmids, and plasmid DNA isolation with the NucleoSpin® Plasmid kit (Macherey-Nagel). Subsequently, plasmids were digested with the corresponding

restriction enzymes, ethanol-precipitated and resuspended at 1 mg/ml in sterile H_2O. In the specific case of DNA fragments aimed to be recombined, prior to the ethanol-precipitation step, the insert was purified from an agarose gel using the NucleoSpin® Gel and PCR Clean-up kit (Macherey-Nagel). Transfected cell lines were then obtained following electroporation protocols previously described (Wirtz *et al.* 1999).

For transfection of *T. brucei* BSF, $2.4 \cdot 10^7$ parasites were collected by centrifugation, washed twice with Cytomix buffer (Table C4) at room temperature (RT) and mixed with 10 μg of linearized DNA in a total volume of 400 μl. Transfection was performed by electroporation using a BTX ECM 630 electroporator at 1.7 kV, 25 μF and 25 Ω. After pulse, the cells were diluted in 12 ml of fresh media and uniformly distributed in a 24-well plate. Parasites were left to recover at 37ºC and 5% CO_2 for 18 h before the addition of 1 ml of fresh media with the corresponding drug used as selectable marker. For the generation of *TbHD52*-dKO and derivative cell lines, the culture media was always supplemented with 0.6 mM dThd.

For transfection of *T. brucei* PCF, $2 \cdot 10^7$ parasites were harvested at 4ºC and washed twice with cold ZPFM medium (Table C4). Parasites were mixed with 10 μg of linearized DNA in a total volume of 500 μl, and after incubation in ice for 5 min, electroporation was carried out at 1.6 kV, 25 μF and 25 Ω. Cells were then transferred to a culture flask in 12 ml of fresh media and allowed to recover overnight at 28ºC. Finally, the culture was distributed along the upper row of two 24-well plates and was dispensed in a 1:2 serial dilution across the columns in 0.5 ml of fresh media with the corresponding drug used as selectable marker. *TbHD52*-dKO and derivative cell lines were also supplemented with 0.6 mM dThd.

C.2.1.3. Generation of transgenic cell lines

The general information about the cell lines generated in this thesis, as well as the parental parasites (BSF or PCF) and selectable markers used for each case, are described in Table C2. The procedure is briefly reported in the following subsections and the information about all oligonucleotides and plasmids produced are listed in Table C8 and Table C9, respectively.

C.2.1.3.1. Generation of *TbHD82* and *TbHD52* knock-out cell lines

In order to completely eliminate the expression of TbHD82 and TbHD52, allelic replacement by recombination was accomplished. Allele replacement was achieved by the sequential transfection of two gene cassettes containing the *BSD* or *HYG* resistance markers, flanked by a region of the 5'- and 3'-UTR (untranslated region) sequences of *TbHD82* and *TbHD52*. Thus, the 5' and 3'-UTR fragments of the regions flanking the open reading frame (ORF) of both genes were amplified by polymerase chain reaction (PCR) using wild type *T. brucei* 427 genomic DNA. For the amplification of the 5'- and 3'-UTRs from *TbHD82*, VCA171-VCA172 and VCA173-VCA174 oligonucleotides were respectively used. On the other hand, the amplification of the 5' and 3'UTRs from *TbHD52* was performed with VCA202-VCA203 and VCA204-VCA205 oligonucleotides, respectively. The resulting sequences were then cloned in a pGEM-T plasmid (Promega), resulting in pGRV185 and pGRV186 plasmids, in the case of *TbHD82*, and pGRV213a and pGRV214a plasmids for *TbHD52*. The inserts were then released by enzymatic digestion and cloned flanking the *BSD* resistance gene in the pHD887 plasmid (Helfert *et al.* 2001). As a result, pGRV188 and pGRV216 constructs were originated for *TbHD82* and *TbHD52*, respectively. After isolation and purification of the cassette, the parental cell line was transfected, leading to a single-KO cell line.

The second cassette was generated through replacement of the *BSD* marker gene with the *HYG* resistance gene coming from SnaBI-digested pGRV28. The yielding constructs, pGRV189 for *TbHD82* and pGRV217 for *TbHD52*, were finally employed for null-mutants generation.

C.2.1.3.2. Generation of TbHD82 and TbHD52-RNAi cell lines

To down-regulate the expression of the *TbHD82* and *TbHD52* transcripts, the interference RNA (RNAi) stem-loop strategy was used. To this purpose, a fragment from the corresponding coding sequences was cloned twice into the pGR19 vector (Clayton *et al.* 2005), with the inverted sequences separated by the stuffer region, which enables the stem-loop structure. The DNA sequences selected for gene silencing corresponded to the 1135-1640 bp fragment of *TbHD82* ORF and 387-978 bp fragment of *TbHD52* ORF. These sequences were amplified by PCR from *T. brucei* 427 genomic DNA, using Pwo DNA polymerase (Roche) and the specific primers: VCA151-VCA152 for *TbHD82*, and VCA153-VCA154 for *TbHD52*. Subsequently, PCR products were first digested with HindIII and ApaI restriction enzymes and cloned into pGR19, yielding pGRV169 (*TbHD82*) and pGRV171 (*TbHD52*) plasmids. The cloning of the second fragment in opposite sense was introduced by digestion with BamHI and HpaI restriction enzymes. The resulting plasmids, pGRV170 (*TbHD82*) and pGRV172 (*TbHD52*), were linearized with NotI enzyme for further transfection of parental cell lines, obtaining this way both the *Tb* HD82-RNAi and *Tb* HD52-RNAi cell lines.

C.2.1.3.3. Generation of TbHD82 and TbHD52-cmyc and overexpressing cell lines

In order to perform the localization analysis, cell lines overexpressing TbHD82 or TbHD52, either native or c-myc-fused proteins, were generated. For this purpose, the coding sequences of both proteins were amplified by PCR using *T. brucei* 427 genomic DNA as template with specific primers: VCA177-VCA148 and VCA191-VCA150 for TbHD82 and TbHD52 native proteins, respectively. For the c-myc fusion protein overexpression, 3' end oligonucleotides lacking a stop codon were designed and used to amplify the *TbHD82* (VCA177 and VCA178c) and *TbHD52* (VCA149 and VCA180) ORF sequences. PCR products were cloned in pGEM-T (Promega), yielding pGRV191a, pGRV194a, pGRV190a and pGRV197a plasmids. Subsequently, the native sequences were digested and the inserts were subcloned in pGRV23b, resulting in the pGRV190 and pGRV197 constructs for TbHD82 and TbHD52 overexpression, respectively. For the c-myc fused forms, the sequences were subcloned in pGRV33 plasmid (Castillo-Acosta *et al.* 2012b) containing the carboxy-terminal tag with SKGKVNEE<u>QKLISEEDL</u>* additional amino acid sequence (c-myc sequence is underlined, asterisk indicates stop codon). Hence, the pGRV191 and pGRV194 plasmids were generated for the expression of TbHD82 and TbHD52 fused to c-myc, respectively. All plasmids were linearized with NotI restriction enzyme for further transfection of parental cell lines and *TbHD52*-null mutants, yet the TbHD52-deficient cells were only transfected with the native TbHD52 protein. The expression from the resulting plasmids is regulated by a tetracycline-inducible *parp* promoter allowing protein expression after Dox addition, and puromycin was used as selectable drug.

C.2.1.3.4. Overexpression of HsDCTD and TbCDA in the *TbHD52*-dKO cell line

Overexpression of TbCDA and HsDCTD in the *TbHD52*-dKO cell line was obtained by transfection with the pGRV192 and pGRV23b+DCTD plasmids, respectively, which had been previously generated in the lab (Moro-Bulnes *et al.* 2019). As aforementioned in the previous section, both plasmids were linearized with NotI prior to *TbHD52*-dKO transfection. The expression of these plasmids is also regulated by a tetracycline-inducible *parp* promoter, and puromycin was used as selectable drug.

C.2.2. Immunological assays

C.2.2.1. Protein extraction and western blot analysis

The protein extract was obtained from $5 \cdot 10^6$ parasites per sample from a logarithmic phase culture. Trypanosomes were collected at 1,400 x *g* for 10 min, washed once with PBS 1x and resuspended in urea-cracking buffer (Table C4). The cell suspension was lysed by vortexing and, after addition of sample buffer (Table C4), the proteins were denatured by incubation at 99ºC for 5 min.

Whole cell extracts were separated based on their molecular weight by SDS-PAGE electrophoresis. The electrophoresis was performed in running buffer (Table C4) at 200 V for 45-60 min in 8-12% polyacrylamide gel, according to the protein. The proteins were then transferred to a polyvinylidene difluoride membrane (PVDF, GE Healthcare), previously activated with methanol, using the *Mini Trans-Blot*® *Electrophoretic Transfer Cell* (Bio-Rad) at 100 V for 45 min in transfer buffer (Table C4). In order to label the markers and confirm efficient transfer, the membrane was stained with Ponceau-S red for 1 min, followed by washing with PBS-Tween 20 0.1%. The membrane was then blocked for 30 min in blocking solution

(PBS-Tween 20 0.1%, milk 5%) at RT, probed with primary antibodies diluted in blocking solution overnight at 4ºC, revealed by using secondary antibodies in blocking solution for 1 hour at RT, and detected with the Amersham® ECL Select® reagents (GE Healthcare) and Amersham® Hyperfilm® ECL (GE Healthcare).

C.2.2.2. Antibody generation and purification

For antibody generation, TbHD82 and TbHD52 were first expressed and purified fused to a His-tag. To this purpose, the coding sequences of both proteins were amplified by PCR using *T. brucei* 427 genomic DNA as template. The specific primers used were VCA147-VCA148 and VCA149-VCA150 (Table C8) for TbHD82 and TbHD52, respectively. PCR products were cloned in pGEM-T (Promega), resulting in pGRV165 (TbHD82) and pGRV166 (TbHD52) plasmids (Table C9), and subsequently, the sequences were digested and subcloned in the expression vector, pET28a (Novagen), yielding pGRV167 (TbHD82) and pGRV168 (TbHD52) (Table C9). *E. coli* BL21(DE3) strains were then transformed and protein expression was induced by adding 1 mM isopropyl-β-D-thiogalactopyranoside (IPTG) when an OD_{600} of 0.6 was reached, and incubated for 4 h at 37ºC.

For purification, the bacterial pellet was lysed in 50 ml of binding buffer (Table C4) at 4ºC by sonication 4 times for 40 s. The whole cell extract was incubated for 1 h with *NiSepharose® High Performance affinity media* (GE Healthcare), a nickel-charged immobilized metal ion-affinity chromatography resin, following a batch procedure. Prior to the elution step, the resin was equilibrated and washed twice with Wash buffer (Table C4) to remove unspecific binding. Consecutive elution steps were performed at high imidazole concentrations (Elution buffer, Table C4), resulting in

7 sample fractions. The fractions were quantified by Bradford and analyzed by SDS-PAGE. For further purification of the pooled fractions, large SDS-PAGE was carried out with the *Protean® II Xi Cell System* (Bio-Rad) using 10% polyacrylamide gels at 70 mA for 4.5 h. Selected bands were isolated from the gel by electroelution using the *Electro-Eluter 422* (Bio-Rad) at 30 mA for 5.5 hours. The fractions were quantified again by Bradford and verification of the protein purity was accomplished both by SDS-PAGE (Fig. C1) and Peptide Mass-Fingerprint (MALDI-TOF) analysis.
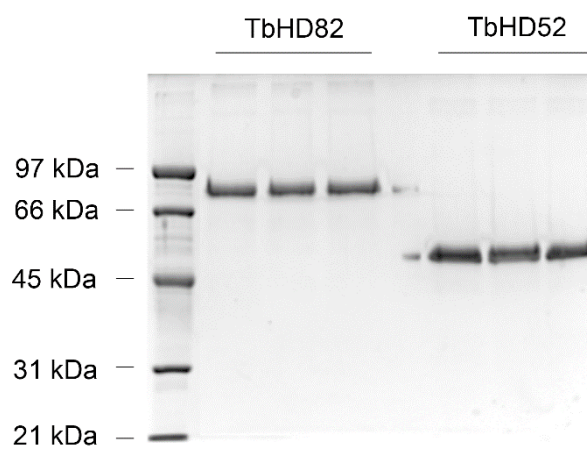
Figure C1. Determination of TbHD82 and TbHD52 purity by SDS-PAGE. Purified fractions of each protein, TbHD82 and TbHD52, were validated by SDS-PAGE (TbHD82-HisTag, 84.2 kDa and TbHD52-HisTag, 54.6 kDa).

Denatured and purified recombinant proteins were used to immunize a rabbit for the generation of polyclonal anti-TbHD82 and anti-TbHD52 antibodies. Approximately 200 μg of each protein were used in each inoculation, which were resuspended in sterile PBS and mixed with complete Freund's adjuvant (Sigma-Aldrich) in the first injection or with incomplete Freund's adjuvant (Sigma-Aldrich) for the three remaining inoculations, at 1:1 ratio. One month later after the fourth injection, rabbits were sacrificed and serum containing anti-TbHD82 and anti-TbHD52 antibodies was separated from blood. Next, antibodies were purified by affinity chromatography using

0.5 mg of the pure recombinant protein coupled to Affi-Gel® 10 resin (Bio-Rad) and Poly-Prep® Chromatography Columns (Bio-Rad), according to the manufacturers' instructions (the composition of the solutions employed are specified in Table C4). The specificity of the antibodies was validated by the incubation of antibodies with the corresponding antigen in 10-fold excess overnight and visualization by SDS-PAGE (Fig. C2).
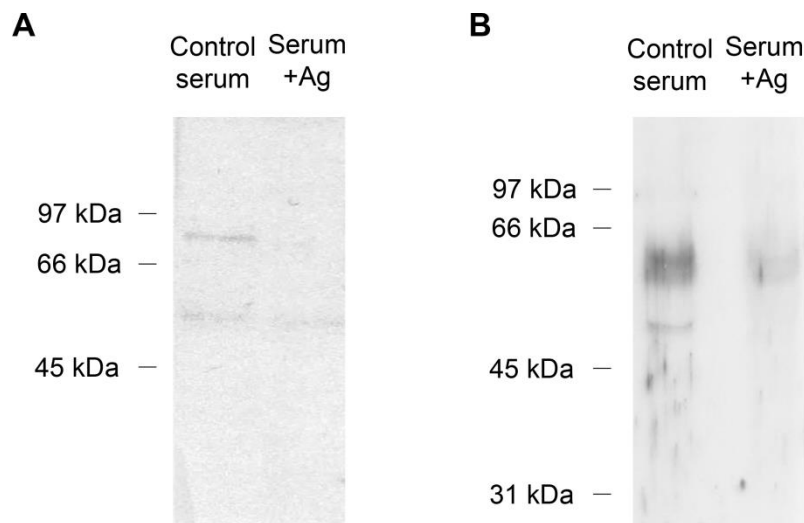
Figure C2. Evaluation of anti-TbHD82 and anti-TbHD52 antibody specificity. Western blot analysis of purified anti-TbHD82 (A) and anti-TbHD52 (B) antibodies. Protein samples from $5 \cdot 10^6$ trypanosomes were used per well and incubated overnight with "Control serum", which corresponds to the 1:10,000 diluted antibody for each case, or "Serum +Ag", which is the saturated serum with an excess of antigen (TbHD82, 81.73 kDa and TbHD52, 52.2 kDa).

C2.2.3. Immunofluorescence studies

Immunofluorescence studies were carried out using anti-TbHD82, anti-TbHD52 and anti-c-myc antibodies in order to determine the intracellular localization. The anti-γH2A antibody was used for quantification of DNA damage.

For colocalization analysis, $5 \cdot 10^6$ parasites were incubated with MitoTracker® Red (ThermoFisher Scientific) for 15 min in 1 ml of culture medium without FBS. After

recovery in fresh culture medium without FBS, the culture was washed twice with PBS. In the case of DNA damage determination, $5 \cdot 10^6$ parasites were directly washed twice with TDB-Glucose (Table C4). Afterwards, in both cases, $1 \cdot 10^6$ parasites per sample were fixed at RT for 20 min with 4% *p*-formaldehyde (PFA) prepared in PBS, and mounted in a poly-L-lysine coated slide. Next, the samples were washed twice with PBS-Tween 20 0.2% and blocked and permeabilized for 75 min at RT with 1% NP-40 in blocking solution (1% Blocking Reagent from Roche). Preparations were then incubated with the corresponding primary antibody diluted in blocking solution for 1 h at RT, washed six times with PBS-Tween 20 0.2% of 5 min each one and probed with the secondary antibody in blocking solution for 1 h at RT. After washing, coverslips were then dehydrated in methanol for 1 min and stained with *ProLong* Gold Antifade Mountant with DAPI (Invitrogen). Finally, vertical stacks of 30 - 40 slices (0.2 μm steps) were captured using an Olympus microscope and Cell R IX81 software. Deconvolution and pseudo-colouring was performed using Huygens Essential software (version 3.3; Scientific Volume Imaging) and Fiji software (version 1.5e; ImageJ), whereas colocalization analysis was carried out using JACoP plugin. Images for γH2A foci counting were obtained using Zeiss Axio Imager A1 microscope and analysed with Fiji software (version 1.5e; ImageJ) following the Duke University Light Microscopy Core Facility protocol (microscopy.duke.edu).

C.2.3. Procedures used in the characterization of nucleotidases

C.2.3.1. Fluorescence activated cell sorting (FACS) analysis

Flow cytometry studies were used to evaluate the effects of the lack of TbHD52 on the cell cycle, DNA damage and kinetoplast integrity. In all cases, fluorescence was monitored by FACS in a Becton Dickinson FACSAria III using BD CellQuest[®] Pro version 4.0.2 software and analysis were performed with FlowJo[®] software (Tree Star Inc).

For cell cycle studies, parental and TbHD52-deficient cell lines were cultured in the presence or absence of 0.6 mM dThd for 24 h (BSFs) or 10 days (PCFs). Cells (10^7 trypanosomes per sample) were washed twice in PBS and fixed overnight at -20ºC with 70% ice-cold ethanol prepared in PBS. Samples were finally washed in PBS and stained at 37ºC for 30 min with 40 µg/ml of propidium iodide (PI) (Sigma-Aldrich) prepared in PBS containing 10 µg/ml of RNAse A (Sigma-Aldrich).

In the case of DNA damage measurement, $5 \cdot 10^7$ parasites were fixed in a suspension of 4% PFA diluted in TDB-Glucose (Table C4) for 2.5 h. Cells were then incubated 15 min in 0.1 M Na_2HPO_4/1M glycine (pH 7.2) solution and permeabilized with 2% NP-40 for 1 h. Finally, DNA damage was established by probing with the anti-TbγH2A antibody and labelling with secondary antibodies for 1 h per incubation at RT.

Dihydroethidium (DHE) staining of living cells was used to analyze the kDNA content. To this purpose, $5 \cdot 10^6$ parasites were collected and incubated with 10 µg/ml DHE (Sigma-Aldrich) for 10 min at RT, and washed twice with Cytomix (Table C4) prior to FACS analysis.

C.2.3.2. Morphological phenotypic evaluation

Additional information about cell cycle progression was obtained from the nuclei and kinetoplast content of TbHD52-null mutants as revealed by DAPI staining and fluorescence microscopy. For the morphological phenotypic analysis, $1 \cdot 10^6$ parasites were washed twice with TDB-Glucose (Table C4) and fixed in 4% PFA for 20 min on a poly-L-lysine. The samples were then washed twice with PBS-Tween 20 0.2% and stained with *ProLong* Gold Antifade Mountant with DAPI (Invitrogen). Digital images were acquired with a Zeiss Axio Imager A1 microscope and evaluated with Fiji software (version 1.5e; ImageJ). The subsequent analysis was performed by categorization of different populations according to the number of nuclei and kinetoplasts in individual cells from three independent experiments (>300 cells in total).

C.2.3.3. Measurement of intracellular nucleotides

The four canonical dNTPs (dTTP, dCTP, dATP and dGTP) were quantified using a modified DNA polymerase assay (Sherman and Fyfe 1989) in BSF parental and *HD52*-dKO cell lines cultured under dThd starvation for 24 h. The DNA polymerase assay is based on the incorporation of dATP or dTTP labelled with tritium (^{3}H) in oligonucleotides with a defined sequence. A shared template (P255, see Table C8) is employed for the determination of all nucleotides, in combination with specific templates (P256 for dCTP, P257 for dTTP, P258 for dGTP and Pol dATP for dATP, see Table C8) depending on the quantified dNTP. As the ^{3}H-labelled nucleotide is added in excess, the radioactivity incorporated during DNA synthesis is proportional to the nucleotides present in the cell extract. Briefly, $2 \cdot 10^6$ parasites per sample were

harvested by centrifugation, washed once in PBS and intracellular dNTPs were extracted by incubation in 250 µL of cold 60% methanol overnight at −20 °C. Next, samples were denatured by boiling in a water-bath for 5 min, centrifuged for 20 min at 17,000 x *g*, and the supernatant was transferred to a fresh tube and vaccum-dried. In order to eliminate dUTP interference, in the case of dTTP determination, the residue was dissolved in 40 µl of dUTPase buffer (Table C4) with 30 ng of human dUTPase and incubated for 20 min at 37 °C. The reaction was stopped by the addition of 60 µl of 100% methanol and incubation for 1 hour at −20°C, followed by centrifugation for 20 min at 17,000 x *g* allowed to remove the protein fraction. After another step of vaccum-dry, residues were dissolved in 100 µl of reaction mixture in DNA Polymerase buffer (Table C4) containing 32 nM DNA template, 32 nM DNA primer, NEBuffer 2 (New England BioLabs), 0.3 units of DNA polymerase I Klenow fragment (New England Biolabs) and 0.0032 µCi/µl [^{3}H]dATP (Moravek) (for dTTP, dCTP and dGTP measurements) or [^{3}H]dTTP (PerkinElmer) (for dATP determination). For quantification of dCTP, dGTP or dATP, the samples were directly resuspended in the described mixture after the first vacuum-drying, and the protocol continued for all determinations as follows. Samples were incubated for 15 min at 25°C, followed by addition of 10 mM EDTA and heating at 75°C for 20 minutes to stop the reaction. DNA was finally precipitated with 10% (v/v) TCA (see Precipitation buffer, Table C4) for 30 min at 4°C. The solution was blotted on Glass Microfibre Filters GF/C (Whatman) and each filter was washed under vacuum with 30 ml of 5% TCA, rinsed with 3 ml of ethanol, dried and the radioactivity was measured in a LS 6500 Multi-Purpose Scintillation counter (Beckman Coulter). Individual data results from interpolation in standard curves.

C.2.3.4. Metabolomics

The metabolomics analysis was conducted by Metabolon, Inc., in HD52-null and BSF parental parasites subjected to dThd deprivation for 24 h. Briefly, four independent biological replicates of $1 \cdot 10^9$ parasites were collected and washed with fresh medium without FBS at 4ºC, and the cellular pellet was flash-frozen in liquid nitrogen. The samples were transported to Metabolon, Inc., which determined 565 metabolites by several mass spectrometry methods, including two separated reverse phase (RP)/UPLC-MS/MS methods with positive ion mode electrospray ionization (ESI), RP/UPLC-MS/MS with negative ion mode ESI and HILIC/UPLC-MS/MS with negative ion mode ESI.

C.2.4. Methods employed for *in vivo* DNA damage studies

C.2.4.1. Animal studies and parasite isolation

Four female C57BL/6J mice per group (6-8 weeks old) were housed under conventional conditions, given water and chow *ad libitum*, and infected via intraperitoneal injection with 4,800 monomorphic *T. brucei* parasites of either BSF parental, *UNG*-KO or *UNG*-KO/OE cell lines. Dox (1 mg/ml, Sigma-Aldrich) or 2.5% AG (Sigma-Aldrich) were administered, protected from light, and refreshed every 48 h in the drinking water. Dox was only provided to the murine group infected with *UNG*-KO/OE trypanosomes in order to induce UNG overexpression. Parasitaemia was daily monitored by dilution 1:1,000 of 1 μl tail blood in TDB-Glucose and counting in a haemocytometer chamber.

In order to isolate trypanosomes, blood of infected mice at day 5 or 10 *post-infection* was collected in 1.3 ml K3E microtubes (Sarstedt), to avoid sample

coagulation, and parasites were isolated from the buffy-coat interphase by centrifugation at 5,000 x *g* for 5 min. To remove residual blood components, parasites were further purified and eluted in SB-Glucose (Table C4) by anion exchange chromatography using a DEAE-cellulose column (Whatman Chromedia, DE-52) (Lanham 1968).

C.2.4.2. Pfu sensitive sites determination

Different processivity exhibited by different DNA polymerases is a property exploitable in the determination of the uracil content as well as of other lesions present in genomic DNA. Thus, product formation obtained by *Pyrococcus furiosus* (Pfu) and *Thermus aquaticus* (Taq) DNA polymerases was proportional to the amount of Pfu sensitive sites, mainly as result of the presence of uracil and AP sites. The methodology provides a relative quantification with respect to the control, which is considered as a Pfu sensitive site-free sample.

First, genomic DNA was isolated from parasites, either cultured *in vitro* or from murine infection, by phenol/chloroform extraction. Briefly, $1 \cdot 10^8$ cells were harvested, washed twice with PBS and incubated overnight in lysis buffer at RT (Table C4). After phenol-chloroform extraction and DNA ethanol-precipitation, samples were incubated in TE buffer (Table C4) with 10 μg/ml RNase (Sigma-Aldrich) overnight. After a new step of phenol/chloroform extraction and ethanol-precipitation, DNA was finally purified and resuspended in H_2O. Pure genomic DNA was then digested with XhoI-HF (NE Biolabs) at 37ºC overnight and 4.3–6.5 kb fragments containing the *myosin* gene were extracted and purified from a 0.8% agarose gel using Illustra® GFX® PCR DNA and Gel Band Purification Kit (GE Healthcare). Two-fold dilution series of the DNA

samples were then amplified with Pfu Turbo Hotstart (Agilent Technologies) or Taq Polymerase (Bioline). Real-time quantitative PCR (RT-qPCR) was carried out in the CFX96® Real-time System C1000 Thermal Cycler (Bio-Rad Laboratories) using TbMyo1 and TbMyo2 oligonucleotides (Table C8) and the following reaction conditions: initial step at 95°C for 2 min, 40 cycles with 95°C for 15 s, 58°C for 20 s, 72°C for 1 min 10 s and a final cycle at 95°C for 1 min. The melting curve program consisted of temperatures between 55°C and 95°C with a heating rate of 0.2°C/s and a continuous fluorescence measurement. Resulting Cq values were associated to Pfu sensitive sites according to equations previously described (Horvath and Vertessy 2010) referred to a control sample.

C.2.4.3. AP sites

Genomic DNA was isolated from $3 \cdot 10^7$ parasites, either cultured *in vitro* or from murine infection, by using DNAzol Reagent (Invitrogen), according to the manufacturer's instructions. DNA samples were first diluted at 100 µg/ml in H_2O and were then analyzed with the OxySelect® Oxidative Damage Quantitation Kit (AP sites) (Cell Biolabs) following the manufacturer's instructions. This method derivatizes DNA samples with a biotin tag containing an aldehyde reactive probe (ARP) that specifically reacts with the aldehyde group located on the open ring form of AP sites. The probe is detected with a streptavidin-enzyme conjugate by spectrophotometry based on the values of a standard curve. Absorbance was quantified with an Infinite® F200 Fluorescence Microplate Reader (TECAN) and each biological replicate was assayed in duplicate.

C.2.4.4. NO determination

During AG treatment, and in order to confirm the efficient iNOS inhibition, every day *post-infection* blood samples were obtained by cardiac puncture from each group to compare concentration of NO derivatives in plasma. Briefly, blood of infected mice was harvested in 1.3 ml K3E microtubes (Sarstedt) and plasma was collected by centrifugation at 5,000 x g for 5 min. To reduce hemoglobin (64 kDa) background absorbance, plasma samples were ultrafiltered through a NanoSep® Centrifugal device with 10-kDa Omega® membrane (PALL) pre-equilibrated with H_2O. NO derivatives were measured by the Griess method using the Nitrate/Nitrite Colorimetric Assay (Cayman Chemical) as indicated by the manufacturer's instructions. Absorbance was quantified with Infinite® F200 Fluorescence Microplate Reader (TECAN) and each biological replicate was assayed in duplicate.

RESULTS

D. RESULTS

D.1. CHARACTERIZATION OF *Hs*SAMHD1 ORTHOLOGUES IN *Trypanosoma brucei*

D.1.1. Identification of *Hs*SAMHD1 orthologues in *Trypanosoma brucei*

In order to identify enzymes that could have a similar role to *Hs*SAMHD1 in *T. brucei*, a bioinformatics analysis was performed using PANTHER (Protein ANalysis THrough Evolutionary Relationships). *Hs*SAMHD1 belongs to the SAM domain and HD domain-containing protein-related family (PTHR11373), for which the analysis identified a total of 193 genes (Fig. D1). Within this family, two members were *T. brucei* proteins that correspond to Tb927.6.2900 and Tb927.7.4810 genes (TriTrypDB Kinetoplastid Genomics Resource). Tb927.6.2900 gene encodes a 735 amino acid protein with an estimated molecular mass of 81.734 Da (Universal Protein Resource, UniProtKB, protein ID Q583P4) and belongs to the deoxynucleoside triphosphate triphosphohydrolase subfamily (PTHR11373:SF4) that also includes *Hs*SAMHD1 (Fig. D1). On the other hand, Tb927.7.4810 encodes a protein of 458 amino acids with an estimated molecular mass of 52.176 Da (UniProtKB protein ID Q57X97), and appears as a member of a kinetoplastid-specific subfamily named PTHR11373:SF33. The analysis also identified a *L. major friedlin* orthologue (LMJF_06_0160) (Fig. 1D) as member of this subfamily and the further identification of the *T. cruzi* orthologue (TcCLB.508579.10) was accomplished by sequence similarity analysis (BLAST). Both Tb927.6.2900 and Tb927.7.4810 were named according to their molecular mass as TbHD82 and TbHD52, respectively.

Family ID	Family Name	Number of genes
PTHR11373	SAM DOMAIN AND HD DOMAIN-CONTAINING PROTEIN-RELATED	193
PTHR11373:SF4	Deoxynucleoside triphosphate triphosphohydrolase	150
PTHR11373:SF32	Subfamily not named	10
PTHR11373:SF25	Subfamily not named	9
PTHR11373:SF35	Subfamily not named	8
PTHR11373:SF26	Subfamily not named	5
PTHR11373:SF34	Subfamily not named	5
PTHR11373:SF29	Deoxyguanosinetriphosphate triphosphohydrolase	4
PTHR11373:SF33	Subfamily not named	2

NG_017059.1 (HsSAMHD1)
Tb927.6.2900 (**TbHD82**)

LMJF_06_0160
Tb927.7.4810 (**TbHD52**)

Figure D1. Identification of *T. brucei* genes in the SAM domain and HD domain-containing protein-related family. Description of the subfamilies and number of genes that belong to the SAM domain and HD domain-containing protein-related family (PTHR11373) according to PANTHER. HsSAMHD1 as well as the two putative orthologues in *T. brucei* and the orthologue in *L. major* are highlighted.

To further predict the putative catalytic domains of these enzymes, the amino acidic sequences of HsSAMHD1, TbHD82 and TbHD52 were introduced in SMART (Simple Modular Architecture Research Tool) and InterPro (Interpro protein sequence analysis & classification) software packages, which identified an HD domain in all the proteins analysed (Fig. D2). The tools used identified an HD domain in the HsSAMHD1 between the 160 and 325 residues, though it has been already reported that the catalytic core of the protein embraces up to residue 599 of the protein (Ji *et al.* 2013; Zhu *et al.* 2013; Ahn 2016). The HD domain is characteristic of metalloenzymes with phosphohydrolase activity, and is characterized by the presence of motifs with histidine and aspartate doublets that act as metal-chelating residues (Aravind and Koonin 1998).

However, the analysis revealed that a canonical SAM domain, involved in protein-protein and protein-RNA interactions (Kim and Bowie 2003; Qiao and Bowie 2005), is absent in the trypanosomal proteins (Fig. D2). Several studies have shown that the SAM domain is not required for oligomerization and thereby for its enzymatic activity (White *et al.* 2012; Yan *et al.* 2013; Seamon *et al.* 2015). In fact, it has been reported that the human HD domain *per se* possesses higher activity than the full-length protein (Buzovetsky *et al.* 2018).

Figure D2. TbHD82 and TbHD52 sequences present an HD domain. Prediction of the conserved domains of HsSAMHD1, TbHD82 and TbHD52 by SMART software. Both SAM and HD domains are illustrated within the amino acid sequences of the proteins.

Both sequences were aligned with orthologues characterized from different eukaryotic and prokaryotic species using ClustalOmega (Goujon *et al.* 2010; Sievers *et al.* 2011; McWilliam *et al.* 2013). The alignment was visualized in JalView with the colour scheme from Clustal. The selected proteins were SAMHD1 from *H. sapiens* and *M. musculus,* and in order to take into account a prokaryotic protein in the analysis, due to the absence of SAMHD1 in these organisms, we also included *E. faecalis* EF1143 protein. It is a well-characterized dNTPase, considered as a prokaryotic homologue of HsSAMHD1 because of its structural and functional similarities, as it hydrolyses dCTP

and dATP in the presence of Mg^{2+} using dGTP as an effector (Vorontsov *et al.* 2011; Mauney and Hollis 2018).
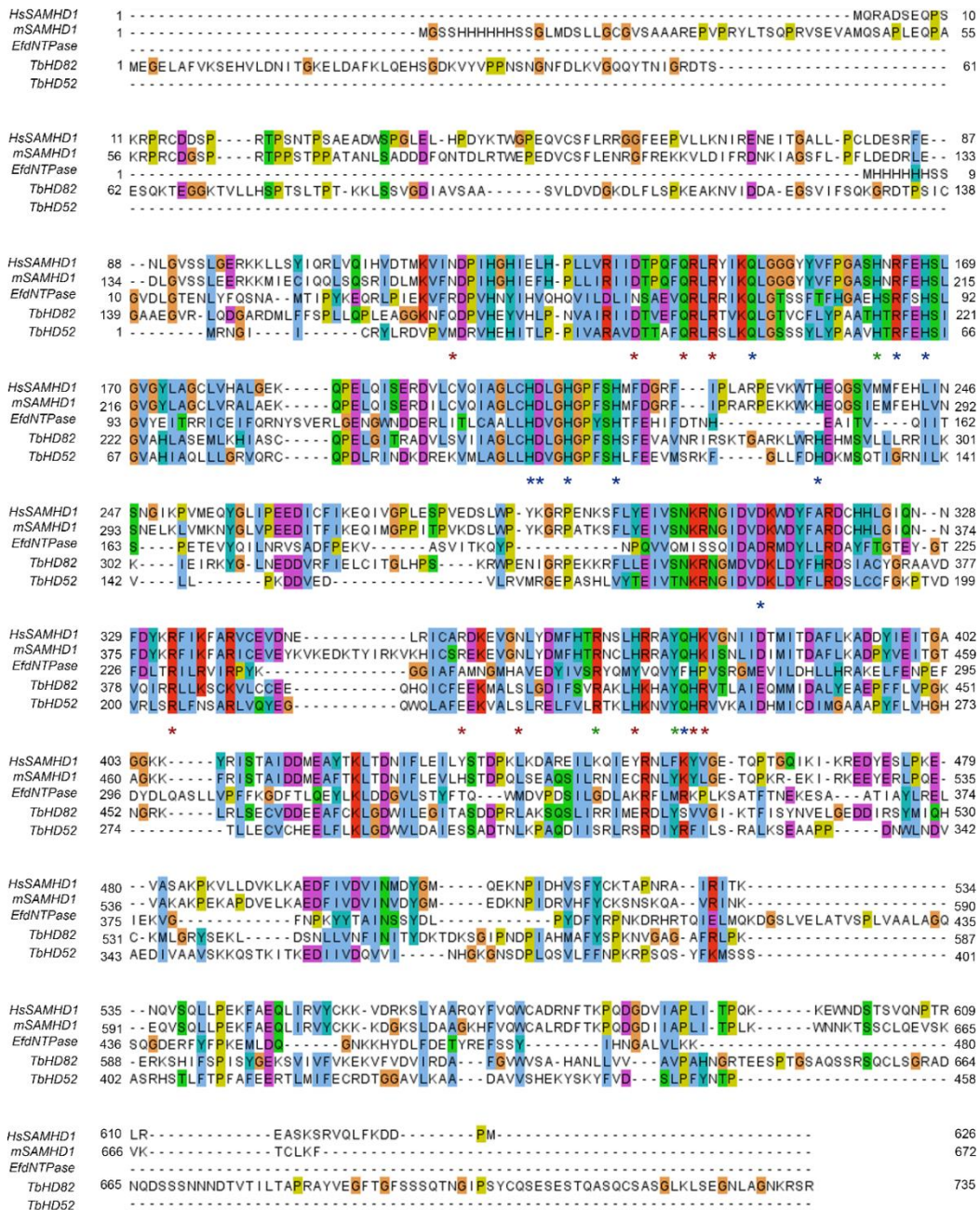
Figure D3. Alignment of representative HD containing proteins from several organisms. Alignment was performed using ClustalOmega and visualized with JalView, and includes the sequences obtained from UniProt database with the following sequence IDs: HsSAMHD1 (Q9Y3Z3), mSAMHD1 (Q60710-1), EfdNTPase (Q836G9), TbHD82 (Q583P4), TbHD52 (Q57X97). Red asterisks indicate residues involved in the allosteric sites; blue asterisks show residues involved in catalytic activity; and green asterisks denote residues involved in deoxyribose specificity.

The catalytic site of HsSAMHD1 requires the coordination of a Zn^{2+} ion, which is established with the side chains of two histidines (His167 and His206), two aspartates (Asp207 and Asp311) and a phosphate oxygen. It has been suggested that the Zn^{2+}-coordinated phosphate could correspond to an α-nucleotidyl phosphate, which additionally forms salt bridges with four basic residues (Arg164, His210, His215 and His233) adjacent to the active site and a hydrogen bond to a water molecule (Goldstone *et al.* 2011). Gln149 and Gln375 have also been reported as fundamental for the catalytic activity of HsSAMHD1.

The primary allosteric site compels the formation of five hydrogen bonds with the residues Asp137, Gln142 and Arg145 (Koharudin *et al.* 2014), as well as stacking interactions with Arg451 (Arnold *et al.* 2015). Hence, guanine is the only base that fits in the primary allosteric site. In the human SAMHD1 the secondary dNTP allosteric site is mainly characterized by the presence of Asn119, Arg333 and Asn358 (Ahn 2016). In the two orthologues of *T. brucei*, the amino acids aligned in the positions of Asn119 and Asn358 were Gln171 and Ser407 for TbH82, and Met16 and Ser229 for TbHD52, though in general the chemical and physical properties are preserved. Finally, the Arg366 and Tyr374 residues involved in deoxyribose specificity in the human protein are conserved in the trypanosomal proteins (Zhu *et al.* 2013).

The alignment shows that TbHD82 and TbHD52 conserve most motifs identified as essential for the activity of HsSAMHD1 (Fig. D3). Due to the similarity observed in the conserved motifs between the human protein and the two orthologues of *T. brucei,* we postulated that TbHD82 and/or TbHD52 perform in *T. brucei* a comparable role to that of HsSAMHD1.

D.1.2. Intracellular localization of TbHD82 and TbHD52

SAMHD1 is expressed in a wide variety of human cell lines. It is predominantly located in the nucleus (Rice *et al.* 2009; Brandariz-Nunez *et al.* 2012), though a small fraction has also been found in the cytoplasm of CD4(+) T cells and monocytes (Baldauf *et al.* 2012; Ryoo *et al.* 2014). In order to determine the intracellular localization of TbHD82 and TbHD52 in *T. brucei,* indirect immunofluorescence studies were performed in BSF and PCF parasites using polyclonal primary antibodies generated in our lab against both proteins (see Methods). Apart from including the parental cells in the analysis, several overexpressing-cell lines were generated that produce high levels of both the native and a c-myc-fusion protein.

TbHD82 is mostly localized in the nuclear compartment both in BSF and PCF trypanosomes (Fig. D4), though a small amount of the protein was observed in the cytoplasm of BSF parasites. The nuclear localization was confirmed by co-localization analysis. The Manders coefficient obtained for the green (TbHD82) and blue (DAPI) signal colocalization was 0.98 ± 0.02 and 0.83 ± 0.13 for TbHD82-OE and TbHD82-myc parasites, respectively.
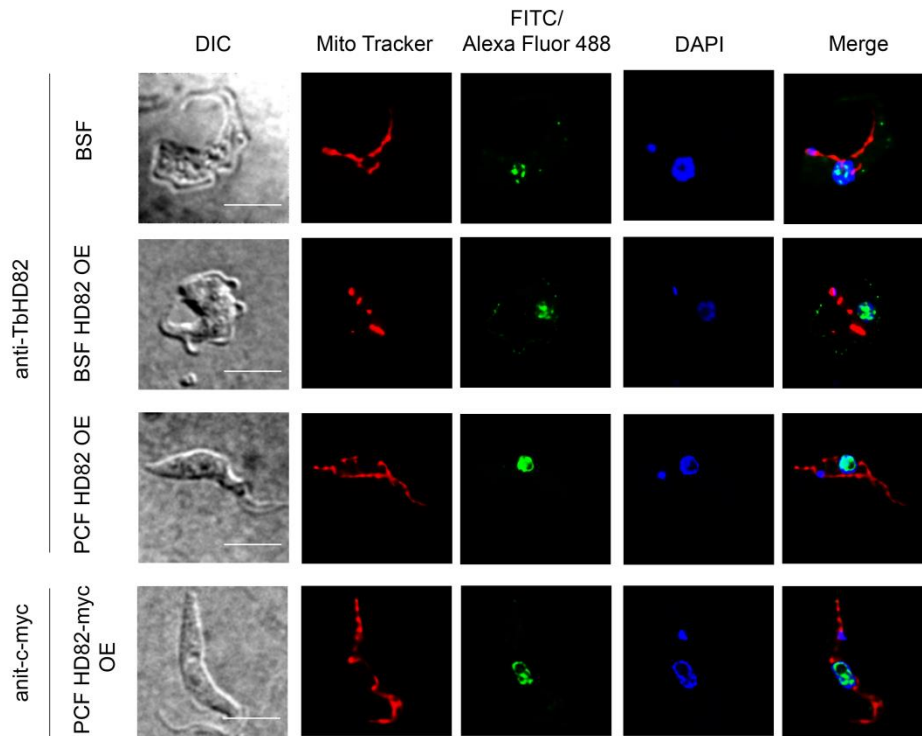
Figure D4. TbHD82 is detected mostly in the nucleus. Immunofluorescence analysis of the intracellular localization of TbHD82 in parental (BSF) and overexpressing (BSF HD82 OE) bloodstream forms as well as procyclic cell lines overexpressing the native protein (PCF HD82 OE) and a c-myc tagged fusion protein (PCF HD82-myc OE). HD82 signal (green) was detected by anti-TbHD82 or anti-c-myc primary antibodies and FITC-conjugated anti-rabbit or Alexa Fluor 488-conjugated goat anti-mouse secondary antibody, respectively. DAPI (blue) and MitoTrackerVR Red CMXRos (red) were used to stain nuclear and kinetoplast DNA and mitochondria, respectively. Images were collected with an Olympus IX81 microscope and Xcellence software, deconvolved using Huygens Professional from Scientific Volume Imaging (version 3.3) and pseudo-colored by using Fiji software (Schindelin *et al.* 2012). Bar, 5 μm.

On the other hand, the immunofluorescence analysis revealed that TbHD52 is predominantly mitochondrial (Fig. D5) and the Manders coefficients obtained for the green (TbHD52) and red (MitoTracker) signals were 0.86 ± 0.07 and 0.92 ± 0.05 for procyclic TbHD52-OE and TbHD52-myc parasites, respectively.
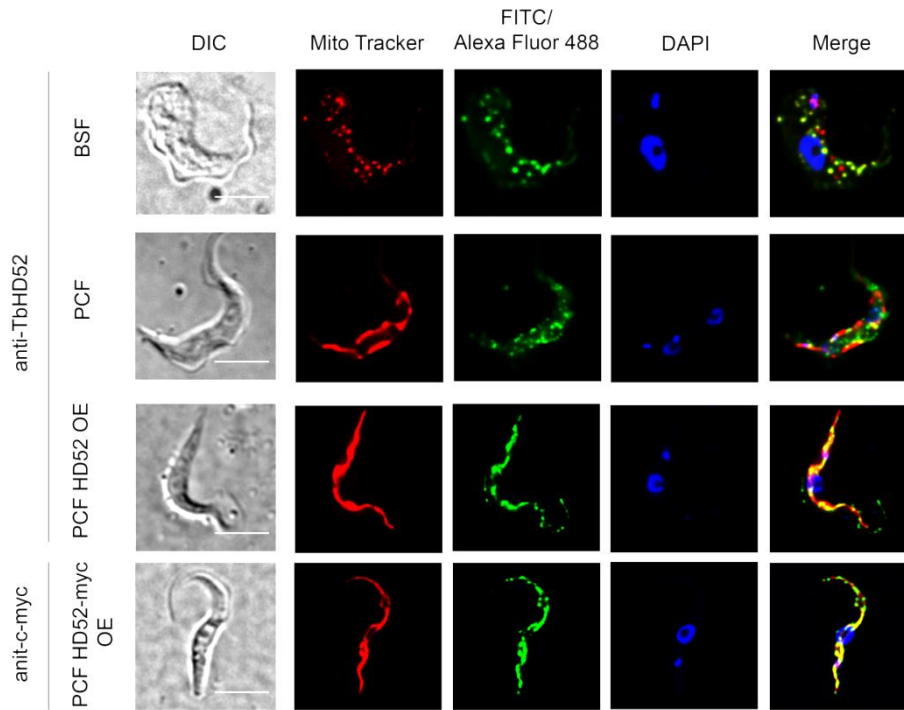
Figure D5. TbHD52 is predominantly located in the mitochondria. Immunofluorescence analysis of the intracellular localization of TbHD52 in parental bloodstream form (BSF) and procyclic forms of parental (PCF) and overexpressing native (PCF HD52 OE) or myc tagged fusion protein (PCF HD52-myc OE) cell lines. HD52 signal (green) was detected by anti-TbHD52 or anti-c-myc primary antibodies and FITC-conjugated anti-rabbit or Alexa Fluor 488-conjugated goat anti-mouse secondary antibody, respectively. DAPI (blue) and MitoTrackerVR Red CMXRos (red) were used to stain nuclear and kinetoplast DNA and mitochondria, respectively. Images were collected with an Olympus IX81 microscope and Xcellence software, deconvolved using Huygens Professional from Scientific Volume Imaging (version 3.3) and pseudo-colored by using Fiji software (Schindelin *et al.* 2012). Bar, 5 μm.

D.1.3. Role of TbHD82 and TbHD52 in cell viability and cell cycle progression in bloodstream and procyclic forms of *Trypanosoma brucei*

D.1.3.1. TbHD82 is not required for BSF survival

As the control of a balanced pool of deoxyribonucleotides is vital for DNA replication and repair, the impact of TbHD82 on cell proliferation was evaluated. To this purpose, gene silencing of *TbHD82* was performed by RNAi. We observed that

parasite growth rate was not significantly affected upon TbHD82 depletion (Fig. D6, panels A and B).

Since low levels of the protein can remain after RNAi induction and may be able to maintain cell viability, a TbHD82 null mutant was obtained through two allelic replacements with cassettes containing blasticidin and hygromycin resistance markers. Thus, an assessment of the genotype showing the presence of resistance genes and the replacements in the correct locus was performed by PCR using specific primers in combination with the *TbHD82* flanking sequences. In addition, the elimination of *TbHD82* was evaluated by PCR with specific oligonucleotides of the ORF as well as by analysis of protein expression by western blot (Fig. D6, panels C-E). While the absence of TbHD82 resulted in a slight growth defect compared to the parental cell line (Fig. D6 panel F), the cells were viable, revealing a non-essential role for the enzyme.
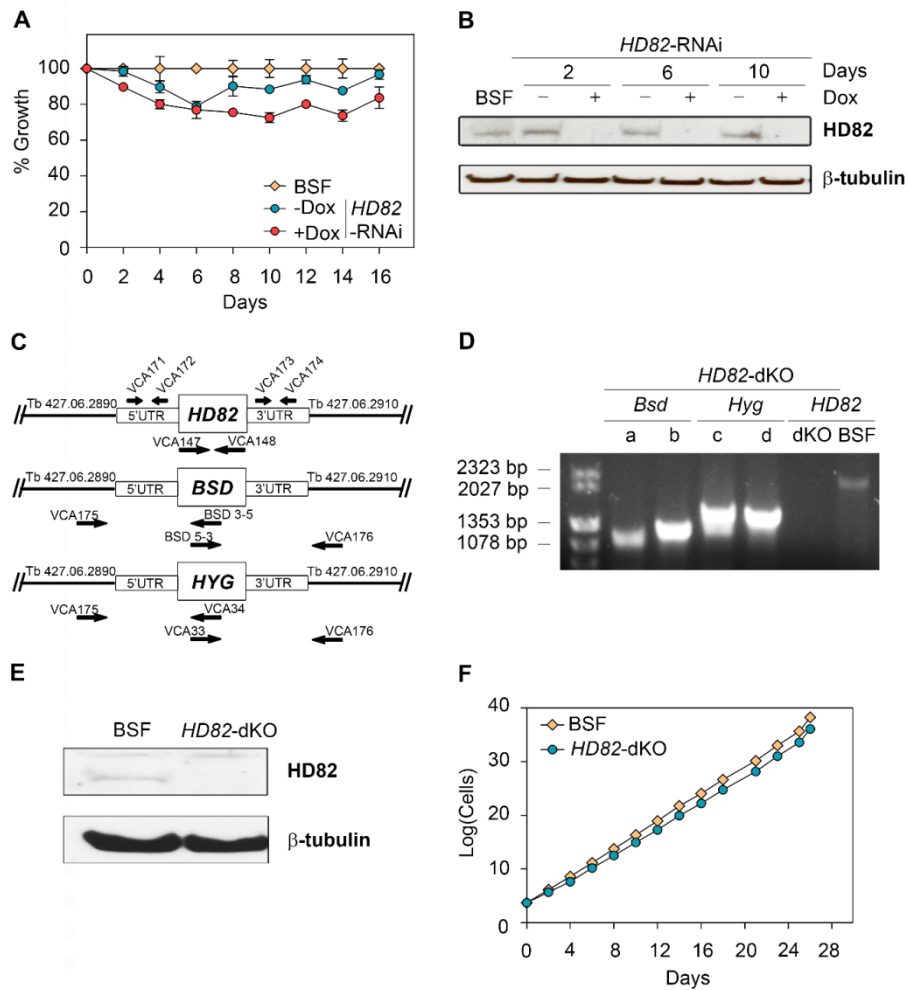
Figure D6. TbHD82 is not essential for cell viability in *Trypanosoma brucei* BSFs. (A) Plot showing the *HD82*-RNAi cell line growth minus or plus doxyxycline (1 µg/ml) calculated as growth percentage compared to the BSF parental cell line. (B) Evaluation of RNAi induction by western blot analysis using the polyclonal anti-TbHD82 antibody (TbHD82, 81.73 kDa). Anti-Tbβtubulin antibody (Tbβ-tubulin, 50.0 kDa) (Sigma) was used as loading control. (C and D) Genotypic analysis of *TbHD82*-dKO cell line. Scheme in (C) represents *TbHD82* locus architecture (Gene DB database, Tb927.6.2900 as systematic name) and the corresponding two allele replacements by *BSD* and *HYG* resistance genes for generation of the *HD82* double knockout cell line (BSF *HD82*-dKO). The open reading frames flanking the 5'UTR and 3'UTR of the *TbHD82* locus are Tb427.06.2890 (upstream) and Tb427.06.2910 (downstream), whereas arrows indicate the complementary sequences of the oligonucleotides used to check the genotype. The correct allelic replacement was verified by PCR (D) using different combinations of oligonucleotides. The *BSD* replacement was checked using VCA175/BSD 3-5 (a, 1227 bp) and VCA176/BSD 5-3 (b, 1288 bp) oligonucleotides. *HYG* replacement was verified using VCA175/VCA34 (c, 1756 bp) and VCA176/VCA33 (d, 1808 bp) oligonucleotides. The open reading frame of the *HD82* gene (2221 bp) was amplified with VCA147 and VCA148 oligonucleotides in dKO and parental BSF. (E) TbHD82 levels were determined by western blot in *TbHD82*-dKO and parental lines using polyclonal anti-TbHD82 antibody. Anti-Tbβtubulin antibody (Tbβ-tubulin, 50.0 kDa) (Sigma) was used as loading control. (F) Cumulative growth of *HD82*-dKO and parental lines monitored for 28 days.

D.1.3.2. TbHD52 is essential for Trypanosoma brucei

As described above, TbHD52 belongs to a protein subfamily that is only present in kinetoplastids, so its role might be particularly relevant in these organisms. Thus, we explored the effects of *TbHD52* knockdown on the growth of the BSF parasites by RNAi. Upon induction of *HD52*-RNAi, protein levels were efficiently reduced, which led to acute defects in proliferation, reaching a maximum growth inhibition of 90% after 6 days of RNAi induction (Fig. D7, panels A and B).

Bearing in mind that the human SAMHD1 is involved in deoxynucleoside formation and that deoxynucleoside salvage by thymidine kinase is important for *de novo* thymidylate biosynthesis in *T. brucei* (Leija *et al.* 2016; Valente *et al.* 2016), we hypothesized that TbHD52 could be crucially involved in dTTP homeostasis. To examine if TbHD52 knockdown affects pyrimidine availability, parasites were grown in HMI-9 medium supplemented with a high and non-physiological concentration of dThd (0.6 mM). Indeed, high concentrations of dThd counteracted the deleterious effects of TbHD52 deficiency and restored normal proliferation, thus suggesting a role in the provision of metabolites essential for cell proliferation, mainly dTTP (Fig. D7, panel C).
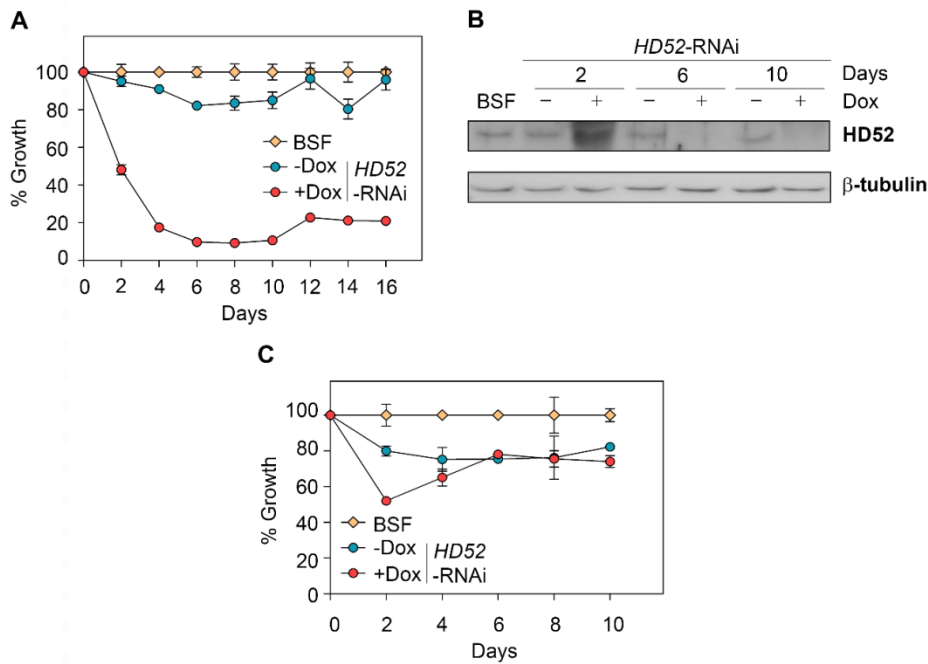
Figure D7. TbHD52 knockdown compromises cell viability in the absence of thymidine. (A) Relative growth rate of the *HD52*-RNAi cell line minus or plus doxyxycline (1 µg/ml) compared to the BSF parental line. (B) RNAi efficiency during the growth curve was confirmed by western blot using polyclonal anti-TbHD52 (TbHD52, 52.2 kDa) antibody. Anti-Tbβtubulin antibody (Tbβ-tubulin, 50.0 kDa) (Sigma) was used as loading control. (C) Time course showing relative growth rate of *HD52*-RNAi cell line minus or plus doxycycline (1 µg/ml) with regard to the BSF parental line, grown in HMI-9 medium supplemented with 0.6 mM dThd.

TbHD52 knockout parasites were also generated as previously described. Thus, replacement of the first *HD52* allele was easily attained resulting in heterozygote parasites. Nevertheless, after several attempts to eliminate the second allele of the gene, it was only achieved in the presence of 0.6 mM dThd, generating *HD52*-dKO parasites that were dThd auxotrophs. The genotype of the null mutants was verified by PCR through the amplification of the *BSD* and *HYG* resistance markers together with the use of primers complementary to the flanking sequences of *TbHD52*. TbHD52 protein was also not detectable by western blot (Fig. D8, panels A-C). As mentioned, *Tb* BSF *HD52*-dKO parasites require exogenous dThd supplementation, and dThd withdrawal

induced early defects on viability. Thereby, a 30% inhibition was obtained 8 h after dThd starvation and there was a complete loss of viability after 6 days (Fig. D8, panels D-E).
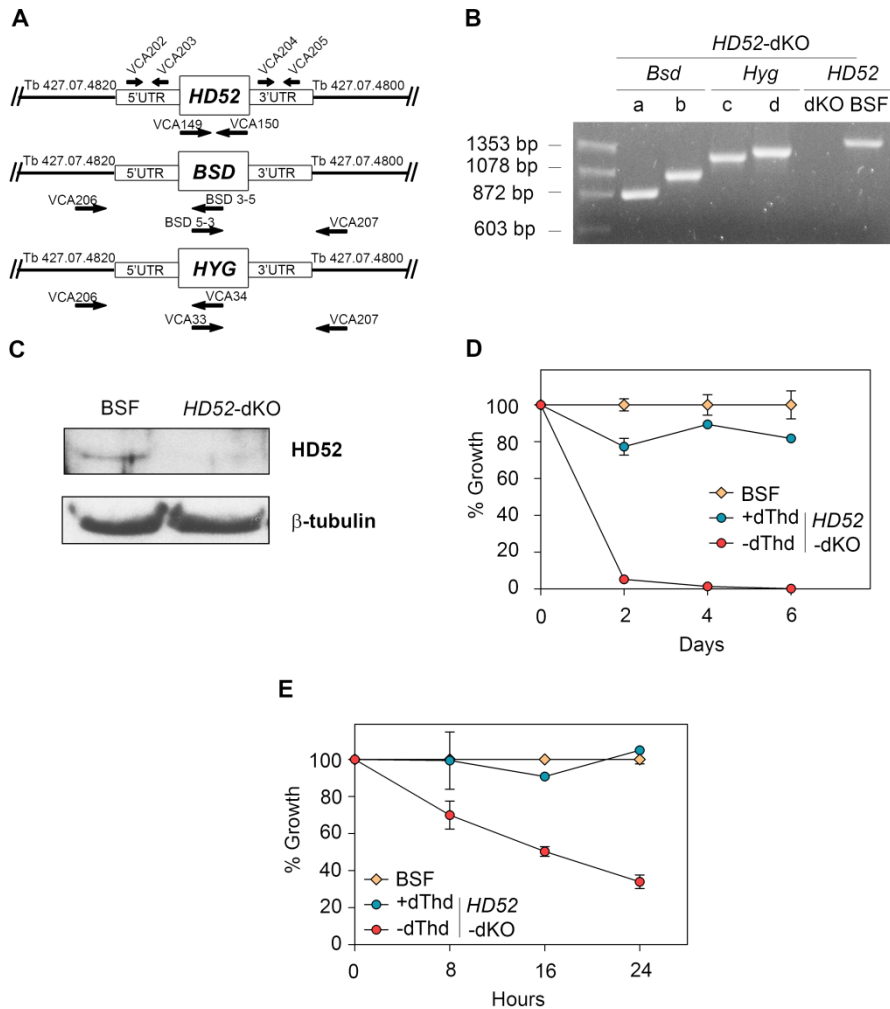
Figure D8. *TbHD52*-null mutants are thymidine auxotrophs in BSFs. (A and B) Genotypic analysis of the *TbHD52*-dKO cell line. Scheme in (A) represents *TbHD52* locus architecture (Gene DB database, Tb927.7.4810 as systematic name) and the corresponding two allele replacements by *BSD* and *HYG* resistance genes for generation of the HD52 double knockout (BSF *HD52*-dKO). The open reading frames flanking the 5'UTR and 3'UTR of *TbHD52* locus are indicated (Tb427.07.4820 (upstream) and Tb427.07.4800 (downstream)), whereas the arrows show the complementary sequences of the oligonucleotides used to verify the genotype. The correct allelic replacement was verified by PCR in (B) using different combination of oligonucleotides. *BSD* replacement was checked using VCA206/BSD 3-5 (a, 866 bp) and VCA207/BSD 5-3 (b, 1020 bp) oligonucleotides. *HYG* replacement was checked using VCA206/VCA34 (c, 1205 bp) and VCA207/VCA33 (d, 1264 bp) oligonucleotides. The open reading frame of the *HD52* gene (1393 bp) was amplified with VCA149 and VCA150 oligonucleotides in dKO and parental (BSF). (C) Western blot representing TbHD52 levels in *TbHD52*-dKO and parental lines

using polyclonal anti-TbHD52 (TbHD52, 52.2 kDa) antibody. Anti-Tbβtubulin antibody (Tbβ-tubulin, 50.0 kDa) (Sigma) was used as loading control. (D) Cumulative growth in dThd-free HMI-medium of *HD52*-dKO and parental cell lines cultured in absence or presence of 0.6 mM dThd for 28 days. (E) Time course of the growth rate of *HD52*-dKO cell line minus or plus 0.6 mM dThd with regard to the parental line.

The role of TbHD52 in the viability of *T. brucei* PCFs was also evaluated. Knockdown of TbHD52 by RNAi affected significantly cell proliferation, though the defects were less pronounced than in BSFs. Induction of TbHD52 depletion provoked a sudden decline of 30% in growth after 48 h and a 70% growth inhibition at day 12 post-induction (Fig. D9 panel A). Western blot analysis confirmed the efficient RNAi-mediated enzyme depletion over the time course of the experiment (Fig. D9 panel B).

In a similar fashion to BSFs, *Tb* PCF *HD52*-dKO cells were also obtained in the presence of 0.6 mM dThd (Fig. D9 panels C-D). However, in contrast to BSFs, dThd supplementation did not fully efficiently sustain proliferation, as under these conditions parasites exhibited around 30-40% growth inhibition compared to the parental cell line. Additionally, dThd withdrawal resulted in 90% growth inhibition compared to the parental cell line, yet a small remaining population was observed after 16 days (Fig D9 panel E).
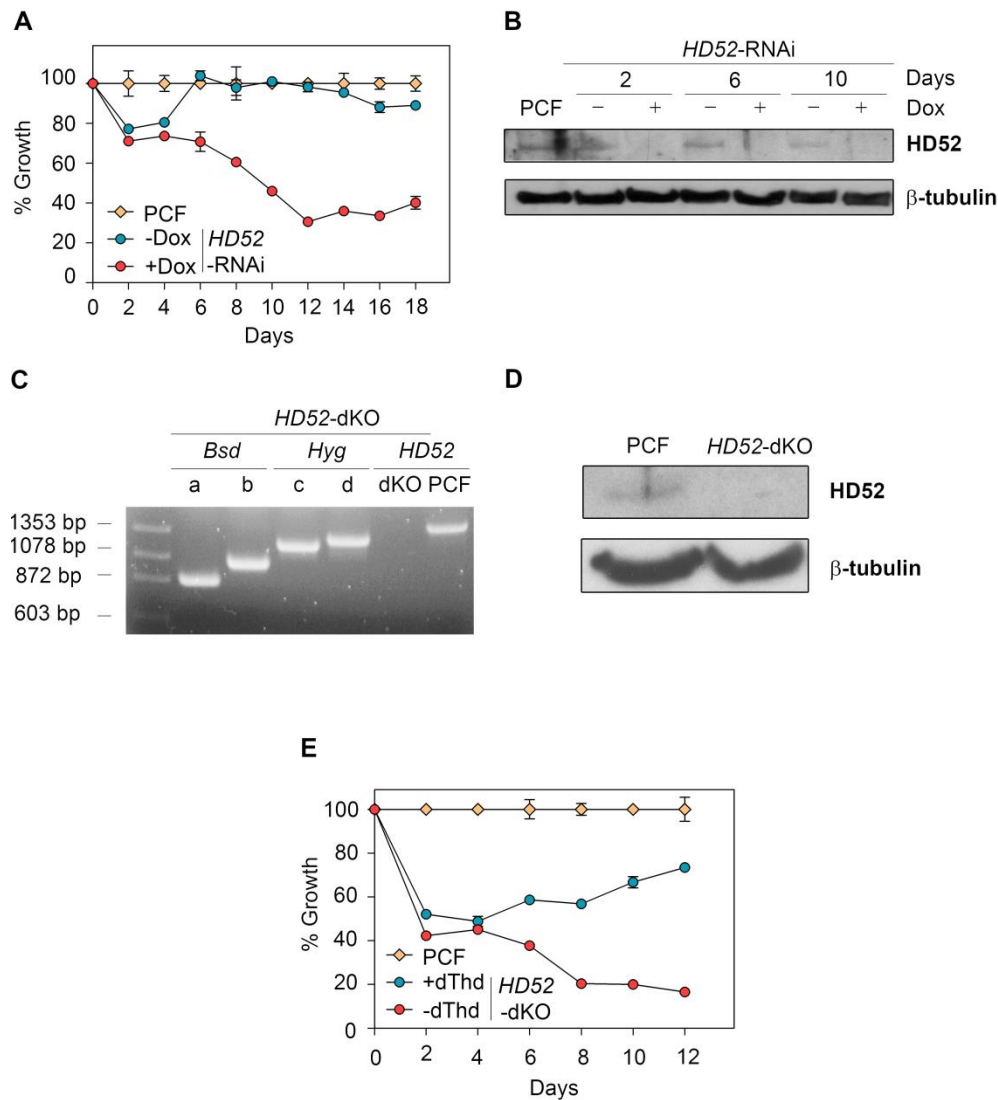
Figure D9. TbHD52 knockdown or knockout affects cell proliferation of procyclic parasites under thymidine deprivation. (A) Proliferation rate of the *HD52*-RNAi cell line minus or plus doxyxycline (1 µg/ml) compared to the PCF parental line. (B) Expression profile of TbHD52 as determined by western blot using the polyclonal anti-TbHD52 antibody (TbHD52, 52.2 kDa). The Anti-Tbβtubulin antibody (Tbβ-tubulin, 50.0 kDa) (Sigma) was used as loading control. (C) Genotypic analysis of *TbHD52*-dKO cell line in PCFs by PCR. As previously described, *BSD* replacement was checked using VCA206/BSD 3-5 (a, 866 bp) and VCA207/BSD 5-3 (b, 1020 bp) oligonucleotides, and *HYG* replacement was verified using VCA206/VCA34 (c, 1205 bp) and VCA207/VCA33 (d, 1264 bp) oligonucleotides. The open reading frame of the HD52 gene (1393 bp) was amplified with VCA149 and VCA150 oligonucleotides in *Tb* PCF *HD52*-dKO and parental lines. (D) Expression levels of TbHD52 analyzed by western blot in and *TbHD52*-dKO and parental lines as described above. (E) Growth percentage of *Tb* PCF *HD52*-dKO cell line grown with or without 0.6 mM dThd compared to the parental line.

To further validate the relationship between the lack of TbHD52 and the phenotype observed, a conditional knockout was generated in both BSFs and PCFs, where parasites harboured an inducible ectopic copy of *TbHD52* (*HD52*-dKO/OE). In BSFs, growth of this cell line was completely restored after induction of the ectopic copy, both in the presence and absence of dThd. Non-induced parasites exhibited proliferation defects when dThd was not available, yet growth was fully re-established after 10 days of dThd withdrawal (Fig. D10 panel A). This observation can be associated to the leakiness of the inducible system, since at day 10, HD52 was beginning to be expressed even in the absence of Dox (Fig. D10 panel B). Again, in a similar fashion, in PCFs the induction of the ectopic copy in the absence of dThd also restored cell growth (Fig. D10 panel C). TbHD52 was not detected by western blot under non-induced conditions (Fig. D10 panel D), yet the *HD52*-dKO/OE cell line grew slightly better than the null mutants after dThd withdrawal. It is possible that a small basal level of protein is sufficient to sustain growth in this form of the parasite.
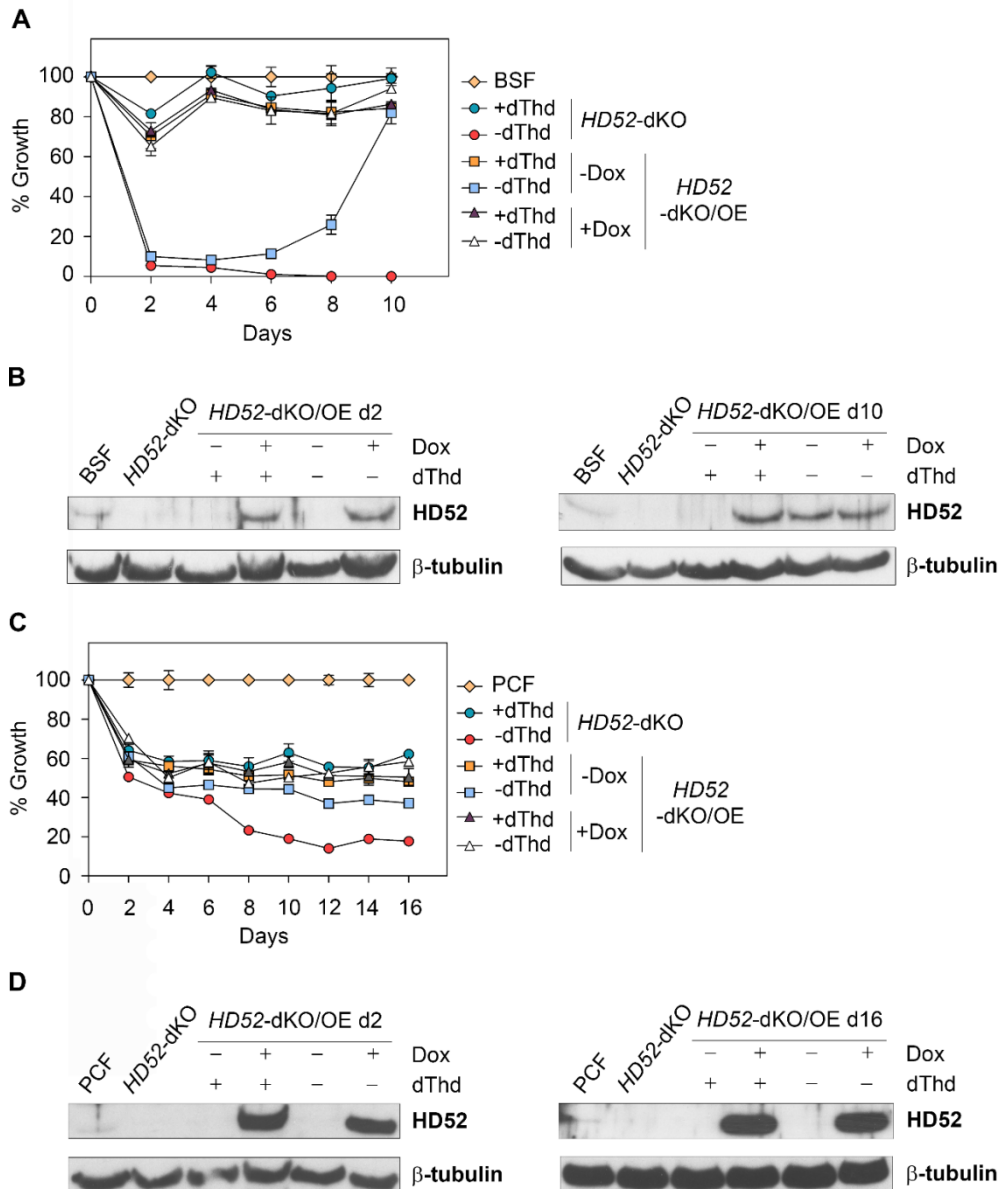
Figure D10. Expression of an inducible TbHD52 ectopic copy in null-mutants restores cell growth. (A) Time course of the proliferation rate in the *HD52*-dKO and *HD52*-dKO/OE cell lines compared to parental parasites grown in dThd-free medium for 10 days with the different combinations of 1 µg/ml Dox and 0.6 mM dThd. (B) Expression profile of TbHD52 at the beginning and the end of the growth curve was determined by western blot using the polyclonal anti-TbHD52 antibody (TbHD52, 52.2 kDa). Anti-Tbβtubulin antibody (Tbβ-tubulin, 50.0 kDa) (Sigma) was used as loading control. (C) Plot showing the growth of the *HD52*-dKO and *HD52*-dKO/OE cell lines compared to the PCF parental parasites as described in (A). (D) TbHD52 levels were monitored by western blot at day 2 and 16 as described in (B).

D.1.3.3. The absence of TbHD52 impairs cell cycle progression and DNA segregation

In order to evaluate the effects of TbHD52 deficiency on cell cycle progression, *Tb* BSF *HD52*-dKO cells were subjected to dThd deprivation for 24 hours and cell cycle progression was analysed by flow cytometry. As shown (Fig. D11 panel A), the absence of TbHD52 gave rise to an increase of parasites in S and G2/M phases, whereas the G1 population was drastically reduced. In addition, a significant number of cells containing an abnormal DNA amount, such as sub-G1 and post-G2/M population, were also observed. Additionally, a more detailed study of the cell cycle and morphology was performed by DNA staining with DAPI. In agreement with flow cytometry analysis, TbHD52-deficient parasites displayed an important reduction in 1N1K and 1N1K* populations, corresponding to the G1 phase. Likewise, we found several aberrant populations with defects in DNA replication and segregation of nucleus and kinetoplast: 1N*1K* (17%) where nuclear DNA replication initiates before the completion of kinetoplast segregation; 1N2K* (1%) where one segregated kinetoplast is replicating again before nuclear DNA replication; 1N*2K* (3%) where a new event of kinetoplast replication occurs although there is an arrest in mitosis; and 1N0K (2.8%) which comes from the progression of mitosis without complete kinetoplast segregation. Moreover, cytokinesis was also considerably perturbed, as we observed cells with an abnormal number of nuclei and kinetoplasts (xNxK, 4.6%), where mitosis is blocked but both nuclei and kinetoplasts enter a new replication round, as well as 2N2K* cells (1.5%) (Fig. D11 panels B and C).
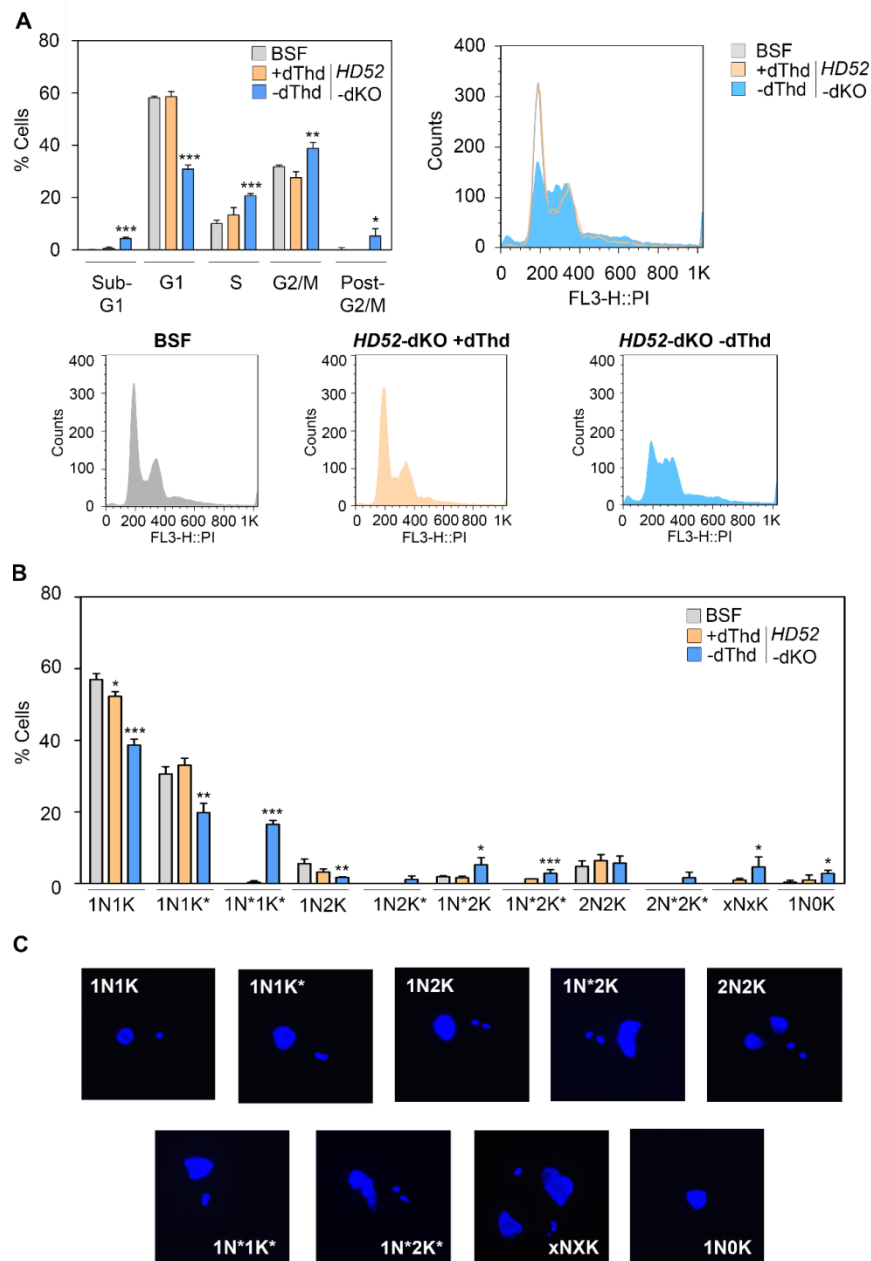
Figure D11. BSF *TbHD52*-deficient parasites present severe cell cycle defects. Cell cycle progression was determined by propidium iodide and DAPI staining in parental and *HD52*-dKO cell lines grown in the presence or absence of 0.6 mM dThd for 24 h. (A) Plot and histograms obtained by flow cytometry of cells stained with propidium iodide. Left panel corresponds to the percentages of cells in each of the different cell cycle stages (sub-G1, G1, S, G2/M and post-G2/M). Right panel shows the FACS layout that results from overlapping the separate histograms obtained for each condition (see histograms below). Bars represent the mean (±S.D.) calculated from three independent experiments. (B) Quantification of cell populations according to the number of nuclei (N) and kinetoplasts (K) stained with DAPI and observed by immunofluorescence microscopy. N or K undergoing duplication is denoted with an asterisk. Data are shown as the mean (±S.D.) of more than 300 cells coming from three independent experiments. (C) Representative images obtained with the Zeiss Axio Imager A1 fluorescence microscope after DAPI staining, which illustrates populations described in (B). The asterisks show significant difference calculated by the Student's t-test (n=3) *p<0.05, **p<0.01 and ***p<0.001.

Kinetoplast integrity was also studied by the use of DHE. It specifically stains the kDNA network in living cells, since it is oxidized to ethidium, a DNA intercalating molecule, inside the mitochondrion (Wang *et al.* 2002). We observed that, after dThd removal, TbHD52-deficient parasites displayed an increase in DHE signal, corresponding to enlarged kinetoplasts, which could be associated to the aberrant populations already detected (1N*1K*, 1N2K*, 1N*2K* and 2N*2K*) (Fig. D12). In conclusion, these results suggest that, although TbHD52 is a mitochondrial enzyme, its depletion has an impact on both nuclear and kinetoplast replication and segregation.
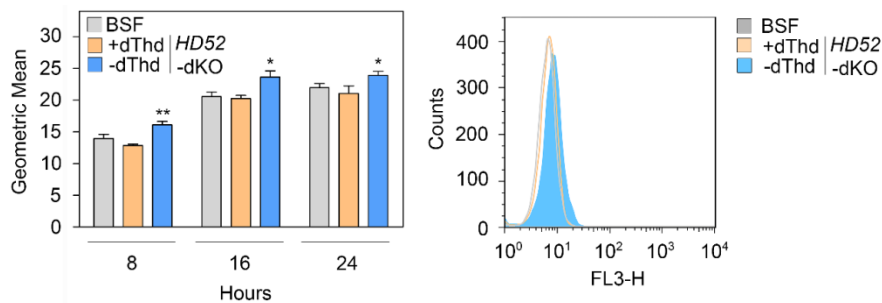
Figure D12. *TbHD52*-null mutants exhibit defects in kinetoplast segregation in BSFs. kDNA was stained with DHE in *HD52*-dKO and parental lines (BSF) grown in dThd-free HMI-9 medium with or without 0.6 mM dThd, and the signal was measured with FACS. Samples were measured at different times (8, 16 and 24 h) after dThd withdrawal. Left panel represents geometric mean of kDNA signal and right panel shows the overlapped histograms of the samples collected at 24 h. Data represent the geometric mean (±S.D.) coming from three independent experiments. The asterisks show significant differences calculated by the Student's t-test (n=3) *p<0.05, **p<0.01 and ***p<0.001.

Since PCF HD52-deficient trypanosomes exhibited important defects in cell proliferation, the cell cycle progression was also determined in these cells. Thus, the *Tb* PCF *HD52*-dKO cell line was maintained both in the presence and absence of dThd for 10 days and then parasites were stained with propidium iodide and DAPI to evaluate cell cycle progression and morphology. FACS analysis showed that the remaining parasites (without dThd) exhibit a normal population distribution based on the DNA content (Fig. D13 panel A). However, whereas nuclear defects were not apparently

observed, a more detailed analysis of cell populations by DAPI staining confirmed that

kinetoplast replication was seriously affected (Fig. D13 panel B and C).
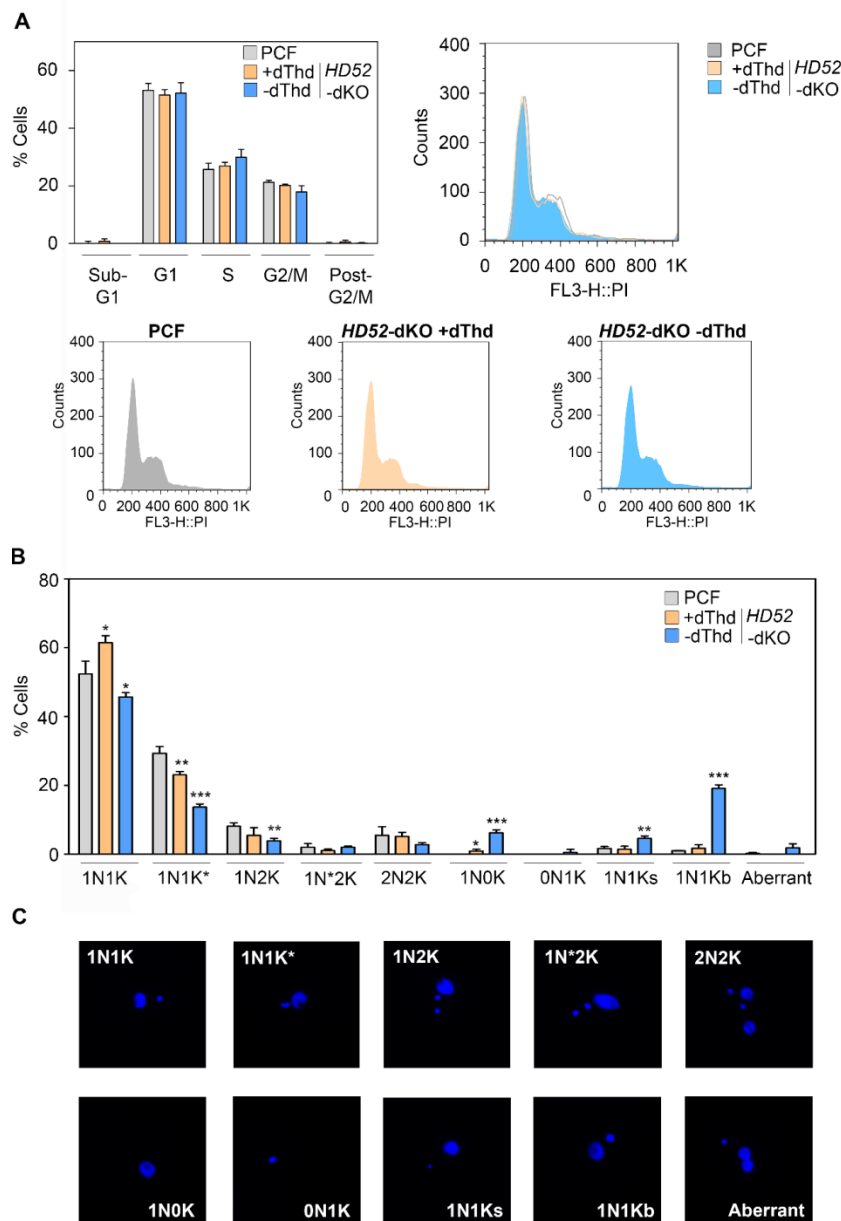
Figure D13. Cell cycle progression is not altered in HD52 deficient PCF trypanosomes. *HD52*-dKO and parental cell lines were cultured for 10 days with or without 0.6 mM dThd and cell cycle progression was subsequently determined by propidium iodide and DAPI staining. (A) Resultant plot and histograms from FACS analysis in cells stained with propidium iodide. Left panel corresponds to the percentages of cells in each of the different cell cycle stage (sub-G1, G1, S, G2/M and post-G2/M). Right panel shows the FACS layout that results from overlapping the separate histograms obtained for each condition (see histograms below). Bars represent the mean (±S.D.) calculated from three independent experiments. (B) Quantification of cell populations according to the number of nuclei (N) and kinetoplasts (K) stained

with DAPI and observed by immunofluorescence microscopy. N or K undergoing duplication is denoted with an asterisk. Ks and Kb correspond to smaller or bigger kinetoplasts than usual, respectively, whereas aberrant cells are considered as those populations with an abnormal number of N or K. Data are shown as the mean (±S.D.) of more than 300 cells coming from three independent experiments. (C) Representative images obtained with the Zeiss Axio Imager A1 fluorescence microscope after DAPI staining, which illustrates populations described in (B). The asterisks show significant difference calculated by the Student's t-test (n=3), *p<0.05, **p<0.01, ***p<0.001.

Thus, in this cell line, the lack of TbHD52 in the absence of dThd led to the appearance of two additional 1N1K sub-populations presenting either a bigger (1N1Kb) or smaller (1N1Ks) kinetoplast, as well as a meaningful decrease in cells containing 1N1K* (13.6%) compared to parasites coming from both parental and *HD52*-dKO cell lines cultured with dThd. Taking into account the distribution of the kinetoplast perimeter value in parental parasites, we considered a normal range of $0.09 < K < 0.180$ pixel units, which was determined using Fiji software. Thus, the percentage of cells corresponding to the 1N1Kb population was 19.1%, whereas 1N1Ks cells were 4.6%. Finally, we also found a significant number of parasites that lacked a kinetoplast (1N0K, 6.2%).

Fig. D14 shows the kinetoplast perimeter of the1N1K population *versus* its frequency, analysed by IBM SPSS statistics software. Thus, we observed an augmented dispersion degree of the kinetoplast perimeter in the PCF *HD52*-null parasites maintained in absence of dThd for 12 days compared to the same cell line grown in the presence of dThd and parental parasites. *Tb* PCF *HD52*-dKO parasites grown in the absence of dThd also exhibited a significant higher average perimeter value determined by the ANOVA test (p<0.001), being 0.152 ± 0.044 pixel units in the absence of dThd and 0.132 ± 0.024 and 0.134 ± 0.022 pixel units in HD52-deficient parasites in the presence of dThd and parental cells, respectively (Fig. D14). These observations

indicate that the 1N1K population contains enlarged kinetoplasts, which is consistent with the observation of parasites with an abnormal kinetoplast size (1N1Kb and 1N1Ks) already detected by DAPI staining.
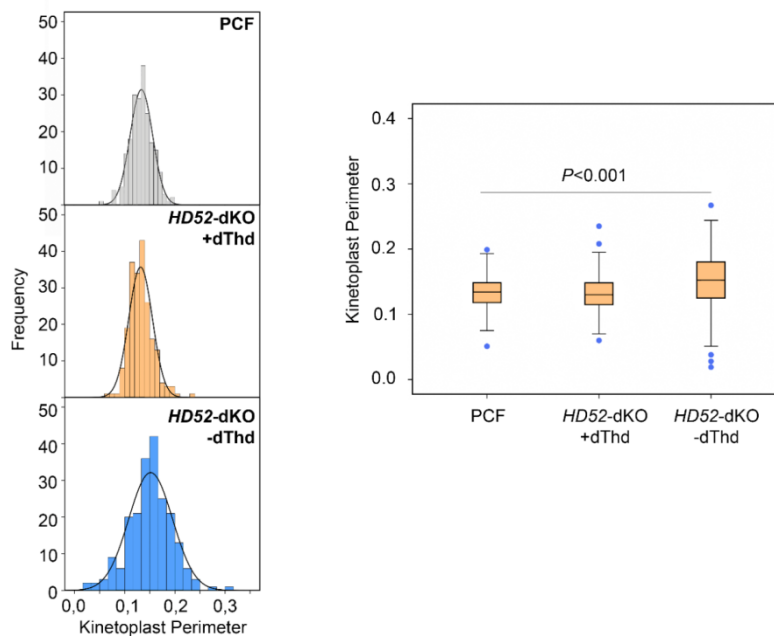
Figure D14. In the absence of TbHD52, PCF parasites present heterogeneous kinetoplast sizes. *HD52*-dKO cells were grown with 0.6 mM dThd and for 10 days without dThd, and, together with parental PCFs, were subjected to DAPI staining. Images were collected with a Zeiss Axio Imager A1 fluorescence microscope and kinetoplast perimeter was quantified with Fiji software selecting 1N1K cells. Left panel shows the histograms representing kinetoplast perimeter *versus* its frequency. The corresponding box plots are indicated in the right panel where the line is the mean of the values; the box exhibits the interquartile range; whiskers correspond to the maximum and minimum values and dots are outlying data points.

As in BSFs, DHE staining was carried out in PCF parasites, showing that total fluorescence, represented as geometric mean, was not modified. However, in agreement with the Fiji analysis, we found a wider distribution in the kDNA signal, which indicates more profound differences in kinetoplast size within the cell population (Fig. D15).
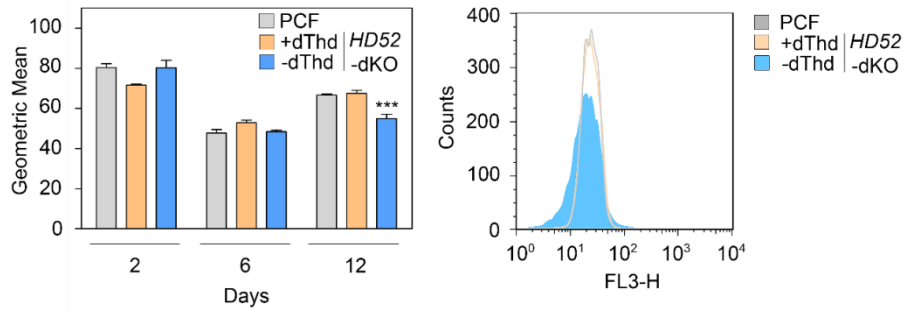
Figure D15. DHE staining in PCF *TbHD52*-null mutants. kDNA was stained with DHE in *Tb* PCF parental cells and *HD52*-dKO cells cultured with or without 0.6 mM dThd for 12 days, and fluorescence was measured by flow cytometry. Determinations were performed at different time points, corresponding to 2, 6 and 12 days after dThd removal. Left panel shows the geometric mean of the kDNA signal, whereas the right panel exhibits the overlapped histograms corresponding to 12 days. Data represent the geometric mean ($\pm$S.D.) coming from three independent experiments. The asterisks show significant difference calculated by the Student's t-test (n=3) *$p<0.05$, **$p<0.01$ and ***$p<0.001$.

D.1.4. Role of TbHD52 in the homeostasis of pyrimidine and purine nucleosides in *Trypanosoma brucei*

D.1.4.1. Deficiency of TbHD52 is counteracted by a high concentration of extracellular pyrimidine nucleosides

In order to establish the role of TbHD52 in pyrimidine metabolism, both BSF and PCF *TbHD52*-null mutants were cultured in dThd-free culture media supplemented with different pyrimidine nucleosides. It is known that BSF parasites express two well-characterized transporters, a high-affinity uracil transporter (TbU3) and an extremely low-affinity thymidine transporter (TbT1) (Gudin *et al.* 2006; Ali *et al.* 2013a). As aforementioned, HD52-null mutants were obtained at high dThd concentrations, yet dThd titration was performed to assess whether lower doses of dThd could also support cell growth. Different dThd concentrations (ranging from 25 μM to 0.6 mM) were tested. Viability was dose-dependent and below 0.2 mM dThd growth

was severely compromised (Fig. D16 panel A). In view of these observations we decided to maintain the *HD52*-dKO cell line in media supplemented with 0.6 mM dThd.

As *Tb* BSF *HD52*-null mutants are dThd auxotrophs, efforts were performed in order to understand the role of TbHD52 in thymidylate biosynthesis. It is known that dTTP comes from the phosphorylation of dTMP, which can be formed either by salvage of dThd through its phosphorylation by TK or from the *de novo* pathway through dUMP methylation by DHFR-TS. In fact, studies have shown that TbTK plays an essential role in *de novo* biosynthesis of dTTP, providing dUMP via phosphorylation of dUrd (Leija *et al.* 2016; Valente *et al.* 2016). Interestingly, most dUrd is generated by dCyd deamination via CDA (Leija *et al.* 2016), which can also additionally deaminate the non-physiological 5-methyl-2'-deoxycytidine (5M-dCyd) directly to thymidine. Hence, to evaluate the potential role of TbHD52 in the provision and homeostasis of the different pyrimidine deoxynucleosides, we analysed if supplementation with different nucleosides involved in the dTTP biosynthesis pathway (dUrd, Ura, dCyd or 5M-dCyd) could support cell viability in HD52-deficient parasites. It has been documented that transport of pyrimidine deoxynucleosides is deficient in BSF trypanosomes except for Ura (Gudin *et al.* 2006). Bearing this in mind, parasites were supplemented with high doses of dUrd, dCyd and 5M-dCyd to ensure uptake (more than 1 mM), whereas Ura was used at 0.1 mM to avoid cytotoxicity (Ong *et al.* 2013). In the case of supplementation with 5 mM dUrd, cell proliferation was well restored, whereas dCyd and 5M-dCyd were less efficient. Ura could not support the growth of HD52-deficient parasites (Fig. D16 panel B).
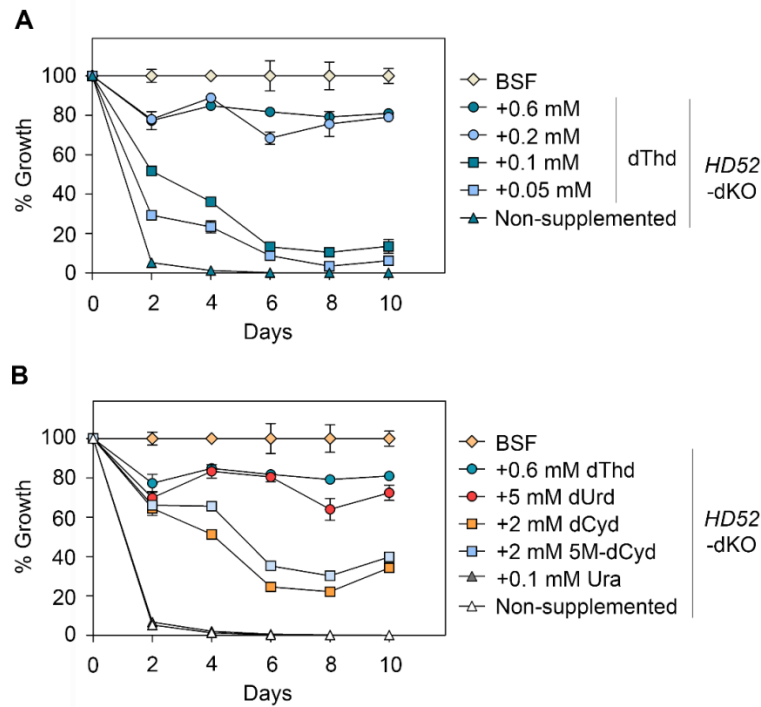
Figure D16. In the absence of TbHD52, thymidine and deoxyuridine supplementation is required for viability of BSF parasites. (A) Plot showing growth of the BSF parental line and *HD52*-dKO parasites in dThd-free HMI-9 medium at different dThd concentrations (0-0.6 mM dThd). (B) Time course of the proliferation rate of the BSF parental line and *HD52*-dKO parasites grown in dThd-free HMI-9 medium supplemented with thymidine (dThd), deoxyuridine (dUrd), deoxycytidine (dCyd), 5-methyl-2'-deoxycytidine (5M-dCyd) or uracil (Ura). Growth is expressed as percentage compared to the parental line.

The effect of pyrimidine supplementation on cell viability was also performed in PCF parasites. Thus, three different pyrimidine transporters have been reported in PCFs: TbU1, TbU2 and TbC1. TbU1 exhibits high-affinity and efficiency with Ura, whereas TbU2 and TbC1 present high-affinity but low-efficiency with Urd and Cyt (de Koning and Jarvis 1998; Gudin *et al.* 2006). No specific dThd transporter has been identified in PCFs. Growth of PCF *HD52*-dKO parasites in the presence of dThd was concentration-dependent and the optimal was 0.6 mM dThd (Fig. D17 panel A). On the other hand, supplementation with dUrd, dCyd, and 5M-dCyd in PCFs lacking TbHD52

alleviated the defective growth phenotype, although the growth rate was always lower than in presence of 0.6 mM dThd (Fig. D17 panel B).
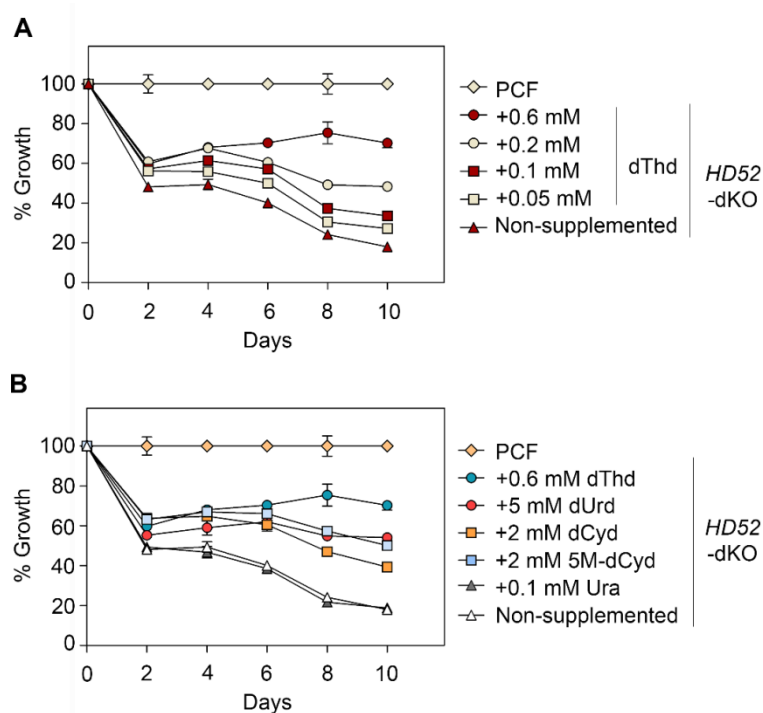
Figure D17. Supplementation of pyrimidine nucleosides enhances cell proliferation in the PCF *HD52*-dKO cell line. (A) Relative growth rate of *HD52*-dKO and PCF parental lines at increasing dThd concentrations (0-0.6 mM). (B) Growth percentage of *HD52*-dKO and PCF parental lines cultured in presence of dThd), dUrd, dCyd, 5M-dCyd or Ura. Growth is expressed as percentage compared to the parental cell line.

Availability of an extracellular source of dTTP precursors is able to counteract the growth defects caused by the lack of HD52. However, only dThd and dUrd supplementation was completely effective, whereas dCyd and 5M-dCyd only partially restored cell growth in the HD52-deficient cells. This observation suggested that perhaps TbCDA levels are low and could be limiting the efficient utilization of dCyd and 5M-dCyd, via deamination to dUrd and dThd respectively, for dTTP formation.

In order to analyse this possibility, BSF *HD52*-null mutants overexpressing an inducible copy of *TbCDA* were generated (*HD52*-dKO/*Tb*CDA). TbCDA overexpression was non-toxic, since the *HD52*-dKO/*Tb*CDA cell line exhibited a similar growth profile as *HD52*-dKO parasites (Fig. D18 panel A). Overexpression of TbCDA had no effect on the growth profile of dCyd-supplemented cells (Fig. D18 panel B), while 5M-dCyd efficiently restored growth of the *HD52*-dKO/*Tb*CDA cell line to levels similar to those attained with dThd (Fig. D18 panel C). Thus, over-expression of TbCDA favours 5M-dCyd-mediated rescue of cell viability in *HD52*-dKO cell lines but not in the case of dCyd.
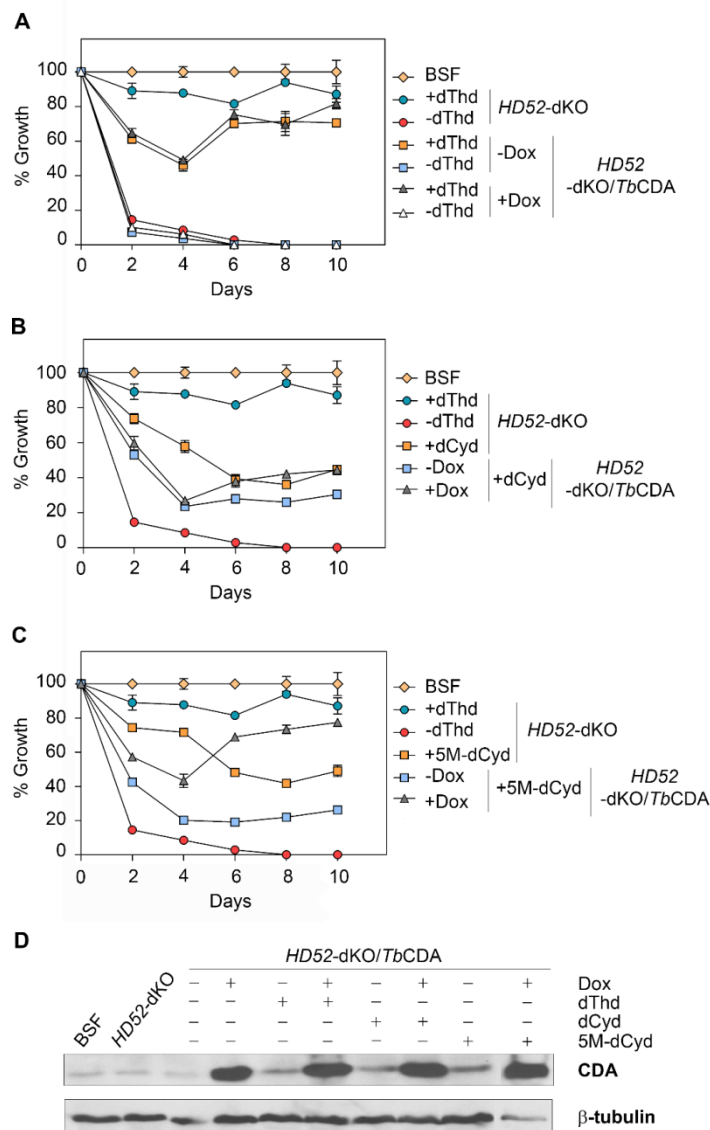
Figure D18. **TbCDA overexpression in BSF HD52-dKO cell lines restores cell growth in the presence of 5-methyl-2'-deoxycytidine.** *HD52*-dKO, *HD52*-dKO/*Tb*CDA and parental lines were grown in dThd-free HMI- medium for 10 days with different combinations of 1 μg/ml Dox, 0.6 mM dThd, 2 mM dCyd and 2 mM 5M-dCyd. Proliferation is expressed as growth percentage compared to the parental line. (A) Time course analysis showing the relative growth rate of *HD52*-dKO and *HD52*-dKO/*Tb*CDA cell lines in the presence or absence of 0.6 mM dThd, as well as minus/plus 1 μg/ml Dox in the case of *HD52*-dKO/*Tb*CDA parasites. (B and C) Growth percentage of *HD52*-dKO and *HD52*-dKO/*Tb*CDA cell lines in the presence or absence of 2 mM dCyd (B) and 2 mM 5M-dCyd (C), in combination with 1 μg/ml Dox in the case of *HD52*-dKO/*Tb*CDA parasites. dThd supplementation in *HD52*-deficient parasites is also plotted as a positive and negative control of growth in this cell line. (D) Expression profile of TbCDA determined by western blot analysis in extracts isolated at day 2 of the growth curve using polyclonal anti-TbCDA (TbCDA, 21.0 kDa) antibody. Anti-Tbβtubulin antibody (Tbβ-tubulin, 50.0 kDa) (Sigma) was used as loading control. *HD52*-dKO extracts corresponds to the cell line supplemented with 0.6 mM dThd.

D.1.4.2. The expansion of the dUMP pool supports thymidylate biosynthesis when TbHD52 is absent

It has been described that dUMP is a pivotal intermediate for *de novo* biosynthesis of dTTP in *T. brucei* (Leija *et al.* 2016; Valente *et al.* 2016). In mammalian cells, dUMP is mainly originated through deamination of dCMP by a deoxycytidine monophosphate deaminase (DCTD, EC3.5.4.12) (Bianchi *et al.* 1987). However, a DCTD activity has not been identified in trypanosomes, so dUMP synthesis could only come from dUrd phosphorylation via TK (Leija *et al.* 2016; Valente *et al.* 2016) and dUDP/dUTP hydrolysis by dUTPase (Castillo-Acosta *et al.* 2013). Thus, as previously described, high concentrations of dUrd could be able to sustain *TbHD52*-deficient parasites growth as it is converted to dUMP, the substrate for dTMP biosynthesis, via TK phosphorylation

We reasoned that if we provide an alternative source of dUMP, the need for dUrd formation via HD52 could be by-passed. We therefore introduced an inducible copy of human dCMP deaminase (*HsDCTD)* in BSF *HD52*-null mutants (*HD52*-dKO/*Hs*DCTD). Indeed, upon induction of the expression of HsDCTD, *HD52*-dKO/HsDCTD parasites exhibited normal proliferation in the absence of an extracellular source of dThd (Fig. D19 panel A). The construct was somehow leaky, as HsDCTD basal expression was detected at day 10 (Fig. D19 panel B). In conclusion, the provision of dUMP for further dTTP biosynthesis is able to compensate the lack of TbHD52 in *T. brucei*.
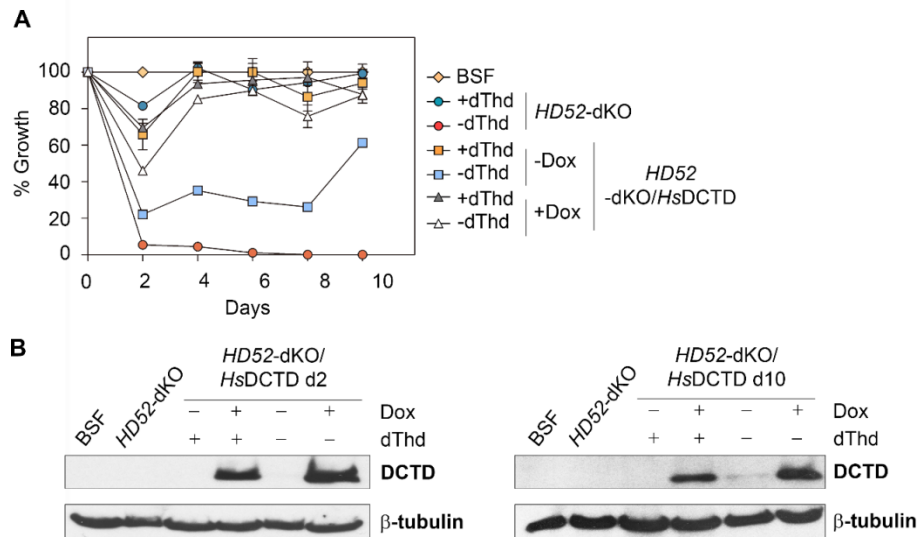
Figure D19. Expression of human dCMP deaminase reverts the *HD52*-dKO lethal phenotype in BSFs. (A) Parental lines and *HD52*-dKO, *HD52*-dKO/*Hs*DCTD   lines were grown in dThd-free HMI- medium for 10 days with or without different combinations of 1 µg/ml Dox and 0.6 mM dThd. Plot represents growth percentage compared to the BSF parental cell line. (B) HsDCTD levels were determined by western blot using monoclonal anti-HsDCTD (HsDCTD, 20.0 kDa) antibody (Santa Cruz Biotechnology) in cultures described in (A) isolated at day 2 or 10 of the growth curve. Anti-Tbβtubulin antibody (Tbβ-tubulin, 50.0 kDa) (Sigma) was used as loading control. *HD52*-dKO extracts correspond to the cell line supplemented with 0.6 mM dThd.

D.1.4.3. The essential role of TbHD52 is not related to purine metabolism

HsSAMHD1 exhibits dNTPase activity against the four canonical dNTPs (Goldstone *et al.* 2011; Powell *et al.* 2011; Ji *et al.* 2013; Zhu *et al.* 2015), therefore, we sought to assess whether purines are related to the essential function of TbHD52.

T. brucei, as other parasitic protozoa, cannot synthesize the purine ring *de novo* (Hammond and Gutteridge 1984; de Koning *et al.* 2005), and depends on salvage of an extracellular source of purines for growth. For this reason, HMI-9 medium contains 1 mM hypoxanthine, which cannot be removed without compromising cell viability. As previously indicated, *HD52*-dKO cells present severe growth defects even in the presence of hypoxanthine, yet we evaluated if modulating purine availability had any

impact on the proliferation of TbHD52 deficient parasites. Hence, *HD52*-null parasites were cultured in the presence of different purine nucleobase/nucleosides such as dAdo, dGuo, Ado and Guo. Purine supplementation was carried out in the absence of an extracellular pyrimidine source, as well as in combination with a low (0.1 mM) concentration of dThd. However, the lethal phenotype of TbHD52 lack was not rescued with any of the purines tested. In fact, combined supplementation of purine nucleobase/nucleosides with 0.1 mM dThd resulted to be more detrimental for cell growth than the addition of solely dThd (Fig. D20 panels A-D). Hence, although we cannot rule out that purine dNTPs are substrates of TbHD52, these results highlight that the pivotal role of TbHD52 is related to pyrimidine biosynthesis.
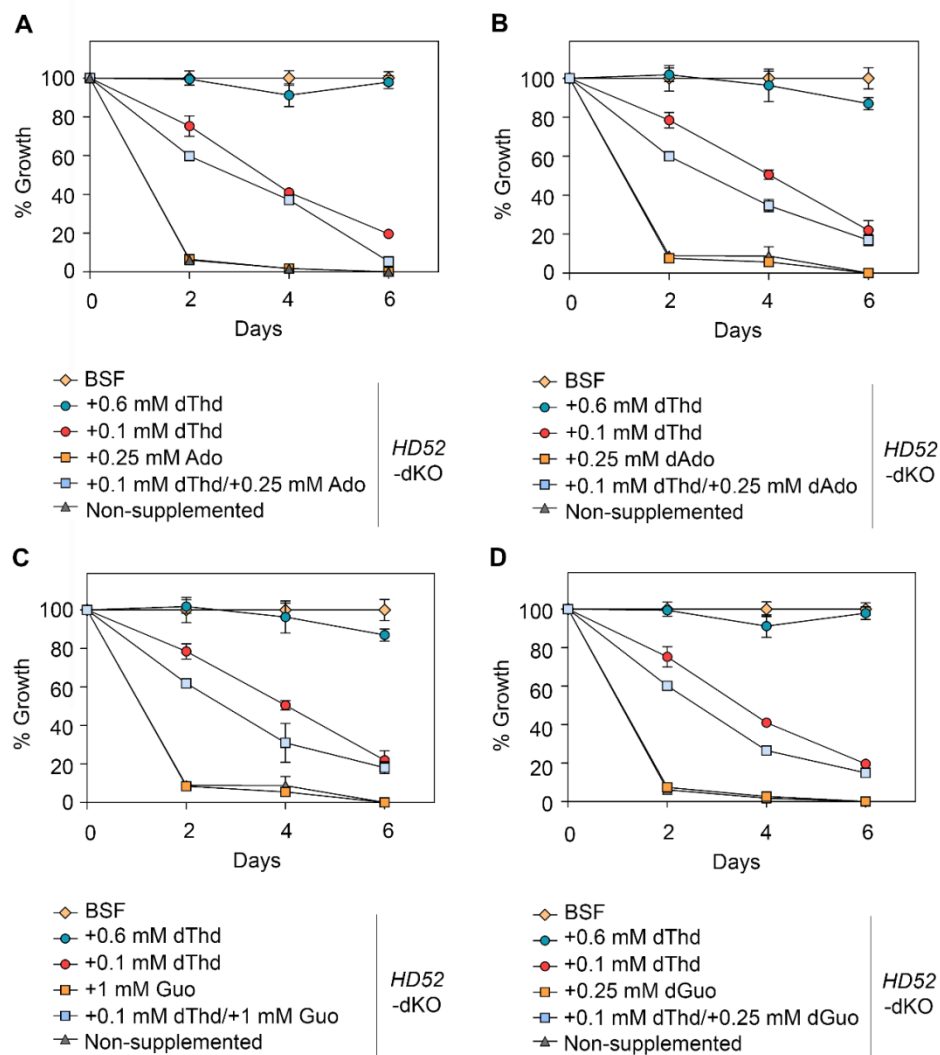
Figure D20. Effect of supplementation with purine nucleosides on BSF *HD52*-dKO cell growth. Cell proliferation was evaluated in parental cells and in *HD52*-dKO parasites cultured in dThd-free HMI- medium for 6 days. HD52-deficient cell lines were grown in the presence of either dThd (0.1 and 0.6 mM) or different purine nucleosides (0.25 mM Ado (A), 0.25 mM dAdo (B), 1 mM Guo (C) and 0.25 mM dGuo (D)). Growth rate was expressed as percentage compared to the parental cell line.

D.1.5. Role of TbHD52 in dNTP homeostasis and nucleotide metabolism in *Trypanosoma brucei*

D.1.5.1. dCTP and dTTP levels are altered in the absence of TbHD52

In line with the dNTPase activity of SAMHD1 and its role in the maintenance of dNTP levels (Mauney *et al.* 2017), several studies show how HsSAMHD1 depletion induces the expansion of the four canonical dNTP pools (Goldstone *et al.* 2011; Franzolin *et al.* 2013; Gramberg *et al.* 2013; Lahouassa *et al.* 2013). We therefore postulated that TbHD52 might have an important role in dNTP homeostasis also in *T. brucei*. Thus, first, dNTP levels were determined using a polymerase-based dNTP quantification assay.

In the presence of dThd, BSF *TbHD52*-null mutants exhibited an increase in dTTP associated to the high dThd concentration required for growing, whereas the other three dNTPs remained unaltered compared to parental parasites. Interestingly, we observed a 5-fold expansion of the dCTP pool and a statistically significant 1.6-fold reduction of dTTP in HD52-deficient parasites after dThd withdrawal for 24 hours. Remarkably, no significant alterations in purine dNTP pools were found in the absence of dThd (Fig. D21 panel A).

Nucleotide homeostasis involves a coordinated control of dNTP pools (Pai and Kearsey 2017), therefore, an imbalance in dTTP could lead to the perturbation of other dNTPs. In order to corroborate whether dCTP pools are expanded due to the intrinsic lack of TbHD52 and not to the retrieval of dThd, BSF parental cells were cultured for 7 days in the presence of a high concentrations of dThd, which was subsequently removed for 24 h. Indeed, while dThd supplementation results in the expansion of the dTTP pool, upon dThd removal, dTTP levels were restored, and dCTP levels were not

modified in control BSFs (Fig. D20 panel B). Thus, changes observed in dCTP and

dTTP are due to the absence of TbHD52.
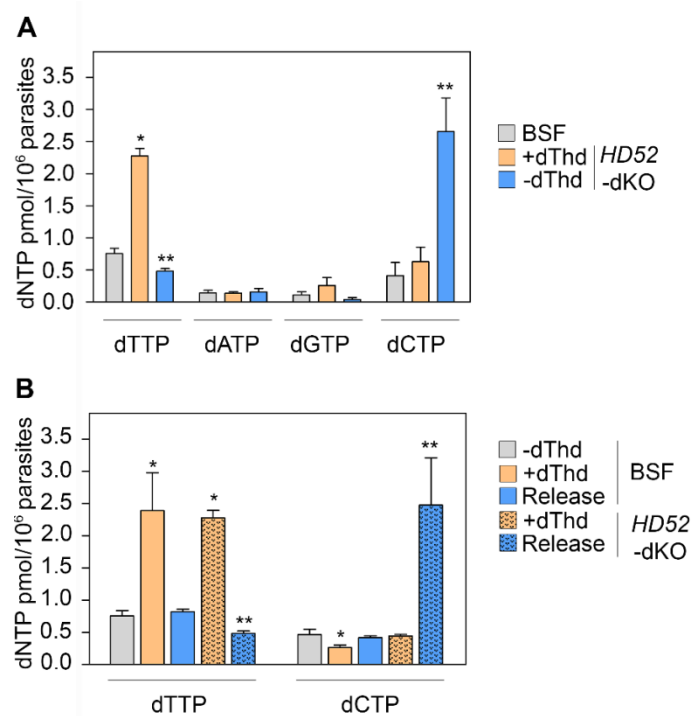
Figure D21. The *TbHD*52-dKO cell line exhibits expanded dCTP and reduced dTTP pools.
(A) *HD52*-dKO and BSF parental lines were grown in dThd-free HMI-9 medium with or without
0.6 mM dThd for 24 hours and cell extracts were collected for dNTP quantification using the
polymerase-based assay. (B) *HD52*-null parasites and BSF parental lines were cultured for 7 days in
dThd-free HMI-9 medium in the presence or absence of 0.6 mM dThd. dThd was withdrawn for 24 h and
dCTP and dTTP levels were measured. Bars represent mean ($\pm$S.D.) from three independent experiments.
The asterisks show significant differences calculated by the Student's t-test (n=3) *p<0.05, **p<0.01, *vs*
parental line non-supplemented.

D.1.5.2. The global metabolomic profile is disturbed in TbHD52-null parasites

In order to perform a more detailed study of the role of TbHD52 in nucleotide metabolism, we sought to determine global disturbances in the metabolomic profile of the *TbHD52*-dKO cell line. Hence, a dataset that comprises a total of 565 metabolites was obtained using different mass spectrometry methods.

The metabolomic profile of thymidine-supplemented TbHD52-null parasites was very similar to that of BSF parental cells. Thus, only a small number of changes were denoted, with 14 metabolites significantly altered, most of them derived from the expansion of dTTP (Fig. D22 panel A). Nonetheless, upon dThd withdrawal for 24 h, the profile was significantly perturbed; up to 230 metabolites were significantly altered compared to TbHD52-null parasites grown in the presence of dThd. Specifically, a series of nucleotide-related metabolites was significantly modified. Cytosine-derived metabolites were increased (Cyd (4-fold), Cyt (3-fold), dCMP (25-fold) and dCyd (50-fold)) while conversely dThd-derived metabolites were decreased (3, 7 and 10-fold decrease in dTMP, thymine and dThd, respectively). In addition, there was a significantly lower amount of Urd and 5-methyluridine. Certain purine metabolites in dThd-deprived cells such as IMP, GMP, dAMP, AMP and ADP were also diminished, suggesting significant crosstalk between purine and pyrimidine metabolism (Fig. D22 panel B).
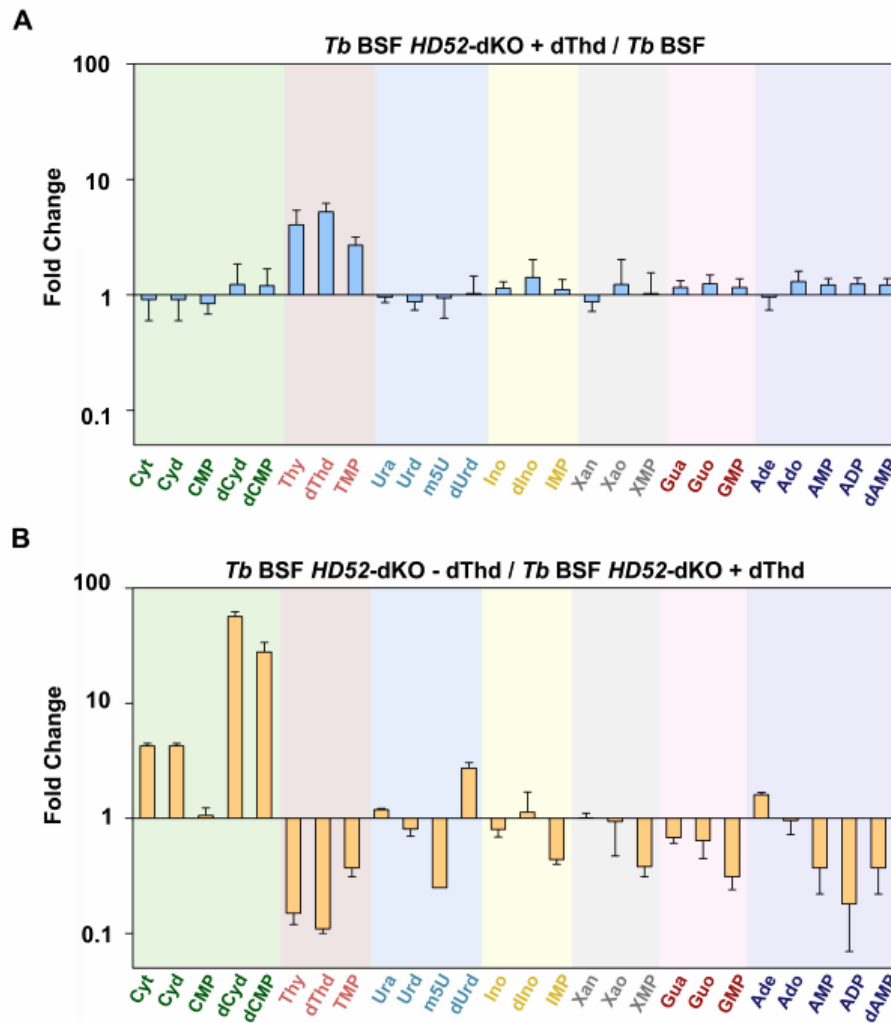
Figure D22. Nucleotide metabolism is perturbed in the absence of TbHD52. BSF parental lines and *HD52*-deficient parasites (with or without 0.6 mM dThd for 24 h) were cultured in dThd-free HMI-9 medium. Cell extracts were flash-frozen and metabolomic profiles were determined by mass spectrometry. (A) Fold change of disclosed metabolites involved in nucleotide metabolism in *TbHD52*-dKO grown in the presence of 0.6 mM dThd compared to the BSF parental line. (B) Relative quantification of nucleotide-derived metabolites detected in *HD52*-deficient parasites cultured for 24 h in the absence of dThd compared to the same cell line grown in the presence of dThd. Bars represent mean (±S.D.) from four independent biological replicates.

Other metabolites, some related to nucleotide metabolism, were also altered in the absence of TbHD52. Interestingly, different UDP sugars (involved in protein glycosylation) such as UDP-glucose, UDP-galactose and UDP-N-acetylglucosamine/galactosamine, were considerably reduced in the *TbHD52*-dKO cells upon withdrawal of dThd (Fig. D23 panel A).

On the other hand, several lipid classes increased in *TbHD52*-dKO parasites in the absence of dThd. Long chain fatty acids, polyunsaturated fatty acids, acyl carnitines, acyl cholines, lysophospholipids, and sphingomyelins (Fig. D23 panel B) were all augmented. Stress and apoptotic processes have been associated to an increase in cytoplasmic lipid formation (Taketo and Sonoshita 2002; Boren and Brindle 2012). Hence, the HD52-deficient cell line could be undergoing a stress response or cytotoxic phenotype which disturbs overall cell metabolism.
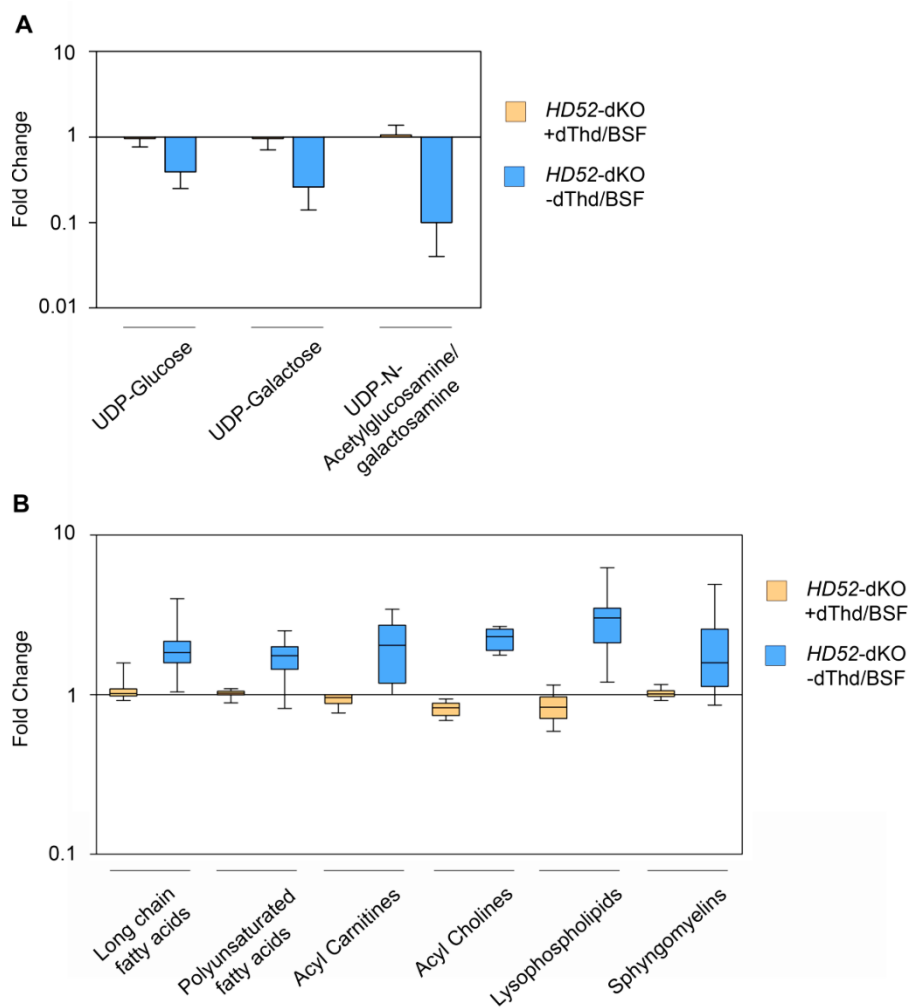
Figure D23. BSF *TbHD52*-null parasites exhibit an altered carbohydrate and lipidic profile in the absence of an extracellular source of dThd. *HD52*-dKO parasites were cultured in dThd-free HMI-9 medium for 24 h in the presence or absence of 0.6 mM dThd, and cell extracts were flash-freezed for metabolomics determination by mass spectrometry compared to parental cells. (A) Fold change of altered sugar metabolites detected in *TbHD52*-dKO compared to the parental line. (B) Box plot indicates the relative quantification of modified lipid metabolites, classified by classes related to BSF parental line. Data are obtained from four independent biological replicates. Bars represent mean (±S.D.), whereas in the box plot the line is the mean of the values, the box exhibits the interquartile range and whiskers correspond to the maximum and minimum values.

D.1.6. Coordinated regulation of the expression of enzymes involved in pyrimidine metabolism in *TbHD52*-null parasites

Taking into account the high plasticity of trypanosomes to circumvent a hostile situation, we sought to study the potential modulation of enzymes involved in pyrimidine metabolism in response to the absence of TbHD52. To this purpose, we analysed by western blot the expression of TbdUTPase, TbTK and TbHD82 in *Tb* BSF *HD52*-dKO cells in the presence or absence of dThd for 24 h. The rationale for selecting TbdUTPase was its possible role in dUMP formation from dUTP/dUDP hydrolysis, while TbTK is directly generating dTMP and dUMP for the salvage and *de novo* dTTP biosynthetic pathways. Finally, as TbHD82 is a HD domain-containing belonging to the same family as TbHD52, they may perform related functions.

No significant changes were observed in the levels of TbdUTPase and TbHD82 upon dThd withdrawal, whereas a 2-fold increase in TbTK was obtained (Fig. D24 panels A-C). It is possible that the increase in TbTK is destined to counteract dTTP-deficient biosynthesis in the absence of dThd.
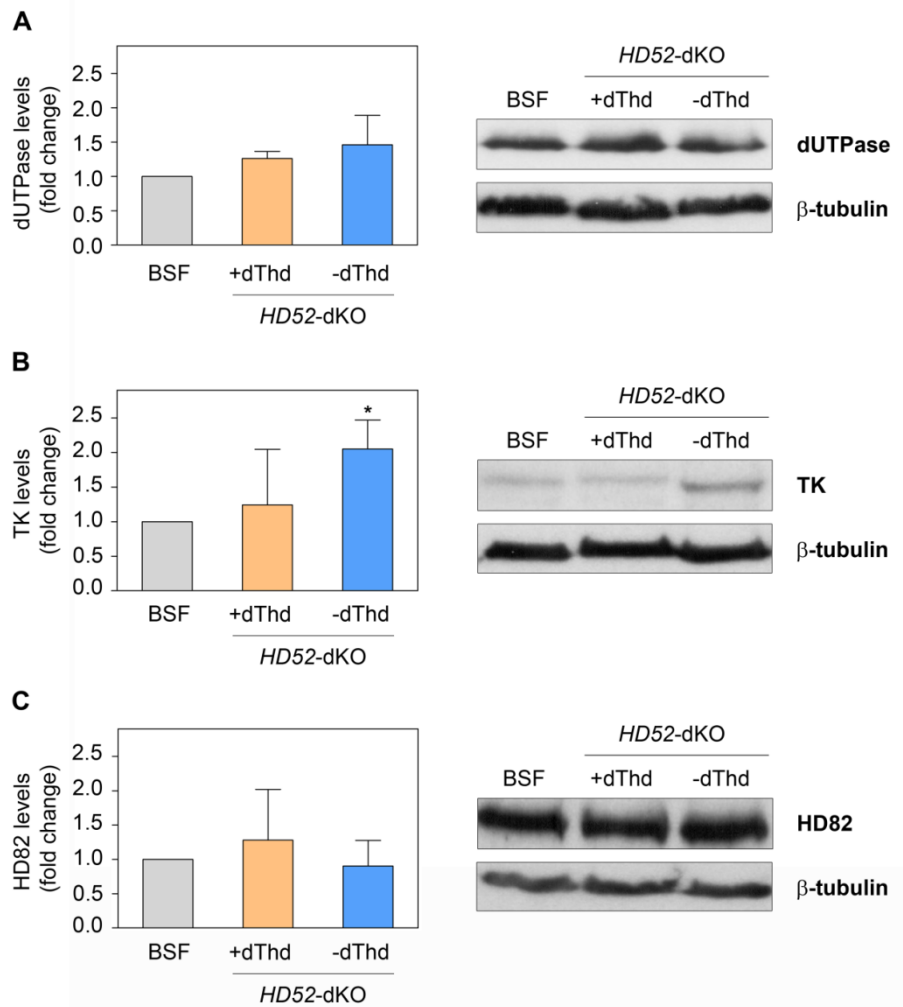
Figure D24. TbTK levels are increased in *Tb* BSF *HD52*-dKO parasites upon removal of extracellular dThd. *HD52*-null parasites were grown for 24 h with or without 0.6 mM dThd in dThd-free HMI-9 medium and protein extracts were isolated. The BSF parental line was also analysed. Levels of several enzymes involved in pyrimidine metabolism were measured by western blot using polyclonal anti-TbdUTPase (TbdUTPase, 34 kDa) antibody (A), polyclonal anti-TbTK (TbTK, 53 kDa) antibody (B) or polyclonal anti-TbHD82 (TbHD82, 81.73 kDa) antibody (C). Anti-Tbβtubulin antibody (Tbβ-tubulin, 50.0 kDa) (Sigma) was used as loading control. Fold changes are shown in the left panels, where bars indicate mean (±S.D.) from three independent replicates. Representative western blot images are shown in the right panels. Asterisks show significant differences calculated by the Student's t-test (n=3) *p<0.05, *vs* the parental line.

D.1.7. TbHD52 and genome integrity

DNA damage, such as double-strand breaks, elicits phenomena aimed at the activation of the DNA damage repair response. In this context, one of the earliest events is phosphorylation of trypanosomal histone H2A at Thr[130] (identified as trypanosomal γH2A), which is involved in both the DNA damage signalling cascade and cell cycle arrest. Therefore, quantification of nuclear γH2A foci has been established as a prominent repair marker (Glover and Horn 2012).

In order to investigate if the loss of cell viability in the *Tb* BSF *HD52*-dKO cell line is related to DNA damage, we monitored the presence of γH2A nuclear foci using an anti-TbγH2A antibody in *HD52*-null parasites and parental lines grown for 24 h in the presence or absence of dThd. First, we quantified the γH2A signal by flow cytometry, which evidenced an increased γH2A-positive population in *HD52*-deficient parasites in the absence of dThd (31.1% versus 21.0% in the parental line), while in dThd-supplemented cells values were similar to those observed in parental parasites (Fig. D25 panel A). These results were further corroborated by immunofluorescence microscopy. Thus, after quantification of more than 300 cells, an increased number of γH2A foci in *Tb* BSF *HD52*-dKO cells without dThd was established (34.0%) when compared to the parental line (19.7%) (Fig. D24 panels B and C). Hence, the lack of TbHD52 has detrimental consequences on DNA integrity and γH2A nuclear foci are increased upon activation of the DNA damage signalling response.
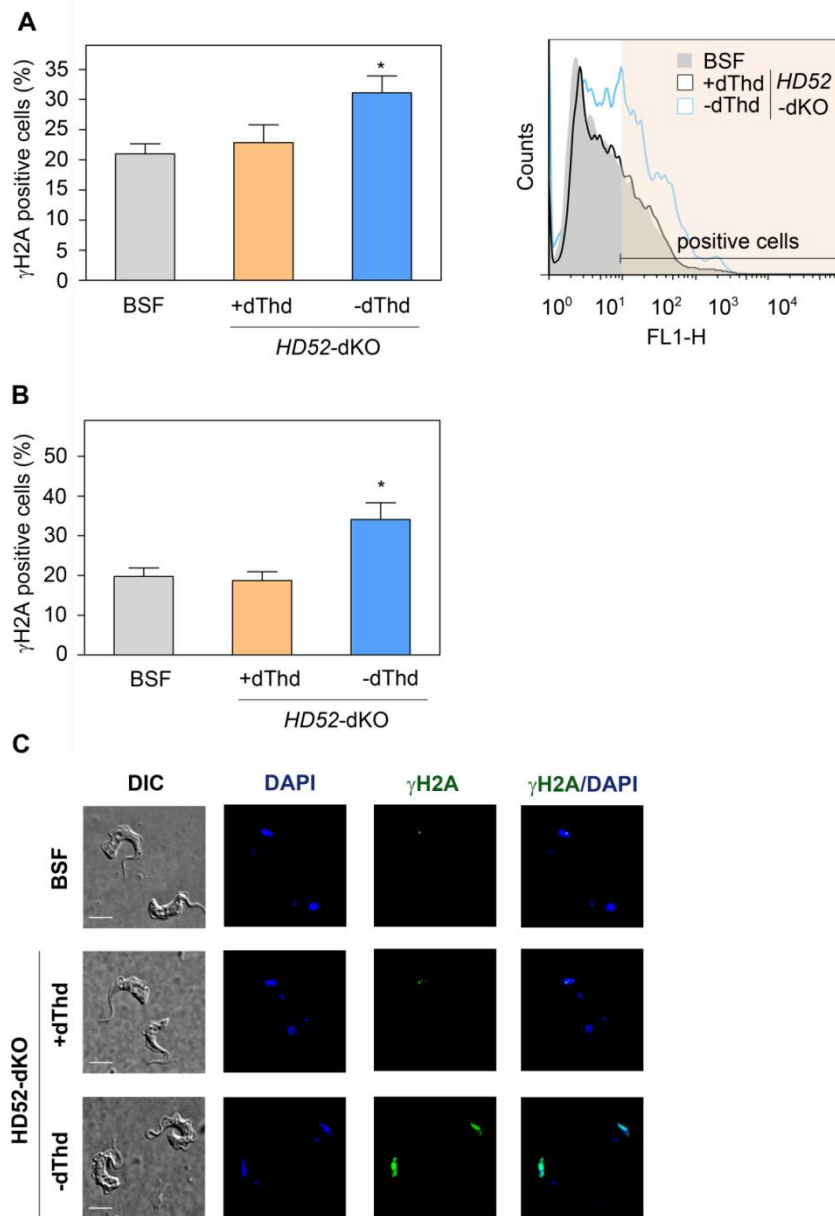
Figure D25. TbHD52 deficiency activates the γH2A-mediated DNA damage response. The quantification of γH2A foci was performed by immunofluorescence and flow cytometry in *HD52*-null parasites grown for 24 h in the presence or absence of 0.6 mM dThd and BSF parental cell lines, all cultured in dThd-free HMI-9 medium. (A) The left panel represents the percentage of γH2A positive cells, as determined by flow cytometry using an anti-TbγH2A antibody and an Alexa Fluor 488-conjugated anti-rabbit secondary antibody. The corresponding overlaid histogram of the different cell lines is shown in the right panel, where the red area indicates the γH2A-positive populations. (B) Percentage of γH2A positive cells quantified by immunofluorescence microscopy (n>300 for each condition). We considered positive cells those showing at least one nuclear γH2A focus. (C) Immunofluorescence microscopy images showing the representative γH2A stain for each condition. Nuclei and kinetoplasts were DAPI stained. Bars, 5 μm. Plots exhibit mean (±S.D.) from three independent replicates, and the asterisks show significant differences calculated by the Student's t-test. *p<0.01, *vs* parental line.

D.2. Evaluation of the participation of base excision repair in the response to oxidative stress in *Trypanosoma brucei*

We have shown that impairment of canonical nucleotide biosynthesis leads to severe DNA damage in *T. brucei*. In the second part of this work, we have completed a study on the occurrence of damage and non-canonical nucleotides, namely uracil, in DNA upon oxidative stress both *in vitro* and *in vivo*. Since the major pathway involved in removal of oxidized bases in DNA is BER, we have used a cell line deficient in the first enzyme involved in uracil repair, UNG, in order to explore the role of the BER pathway in oxidative defence.

While uracil is considered as deleterious when present in DNA, it is a frequent modification that may arise via two main processes: spontaneous or enzymatic cytosine deamination or dUTP misincorporation instead of dTTP during DNA replication. Since uracil can be highly mutagenic, removal is accomplished by the action of UNG, which as previously indicated is the first enzyme involved in the BER pathway (Schormann *et al.* 2014; Wallace 2014). Previous studies performed in the lab revealed the importance of UNG in *T. brucei*. UNG-defective parasites exhibited reduced infectivity *in vivo* and a hypermutator phenotype, as well as an increase in DNA fragmentation and enhanced sensitivity to oxidizing agents, such as hydrogen peroxide (Castillo-Acosta *et al.* 2012b). Taking into account the data already reported, here we were interested in characterizing uracil occurrence and DNA damage upon oxidative stress induced by NO or exposure to the host immune response during infection.

D.2.1. Determination of the occurrence of uracil upon *in vitro* and *in vivo* oxidative stress

D.2.1.1. Exposure to RNS induces an accumulation of uracil in DNA

NO is a highly reactive molecule that, in combination with oxygen, generates nitrous anhydride, which attacks amine groups, thiols, as well as other nucleophile molecules. Therefore, important oxidative and nitrosative stress arises as a consequence of exposure to NO, leading to diverse DNA damage such as strand breaks and base deamination and oxidation (Vasudevan and Thomas 2014). In this context, deamination of cytosine, guanine and adenine leads to uracil, xanthine and hypoxanthine formation, respectively, which in turn may generate mutagenesis and genomic instability if unrepaired (Caulfield *et al.* 1998). Previous work performed in the lab showed that cells treated with NO donors exhibited a 6.4-fold increase in the mutation rate (Fig. S1 panel A), specially characterized by the presence of large deletions, whereas UNG-deficient parasites exhibited NO-induced insertions and base substitutions at G:C pairs (Fig. S1 panel B), probably as a consequence of uracil resulting from cytosine deamination. It was therefore of interest to corroborate the presence of uracil, which cannot be repaired through the BER pathway in *UNG*-KO cells exposed to oxidative stress.

A

	PCF TK								PCF UNG-KO/TK			
	-DETA-NO[a]	-DETA-NO	+ DETA-NO (µM)				-DETA-NO[a]	-DETA-NO	+ DETA-NO (µM)			
			10	20	30	40			10	20	30	40
Initial number of trypanosomes, Ni	200	200	200	200	200	200	200	200	200	200	200	200
Final number of trypanosomes, Nf (10^5)	9.92	13.30	8.43	7.45	5.54	2.99	9.06	7.04	6.08	5.28	4.10	2.26
Total number of cell generations per culture, (Nf - Ni)/Ln 2 (10^6)	1.43	1.92	1.22	1.07	0.799	0.431	1.31	1.02	0.877	0.762	0.591	0.326
Number of experimental cultures	96	192	192	192	192	192	96	192	192	192	192	192
Cultures without growth	69	158	141	140	145	146	31	39	32	40	43	58
Proportion of wells without cell growth, P_0	0.72	0.82	0.73	0.73	0.76	0.76	0,16	0.2	0.17	0.21	0.22	0.30
Average number of mutants per culture, $m = -Ln\ P_0$	0.33	0.19	0.31	0.32	0.28	0.27	1.86	1.59	1.79	1.57	1.50	1.20
Mutation rate, m/total number of generations (cell/generation) (10^{-6})	0.23	0.10	0.25	0.29	0.35	0.64	1.42	1.57	2.04	2.06	2.53	3.67

B

Genotype	+ DETA-NO (40 µM)			- DETA-NO[a]		
	Mutation	Occurrence	Mutation rate (10^{-7})[b]	Mutation	Occurrence	Mutation rate (10^{-7})[b]
PCF TK	(−1) deletion	2/24(8%)	0.50 [5.5][d]	(−1) deletion	1/23 (4%)	0.09
	deletions	11/24(46%)	2.92 [13.9][d]	deletions	2/23 (9%)	0.21
	(+1) insertion	1/24(4%)	0.25	(+1) insertion	3/23 (13%)	0.31
	insertions	1/24(4%)	0.25	insertions	2/23 (9%)	0.20
	GC → AT	3/24(12%)	0.76	GC → AT	7/23 (30%)	0.69
	GC → TA	2/24(8%)	0.50	GC → TA	4/23 (17%)	0.41
	GC → CG	1/24(4%)	0.25	GC → CG	3/23 (13%)	0.31
	AT → CG	2/24(8%)	0.50 [5.6][d]	AT → CG	1/23 (4%)	0.09
	AT → GC	1/24(4%)	0.25	AT → GC	–	–
PCF UNG-KO/TK	(−1) deletion	1/51(2%)	0.7 [1.4][c]	(−1) deletion	1/24 (4%)	0.57
	deletions	–	–	deletions	1/24 (4%)	0.57
	(+1) insertion	4/51(8%)	2.9 [11.6] [c][2.5][d]	(+1) insertion	2/24 (8%)	1.14
	insertions	14/51(27%)	9.9 [39.6] [c][4.1][d]	insertions	4/24 (17%)	2.41[12.1][c]
	GC → AT	21/51(41%)	15.0 [19.7] [c][2.5][d]	GC → AT	10/24 (42%)	6.00 [8.7][c]
	GC → TA	4/51(8%)	2.9 [5.8][c]	GC → TA	5/24 (21%)	3.00
	GC → CG	3/51(6%)	2.2 [8.8] [c][3.8][d]	GC → CG	1/24 (4%)	0.57
	AT → CG	2/51(4%)	1.5 [3.0][c]	AT → CG	–	–
	AT → TA	2/51(4%)	1.5 [6.0][c]	AT → TA	–	–

Figure S1. Mutation rate and spectra performed in PCF and UNG-KO cell lines exposed to NO donors. (A) Experimental data for the Luria–Delbrück fluctuation analysis of reversion in TK transformed trypanosome lines. The mutation rate to ganciclovir resistance for HSV-1 TK transfectants was calculated using the Luria–Delbrück fluctuation test equation. (B) Spectra of Herpes simplex virus TK gene mutations. *a* Mutation rate and spectra for parental PCF and UNG-KO trypanosomes in the absence of DETA-NO obtained in previous studies (Castillo-Acosta *et al.* 2012b). *b* Mutation rates are the product of the proportion of a mutation specific class and the total mutation rate for each strain. In this experiment, the overall mutation rates for procyclic forms of parental and UNG-KO strains exposed to 40 µM DETA-NO were $0.635 \cdot 10^{-6}$ and $3.67 \cdot 10^{-6}$ per cell generation, respectively. *c* Number in brackets is the fold induction of a specific class of mutation relative to the corresponding parental line. *d* Number in brackets is the fold induction of a specific class of mutation upon exposure to DETA-NO relative to the corresponding untreated cell line. Figures from PhD thesis entitled "Descifrando el papel de la endonucleasa V en el metabolismo de ácidos nucleicos de *Trypanosoma brucei*". Daniel García-Caballero, 2017.

To this purpose, parental and UNG-deficient cells were subjected to 48 h incubation with the diethylenetriamine/nitric oxide adduct (DETA-NO) as NO donor. UNG-deficient cells expressing an inducible ectopic copy of UNG were also included in the study. The EC_{50} (half maximal effective concentrations) value of DETA-NO in *T. brucei* was formerly established as 25 μM (Fig. S2), so both the EC_{50} and an intermediate concentration (25 and 10 μM DETA-NO, respectively) were selected.
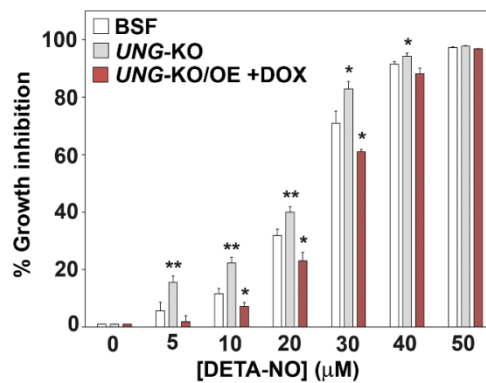
Figure S2. Sensitivity to DETA-NO exposure. Effect of NO treatment on cell growth of trypanosomes exposed to different concentrations of DETA-NO for 48 h. Inhibition of proliferation was calculated with respect to the number of parasites determined in the absence of NO donors for each cell line. The asterisks show significant differences calculated by the Student's t-test. *$p < 0.05$, **$p < 0.01$, *vs* the BSF parental cell line. Data obtained from studies conducted by Fernando Aguilar Pereyra and reported in the PhD thesis entitled "Establecimiento del papel del uracilo en la integridad genómica y la infectividad en *Trypanosoma brucei*", 2014.

For uracil determination we employed a qPCR method that relies on the different uracil processivity of the *Pyrococcus furiosus* (Pfu) and *Thermophilus aquaticus* (Taq) B-type DNA polymerases during DNA replication, since *Pfu* DNA polymerase irreversibly binds to uracil residues whereas Taq DNA polymerase is able to replicate DNA regardless of uracil content. Thus, differences in DNA replication may be correlated to the uracil content in the DNA sample (Horvath and Vertessy 2010). Nevertheless, the technique presents a pitfall to take into account, as other lesions such

as abasic sites or hypoxanthine may also affect processivity of both polymerases, influencing the uracil measurement (Gruz *et al.* 2003; Heyn *et al.* 2010). Therefore, results are not referred to as "uracil content" but as "Pfu sensitive sites". It should be also noted that the procedure provides a relative quantification compared to a uracil-free sample. In our experiments, we considered untreated parental BSF cells as the uracil zero-content sample and the quantifications were related to this control.

The study revealed that untreated *UNG*-KO cells contain a higher number of Pfu sensitive sites in DNA compared to parental BSF parasites, thus corroborating the pivotal role of UNG in uracil removal. Unexpectedly, Pfu sensitive sites were not restored to basal levels in *UNG-KO*-overexpressing cells, which exhibited a similar content than *UNG*-null parasites (Fig. D26 panel A). The *UNG*-KO/OE Pfu sensitive sites may correspond to unrepaired abasic sites, as previous studies have demonstrated that UNG overexpression promotes UNG binding to abasic sites, which results in impaired access of the BER machinery to the resultant abasic sites and eventually block of the BER pathway (Elder *et al.* 2003). Western blot analysis confirmed the absence or overexpression of UNG (Fig. D26 panel B) and demonstrated that the amount of protein in overexpressing cells was approximately 6-fold than detected in parental BSFs. NO treatment gave rise to a significant increase in Pfu sensitive sites, in both parental and *UNG*-KO cells, probably due to the presence of uracil generated by NO-mediated cytosine deamination. The amount of Pfu sensitive sites in *UNG*-KO/OE cells was not modified after NO exposure, highlighting the protective role of the enzyme against oxidative stress (Fig. D26 panel A).
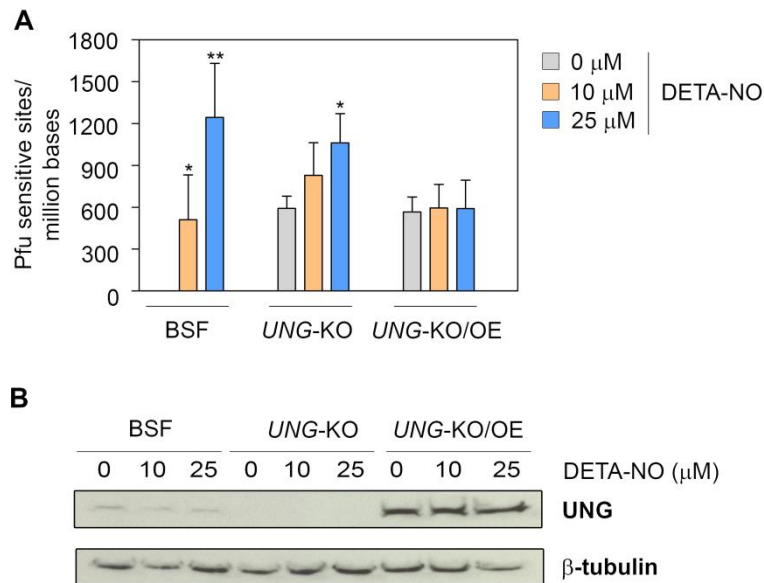
Figure D26. Effect of DETA-NO treatment on the Pfu-sensitive site content in BSFs. *UNG-KO*, *UNG*-KO/OE and parental cell lines were exposed to different concentrations of DETA-NO (0, 10 and 25 μM) for 48 h, and subsequently DNA and proteins were isolated from the cell extracts. (A) Determination of Pfu sensitive sites content in DNA by qPCR using Pfu and Taq polymerases. All values are referred to the untreated BSF cell line considered as control. Bars exhibit the mean (±S.D.) of at least three independent experiments with duplicated determinations. The asterisks show significant differences calculated by the Student's t-test. *$p<0.01$, **$p<0.001$ *vs* the corresponding non-treated cell line. (B) Representative western blot showing TbUNG levels using polyclonal anti-TbUNG (TbUNG, 32 kDa) antibody. Anti-Tbβtubulin antibody (Tbβ-tubulin, 50.0 kDa) (Sigma) was used as loading control.

D.2.1.2. Pfu sensitive sites increase during murine infection

During infection, parasites are highly exposed to NO and oxidative stress (Sternberg *et al.* 1998; Keita *et al.* 2000; MacLean *et al.* 2001) as a result of the host early innate immune response. NO is synthesized early in infection by macrophages (Hibbs *et al.* 1988; Marletta *et al.* 1988), thereby contributing to oxidative stress. In previous studies conducted by Castillo-Acosta *et al.*, it was demonstrated that UNG-defective trypanosomes presented reduced infectivity, which was characterized by

a parasitaemia clearance at day 5 post-infection and an expanded life-span compared to parental BSF parasites (10 days *vs* 5 days) (Castillo-Acosta *et al.* 2012b). The parasitaemia peak in UNG-defective parasites coincides with an abrupt increase in RNS levels (Fig. S3). Taking into consideration this data, we analysed the impact of infection on DNA uracil content (Pfu senstive sties) in *T. brucei*.
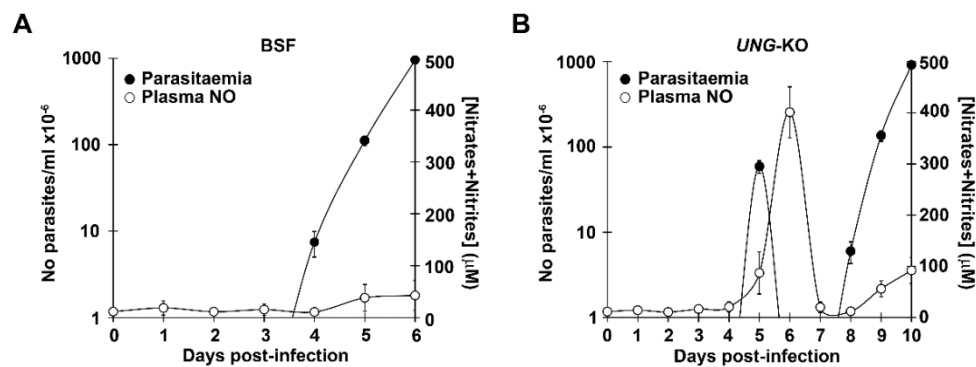
Figure S3. Parasitaemia and nitric oxide levels in mice infected with *T. brucei*. Mice were infected with 4,800 parasites of the following cell lines: parental BSF (A) and UNG-KO (B). Parasitaemia and nitric oxide (nitrates+nitrites) levels were monitored every 24 h. Data from studies conducted by Fernando Aguilar Pereyra and reported in the PhD thesis entitled "Establecimiento del papel del uracilo en la integridad genómica y la infectividad en *Trypanosoma brucei*", 2014.

To this end, mice were infected with 4,800 *UNG*-KO or parental BSF trypanosomes, and parasites were isolated at 5 or 10 days *post-infection*. Pfu sensitive sites were measured by RT-qPCR in genomic DNA samples coming from parasites cultured *in vitro* as well as from *in vivo* infection. The uracil zero-content considered in this experiment was the sample corresponding to the parental BSF cell line cultured *in vitro*. We observed an increased content in Pfu sensitive sites in all cell lines recovered from mice (Fig. D27 panel A). In addition, at day 10 *post-infection* parasites exhibited a reduced number of Pfu sensitive sites, observation that correlated with

enhanced virulence and lower concentration of nitric oxide derivatives in mice blood (Fig. S3). Western blot analysis was performed in order to confirm the *UNG*-KO genotype (Fig. D27 panel B). These results corroborate that parasites are exposed to intense oxidative stress during murine infection, which leads to the accumulation of significant lesions in DNA.
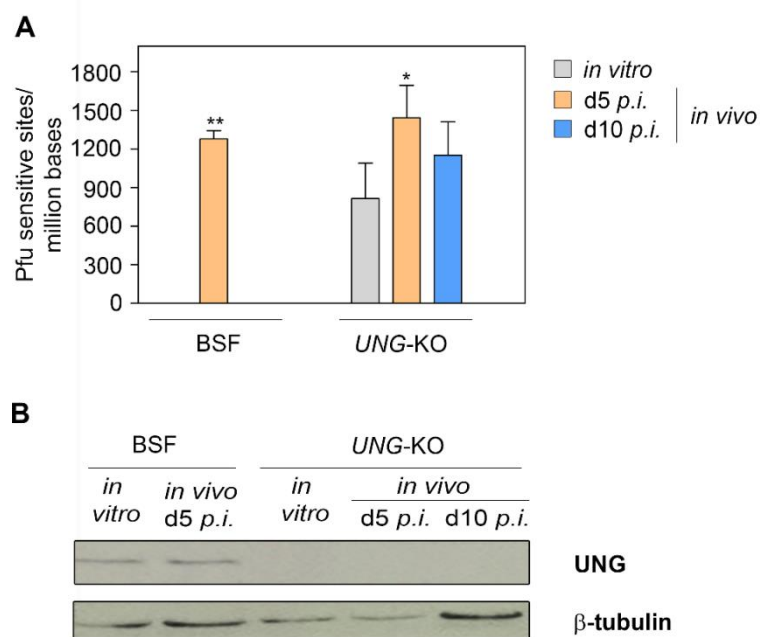
Figure D27. BSF parental and *UNG*-KO parasites show higher content in uracil and Pfu sensitive sites in DNA during infection. Mice were infected with 4,800 parasites of *UNG*-KO and parental lines, and parasites were isolated at 5 or 10 days *post-infection* (d5 *p.i.* and d10 *p.i.,* respectively) for DNA and protein extraction. (A) Relative quantification of Pfu sensitive sites by RT-qPCR in genomic DNA from parasites isolated after murine infection as well as trypanosomes cultured *in vitro*. All values are normalized with regard to the *in vitro* BSF cell line considered as the control sample. Plots show the mean (±S.D.) of parasites from at least four infected mice. The asterisks show significant differences calculated by the Student's t-test. *p<0.05, **p<0.001 *vs* the corresponding cell line cultured *in vitro*. (B) Illustrative western blot analysis of TbUNG expression in parasites cultured *in vitro* or after murine infection using polyclonal anti-TbUNG (TbUNG, 32 kDa) antibody. Anti-Tbβtubulin antibody (Tbβ-tubulin, 50.0 kDa) (Sigma) was used as loading control.

D.2.2. UNG-deficient parasites exhibit a lower content in abasic sites in response to oxidative stress

AP sites are the most common lesions in DNA (Lindahl 1993). They are highly cytotoxic and mutagenic if unrepaired, by causing both blockage of the replication fork or incorrect incorporation of nucleotides (Loeb and Preston 1986; Abbotts and Wilson 2017). The assay used to quantify Pfu sensitive sites has been previously described as a specific methodology of uracil quantification (Horvath and Vertessy 2010) based on the fact that the archaeal DNA polymerase from *Pyrococcus furiosus* stalls on uracil-containing templates. However, Pfu polymerase activity is also reduced by the occurrence of abasic sites. Pfu terminates the extension before the site, while all other polymerases extend one or a few bases across the site before terminating (Gruz *et al.* 2003; Heyn *et al.* 2010).

AP sites were therefore quantified in DNA samples from parasites exposed *in vitro* to increasing concentrations of DETA-NO and in BSFs isolated from *in vivo* infection (Fig. D28) and were slightly increased in UNG overexpressing cells and significantly enhanced in UNG-deficient parasites (Fig. D28). Strikingly, upon oxidative stress, UNG-KO cells showed a progressive reduction in AP sites (Fig. D28), probably due to the occurrence of single-strand and double-strand breaks which have been shown to appear upon AP site formation (Kuzminov 2001; Boiteux and Guillet 2004).
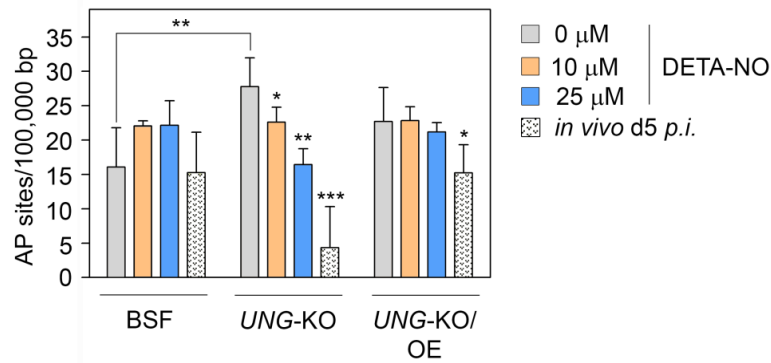
Figure D28. Determination of abasic sites in *UNG*-KO, *UNG*-KO/OE and parental BSF parasites exposed either *in vitro* or *in vivo* to oxidative stress. Estimation of AP sites *per* 100,000 base pairs generated in *UNG*-KO, *UNG*-KO/OE and parental lines treated *in vitro* with increasing concentrations of DETA-NO (0, 10 and 25 μM) for 48 h, as well as in parasites isolated from mice after 5 days of infection (*in vivo* d5 *p.i.*). DNA was extracted and abasic sites were quantified using Oxiselect DNA Damage Quantitation Kit (AP sites). Plot refers to the mean (±S.D.) of three independent experiments. The asterisks show significant differences calculated by the Student's t-test. *p<0.05, **p<0.01, ***p<0.001 *vs* the corresponding non-treated cell line cultured *in vitro*.

D.2.3. Determination of the impact of oxidative stress on DNA damage

D.2.3.1. DETA-NO exposure triggers the activation of the DNA damage response

Preceding studies demonstrated a meaningful DNA fragmentation in *UNG*-KO parasites, which was enhanced after exposure to NO (Fig. S4). Given this information and the significant accumulation of uracil and AP sites in DNA, we sought to evaluate the activation of the DNA damage response against oxidative stress.
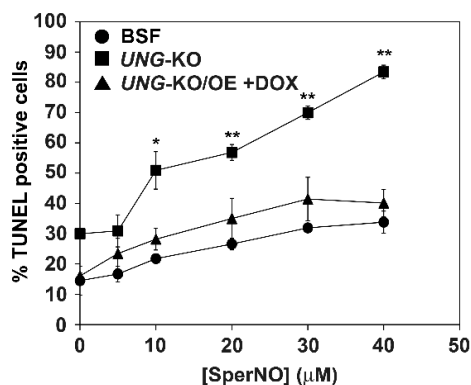
Figure S4. Fragmentation of DNA in parasites exposed to increasing concentrations of Spermine-NO. Parasites were exposed to increasing concentrations of Spermine-NO and TUNEL positive cells were determined by TUNEL labelling and FACS analysis. The asterisks show significant differences calculated by the Student's t-test. *p < 0.05, **p < 0.01, *versus* the BSF parental cell line. Data are presented as the mean (±S.D.) of two independent experiments where determinations were performed in triplicate. Figures obtained from experiments conducted by Fernando Aguilar Pereyra and reported in the PhD thesis entitled "Establecimiento del papel del uracilo en la integridad genómica y la infectividad en *Trypanosoma brucei*", 2014.

To this purpose, an immunofluorescence analysis was performed in cells exposed to the EC_{50} concentration of DETA-NO using the anti-TbɣH2A antibody. Positive cells were considered as those that showed at least one nuclear ɣH2A focus, and the percentage of ɣH2A-positive cells was obtained by counting more than 300 cells per sample. *UNG*-KO and *UNG*-KO/OE cells exhibited a higher basal proportion of ɣH2A-positive cells compared to the parental BSF cells. DETA-NO treatment led to the activation of the ɣH2A repair pathway, both in *UNG*-KO and parental BSF parasites, yet no significant effect was observed in the UNG overexpressing cell line (Fig. D29 panel A). As aforementioned, UNG overexpression may cause detrimental non-specific binding that could trigger DNA repair signalling, yet it could also confer protection to additional damage from oxidizing agents. On the other hand, it has been reported that the number of phosphorylated ɣH2A molecules is proportional to the level of damage (Rogakou *et al.* 1998). Thus, we decided to

distinguish different γH2A populations according to the amount of nuclear foci or staining observed. This categorization revealed significant γH2A signal of the whole nucleus in UNG-null parasites, which indicated massive DNA damage in this cell line. On the other hand, while the percentage of γH2A-positive cells in untreated *UNG*-KO/OE parasites was similar to *UNG*-KO trypanosomes, the intensity of γH2A stain was somehow different, being less pronounced in overexpressing cells (Fig. D29 panels B and C). In conclusion, these results suggest that NO exposure gives rise to important DNA lesions that require the involvement of the BER pathway to be correctly repaired.
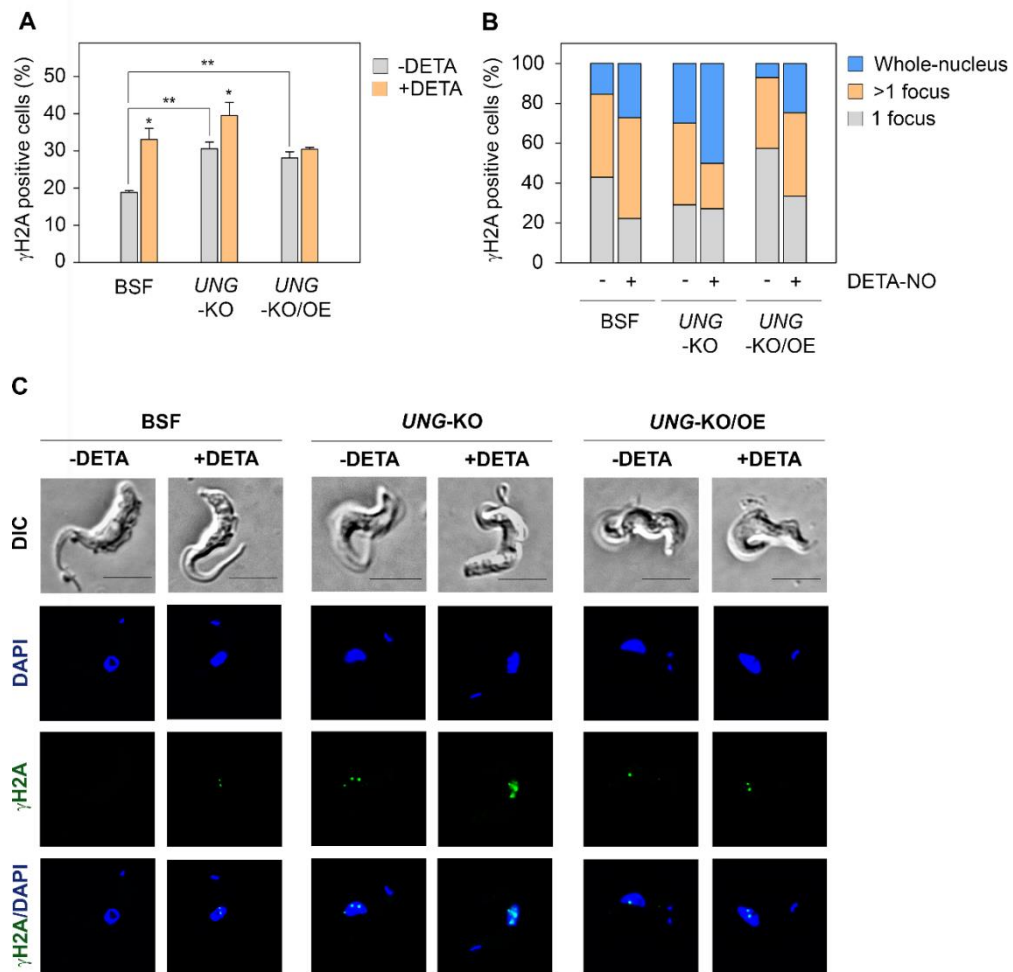
Figure D29. Analysis of DNA damage in *UNG*-KO, UNG-KO/OE and parental BSF parasites exposed to *in vitro* oxidative stress. *UNG-KO*, *UNG*-KO/OE and parental BSF parasites were cultured in the absence (-DETA) or presence of 25 µM DETA-NO (+DETA). After 48 h, the ɣH2A signal was determined by immunofluorescence analysis using the anti-TbɣH2A antibody and Alexa Fluor® 488–conjugated anti-rabbit secondary antibody. (A) Percentage of ɣH2A positive cells measured by immunofluorescence microscopy. Positive cells were considered those showing at least one nuclear ɣH2A focus (n>300 for each condition). (B) Percentage of positive cells showing distinct ɣH2A staining, classified as whole-nucleus staining, a single focus or more than one focus (n>300 for each condition). (C) Immunofluorescence microscopy images showing representative ɣH2A staining under each condition. Nuclei and kinetoplasts were DAPI stained (blue). Bars, 5 µm. Plots exhibit mean (±S.D.) from three independent replicates, and the asterisks show significant differences calculated by the Student's t-test. *p<0.05, **p<0.01 *vs* the corresponding untreated cell line.

D.2.3.2. The immune response during murine infection induces DNA damage in T. brucei

In order to identify the activation of DNA repair mechanisms during infection *in vivo*, ɣH2A staining was measured using the anti-TbɣH2A antibody by immunofluorescence analysis in parasites recovered from mice blood. To this purpose, mice were infected with 4,800 *UNG*-KO or parental cells and parasites were isolated 5 or 10 days *p.i.* Positive cells exhibiting DNA damage were considered those with at least one nuclear ɣH2A focus. Thus, number of ɣH2A-positive cells at 5 days *p.i.* was notably increased both in UNG-deficient and parental cells compared to the corresponding parasites cultured *in vitro* (Fig. D30 panel A). However, after parasite clearance at day 10 *p.i.*, UNG-null trypanosomes exhibited similar levels of γH2A than those cultured *in vitro*. Whole-nucleus staining was prevalent in parasites collected during *in vivo* infection (Fig. D30 panel B and C), suggesting that upon exposure to the primary immune response, significant DNA damage is inflicted upon BSFs.
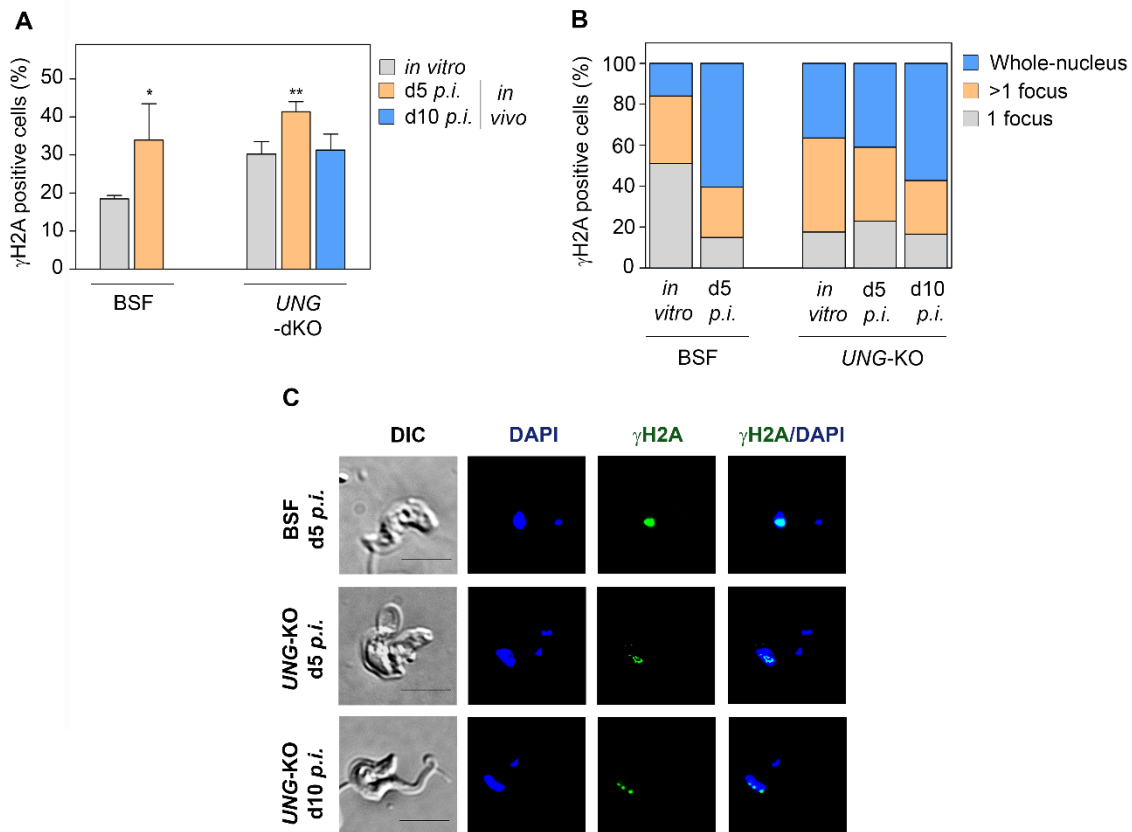
Figure D30. ɣH2A activation in *T. brucei* is promoted during murine infection. Mice were infected with 4,800 parental and *UNG*-KO trypanosomes and parasites were isolated at 5 or 10 days *p.i.* ɣH2A positive cells were quantified by immunofluorescence analysis in parasites isolated from murine infection (*in vivo*) as well as in parasites cultured *in vitro* using the anti-TbɣH2A antibody and Alexa Fluor® 488–conjugated anti-rabbit secondary antibody. (A) Graph displays the percentage of ɣH2A positive cells. At least one nuclear ɣH2A focus was present in positive cells (n>300 for each condition). (B) Percentage of positive cells showing distinct ɣH2A stain, categorized as whole-nucleus staining, a single focus or more than one focus (n>300 for each condition). (C) Representative immunofluorescence microscopy images showing ɣH2A stain at each cell line isolated from mice infection. Nuclei and kinetoplasts were stained with DAPI (blue). Bars, 5 µm. Plots represent mean (±S.D.) from three independent replicates, and the asterisks denote significant differences calculated by the Student's t-test. *p<0.05, **p<0.01 *vs* corresponding *in vitro* cell line.

D.2.4. Contribution of NO to DNA damage produced during murine infection

Considering previous results, we sought to investigate whether NO released during infection was contributing directly to damage. To this purpose, we specifically inhibited the production of NO by macrophages in mice and analysed the consequences on virulence and DNA damage.

NO is produced in the mammalian host by several isoforms of the NOS, yet macrophages only express iNOS (Stuehr *et al.* 1991; Panaro *et al.* 2003). While several NOS inhibitors exist, we administered mice AG, which is able to selectively inhibit iNOS (Griffiths *et al.* 1993; Misko *et al.* 1993), preventing the release of NO.

D.2.4.1. Effect of aminoguanidine on NO levels and parasitaemia

In order to inhibit murine iNOS, mice were treated with AG 2.5% in drinking water, which was replaced every two days. Infection of mice was performed with 4,800 UNG-null and parental parasites, and NO levels and parasitaemia were evaluated. Determination of NO derivatives (NO_2 and NO_3) corroborated the effectiveness of AG, as all treated mice exhibited a significant drop in NO derived species. In the case of parental trypanosomes, the reduction was less evident since NO levels were *per se* lower (Fig. D31 panel A) than in *UNG*-KO parasites (Fig. D31 panel B).

The inhibition of NO synthesis has been previously studied in mice infected with *T. brucei* (Millar *et al.* 1999) (Sternberg *et al.* 1994). Thus, the observation that AG-mediated NO inhibition controlled parasitaemia and extended the life span of mice both in *UNG*-KO and parental trypanosomes agrees with previous observations (Fig. D31 panels C and D).
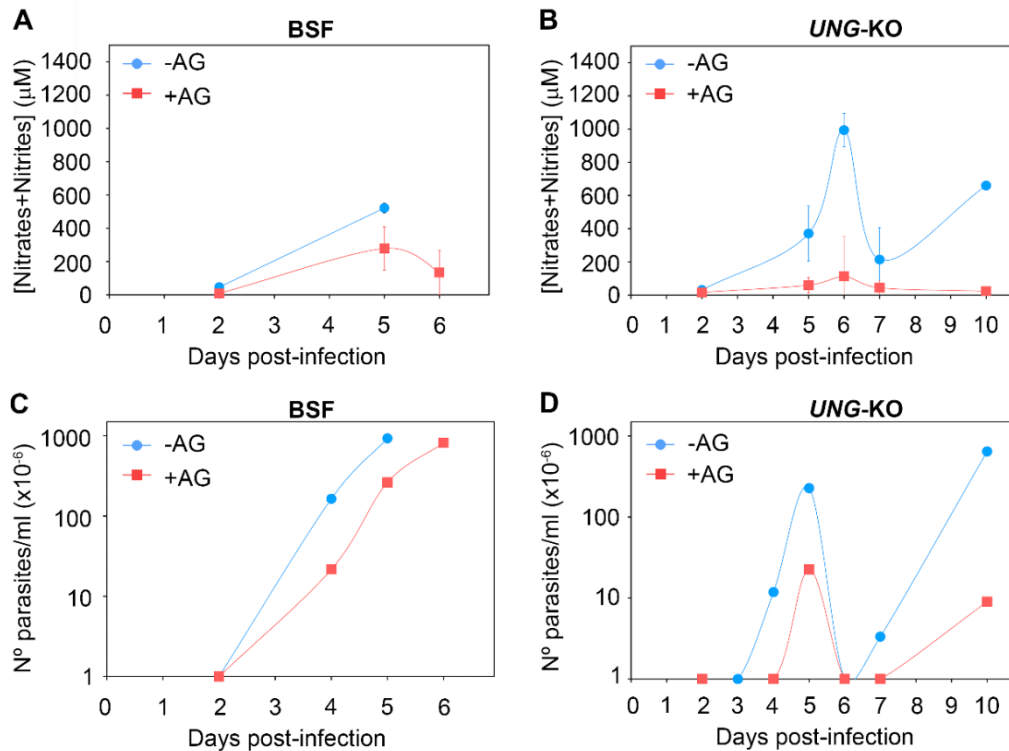
Figure D31. Evaluation of parasitaemia and nitric oxide levels upon aminoguanidine treatment in mice infected with *UNG*-KO and parental parasites. Mice were infected with 4,800 *UNG*-KO and parental trypanosomes and 2.5% aminoguanidine (AG) was added to the drinking water. Nitric oxide (nitrates+nitrites) levels (±S.D.) (A and B) and parasitaemia (C and D) were monitored during the time course of infection. At least four infected mice per condition were used in the study.

D.2.4.2. *Aminoguanidine treatment has no impact on γH2A activation during murine infection*

The occurrence of repair foci was also investigated upon 2.5% AG administration to mice infected with 4,800 *UNG*-null and parental parasites. γH2A signal determination was evaluated by immunofluorescence analysis using the anti-TbγH2A antibody. However, no significant differences were observed in γH2A-positive parasites isolated from AG-treated mice compared to the untreated condition (Fig. D32). Hence, NO is probably not solely responsible for DNA damage in parasites during infection.
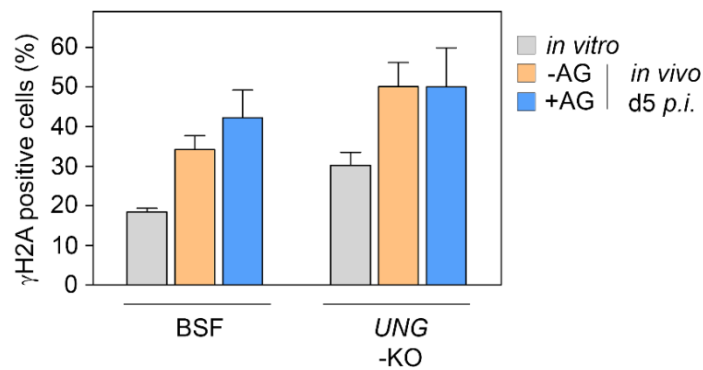
Figure D32. ɣH2A foci determination in *UNG*-KO and parental parasites recovered from mice after aminoguanidine-mediated iNOS inhibition. Mice were infected with 4,800 *UNG*-KO and parental parasites and 2.5% AG was administered in the drinking water. Parasites were isolated at 5 days *p.i.* and immunofluorescence analysis was performed using an anti-ɣH2A antibody and Alexa Fluor® 488-conjugated anti-rabbit secondary antibody. The corresponding cell lines cultured *in vitro* were also subjected to immunofluorescence analysis as a control. Percentage of ɣH2A positive cells was determined considering that at least one nuclear ɣH2A focus was present in positive cells (n>300 for each condition). Graph represent the mean (±S.D.) corresponding to four infected mice per condition (*in vivo*) or three independent replicates (*in vitro*).

DISCUSSION

E. DISCUSSION

Human African Trypanosomiasis is a neglected tropical disease that has led to severe epidemics throughout history. While the number of cases has been considerably reduced, current treatments are still highly toxic, and an additional handicap is the development of drug resistance (Buscher *et al.* 2017). The identification of new drug targets to improve therapies for the disease remains a research priority.

Since balanced dNTP levels are necessary for correct DNA replication and repair, the components of nucleotide metabolism represent a meaningful source of therapeutic drug targets. Due to the importance of nucleotide metabolism in the preservation of correct cell proliferation, the use of nucleoside analogs is being currently exploited for the development of antibiotics, antivirals and cancer therapies. Indeed, the Food and Drug Administration (FDA) has approved in recent years the use of 15 nucleoside analogs against several types of cancer (Shelton *et al.* 2016).

dNTPs are susceptible to diverse modifications induced by both endogenous and exogenous agents, which may lead to potential cytotoxicity when incorporated during replication. To circumvent this, the cell is endowed with multiple DNA repair pathways as well as "housecleaning" enzymes that remove potentially deleterious nucleotides (Fig. E1). For instance, dUTPase hydrolyzes dUTP or dUDP to dUMP, maintaining low the dUTP/dTTP ratio and thereby avoiding dUTP misincorporation into DNA during replication. In fact, the activity of dUTPase is essential for *T. brucei* unless an exogenous source of thymidine is provided in the media (Castillo-Acosta *et al.* 2013).
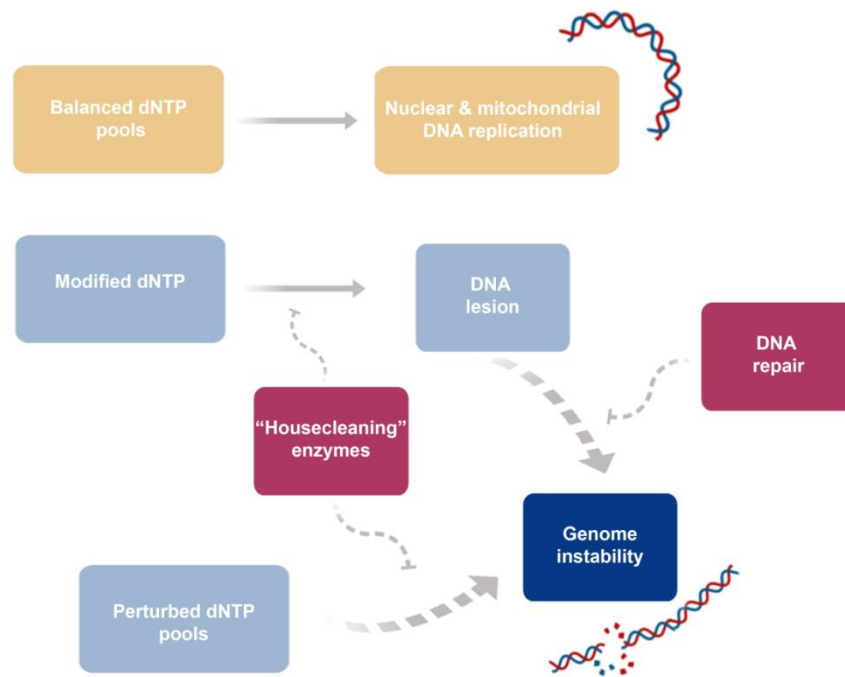
Figure E1. General pathways involved in the preservation of genome integrity. Nuclear and mitochondrial DNA replication requires the adequate supply of dNTPs. Misbalanced dNTP pools, as well as incorporation of non-canonical nucleotides into DNA may lead to genome instability. However, to avoid these processes, the cell expresses housecleaning enzymes and activates DNA repair pathways. Adapted from Rudd *et al.*, 2016 and created with Biorender®.

Given the importance of genome integrity preservation, the present thesis was focused on identifying novel features of nucleotide homeostasis control and repair in *T. brucei* in order to reveal novel drug targets or aspects that may be exploited in antitrypanosomal therapies.

E.1. TbHD52 is an essential enzyme in pyrimidine nucleotide metabolism in *Trypanosoma brucei*

As aforementioned, it has been widely reported that dysregulation of enzymes involved in nucleotide metabolism results in inadequate dNTP supply, provoking severe genome instability. For instance, upregulation of RNR activity in budding yeast expands dNTP levels, a situation that leads to increased spontaneous mutagenesis (Davidson *et al.* 2012). Whereas RNR is the main enzyme involved in the *de novo* biosynthesis of deoxyribonucleotides, dNTP catabolism relies on the activity of 5'-nucleotidases, nucleoside phosphorylases and deaminases, which are vital in the maintenance of balanced intracellular dNTP pools.

Hence, augmented expression of CDA (the enzyme responsible for deamination of dCyd/Cyd to dUrd/Urd) in cancer cells inhibits cell proliferation (Ye *et al.* 2015), whereas expansion of dCTP pools due to CDA deficiency causes under-replication of DNA (Gemble *et al.* 2015). In *T. brucei*, CDA depleted and null parasites rely on dThd supplementation to proliferate (Leija *et al.* 2016; Moro-Bulnes *et al.* 2019). Similarly, it has been described that overexpression of SAMHD1 reduces proliferation of several cancer cell lines, presumably due to the insufficient dNTP supply required for DNA replication (Clifford *et al.* 2014; Wang *et al.* 2014; Kodigepalli *et al.* 2017). Transient and stable silencing of SAMHD1 in lung and skin fibroblasts and THP-1 cells, respectively, also generated an expansion of intracellular dNTP levels in combination with altered proliferation (Franzolin *et al.* 2013; Bonifati *et al.* 2016). Bearing in mind the relevance of this dNTPase in mammalian cells, we explored the implication of trypanosomatid orthologues of SAMHD1 in the maintenance of dNTP homeostasis in *T. brucei*.

E.1.1. Two orthologues of HsSAMHD1 with different roles in parasite dNTP metabolism are present in *Trypanosoma brucei*

With regard to the identification of nucleotidases involved in deoxynucleoside homeostasis, previous studies have characterized a *T. brucei* homologue for the *E. coli* YfbR 5'-nucleotidase (Tb09.211.2190). This protein was cloned and expressed in a heterologous system and was shown to be involved in nucleoside generation via its activity against deoxyribonucleoside and ribonucleoside 5'-monophosphates. Activity was metal-dependent and while both purine and pyrimidine nucleotides were substrates, it was more active towards dCMP, dUMP and dTMP (Leija *et al.* 2016). However, studies destined at establishing its role in providing deoxynucleosides for dTMP synthesis were not performed. Due to its crucial role in controlling the dNTP/deoxynucleoside ratio we focused on proteins related to SAMHD1 and identified two members of the SAM domain and HD domain-containing protein-related family (PTHR11373), which were named TbHD82 and TbHD52 taking into account their predicted molecular mass.

TbHD82 and TbHD52 exhibited a differential localization as well as different roles in BSFs. Thus, deficiency of mitochondrial TbHD52 protein had a profound impact on parasite viability, whereas the depletion of nuclear TbHD82 only caused slight defects in the growth rate. The existence of two paralogues was common to Kinetoplastida and appeared as a unique feature not present in other organisms. The work here presented was centered on the role of TbHD52 in nucleotide metabolism since its initial characterization as a thymidine auxotroph suggested that it may have a central role in dTMP biosynthesis. In addition, the enzyme may present unique features and exhibits potential as a drug target due to its essential character.

E.1.2. TbHD52 is involved in the homeostasis of pyrimidine nucleotide pools

Human SAMHD1 is involved in the hydrolysis of the four canonical dNTPs to their corresponding nucleosides by means of its dNTPase activity. It has been demonstrated that there is no direct interaction between the enzyme and the dNTP substrate, but instead, binding is mediated by a series of water molecules. For this reason, although the enzyme can catalyze degradation of all dNTPs, interaction with pyrimidine nucleotides (dCTP and dTTP) is favoured (Ji *et al.* 2014).

While characterization of the recombinant enzyme was not performed in this study, the metabolomics profile in TbHD52-deficient cells was globally disturbed and particularly many intermediate compounds associated with pyrimidine metabolism, thus suggesting that pyrimidine dNTPs are the preferred substrates. Indeed the intracellular accumulation of dCTP advocates that this dNTP is the major substrate of TbHD52.

To further establish the role of TbHD52 in pyrimidine metabolism, both salvage and *de novo* dTTP biosynthesis should be considered. First, salvage of exogenous dThd seems highly unlikely in a physiological context, as *T. brucei* only expresses one transporter that mediates the incorporation of exogenous dThd, TbT1. The transporter exhibits an extremely low affinity and efficiency, since the K_m for dThd is 1.24 mM (Ali *et al.* 2013a). Ineffective transport via TbT1, along with the observation that dThd concentration in mice plasma is approximately 1 μM (Clarke *et al.* 2000), and in human plasma lower than 0.05 μM (Spinazzola *et al.* 2002) led us to assume that *T. brucei* is highly dependent on *de novo* biosynthesis for satisfying the intracellular requirements of dTTP .

In mammalian cells, dUMP for *de novo* biosynthesis of dTTP can come from two sources, either through dCMP deamination to dUMP by the action of DCTD, or through the reduction of UDP to dUDP via RNR. In human cells, most dTTP is derived from dCMP deamination, as has been demonstrated in the fibroblast CCL39 cell line, where DCTD deficiency caused a depletion in dTTP pools and acutely affected cell growth if dThd or dUrd were not exogenously supplemented (de Saint Vincent *et al.* 1980). *T. brucei* lacks a canonical DCTD in its genome and is unable to produce dUMP from dCMP. Indeed, it has been reported that trypanosomes contain extremely low concentrations of CDP and CTP, yet there is a significant pool of dCTP presumably because RNR preferentially reduces CDP (Hofer *et al.* 1997; Hofer *et al.* 1998). Hence, it has been postulated that the aim of the lack of DCTD in *T. brucei* together with the efficient reduction of CDP to dCDP is to avoid the exhaustion of metabolic intermediates and promote *de novo* dCTP biosynthesis (Ranjbarian *et al.* 2012).

On the other hand, studies performed with TK and CDA in *T brucei* (Valente *et al.* 2016; Moro-Bulnes *et al.* 2019) clearly indicate that thymidylate synthesis relies on TK-mediated dUMP formation (Fig. E2). In theory, dUMP could also be generated through the reduction of UDP and hydrolysis of dUDP/dUTP by the action of RNR and dUTPase, respectively (Hofer *et al.* 1997; Castillo-Acosta *et al.* 2008). However, the essential character of TK and CDA together with the observation that CDA-null mutants are dThd/dUrd auxotrophs (Leija *et al.* 2016) firmly support the idea that dTTP biosynthesis requires an intracellular-derived source of dUMP (Leija *et al.* 2016; Valente *et al.* 2016), and that dUTPase is not involved in *de novo* dTMP biosynthesis (Moro-Bulnes *et al.* 2019). CDA is a mitochondrial enzyme (Moro-Bulnes *et al.* 2019) while TK is present in both the nucleus and the cytosol (Valente *et al.* 2016).
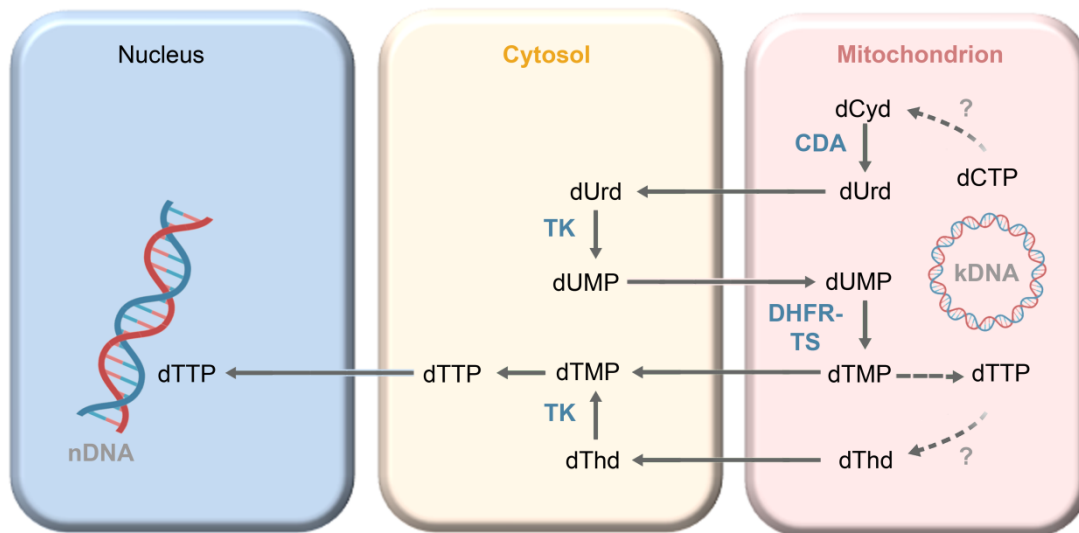
Figure E2. Proposed compartmentalization of the pyrimidine biosynthetic pathway. dTTP biosynthesis could be derived from dThd salvage and further phosphorylation or by dCyd salvage. In the latter case, dCyd is deaminated to dUrd via CDA in the mitochondrion, and subsequently TK mediates phosphorylation of dUrd to dUMP. By the action of DHFR-TS in the mitochondrion, dUMP is converted to dTMP, which ultimately enables formation of dTTP for DNA replication. However, the source of dCyd and dThd in the mitochondrion remains to be unravelled. Created with Biorender®.

In line with our initial hypothesis, the results obtained point towards a major role for TbHD52 in dTTP metabolism, consisting in the provision of an intracellular source of dCyd (Fig. E3). This assumption is supported both by the auxotrophy of the TbHD52 knock-out cell line for dThd and dUrd, as well as by the fact that cell viability is restored upon the expression of hDCTD, as both strategies provide dUMP and/or dTMP for dTTP biosynthesis. In the absence of TbHD52, there is a build-up of of dCTP and Cyt-derived nucleosides and nucleotides including dCyd. We hypothesize that a cellular accumulation of dCTP (both cytosolic and mitochondrial) takes place in the absence of TbHD52. dCTP-derived dCyd probably occurs in the cytosol and is not available for deamination by mitochondrial CDA.
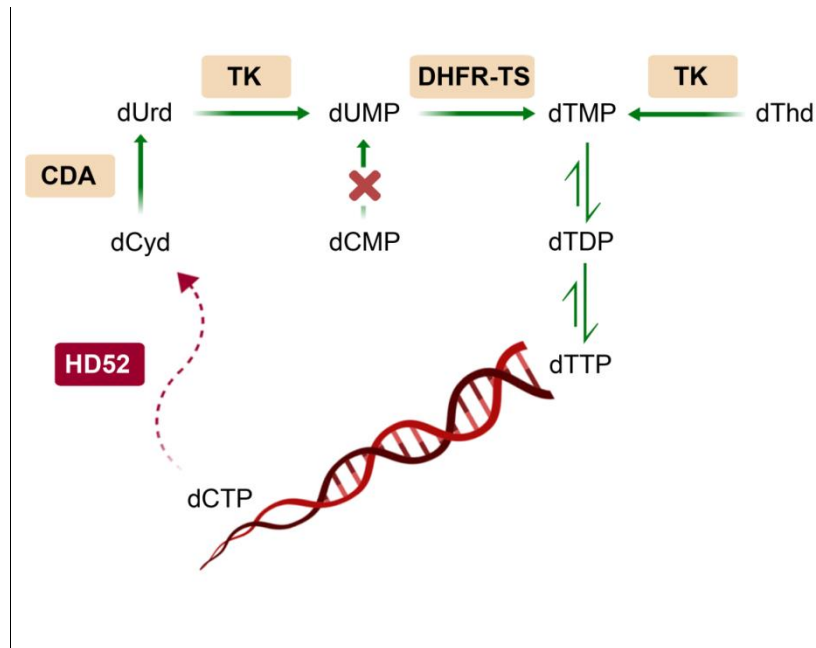
Figure E3. Potential role for HD52 in the pyrimidine biosynthetic pathway. TbHD52 may be a major component of dTTP biosynthesis through the hydrolysis of dCTP to its corresponding nucleoside. Thus, dCyd is then deaminated to dUrd via CDA, and subsequently TK mediates phosphorylation of dUrd and dThd to dUMP and dTMP, respectively. As *T. brucei* lacks DCTD, it is unable to generate dUMP from dCMP. Ultimately, dUMP and dTMP enable formation of dTTP for DNA replication. Created with Biorender®.

E.1.3. Mitochondrial and nuclear nucleoside pools are interconnected

The impact of TbHD52 knockdown, a mitochondrial protein, on the levels of intracellular nucleotides points towards a dynamic exchange between mitochondrial and nuclear dNTPs. In mammals connection between both compartments has been shown to be crucial for cell viability. Several studies have demonstrated the existence of a flux between mitochondrial and nuclear nucleotides and the importance of a correct balance of mitochondrial dNTP pools for the maintenance of nuclear genome integrity. Mitochondrial dNTP pools are separated from the cytosolic ones owing to the double membrane structure of the mitochondria, and are formed by the salvage enzymes TK2 and deoxyguanosine kinase (dGK) together with nucleoside monophosphate kinase (NMPK) and NDPK in postmitotic tissues, while in proliferating cells the mitochondrial

dNTPs are mainly imported from the cytosol produced by the cytosolic pathways (Wang 2016).

Thus, it has been demonstrated that the depletion of SAMHD1 reverts the deleterious phenotype of dGK-deficient fibroblasts, apparently by restoring an adequate level of mitochondrial dNTPs. This effect would be an indirect consequence of the expansion of cytosolic dNTPs in the absence of the SAMHD1 dNTPase activity, thereby also increasing mitochondrial dNTPs (Franzolin *et al.* 2015). In proliferating cells, specifically in human osteosarcoma (HOS) and mouse fibroblasts (3T3) cell lines, Rampazzo *et al*. have reported a bidirectional influx of dThd phosphates from the cytosol to the mitochondria and *vice versa*, in the first case derived from *de novo* biosynthesis and in the latter from dThd salvage (Rampazzo *et al.* 2004).

The mitochondrial membrane is not permeable to numerous metabolites, so transport between cytosol and mitochondria requires additional mechanisms. In this context an important role is accomplished by the family of mitochondrial carrier proteins (MCP), a group of structurally conserved proteins that transfer a wide range of metabolic intermediates across the mitochondrial membrane. A total of 24 putative homologues for MCPs have been identified in the genome of *T. brucei*, by either sequence or phylogenetic analysis (Colasante *et al.* 2009). For instance, TbMCP5 has been characterized as an ADP/ATP exchanger involved in the cytosolic and mitochondrial influx of ADP and ATP. This transporter has special importance in BSF trypanosomes, since in this life stage most ATP is generated by glycolysis and a mitochondrial ATP source by oxidative phosphorylation is lacking (Pena-Diaz *et al.* 2012). Interestingly, a MCP corresponding to the gene Tb927.5.1550, codes for a protein with a hypothetical pyrimidine nucleotide transporter activity. The analysis identified homology with the human pyrimidine nucleotide carrier, SLC25A36

(Colasante *et al.* 2009), which has been reported to efficiently mediate the interexchange, both by uniport and antiport transport, of (deoxy)nucleoside mono-, di- and triphosphates of Cyt and Ura, yet it also accepts Gua-derived nucleotides (Di Noia *et al.* 2014). Thereby, Tb927.5.1550 could be involved in pyrimidine influx between the cytosol and mitochondria in the parasite.

Furthermore, as previously indicated, mitochondrial enzymes involved in thymidylate biosynthesis have been reported to be essential. Moro-Bulnes *et al*., have recently shown that CDA, which catalyses the deamination of dCyd to dUrd, as well as DHFR-TS, which is involved in dUMP methylation to dTMP, present a mitochondrial intracellular localization (Moro-Bulnes *et al.* 2019). It is pertinent to note that CDA deficient-parasites are auxotrophes for dThd or dUrd (Leija *et al.* 2016; Moro-Bulnes *et al.* 2019). In addition, DHFR-TS knock-out cell lines could only be achieved in the presence of 0.16 mM dThd, and, once removed, parasites exhibited severe impairment of cell cycle progression and viability (Sienkiewicz *et al.* 2008). In sum, all combined, these studies suggest that, in *T. brucei,* thymidylate formation comes preferentially from dCyd deamination through the action of CDA in the mitochondria and subsequent dUrd phosphorylation by TK in the cytosol. Thus, the mitochondrial localization of TbHD52 could be relevant to provide dCyd as a substrate for TbCDA (Fig. E4). Our dNTP and metabolomics analysis suggest that the major substrate of TbHD52 is indeed dCTP. This observation together with the established pyridimidine requirements of *TbHD52*-knockout cells suggest that the key role of TbHD52 is to provide the intra-mitochondrial source of dCyd required for the formation of dTTP.
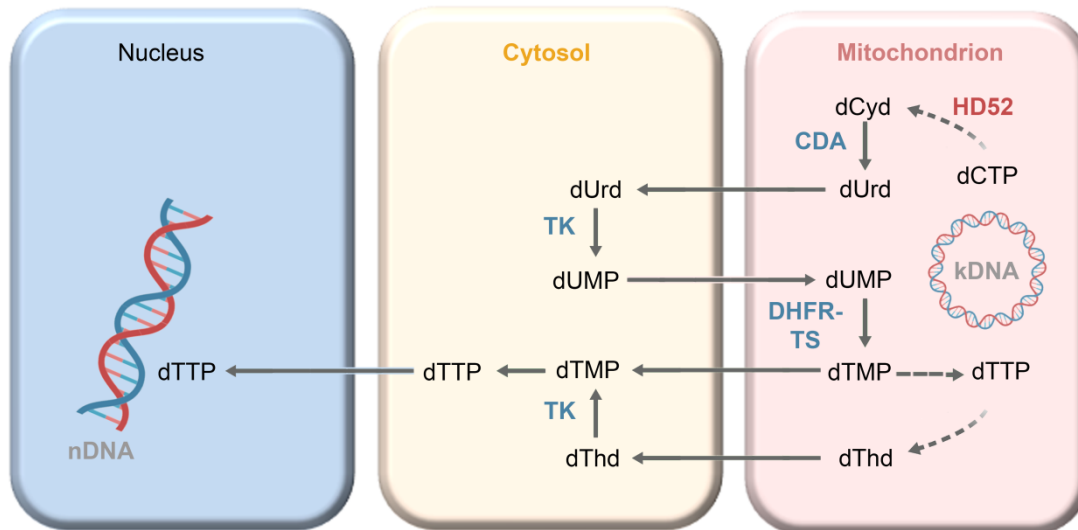
Figure E4. Diagram illustrating nucleoside influx and efflux within cellular compartments and the role of TbHD52 in *T. brucei*. TbHD52 would supply dCyd in the mitochondrion. CDA and DHFR-TS are also mitochondrial enzymes, whereas TK presents a nuclear and cytoplasmic localization. We propose that the influx/efflux of metabolites between the mitochondrion, cytosol and nucleus is required for nuclear dTTP biosynthesis. Created with Biorender®.

E.1.4. The absence of TbHD52 causes thymineless death in *T. brucei*

The absence of TbHD52 in BSFs of *T. brucei* profoundly affects genomic integrity. Cell cycle progression is greatly disturbed, showing arrest in S and G2/M phases, as well as severe difficulties in nuclear and kinetoplast DNA segregation, as demonstrated by the appearance of abnormal populations identified by DAPI staining. Important modifications in cell cycle and viability have been previously demonstrated for enzymes involved in dTTP biosynthesis. Valente *et al*. analysed the effects of TK knockdown in the cell cycle progression of *T. brucei* BSFs, and observed a decline in the percentage of parasites in G1 phase, together with an accumulation of cells in G2/M and post-G2/M. Likewise, populations with an aberrant number of nuclei and kinetoplasts as a consequence of mitotic arrest were visualized (Valente *et al.* 2016). On the other hand, thymidine withdrawal in DHFR-TS-null trypanosomes resulted in

important morphological perturbations, as well as S phase arrest (Sienkiewicz *et al.* 2008).

The defects described after depletion of enzymes involved in *de novo* dTTP synthesis are features of the so-called thymineless death, which is characterized by massive DNA damage in the absence of thymine nucleotides. This response was initially described by Cohen *et al.* in an *E. coli* strain mutant for the thymidylate synthase gene, that exhibited thymine auxotrophy and thymine starvation triggered cell death (Cohen and Barner 1954). To date, thymineless death has also been reported in numerous prokaryotes and eukaryotes, including mammals. The reason why only dThd deprivation, and no other nucleotide, triggers this drastic response was demonstrated by Barclay *et al.*, who identified multiple DNA strand breaks in cells undergoing thymineless death (Barclay *et al.* 1982). Thus, it has been suggested that, if dTTP is not available for DNA replication, DNA polymerase may misincorporate a uracil moiety instead of thymine. In this case, uracil removal by the action of UNG leads to massive single-strand breaks and subsequent DNA fragmentation (Ahmad *et al.* 1998; Khodursky *et al.* 2015). In agreement with this hypothesis, the mode of action of methotrexate towards cancer treatment relies on DHFR inhibition, where it has been reported that not only intracellular dTTP levels are strongly impaired but also more than a 1,000-fold increase in dUTP content occurs (Goulian *et al.* 1986). In the present case, the absence of TbHD52 results in DSB formation and an accumulation of nuclear ɣH2A foci upon removal of dThd, features characteristic of thymineless death and that have also been reported in trypanosomes upon TK depletion (Valente *et al.* 2016). The presence of uracil in DNA remains to be established.

In mammals, imbalances in the dCTP/dTTP ratio negatively affect DNA replication (Zhang *et al.* 2013). Hence, CHEF18 hamster cell lines that are characterised

by the expansion and accumulation of intracellular dCTP, showed an inefficient clearance and removal of misincorporated nucleotides during replication (Rainaldi *et al.* 1996). Recent studies have shown in HeLa cell lines that the accumulation of high intracellular dCTP levels, caused by CDA depletion, negatively affect replication fork progression and gave rise to DNA under-replication. In this latter study, the expansion of dCTP pools, and no other dNTP, specifically inhibited poly [ADP-ribose] polymerase 1 (PARP-1) basal activity (Gemble *et al.* 2015). Consequently, checkpoint kinase 1 (Chk1) activation was impaired, leading to under-replication of DNA and ultimate formation of ultra-fine DNA bridges (Gemble *et al.* 2016). Taking into account this information, apart from defects in dTTP formation, the dead-end accumulation of dCTP and Cyt-derived metabolites in *HD52*-dKO cell lines after dThd removal could be also *per se* enhancing replication stress in the parasite.

In conclusion, our results indicate that TbHD52 is involved in the provision of mitochondrial deoxynucleosides, essential for dTTP biosynthesis via TbTK salvage. When TbHD52 is absent, *de novo* biosynthesis of dTTP is disrupted and the parasite undergoes a reduction in Thy-derived metabolites, including nuclear dTTP. dCyd and Cyt-derived metabolites accumulate probably in the cytosol and are not available for mitochondrial thymidylate biosynthesis and thymineless death is triggered (Fig. E5).
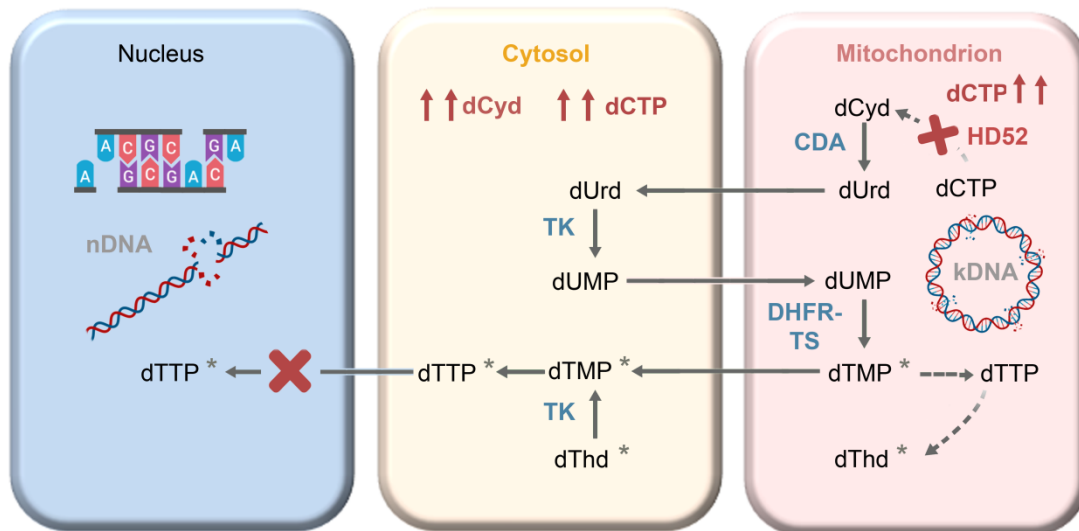
Figure E5. Diagram depicting the pyrimidine metabolic pathway in HD52 deficient cells. The lack of TbHD52 in *T. brucei* blocks supply of mitochondrial dCyd, required for thymidylate biosynthesis. dCyd pools are expanded as a consequence of dCTP accumulation yet dTTP formation is impaired. Grey asterisks highlight the metabolites that were found depleted in *TbHD52*-dKO trypanosomes. Created with Biorender®.

E.2. UNG has a relevant role in counteracting oxidative-derived damage in *Trypanosoma brucei*

All organisms are subjected to diverse damage that compromises genomic integrity. The source of DNA damage can be endogenous or exogenous, yet ROS and RNS are important factors that threaten cell viability. Specifically, since *T. brucei* is an extracellular parasite, it is constantly exposed to oxidative agents generated by the immune system of the host. Hence, cell mechanisms that provide defence and counteract these defects, such as DNA repair, are mostly essential in protozoan parasites.

E.2.1. UNG and BER pathway are crucial in the protection against nitrosative damage

A second part of this thesis was aimed at completing a series of studies focused on establishing the role of the BER pathway, and, specifically, the involvement of UNG in the protection against oxidative stress. The analysis was performed both *in vitro*, through exposure of NO donors, and *in vivo,* where the impact of the response of the host immune system was monitored.

Uracil is the most frequent non-canonical nucleotide in DNA. Uracil can be incorporated instead of thymine by DNA polymerase during replication or can arise as a result of spontaneous or enzyme-mediated cytosine deamination. Although it is estimated that in proliferative cells, 10^4 molecules of dUTP are incorporated in the genome per replication round, the result is harmless if unrepaired, as the polymerase pairs uracil with adenine. In contrast, cytosine deamination, either generated by endogenous or exogenous factors, can also lead to uracil accumulation in DNA, causing U:G mispairs that trigger mutagenesis characterized by C:G to T:A transitions (Alsoe *et al.* 2017). One of the most prevalent causes of cancer comes indeed from this transition, as studies of massive sequencing have detected that, from 1007 somatic mutations identified, 921 corresponded to single base substitutions. Not only in every class of cancer the most frequent mutation were C:G to T:A transitions, but in glioma and melanoma it was virtually the only mutation identified (Greenman *et al.* 2007).

In spite of the existence of additional glycosylases in human cells that can also mediate uracil excision, such as SMUG, TDG and MBD4 (Sousa *et al.* 2007), UNG activity is critical for uracil repair in DNA. Indeed, *E. coli* and *S. cerevisiae* mutant strains deficient in UNG exhibit increased mutation rates (Duncan and Weiss 1982;

Impellizzeri *et al.* 1991), while *Ung*$^{-/-}$ mice present a significant accumulation of uracil in DNA (Nilsen *et al.* 2000). In trypanosomes UNG is the only glycosylase identified that is involved in uracil removal, which underlines its potential importance in BER. Previous studies conducted in the lab have reported that *UNG*-dKO parasites were viable yet exhibited a hypermutator phenotype which was characterized by the presence of insertions and G:C to A:T transitions (Castillo-Acosta *et al.* 2012b). While UNG is not an essential enzyme, it may play a crucial role in defense against oxidative stress where a major genotoxic event is cytosine deamination rendering uracil. In this respect, higher susceptibility to oxidative stress and higher cell death rates were observed in mouse embryonic fibroblasts obtained from *Ung*$^{-/-}$ mice. In addition, they exhibited a higher dU/dC ratio compared to heterozygous and parental cell lines (Nilsen *et al.* 2000).

Here we describe that UNG-null parasites exhibit a higher uracil content in DNA (quantified as Pfu sensitive sites). This observation demonstrates the occurrence of uracil in trypanosomal DNA and the importance of effective BER for maintenance of genomic integrity. Moreover, the uracil content in DNA is further increased by exposure *in vitro* to nitric oxide. The occurrence of uracil upon treatment with NO donors has been previously reported (Endres *et al.* 2004). The present observations suggest that uracil resulting from cytosine deamination is a major genotoxic lesion induced by nitrosative/oxidative stress. In this context, Dizdaroglu *et al.*, evaluated the formation of pyrimidine and purine-derived products in DNA after exposure to oxidative stress, demonstrating that oxidative attack on cytosine leads to the presence of uracil, isodialuric acid, alloxan and 5-hydroxyuracil which are all substrates of human UDG (Dizdaroglu *et al.* 1996). Similar modified bases could be also potential substrates for trypanosomal UNG.

Additional DNA damage that was subject to evaluation was the occurrence of AP sites. Unexpectedly, UNG-null trypanosomes exhibit a higher AP site-content compared to parental parasites. Previous studies in the lab have reported increased DNA fragmentation in the absence of UNG in both BSFs and PCFs, as detected by the TUNEL assay (Castillo-Acosta *et al.* 2012b). In *Bacillus subtilis* UNG is the single glycosylase endowed with uracil-removal activity, yet defective strains exhibit a similar mutation rate to parental cells. However, the disruption of Endonuclease V (EndoV) increased 8-fold the mutation frequency, suggesting that this protein could be involved in the alternative excision of uracil from DNA (Lopez-Olmos *et al.* 2012). Endo V and an alternative excision repair pathway is also potentially present in *T. brucei*. However, studies performed in the laboratory have shown that the preferential substrate of trypanosomal EndoV is ssRNA containing inosine, whereas activity with DNA substrates containing uracil was extremely low (Garcia-Caballero *et al.* 2017). Thus, EndoV does not appear to be involved in alternative uracil removal in *T. brucei*.

The participation of other repair pathways, such as mismatch repair, cannot be discarded (Bell *et al.* 2004). It has been reported that MutSα, an heterodimer composed of MSH2/MDH6, is able to repair U:G mismatches in DNA (Larson *et al.* 2008), indicating that uracil may be repaired by both the BER and MMR pathways. Indeed, *T. brucei* expresses highly conserved MutS homologs, and studies performed by Machado-Silva *et al*., demonstrated that parasites MSH2-deficient presented higher sensitivity upon exposure to hydrogen peroxide-derived oxidative stress (Machado-Silva *et al.* 2008). MMR could be responsible of uracil removal from DNA, though more inefficiently than BER, and consequently explain the accumulation of strand breaks in *UNG*-dKO parasites. Thus, DNA strand breaks could be generated as a consequence of extensive excision during mismatch repair over U:G pairs, as reported

in two colon-cancer-derived cell lines, colon26 from mouse and human HT29, where repair of FU:G lesions by mismatch repair proteins was responsible for nuclear DNA fragmentation and cell death (Li *et al.* 2009).

In pathogenic organisms exposed to situations of intense oxidative stress, as during infection, the role of UNG is critical in order to maintain cell viability, and thus, virulence. In *Salmonella typhimurium*, the inactivation of *ung* gene resulted in a hypermutator phenotype which was enhanced during infection (Richardson *et al.* 2009). Similarly in *Leishmania*, it has been observed that UNG overexpression enables higher macrophage infectivity as well as less susceptibility to ROS agents (Mishra *et al.* 2018). In agreement with these observations, our results show that UNG has a pivotal role in the prevention of DNA damage derived from oxidative agents during infection *in vivo*. Indeed, *UNG*-dKO trypanosomes isolated after murine infection exhibited a high uracil content in DNA and a pronounced activation of the damage signaling cascade. We previously reported that UNG-null parasites present reduced virulence and an increased life-span of mice (Castillo-Acosta *et al.* 2012b). Blood parasite clearance on UNG-null parasites was observed approximately at day 5 post-infection and was followed by the emergence of a virulent population at day 9 that ultimately led to mice death, while parental BSFs caused massive infection and mice died at day 5 post-infection. We postulated that the recovery of virulence in *UNG*-dKO cells was due to the induction of resistance mechanisms that may confer protection against mediators of innate immunity. Indeed, we identified an up-regulation of tryparedoxin peroxidase (TRYP1), a member of the trypanothione/tryparedoxin system, in concurrence with the emergence of high parasitaemia and subsequent mice death. Since the trypanothione/tryparedoxin system is responsible for detoxification of potential reactive oxygen and nitrogen species, it is reasonable to assume that in the absence of UNG, additional mechanisms are activated

that are aimed at providing increased protection against DNA damage derived from the harmful oxidative species released during *in vivo* infection.

E.2.2. NO exposure compromises genomic integrity

Since NO is a small molecule able to diffuse through cell membranes, it is considered an important cell signaling agent, yet it is also highly reactive and thus a critical contributor to many types of damage. The lesions caused by NO have been widely studied, and it is generally accepted that the major potential cytotoxicity of NO is produced by RNS, powerful genotoxic agents generated as a consequence of the reaction of NO with other highly reactive molecules, as ROS. Under aerobic conditions, NO may be oxidized by molecular oxygen, producing $ONOO^-$ or NO_2, which may further react again with NO to form N_2O_3. The ability of RNS to deaminate and oxidize nucleotides in DNA makes them important mutagenic agents, as reported in a great variety of organisms, from bacteria to mammals (Nguyen *et al.* 1992; Routledge *et al.* 1993) and *in vivo* models (Gal and Wogan 1996). Indeed, the treatment of *S. typhimurium* strain TA1535 with different NO-releasing compounds was highly mutagenic, and more than 99% of the mutations found were C:T transitions (Wink *et al.* 1991). In *Trypanosoma,* a major mutagenic event was cytosine deamination to uracil (Fig. E6), which increased pronouncedly in BSF parental cell lines upon exposure to NO-donors.
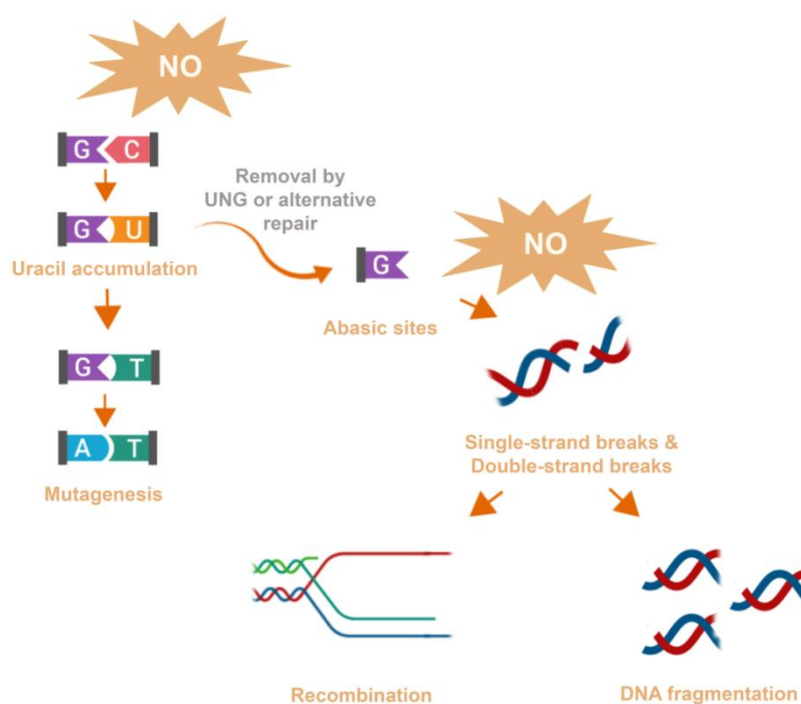
Figure E6. Illustrative description of the effects of NO on DNA integrity. NO generates RNS that ultimately cause DNA damage through different pathways. First, base deamination and oxidation may occur. For instance, cytosine deamination gives rise to uracil accumulation that may either lead to mutagenesis if unrepaired, or be excised, generating an AP site. NO and RNS can directly attack an AP site, triggering SSBs and DSBs, which produce severe cytotoxic events such as recombination or DNA fragmentation. Created with Biorender®.

Apart from uracil, major base damages derived from RNS include 8-oxoG, xanthine and 8-nitroguanine. On the one hand, xanthine can mispair with thymine, causing A:T to G:C transitions, which are prone to depurination, leading to AP sites (Burney *et al.* 1999). On the other hand, 8-oxoG is not recognized as a DNA lesion by DNA polymerase, and gives rise to G:C to T:A transversions if unrepaired (Hsu *et al.* 2004). *T. brucei* expresses a putative orthologue for OGG1 involved in 8-oxoG repair, which has not been studied to date. OGG1 from *T. cruzi* complements OGG1-deficient yeast and suppresses the spontaneous hypermutator phenotype

(Furtado *et al.* 2012), suggesting that TcOGG1, and probably TbOGG1, efficiently removes 8-oxoG from DNA. In contrast, 8-nitroguanine can undergo rapid spontaneous depurination, leading to AP sites (Fig. E6). AP sites are highly cytotoxic as they provoke DNA replication and transcription blockage, as well as mutagenesis. Additionally, AP sites can undergo spontaneous or enzymatic hydrolysis by DNA N-glycosylases/AP lyases and give rise to SSBs (Boiteux and Guillet 2004), which can be further converted to cytotoxic DSBs upon replication fork collapse (Fig. E6) (Kuzminov 2001). It is well established that nitrosating agents can also directly induce the formation of SSBs by reacting with the sugar moiety in DNA (Burney *et al.* 1999). In the present case we did not observe significant modifications in the AP sites content after NO treatment in BSF parental cell lines, suggesting that either it was not the major damage produced by NO or it rapidly progressed to DSBs. Indeed, in UNG-null cell lines, which exhibited a higher basal content of AP sites in DNA, exposure to NO led to a decrease in AP sites, in concurrence with higher fragmentation, suggesting that perhaps AP sites detected are subjected to NO attack and further generation of DSBs. In this respect, Nguyen *et al*. treated TK6 cells with NO and observed a severe base deamination that led to depurination in concurrence with a subsequent high percentage of SSBs, suggesting that SSBs may have arisen via cleavage of the AP sites (Nguyen *et al.* 1992).

DSBs are major contributors to NO cytotoxicity. While NO does not directly induce DSBs, it does provoke SSB accumulation that eventually leads to fragmentation. Currently, one marker widely employed for DSB detection is histone H2AX phosphorylation. An increase in H2AX foci has been described in a variety of cell types upon NO exposure (Tanaka *et al.* 2006; Murata *et al.* 2012). In rat islets, the activation

of H2AX was detected during the exposure to IL-1 and IFN-γ, which surprisingly was prevented with the use of NOS inhibitors. Likewise, direct addition of NO donors also stimulated the accumulation of H2AX foci, suggesting that DSB formation was promoted by the action of NO (Oleson and Corbett 2018). In line with these observations, we detected a massive activation of the DNA damage response upon oxidative stress characterized by whole nuclei staining with the specific antibody. The presence of γH2A whole nuclear staining of trypanosome cells as a DSB marker has been previously reported by Glover *et al*. after treatment with phleomycin, a DSB-producing agent (Glover and Horn 2012). Activation of γH2AX has also been described in *Mycobacterium smegmatis* upon infection of murine macrophages (Ghosh *et al.* 2019), thus supporting our observations that during infection pathogens are subjected to oxidative stress and extensive damage that importantly contributes to virulence control.

E.2.3. Relationship between the components of the immune system and damage during parasitic infection

Our results showed that the parasites, both parental and UNG-deficient, underwent severe genotoxic damage during murine infection, highlighted by the acute uracil accumulation and increased number of repair foci. Since NO donors *in vitro* inflicted similar defects, it is attractive to speculate that NO is also responsible for damage *in vivo*. Indeed, several studies have documented the antitrypanosomal activity of NO donors *in vitro* (Vincendeau *et al.* 1992; Steverding *et al.* 2009), and it is generally accepted that release of pro-inflammatory cytokines, including NO, is required for initial parasitaemia control (Kaushik *et al.* 1999; Gobert *et al.* 2000).

However, inhibition of iNOS involved in the production and release of NO in macrophages, not only did not significantly alter the level of damage, but also unexpectedly, decreased virulence. In relation to this observation Sternberg *et al*. detected that treatment of *T. brucei* infected mice with L-NAME, another NOS inhibitor, resulted in reduced parasitaemia. In this case, the authors argued that oxyhemoglobin is a scavenger for NO and, thus, it is sequestered by erythrocytes, avoiding its antitrypanosomal effects *in vivo* (Sternberg *et al.* 1994). Conversely in a *T. congolense* model, NO exerts protection (Magez *et al.* 2006; Wei *et al.* 2011). Thus, while it is generally agreed that the production of NO is stimulated by infection, the antitrypanosomal activity of NO in *T. brucei* mouse models is questionable (Sternberg *et al.* 1994; Hertz and Mansfield 1999).

Instead of glutathione (GSH), *T. brucei* contains a unique molecule named trypanothione ($T(SH)_2$) as intracellular reducing agent. It has been demonstrated that $T(SH)_2$ it able to intercept NO and iron to form nitrosyl iron complexes, with actually 600-fold higher affinity than GSH. Hence, this particular ability of $T(SH)_2$ to hamper NO and iron could also contribute to explain the lower trypanocidal activity of NO *in vivo* (Bocedi *et al.* 2010).

In addition, it should be considered that NO is not the sole pro-inflammatory agent released *in vivo*, and that additional cytokines have reported antiparasitic effects, yet the trypanocidal role of these molecules is controversial *in vivo*. Firstly, TNF-α has been reported to have trypanocidal activity *in vitro* (Magez *et al.* 1997). However, TNF-α knock-out mice exhibited immunosuppression and lipopolysaccharide hypersensitivity (Magez *et al.* 1999), whereas overproduction led to hypergammaglobulinemia (Okomo-Assoumou *et al.* 1995), since it activates and enhances B cells proliferation and differentiation (Roldan *et al.* 1992). It has also been

reported that the lack of IL-10 led to more virulent parasites and diminished life-span of infected mice (Namangala *et al.* 2001). Similarly, IFN-ɣ knock-out mice presented reduced survival when they were infected with *T. brucei rhodesiense* (Mabbott *et al.* 1998). Hence, these cytokines have also an important trypanocidal role *in vivo* and, in combination with NO, might be contributing to the observed phenotype.

Additionally, the components of the immune system are interconnected, and the interactions are important to understand the mechanisms underlying the infective process. Thus, although macrophages are relevant constituents of the innate immune system, several studies indicate that the activation of macrophages may have different consequences. On the one side, macrophages exert a protective role through the release of cytotoxic compounds, such as RNS and ROS, and through their involvement in parasites phagocytosis (Shi *et al.* 2004). In contrast, it is widely accepted that they trigger down-regulation of the T-cell-dependent response, so they are associated with immunosuppressive events. More in detail, first, myeloid cells sense diverse pathogenic components, such as soluble VSGs (Magez *et al.* 1998; Leppert *et al.* 2007), leading to the activation of T-cells, which release IFN-ɣ via Th1 response (Mansfield and Paulnock 2005). As a consequence, macrophages become fully activated and release several pro-inflammatory cytokines and molecules, such as TNF-α, prostaglandin E_2 (PGE_2) or NO to control parasitaemia (Stijlemans *et al.* 2016). However, these compounds have shown to inhibit T-cell proliferative responses and cause immunosuppression (Sternberg and Mabbott 1996) (Fig. E7). In support of these data, it has been corroborated that inhibition of iNOS activity directly affects T cells. Infection in mice deficient in iNOS triggered the expansion of CD4(+) cells as well as expression of IL-2, whereas CD8(+) and CD25(+)/CD8(+) cells were depleted (Millar *et al.* 1999). In agreement with these observations we observed reduced parasitaemia upon iNOS

inhibition, Hence, NO may limit CD4(+) T cell activation, and the inhibition of NO could be promoting the appearance of cytotoxic cells, leading to a more strict control of the parasitaemia as observed during AG treatment.
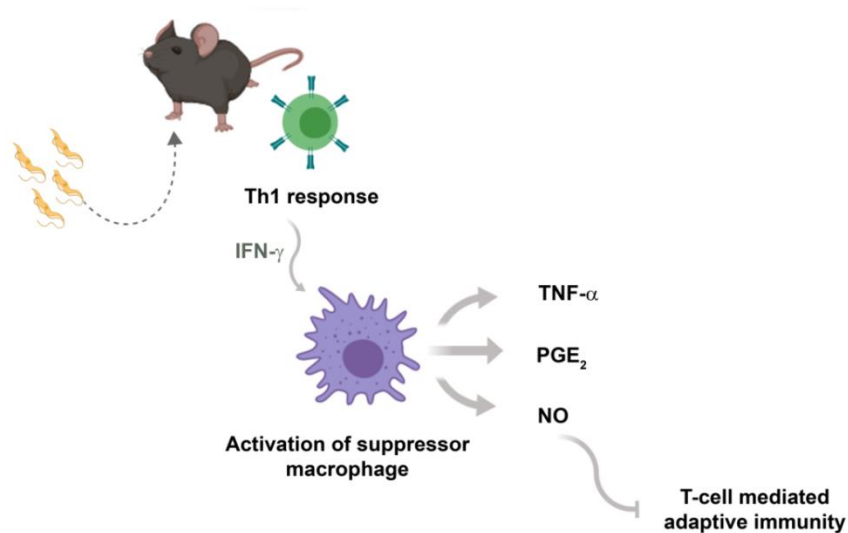
Figure E7. Relationship between NO synthesis and regulation of T-cell response. Once parasites are detected by the immune system, IFN-ɣ is released via a Th1 response, leading to the activation of suppressor macrophages. As a consequence, cytotoxic agents are released, such as NO, which contribute to immunosuppression of T-cells. Created with Biorender®.

On the other side, novel mechanisms for parasite killing are emerging where oxidative stress has a major role. It has been recently reported that NK cells and T lymphocytes also release cytolytic granule molecules, such as granulysin, granzyme proteases and pore-forming perforing. Thus, perforin and granulysin disrupt cell membranes, and help to deliver the granzymes into parasites, where they generate ROS and impair parasite oxidative defences (Dotiwala *et al.* 2016).

In conclusion, although the immune system comprises multiple elements that need to be considered, our results contribute to unravelling the mode of oxidative stress signaling and the molecular mechanisms involved in the counteraction of oxidative damage and provide valuable information for the design of novel strategies directed at compromising parasite survival within the host.

CONCLUSIONS/

CONCLUSIONES

F. CONCLUSIONS/CONCLUSIONES

1. *Trypanosoma brucei* codifica en su genoma dos ortólogos de la proteína SAMHD1 humana, denominados TbHD82 y TbHD52, que presentan un dominio HD con una alta conservación de la mayoría de los residuos implicados en actividad catalítica.

2. TbHD82 es una proteína nuclear cuya depleción y eliminación no afecta de forma significativa a la proliferación celular.

3. TbHD52 es una proteína mayoritariamente mitocondrial tanto en la forma sanguínea como procíclica de *T. brucei* y es esencial para la viabilidad en ambas formas.

4. Las líneas deficientes en TbHD52 son auxótrofas para timidina y desoxiuridina, lo que apoya su papel central en la homeostasis de nucleótidos pirimidínicos.

5. La formación de dUMP mediante la complementación de líneas deficientes en TbHD52 con dCMP desaminasa humana revierte el fenotipo de letalidad, indicando que TbHD52 posee un papel relevante en la biosíntesis de dUMP y dTTP.

6. En ausencia de TbHD52, se producen alteraciones globales del perfil metabolómico del parásito, destacando la acumulación de dCTP y metabolitos derivados de citosina, además de la depleción de dTTP y metabolitos derivados de timidina. Estas observaciones en su conjunto apoyan que el sustrato mayoritario de TbHD52 es dCTP y que la enzima tiene un papel central en la producción de desoxicitidina para la síntesis el dTMP.

7. Las líneas *TbHD52*-dKO mostraron graves alteraciones en la progresión del ciclo celular, observándose una parada en fase S y G2/M así como defectos en la segregación del kinetoplasto.

8. La ausencia de TbHD52 induce una intensa activación de la cascada de señalización de daño mediada por la histona γH2A. Estos defectos, junto a la depleción del pool de dTTP y derivados de timidina, sugieren que está teniendo lugar el proceso de muerte por falta de timina.

9. La enzima UNG posee un papel fundamental en la protección y reparación de daño en el DNA, observándose una mayor sensibilidad al estrés oxidativo en parásitos deficientes en UNG. Las células de la línea *TbUNG*-dKO presentan un mayor contenido en uracilo y sitios abásicos en DNA, así como una activación de la cascada de señalización a daño en DNA mediada por la histona γH2A.

10. La exposición a óxido nítrico *in vitro* produce un daño genotóxico severo en *T. brucei* entre el que cabe destacar la acumulación de uracilo en DNA como consecuencia de la desaminación de citosina, así como la fosforilación de la histona H2A.

11. Durante el proceso de infección en ratones se genera uracilo y daño en el DNA de *T. brucei* lo que no parece ser consecuencia exclusiva de la liberación de óxido nítrico, sino que deben de estar implicados otros componentes de la respuesta inmune del hospedador.

REFERENCES

G. REFERENCES

Abbotts, R. and D. M. Wilson, 3rd (2017) Coordination of DNA single strand break repair. *Free Radic Biol Med*. **107**, 228-244.

Ahmad, S. I., S. H. Kirk and A. Eisenstark (1998) Thymine metabolism and thymineless death in prokaryotes and eukaryotes. *Annu Rev Microbiol*. **52**, 591-625.

Ahn, J. (2016) Functional organization of human SAMHD1 and mechanisms of HIV-1 restriction. *Biol Chem*. **397**, 373-9.

Ahn, J., C. Hao, J. Yan, M. DeLucia, J. Mehrens, C. Wang, A. M. Gronenborn and J. Skowronski (2012) HIV/simian immunodeficiency virus (SIV) accessory virulence factor Vpx loads the host cell restriction factor SAMHD1 onto the E3 ubiquitin ligase complex CRL4DCAF1. *J Biol Chem*. **287**, 12550-8.

Akbari, M., M. Otterlei, J. Pena-Diaz and H. E. Krokan (2007) Different organization of base excision repair of uracil in DNA in nuclei and mitochondria and selective upregulation of mitochondrial uracil-DNA glycosylase after oxidative stress. *Neuroscience*. **145**, 1201-12.

Akinsolu, F. T., P. O. Nemieboka, D. W. Njuguna, M. N. Ahadji, D. Dezso and O. Varga (2019) Emerging Resistance of Neglected Tropical Diseases: A Scoping Review of the Literature. *Int J Environ Res Public Health*. **16**.

Al-Salabi, M. I., L. J. Wallace, A. Luscher, P. Maser, D. Candlish, B. Rodenko, M. K. Gould, I. Jabeen, S. N. Ajith and H. P. de Koning (2007) Molecular interactions underlying the unusually high adenosine affinity of a novel *Trypanosoma brucei* nucleoside transporter. *Mol Pharmacol*. **71**, 921-9.

Ali, J. A., D. J. Creek, K. Burgess, H. C. Allison, M. C. Field, P. Maser and H. P. De Koning (2013a) Pyrimidine salvage in *Trypanosoma brucei* bloodstream forms

and the trypanocidal action of halogenated pyrimidines. *Mol Pharmacol*. **83**, 439-53.

Ali, J. A., D. N. Tagoe, J. C. Munday, A. Donachie, L. J. Morrison and H. P. de Koning (2013b) Pyrimidine biosynthesis is not an essential function for *Trypanosoma brucei* bloodstream forms. *PLoS One*. **8**, e58034.

Alsoe, L., A. Sarno, S. Carracedo, D. Domanska, F. Dingler, L. Lirussi, T. SenGupta, N. B. Tekin, L. Jobert, L. B. Alexandrov, A. Galashevskaya, C. Rada, G. K. Sandve, T. Rognes, H. E. Krokan and H. Nilsen (2017) Uracil Accumulation and Mutagenesis Dominated by Cytosine Deamination in CpG Dinucleotides in Mice Lacking UNG and SMUG1. *Sci Rep*. **7**, 7199.

Antoine-Moussiaux, N., A. Cornet, F. Cornet, S. Glineur, M. Dermine and D. Desmecht (2009) A non-cytosolic protein of *Trypanosoma evansi* induces CD45-dependent lymphocyte death. *PLoS One*. **4**, e5728.

Aravind, L. and E. V. Koonin (1998) The HD domain defines a new superfamily of metal-dependent phosphohydrolases. *Trends Biochem Sci*. **23**, 469-72.

Arnold, L. H., H. C. Groom, S. Kunzelmann, D. Schwefel, S. J. Caswell, P. Ordonez, M. C. Mann, S. Rueschenbaum, D. C. Goldstone, S. Pennell, S. A. Howell, J. P. Stoye, M. Webb, I. A. Taylor and K. N. Bishop (2015) Phospho-dependent Regulation of SAMHD1 Oligomerisation Couples Catalysis and Restriction. *PLoS Pathog*. **11**, e1005194.

Arzumanian, V., E. Stankevicius, A. Laukeviciene and E. Kevelaitis (2003) Mechanisms of nitric oxide synthesis and action in cells. *Medicina (Kaunas)*. **39**, 535-41.

Aslett, M., C. Aurrecoechea, M. Berriman, J. Brestelli, B. P. Brunk, M. Carrington, D. P. Depledge, S. Fischer, B. Gajria, X. Gao, M. J. Gardner, A. Gingle, G. Grant,

O. S. Harb, M. Heiges, C. Hertz-Fowler, R. Houston, F. Innamorato, J. Iodice, J. C. Kissinger, E. Kraemer, W. Li, F. J. Logan, J. A. Miller, S. Mitra, P. J. Myler, V. Nayak, C. Pennington, I. Phan, D. F. Pinney, G. Ramasamy, M. B. Rogers, D. S. Roos, C. Ross, D. Sivam, D. F. Smith, G. Srinivasamoorthy, C. J. Stoeckert, Jr., S. Subramanian, R. Thibodeau, A. Tivey, C. Treatman, G. Velarde and H. Wang (2010) TriTrypDB: a functional genomic resource for the Trypanosomatidae. *Nucleic Acids Res*. **38**, D457-62.

Baldauf, H. M., X. Pan, E. Erikson, S. Schmidt, W. Daddacha, M. Burggraf, K. Schenkova, I. Ambiel, G. Wabnitz, T. Gramberg, S. Panitz, E. Flory, N. R. Landau, S. Sertel, F. Rutsch, F. Lasitschka, B. Kim, R. Konig, O. T. Fackler and O. T. Keppler (2012) SAMHD1 restricts HIV-1 infection in resting CD4(+) T cells. *Nat Med*. **18**, 1682-7.

Barclay, B. J., B. A. Kunz, J. G. Little and R. H. Haynes (1982) Genetic and biochemical consequences of thymidylate stress. *Can J Biochem*. **60**, 172-84.

Beloglazova, N., R. Flick, A. Tchigvintsev, G. Brown, A. Popovic, B. Nocek and A. F. Yakunin (2013) Nuclease activity of the human SAMHD1 protein implicated in the Aicardi-Goutieres syndrome and HIV-1 restriction. *J Biol Chem*. **288**, 8101-10.

Bell, J. S., T. I. Harvey, A. M. Sims and R. McCulloch (2004) Characterization of components of the mismatch repair machinery in *Trypanosoma brucei*. *Mol Microbiol*. **51**, 159-73.

Bell, J. S. and R. McCulloch (2003) Mismatch repair regulates homologous recombination, but has little influence on antigenic variation, in *Trypanosoma brucei*. *J Biol Chem*. **278**, 45182-8.

Benz, C., F. Dondelinger, P. G. McKean and M. D. Urbaniak (2017) Cell cycle synchronisation of *Trypanosoma brucei* by centrifugal counter-flow elutriation reveals the timing of nuclear and kinetoplast DNA replication. *Sci Rep*. **7**, 17599.

Berriman, M., E. Ghedin, C. Hertz-Fowler, G. Blandin, H. Renauld, D. C. Bartholomeu, N. J. Lennard, E. Caler, N. E. Hamlin, B. Haas, U. Bohme, L. Hannick, M. A. Aslett, J. Shallom, L. Marcello, L. Hou, B. Wickstead, U. C. Alsmark, C. Arrowsmith, R. J. Atkin, A. J. Barron, F. Bringaud, K. Brooks, M. Carrington, I. Cherevach, T. J. Chillingworth, C. Churcher, L. N. Clark, C. H. Corton, A. Cronin, R. M. Davies, J. Doggett, A. Djikeng, T. Feldblyum, M. C. Field, A. Fraser, I. Goodhead, Z. Hance, D. Harper, B. R. Harris, H. Hauser, J. Hostetler, A. Ivens, K. Jagels, D. Johnson, J. Johnson, K. Jones, A. X. Kerhornou, H. Koo, N. Larke, S. Landfear, C. Larkin, V. Leech, A. Line, A. Lord, A. Macleod, P. J. Mooney, S. Moule, D. M. Martin, G. W. Morgan, K. Mungall, H. Norbertczak, D. Ormond, G. Pai, C. S. Peacock, J. Peterson, M. A. Quail, E. Rabbinowitsch, M. A. Rajandream, C. Reitter, S. L. Salzberg, M. Sanders, S. Schobel, S. Sharp, M. Simmonds, A. J. Simpson, L. Tallon, C. M. Turner, A. Tait, A. R. Tivey, S. Van Aken, D. Walker, D. Wanless, S. Wang, B. White, O. White, S. Whitehead, J. Woodward, J. Wortman, M. D. Adams, T. M. Embley, K. Gull, E. Ullu, J. D. Barry, A. H. Fairlamb, F. Opperdoes, B. G. Barrell, J. E. Donelson, N. Hall, C. M. Fraser, S. E. Melville and N. M. El-Sayed (2005) The genome of the African trypanosome *Trypanosoma brucei*. *Science*. **309**, 416-22.

Bianchi, V., E. Pontis and P. Reichard (1987) Regulation of pyrimidine deoxyribonucleotide metabolism by substrate cycles in dCMP deaminase-deficient V79 hamster cells. *Mol Cell Biol*. **7**, 4218-24.

Biebinger, S., L. E. Wirtz, P. Lorenz and C. Clayton (1997) Vectors for inducible expression of toxic gene products in bloodstream and procyclic *Trypanosoma brucei*. *Mol Biochem Parasitol*. **85**, 99-112.

Blanc, V. and N. O. Davidson (2010) APOBEC-1-mediated RNA editing. *Wiley Interdiscip Rev Syst Biol Med*. **2**, 594-602.

Bocedi, A., K. F. Dawood, R. Fabrini, G. Federici, L. Gradoni, J. Z. Pedersen and G. Ricci (2010) Trypanothione efficiently intercepts nitric oxide as a harmless iron complex in trypanosomatid parasites. *FASEB J*. **24**, 1035-42.

Bockstal, V., P. Guirnalda, G. Caljon, R. Goenka, J. C. Telfer, D. Frenkel, M. Radwanska, S. Magez and S. J. Black (2011) *T. brucei* infection reduces B lymphopoiesis in bone marrow and truncates compensatory splenic lymphopoiesis through transitional B-cell apoptosis. *PLoS Pathog*. **7**, e1002089.

Boiteux, S. and M. Guillet (2004) Abasic sites in DNA: repair and biological consequences in *Saccharomyces cerevisiae*. *DNA Repair (Amst)*. **3**, 1-12.

Bolte, S. and F. P. Cordelieres (2006) A guided tour into subcellular colocalization analysis in light microscopy. *J Microsc*. **224**, 213-32.

Bonifati, S., M. B. Daly, C. St Gelais, S. H. Kim, J. A. Hollenbaugh, C. Shepard, E. M. Kennedy, D. H. Kim, R. F. Schinazi, B. Kim and L. Wu (2016) SAMHD1 controls cell cycle status, apoptosis and HIV-1 infection in monocytic THP-1 cells. *Virology*. **495**, 92-100.

Boren, J. and K. M. Brindle (2012) Apoptosis-induced mitochondrial dysfunction causes cytoplasmic lipid droplet formation. *Cell Death Differ*. **19**, 1561-70.

Borst, P. (2002) Antigenic variation and allelic exclusion. *Cell*. **109**, 5-8.

Brandariz-Nunez, A., J. C. Valle-Casuso, T. E. White, N. Laguette, M. Benkirane, J. Brojatsch and F. Diaz-Griffero (2012) Role of SAMHD1 nuclear localization in restriction of HIV-1 and SIVmac. *Retrovirology*. **9**, 49.

Bryk, R. and D. J. Wolff (1998) Mechanism of inducible nitric oxide synthase inactivation by aminoguanidine and L-N6-(1-iminoethyl)lysine. *Biochemistry*. **37**, 4844-52.

Bullock WO, F. J., Short JM (1987) XL1-Blue—a high-efficiency plasmid transforming recA *Escherichia coli* strain with β-galactosidase selection. *Biotechniques* **5**, 376-379.

Burchmore, R. J., L. J. Wallace, D. Candlish, M. I. Al-Salabi, P. R. Beal, M. P. Barrett, S. A. Baldwin and H. P. de Koning (2003) Cloning, heterologous expression, and in situ characterization of the first high affinity nucleobase transporter from a protozoan. *J Biol Chem*. **278**, 23502-7.

Burney, S., J. L. Caulfield, J. C. Niles, J. S. Wishnok and S. R. Tannenbaum (1999) The chemistry of DNA damage from nitric oxide and peroxynitrite. *Mutat Res*. **424**, 37-49.

Burton, P., D. J. McBride, J. M. Wilkes, J. D. Barry and R. McCulloch (2007) Ku heterodimer-independent end joining in *Trypanosoma brucei* cell extracts relies upon sequence microhomology. *Eukaryot Cell*. **6**, 1773-81.

Buscher, P., G. Cecchi, V. Jamonneau and G. Priotto (2017) Human African trypanosomiasis. *Lancet*. **390**, 2397-2409.

Buzovetsky, O., C. Tang, K. M. Knecht, J. M. Antonucci, L. Wu, X. Ji and Y. Xiong (2018) The SAM domain of mouse SAMHD1 is critical for its activation and regulation. *Nat Commun*. **9**, 411.

Camacho, C., G. Coulouris, V. Avagyan, N. Ma, J. Papadopoulos, K. Bealer and T. L. Madden (2009) BLAST+: architecture and applications. *BMC Bioinformatics*. **10**, 421.

Campagnaro, G. D., K. J. Alzahrani, J. C. Munday and H. P. De Koning (2018) *Trypanosoma brucei* bloodstream forms express highly specific and separate transporters for adenine and hypoxanthine; evidence for a new protozoan purine transporter family? *Mol Biochem Parasitol*. **220**, 46-56.

Cardamone, F., F. Iacovelli, G. Chillemi, M. Falconi and A. Desideri (2017) A molecular dynamics simulation study decodes the early stage of the disassembly process abolishing the human SAMHD1 function. *J Comput Aided Mol Des*. **31**, 497-505.

Carter, N. S. and A. H. Fairlamb (1993) Arsenical-resistant trypanosomes lack an unusual adenosine transporter. *Nature*. **361**, 173-6.

Castillo-Acosta, V. M., F. Aguilar-Pereyra, J. M. Bart, M. Navarro, L. M. Ruiz-Perez, A. E. Vidal and D. Gonzalez-Pacanowska (2012a) Increased uracil insertion in DNA is cytotoxic and increases the frequency of mutation, double strand break formation and VSG switching in *Trypanosoma brucei*. *DNA Repair (Amst)*. **11**, 986-95.

Castillo-Acosta, V. M., F. Aguilar-Pereyra, D. Garcia-Caballero, A. E. Vidal, L. M. Ruiz-Perez and D. Gonzalez-Pacanowska (2013) Pyrimidine requirements in deoxyuridine triphosphate nucleotidohydrolase deficient *Trypanosoma brucei* mutants. *Mol Biochem Parasitol*. **187**, 9-13.

Castillo-Acosta, V. M., F. Aguilar-Pereyra, A. E. Vidal, M. Navarro, L. M. Ruiz-Perez and D. Gonzalez-Pacanowska (2012b) Trypanosomes lacking uracil-DNA

glycosylase are hypersensitive to antifolates and present a mutator phenotype. *Int J Biochem Cell Biol*. **44**, 1555-68.

Castillo-Acosta, V. M., A. M. Estevez, A. E. Vidal, L. M. Ruiz-Perez and D. Gonzalez-Pacanowska (2008) Depletion of dimeric all-alpha dUTPase induces DNA strand breaks and impairs cell cycle progression in *Trypanosoma brucei*. *Int J Biochem Cell Biol*. **40**, 2901-13.

Caulfield, J. L., J. S. Wishnok and S. R. Tannenbaum (1998) Nitric oxide-induced deamination of cytosine and guanine in deoxynucleosides and oligonucleotides. *J Biol Chem*. **273**, 12689-95.

Clarke, S. J., D. C. Farrugia, G. W. Aherne, D. M. Pritchard, J. Benstead and A. L. Jackman (2000) Balb/c mice as a preclinical model for raltitrexed-induced gastrointestinal toxicity. *Clin Cancer Res*. **6**, 285-96.

Clayton, C. E., A. M. Estevez, C. Hartmann, V. P. Alibu, M. Field and D. Horn (2005) Down-regulating gene expression by RNA interference in *Trypanosoma brucei*. *Methods Mol Biol*. **309**, 39-60.

Clifford, R., T. Louis, P. Robbe, S. Ackroyd, A. Burns, A. T. Timbs, G. Wright Colopy, H. Dreau, F. Sigaux, J. G. Judde, M. Rotger, A. Telenti, Y. L. Lin, P. Pasero, J. Maelfait, M. Titsias, D. R. Cohen, S. J. Henderson, M. T. Ross, D. Bentley, P. Hillmen, A. Pettitt, J. Rehwinkel, S. J. Knight, J. C. Taylor, Y. J. Crow, M. Benkirane and A. Schuh (2014) SAMHD1 is mutated recurrently in chronic lymphocytic leukemia and is involved in response to DNA damage. *Blood*. **123**, 1021-31.

Cohen, S. S. and H. D. Barner (1954) Studies on Unbalanced Growth in *Escherichia Coli*. *Proc Natl Acad Sci U S A*. **40**, 885-93.

Colasante, C., P. Pena Diaz, C. Clayton and F. Voncken (2009) Mitochondrial carrier family inventory of Trypanosoma brucei brucei: Identification, expression and subcellular localisation. *Mol Biochem Parasitol*. **167**, 104-17.

Conway, C., C. Proudfoot, P. Burton, J. D. Barry and R. McCulloch (2002) Two pathways of homologous recombination in *Trypanosoma brucei*. *Mol Microbiol*. **45**, 1687-700.

Coquel, F., M. J. Silva, H. Techer, K. Zadorozhny, S. Sharma, J. Nieminuszczy, C. Mettling, E. Dardillac, A. Barthe, A. L. Schmitz, A. Promonet, A. Cribier, A. Sarrazin, W. Niedzwiedz, B. Lopez, V. Costanzo, L. Krejci, A. Chabes, M. Benkirane, Y. L. Lin and P. Pasero (2018) SAMHD1 acts at stalled replication forks to prevent interferon induction. *Nature*. **557**, 57-61.

Corbett, J. A. and M. L. McDaniel (1996) The Use of Aminoguanidine, a Selective iNOS Inhibitor, to Evaluate the Role of Nitric Oxide in the Development of Autoimmune Diabetes. *Methods*. **10**, 21-30.

Costes, A. and S. A. Lambert (2012) Homologous recombination as a replication fork escort: fork-protection and recovery. *Biomolecules*. **3**, 39-71.

Cribier, A., B. Descours, A. L. Valadao, N. Laguette and M. Benkirane (2013) Phosphorylation of SAMHD1 by cyclin A2/CDK1 regulates its restriction activity toward HIV-1. *Cell Rep*. **3**, 1036-43.

Chandra, V., A. Bortnick and C. Murre (2015) AID targeting: old mysteries and new challenges. *Trends Immunol*. **36**, 527-35.

Chatterjee, A. and K. K. Singh (2001) Uracil-DNA glycosylase-deficient yeast exhibit a mitochondrial mutator phenotype. *Nucleic Acids Res*. **29**, 4935-40.

Chatterjee, N. and G. C. Walker (2017) Mechanisms of DNA damage, repair, and mutagenesis. *Environ Mol Mutagen*. **58**, 235-263.

Daddacha, W., A. E. Koyen, A. J. Bastien, P. E. Head, V. R. Dhere, G. N. Nabeta, E. C. Connolly, E. Werner, M. Z. Madden, M. B. Daly, E. V. Minten, D. R. Whelan, A. J. Schlafstein, H. Zhang, R. Anand, C. Doronio, A. E. Withers, C. Shepard, R. K. Sundaram, X. Deng, W. S. Dynan, Y. Wang, R. S. Bindra, P. Cejka, E. Rothenberg, P. W. Doetsch, B. Kim and D. S. Yu (2017) SAMHD1 Promotes DNA End Resection to Facilitate DNA Repair by Homologous Recombination. *Cell Rep*. **20**, 1921-1935.

Davidson, M. B., Y. Katou, A. Keszthelyi, T. L. Sing, T. Xia, J. Ou, J. A. Vaisica, N. Thevakumaran, L. Marjavaara, C. L. Myers, A. Chabes, K. Shirahige and G. W. Brown (2012) Endogenous DNA replication stress results in expansion of dNTP pools and a mutator phenotype. *EMBO J*. **31**, 895-907.

De Bont, R. and N. van Larebeke (2004) Endogenous DNA damage in humans: a review of quantitative data. *Mutagenesis*. **19**, 169-85.

de Koning, H. P., D. J. Bridges and R. J. Burchmore (2005) Purine and pyrimidine transport in pathogenic protozoa: from biology to therapy. *FEMS Microbiol Rev*. **29**, 987-1020.

de Koning, H. P. and S. M. Jarvis (1997a) Hypoxanthine uptake through a purine-selective nucleobase transporter in *Trypanosoma brucei brucei* procyclic cells is driven by protonmotive force. *Eur J Biochem*. **247**, 1102-10.

de Koning, H. P. and S. M. Jarvis (1997b) Purine nucleobase transport in bloodstream forms of *Trypanosoma brucei* is mediated by two novel transporters. *Mol Biochem Parasitol*. **89**, 245-58.

de Koning, H. P. and S. M. Jarvis (1998) A highly selective, high-affinity transporter for uracil in *Trypanosoma brucei brucei*: evidence for proton-dependent transport. *Biochem Cell Biol*. **76**, 853-8.

de Saint Vincent, B. R., M. Dechamps and G. Buttin (1980) The modulation of the thymidine triphosphate pool of Chinese hamster cells by dCMP deaminase and UDP reductase. Thymidine auxotrophy induced by CTP in dCMP deaminase-deficient lines. *J Biol Chem*. **255**, 162-7.

De Silva, F. S. and B. Moss (2003) Vaccinia virus uracil DNA glycosylase has an essential role in DNA synthesis that is independent of its glycosylase activity: catalytic site mutations reduce virulence but not virus replication in cultured cells. *J Virol*. **77**, 159-66.

Di Noia, M. A., S. Todisco, A. Cirigliano, T. Rinaldi, G. Agrimi, V. Iacobazzi and F. Palmieri (2014) The human SLC25A33 and SLC25A36 genes of solute carrier family 25 encode two mitochondrial pyrimidine nucleotide transporters. *J Biol Chem*. **289**, 33137-48.

Dizdaroglu, M., A. Karakaya, P. Jaruga, G. Slupphaug and H. E. Krokan (1996) Novel activities of human uracil DNA N-glycosylase for cytosine-derived products of oxidative DNA damage. *Nucleic Acids Res*. **24**, 418-22.

Dolezelova, E., D. Teran, O. Gahura, Z. Kotrbova, M. Prochazkova, D. Keough, P. Spacek, D. Hockova, L. Guddat and A. Zikova (2018) Evaluation of the *Trypanosoma brucei* 6-oxopurine salvage pathway as a potential target for drug discovery. *PLoS Negl Trop Dis*. **12**, e0006301.

Dos-Santos, A. L., L. F. Carvalho-Kelly, C. F. Dick and J. R. Meyer-Fernandes (2016) Innate immunomodulation to trypanosomatid parasite infections. *Exp Parasitol*. **167**, 67-75.

Dotiwala, F., S. Mulik, R. B. Polidoro, J. A. Ansara, B. A. Burleigh, M. Walch, R. T. Gazzinelli and J. Lieberman (2016) Killer lymphocytes use granulysin, perforin and granzymes to kill intracellular parasites. *Nat Med*. **22**, 210-6.

Douglas, R. and O. McDonald (2019) Innate Immunity. *Clinical Immunology (Fifth Edition)*, 39-53.

Dranoff, G. (2004) Cytokines in cancer pathogenesis and cancer therapy. *Nat Rev Cancer*. **4**, 11-22.

Duncan, B. K. and B. Weiss (1982) Specific mutator effects of ung (uracil-DNA glycosylase) mutations in *Escherichia coli*. *J Bacteriol*. **151**, 750-5.

Elder, R. T., X. Zhu, S. Priet, M. Chen, M. Yu, J. M. Navarro, J. Sire and Y. Zhao (2003) A fission yeast homologue of the human uracil-DNA-glycosylase and their roles in causing DNA damage after overexpression. *Biochem Biophys Res Commun*. **306**, 693-700.

Endres, M., D. Biniszkiewicz, R. W. Sobol, C. Harms, M. Ahmadi, A. Lipski, J. Katchanov, P. Mergenthaler, U. Dirnagl, S. H. Wilson, A. Meisel and R. Jaenisch (2004) Increased postischemic brain injury in mice deficient in uracil-DNA glycosylase. *J Clin Invest*. **113**, 1711-21.

Engstler, M., T. Pfohl, S. Herminghaus, M. Boshart, G. Wiegertjes, N. Heddergott and P. Overath (2007) Hydrodynamic flow-mediated protein sorting on the cell surface of trypanosomes. *Cell*. **131**, 505-15.

Fang, F. C. (1997) Perspectives series: host/pathogen interactions. Mechanisms of nitric oxide-related antimicrobial activity. *J Clin Invest*. **99**, 2818-25.

Ferguson, M. A., S. W. Homans, R. A. Dwek and T. W. Rademacher (1988) Glycosyl-phosphatidylinositol moiety that anchors *Trypanosoma brucei* variant surface glycoprotein to the membrane. *Science*. **239**, 753-9.

Fish, W. R., D. L. Looker, J. J. Marr and R. L. Berens (1982a) Purine metabolism in the bloodstream forms of *Trypanosoma gambiense* and *Trypanosoma rhodesiense*. *Biochim Biophys Acta*. **719**, 223-31.

Fish, W. R., J. J. Marr and R. L. Berens (1982b) Purine metabolism in *Trypanosoma brucei gambiense*. *Biochim Biophys Acta*. **714**, 422-8.

Forstermann, U. and W. C. Sessa (2012) Nitric oxide synthases: regulation and function. *Eur Heart J*. **33**, 829-37, 837a-837d.

Franco, J. R., G. Cecchi, G. Priotto, M. Paone, A. Diarra, L. Grout, P. P. Simarro, W. Zhao and D. Argaw (2018) Monitoring the elimination of human African trypanosomiasis: Update to 2016. *PLoS Negl Trop Dis*. **12**, e0006890.

Franco, J. R., P. P. Simarro, A. Diarra and J. G. Jannin (2014) Epidemiology of human African trypanosomiasis. *Clin Epidemiol*. **6**, 257-75.

Franzolin, E., G. Pontarin, C. Rampazzo, C. Miazzi, P. Ferraro, E. Palumbo, P. Reichard and V. Bianchi (2013) The deoxynucleotide triphosphohydrolase SAMHD1 is a major regulator of DNA precursor pools in mammalian cells. *Proc Natl Acad Sci U S A*. **110**, 14272-7.

Franzolin, E., C. Salata, V. Bianchi and C. Rampazzo (2015) The Deoxynucleoside Triphosphate Triphosphohydrolase Activity of SAMHD1 Protein Contributes to the Mitochondrial DNA Depletion Associated with Genetic Deficiency of Deoxyguanosine Kinase. *J Biol Chem*. **290**, 25986-96.

Friedberg, E. C. (2005) Suffering in silence: the tolerance of DNA damage. *Nat Rev Mol Cell Biol*. **6**, 943-53.

Frosina, G., P. Fortini, O. Rossi, F. Carrozzino, G. Raspaglio, L. S. Cox, D. P. Lane, A. Abbondandolo and E. Dogliotti (1996) Two pathways for base excision repair in mammalian cells. *J Biol Chem*. **271**, 9573-8.

Furtado, C., M. Kunrath-Lima, M. A. Rajao, I. C. Mendes, M. B. de Moura, P. C. Campos, A. M. Macedo, G. R. Franco, S. D. Pena, S. M. Teixeira, B. Van

Houten and C. R. Machado (2012) Functional characterization of 8-oxoguanine DNA glycosylase of *Trypanosoma cruzi*. *PLoS One*. **7**, e42484.

Gal, A. and G. N. Wogan (1996) Mutagenesis associated with nitric oxide production in transgenic SJL mice. *Proc Natl Acad Sci U S A*. **93**, 15102-7.

Garcia-Caballero, D., G. Perez-Moreno, A. M. Estevez, L. M. Ruiz-Perez, A. E. Vidal and D. Gonzalez-Pacanowska (2017) Insights into the role of endonuclease V in RNA metabolism in *Trypanosoma brucei*. *Sci Rep*. **7**, 8505.

Garcia-Salcedo, J. A., D. Perez-Morga, P. Gijon, V. Dilbeck, E. Pays and D. P. Nolan (2004) A differential role for actin during the life cycle of *Trypanosoma brucei*. *EMBO J*. **23**, 780-9.

Gavegnano, C., E. M. Kennedy, B. Kim and R. F. Schinazi (2012) The Impact of Macrophage Nucleotide Pools on HIV-1 Reverse Transcription, Viral Replication, and the Development of Novel Antiviral Agents. *Mol Biol Int*. **2012**, 625983.

Gemble, S., A. Ahuja, G. Buhagiar-Labarchede, R. Onclercq-Delic, J. Dairou, D. S. Biard, S. Lambert, M. Lopes and M. Amor-Gueret (2015) Pyrimidine Pool Disequilibrium Induced by a Cytidine Deaminase Deficiency Inhibits PARP-1 Activity, Leading to the Under Replication of DNA. *PLoS Genet*. **11**, e1005384.

Gemble, S., G. Buhagiar-Labarchede, R. Onclercq-Delic, D. Biard, S. Lambert and M. Amor-Gueret (2016) A balanced pyrimidine pool is required for optimal Chk1 activation to prevent ultrafine anaphase bridge formation. *J Cell Sci*. **129**, 3167-77.

Genois, M. M., E. R. Paquet, M. C. Laffitte, R. Maity, A. Rodrigue, M. Ouellette and J. Y. Masson (2014) DNA repair pathways in trypanosomatids: from DNA repair to drug resistance. *Microbiol Mol Biol Rev*. **78**, 40-73.

Ghosh, C., A. Sarkar, K. Anuja, M. C. Das, A. Chakraborty, J. J. Jawed, P. Gupta, S. Majumdar, B. Banerjee and S. Bhattacharjee (2019) Free radical stress induces DNA damage response in RAW264.7 macrophages during *Mycobacterium smegmatis* infection. *Arch Microbiol*. **201**, 487-498.

Glover, L., S. Alsford and D. Horn (2013) DNA break site at fragile subtelomeres determines probability and mechanism of antigenic variation in African trypanosomes. *PLoS Pathog*. **9**, e1003260.

Glover, L. and D. Horn (2012) Trypanosomal histone gammaH2A and the DNA damage response. *Mol Biochem Parasitol*. **183**, 78-83.

Glover, L., J. Jun and D. Horn (2011) Microhomology-mediated deletion and gene conversion in African trypanosomes. *Nucleic Acids Res*. **39**, 1372-80.

Glover, L., R. McCulloch and D. Horn (2008) Sequence homology and microhomology dominate chromosomal double-strand break repair in African trypanosomes. *Nucleic Acids Res*. **36**, 2608-18.

Gobert, A. P., S. Daulouede, M. Lepoivre, J. L. Boucher, B. Bouteille, A. Buguet, R. Cespuglio, B. Veyret and P. Vincendeau (2000) L-Arginine availability modulates local nitric oxide production and parasite killing in experimental trypanosomiasis. *Infect Immun*. **68**, 4653-7.

Goldstone, D. C., V. Ennis-Adeniran, J. J. Hedden, H. C. Groom, G. I. Rice, E. Christodoulou, P. A. Walker, G. Kelly, L. F. Haire, M. W. Yap, L. P. de Carvalho, J. P. Stoye, Y. J. Crow, I. A. Taylor and M. Webb (2011) HIV-1 restriction factor SAMHD1 is a deoxynucleoside triphosphate triphosphohydrolase. *Nature*. **480**, 379-82.

Goringer, H. U. (2012) 'Gestalt,' composition and function of the *Trypanosoma brucei* editosome. *Annu Rev Microbiol*. **66**, 65-82.

Goujon, M., H. McWilliam, W. Li, F. Valentin, S. Squizzato, J. Paern and R. Lopez (2010) A new bioinformatics analysis tools framework at EMBL-EBI. *Nucleic Acids Res*. **38**, W695-9.

Goulian, M., B. M. Bleile, L. M. Dickey, R. H. Grafstrom, H. A. Ingraham, S. A. Neynaber, M. S. Peterson and B. Y. Tseng (1986) Mechanism of thymineless death. *Adv Exp Med Biol*. **195 Pt B**, 89-95.

Gramberg, T., T. Kahle, N. Bloch, S. Wittmann, E. Mullers, W. Daddacha, H. Hofmann, B. Kim, D. Lindemann and N. R. Landau (2013) Restriction of diverse retroviruses by SAMHD1. *Retrovirology*. **10**, 26.

Greenman, C., P. Stephens, R. Smith, G. L. Dalgliesh, C. Hunter, G. Bignell, H. Davies, J. Teague, A. Butler, C. Stevens, S. Edkins, S. O'Meara, I. Vastrik, E. E. Schmidt, T. Avis, S. Barthorpe, G. Bhamra, G. Buck, B. Choudhury, J. Clements, J. Cole, E. Dicks, S. Forbes, K. Gray, K. Halliday, R. Harrison, K. Hills, J. Hinton, A. Jenkinson, D. Jones, A. Menzies, T. Mironenko, J. Perry, K. Raine, D. Richardson, R. Shepherd, A. Small, C. Tofts, J. Varian, T. Webb, S. West, S. Widaa, A. Yates, D. P. Cahill, D. N. Louis, P. Goldstraw, A. G. Nicholson, F. Brasseur, L. Looijenga, B. L. Weber, Y. E. Chiew, A. DeFazio, M. F. Greaves, A. R. Green, P. Campbell, E. Birney, D. F. Easton, G. Chenevix-Trench, M. H. Tan, S. K. Khoo, B. T. Teh, S. T. Yuen, S. Y. Leung, R. Wooster, P. A. Futreal and M. R. Stratton (2007) Patterns of somatic mutation in human cancer genomes. *Nature*. **446**, 153-8.

Griffiths, M. J., M. Messent, R. J. MacAllister and T. W. Evans (1993) Aminoguanidine selectively inhibits inducible nitric oxide synthase. *Br J Pharmacol*. **110**, 963-8.

Gruz, P., M. Shimizu, F. M. Pisani, M. De Felice, Y. Kanke and T. Nohmi (2003) Processing of DNA lesions by archaeal DNA polymerases from *Sulfolobus solfataricus*. *Nucleic Acids Res*. **31**, 4024-30.

Gudin, S., N. B. Quashie, D. Candlish, M. I. Al-Salabi, S. M. Jarvis, L. C. Ranford-Cartwright and H. P. de Koning (2006) *Trypanosoma brucei*: a survey of pyrimidine transport activities. *Exp Parasitol*. **114**, 118-25.

Guillet, M., P. A. Van Der Kemp and S. Boiteux (2006) dUTPase activity is critical to maintain genetic stability in *Saccharomyces cerevisiae*. *Nucleic Acids Res*. **34**, 2056-66.

Hammarton, T. C. (2007) Cell cycle regulation in *Trypanosoma brucei*. *Mol Biochem Parasitol*. **153**, 1-8.

Hammond, D. J. and W. E. Gutteridge (1982) UMP synthesis in the kinetoplastida. *Biochim Biophys Acta*. **718**, 1-10.

Hammond, D. J. and W. E. Gutteridge (1984) Purine and pyrimidine metabolism in the Trypanosomatidae. *Mol Biochem Parasitol*. **13**, 243-61.

Harper, J. W. and S. J. Elledge (2007) The DNA damage response: ten years after. *Mol Cell*. **28**, 739-45.

Hassan, H. F. and G. H. Coombs (1988) Purine and pyrimidine metabolism in parasitic protozoa. *FEMS Microbiol Rev*. **4**, 47-83.

He, C. Y., H. H. Ho, J. Malsam, C. Chalouni, C. M. West, E. Ullu, D. Toomre and G. Warren (2004) Golgi duplication in *Trypanosoma brucei*. *J Cell Biol*. **165**, 313-21.

Helfert, S., A. M. Estevez, B. Bakker, P. Michels and C. Clayton (2001) Roles of triosephosphate isomerase and aerobic metabolism in *Trypanosoma brucei*. *Biochem J*. **357**, 117-25.

Henriques, C., M. A. Sanchez, R. Tryon and S. M. Landfear (2003) Molecular and functional characterization of the first nucleobase transporter gene from African trypanosomes. *Mol Biochem Parasitol*. **130**, 101-10.

Hertz, C. J. and J. M. Mansfield (1999) IFN-gamma-dependent nitric oxide production is not linked to resistance in experimental African trypanosomiasis. *Cell Immunol*. **192**, 24-32.

Hess, D. T., A. Matsumoto, S. O. Kim, H. E. Marshall and J. S. Stamler (2005) Protein S-nitrosylation: purview and parameters. *Nat Rev Mol Cell Biol*. **6**, 150-66.

Heyn, P., U. Stenzel, A. W. Briggs, M. Kircher, M. Hofreiter and M. Meyer (2010) Road blocks on paleogenomes--polymerase extension profiling reveals the frequency of blocking lesions in ancient DNA. *Nucleic Acids Res*. **38**, e161.

Hibbs, J. B., Jr., R. R. Taintor, Z. Vavrin and E. M. Rachlin (1988) Nitric oxide: a cytotoxic activated macrophage effector molecule. *Biochem Biophys Res Commun*. **157**, 87-94.

Hofer, A., J. T. Ekanem and L. Thelander (1998) Allosteric regulation of *Trypanosoma brucei* ribonucleotide reductase studied *in vitro* and *in vivo*. *J Biol Chem*. **273**, 34098-104.

Hofer, A., P. P. Schmidt, A. Graslund and L. Thelander (1997) Cloning and characterization of the R1 and R2 subunits of ribonucleotide reductase from Trypanosoma brucei. *Proc Natl Acad Sci U S A*. **94**, 6959-64.

Hofer, A., D. Steverding, A. Chabes, R. Brun and L. Thelander (2001) *Trypanosoma brucei* CTP synthetase: a target for the treatment of African sleeping sickness. *Proc Natl Acad Sci U S A*. **98**, 6412-6.

Hofmann, H., E. C. Logue, N. Bloch, W. Daddacha, S. B. Polsky, M. L. Schultz, B. Kim and N. R. Landau (2012) The Vpx lentiviral accessory protein targets SAMHD1 for degradation in the nucleus. *J Virol*. **86**, 12552-60.

Horvath, A. and B. G. Vertessy (2010) A one-step method for quantitative determination of uracil in DNA by real-time PCR. *Nucleic Acids Res*. **38**, e196.

Hotez, P. J., D. H. Molyneux, A. Fenwick, J. Kumaresan, S. E. Sachs, J. D. Sachs and L. Savioli (2007) Control of neglected tropical diseases. *N Engl J Med*. **357**, 1018-27.

Hsu, G. W., M. Ober, T. Carell and L. S. Beese (2004) Error-prone replication of oxidatively damaged DNA by a high-fidelity DNA polymerase. *Nature*. **431**, 217-21.

Imai, K., G. Slupphaug, W. I. Lee, P. Revy, S. Nonoyama, N. Catalan, L. Yel, M. Forveille, B. Kavli, H. E. Krokan, H. D. Ochs, A. Fischer and A. Durandy (2003) Human uracil-DNA glycosylase deficiency associated with profoundly impaired immunoglobulin class-switch recombination. *Nat Immunol*. **4**, 1023-8.

Impellizzeri, K. J., B. Anderson and P. M. Burgers (1991) The spectrum of spontaneous mutations in a *Saccharomyces cerevisiae* uracil-DNA-glycosylase mutant limits the function of this enzyme to cytosine deamination repair. *J Bacteriol*. **173**, 6807-10.

Jacobs, A. L. and P. Schar (2012) DNA glycosylases: in DNA repair and beyond. *Chromosoma*. **121**, 1-20.

Jacobs, R. T., B. Nare, S. A. Wring, M. D. Orr, D. Chen, J. M. Sligar, M. X. Jenks, R. A. Noe, T. S. Bowling, L. T. Mercer, C. Rewerts, E. Gaukel, J. Owens, R. Parham, R. Randolph, B. Beaudet, C. J. Bacchi, N. Yarlett, J. J. Plattner, Y. Freund, C. Ding, T. Akama, Y. K. Zhang, R. Brun, M. Kaiser, I. Scandale and

R. Don (2011) SCYX-7158, an orally-active benzoxaborole for the treatment of stage 2 human African trypanosomiasis. *PLoS Negl Trop Dis*. **5**, e1151.

James, D. M. and G. V. Born (1980) Uptake of purine bases and nucleosides in African trypanosomes. *Parasitology*. **81**, 383-93.

Ji, X., C. Tang, Q. Zhao, W. Wang and Y. Xiong (2014) Structural basis of cellular dNTP regulation by SAMHD1. *Proc Natl Acad Sci U S A*. **111**, E4305-14.

Ji, X., Y. Wu, J. Yan, J. Mehrens, H. Yang, M. DeLucia, C. Hao, A. M. Gronenborn, J. Skowronski, J. Ahn and Y. Xiong (2013) Mechanism of allosteric activation of SAMHD1 by dGTP. *Nat Struct Mol Biol*. **20**, 1304-9.

Kalinski, P., C. M. Hilkens, E. A. Wierenga and M. L. Kapsenberg (1999) T-cell priming by type-1 and type-2 polarized dendritic cells: the concept of a third signal. *Immunol Today*. **20**, 561-7.

Kaushik, R. S., J. E. Uzonna, J. R. Gordon and H. Tabel (1999) Innate resistance to *Trypanosoma congolense* infections: differential production of nitric oxide by macrophages from susceptible BALB/c and resistant C57Bl/6 mice. *Exp Parasitol*. **92**, 131-43.

Kavli, B., M. Otterlei, G. Slupphaug and H. E. Krokan (2007) Uracil in DNA--general mutagen, but normal intermediate in acquired immunity. *DNA Repair (Amst)*. **6**, 505-16.

Keita, M., P. Vincendeau, A. Buguet, R. Cespuglio, J. M. Vallat, M. Dumas and B. Bouteille (2000) Inducible nitric oxide synthase and nitrotyrosine in the central nervous system of mice chronically infected with *Trypanosoma brucei brucei*. *Exp Parasitol*. **95**, 19-27.

Kennedy, P. G. E. and J. Rodgers (2019) Clinical and Neuropathogenetic Aspects of Human African Trypanosomiasis. *Front Immunol*. **10**, 39.

Khanna, K. K. and S. P. Jackson (2001) DNA double-strand breaks: signaling, repair and the cancer connection. *Nat Genet*. **27**, 247-54.

Khodursky, A., E. C. Guzman and P. C. Hanawalt (2015) Thymineless Death Lives On: New Insights into a Classic Phenomenon. *Annu Rev Microbiol*. **69**, 247-63.

Kim, C. A. and J. U. Bowie (2003) SAM domains: uniform structure, diversity of function. *Trends Biochem Sci*. **28**, 625-8.

Kodigepalli, K. M., M. Li, S. L. Liu and L. Wu (2017) Exogenous expression of SAMHD1 inhibits proliferation and induces apoptosis in cutaneous T-cell lymphoma-derived HuT78 cells. *Cell Cycle*. **16**, 179-188.

Koharudin, L. M., Y. Wu, M. DeLucia, J. Mehrens, A. M. Gronenborn and J. Ahn (2014) Structural basis of allosteric activation of sterile alpha motif and histidine-aspartate domain-containing protein 1 (SAMHD1) by nucleoside triphosphates. *J Biol Chem*. **289**, 32617-27.

Kohl, L., D. Robinson and P. Bastin (2003) Novel roles for the flagellum in cell morphogenesis and cytokinesis of trypanosomes. *EMBO J*. **22**, 5336-46.

Kohnken, R., K. M. Kodigepalli and L. Wu (2015) Regulation of deoxynucleotide metabolism in cancer: novel mechanisms and therapeutic implications. *Mol Cancer*. **14**, 176.

Krokan, H. E., F. Drablos and G. Slupphaug (2002) Uracil in DNA--occurrence, consequences and repair. *Oncogene*. **21**, 8935-48.

Kubota, Y., R. A. Nash, A. Klungland, P. Schar, D. E. Barnes and T. Lindahl (1996) Reconstitution of DNA base excision-repair with purified human proteins: interaction between DNA polymerase beta and the XRCC1 protein. *EMBO J*. **15**, 6662-70.

Kumar, H., T. Kawai and S. Akira (2011) Pathogen recognition by the innate immune system. *Int Rev Immunol*. **30**, 16-34.

Kuo, L. J. and L. X. Yang (2008) Gamma-H2AX - a novel biomarker for DNA double-strand breaks. *In Vivo*. **22**, 305-9.

Kuzminov, A. (2001) Single-strand interruptions in replicating chromosomes cause double-strand breaks. *Proc Natl Acad Sci U S A*. **98**, 8241-6.

Lahouassa, H., W. Daddacha, H. Hofmann, D. Ayinde, E. C. Logue, L. Dragin, N. Bloch, C. Maudet, M. Bertrand, T. Gramberg, G. Pancino, S. Priet, B. Canard, N. Laguette, M. Benkirane, C. Transy, N. R. Landau, B. Kim and F. Margottin-Goguet (2013) SAMHD1 restricts the replication of human immunodeficiency virus type 1 by depleting the intracellular pool of deoxynucleoside triphosphates. *Nat Immunol*. **13**, 223-228.

Lanham, S. M. (1968) Separation of trypanosomes from the blood of infected rats and mice by anion-exchangers. *Nature*. **218**, 1273-4.

Larson, E. D., D. W. Bednarski and N. Maizels (2008) High-fidelity correction of genomic uracil by human mismatch repair activities. *BMC Mol Biol*. **9**, 94.

Leija, C., F. Rijo-Ferreira, L. N. Kinch, N. V. Grishin, N. Nischan, J. J. Kohler, Z. Hu and M. A. Phillips (2016) Pyrimidine Salvage Enzymes Are Essential for De Novo Biosynthesis of Deoxypyrimidine Nucleotides in Trypanosoma brucei. *PLoS Pathog*. **12**, e1006010.

Leppert, B. J., J. M. Mansfield and D. M. Paulnock (2007) The soluble variant surface glycoprotein of African trypanosomes is recognized by a macrophage scavenger receptor and induces I kappa B alpha degradation independently of TRAF6-mediated TLR signaling. *J Immunol*. **179**, 548-56.

Letunic, I. and P. Bork (2018) 20 years of the SMART protein domain annotation resource. *Nucleic Acids Res*. **46**, D493-D496.

Li, J., N. Hou, A. Faried, S. Tsutsumi, T. Takeuchi and H. Kuwano (2009) Inhibition of autophagy by 3-MA enhances the effect of 5-FU-induced apoptosis in colon cancer cells. *Ann Surg Oncol*. **16**, 761-71.

Li, N., W. Zhang and X. Cao (2000) Identification of human homologue of mouse IFN-gamma induced protein from human dendritic cells. *Immunol Lett*. **74**, 221-4.

Li, Q., C. Leija, F. Rijo-Ferreira, J. Chen, I. Cestari, K. Stuart, B. P. Tu and M. A. Phillips (2015) GMP synthase is essential for viability and infectivity of *Trypanosoma brucei* despite a redundant purine salvage pathway. *Mol Microbiol*. **97**, 1006-20.

Lindahl, T. (1993) Instability and decay of the primary structure of DNA. *Nature*. **362**, 709-15.

Loeb, L. A. and B. D. Preston (1986) Mutagenesis by apurinic/apyrimidinic sites. *Annu Rev Genet*. **20**, 201-30.

Lopez-Olmos, K., M. P. Hernandez, J. A. Contreras-Garduno, E. A. Robleto, P. Setlow, R. E. Yasbin and M. Pedraza-Reyes (2012) Roles of endonuclease V, uracil-DNA glycosylase, and mismatch repair in *Bacillus subtilis* DNA base-deamination-induced mutagenesis. *J Bacteriol*. **194**, 243-52.

Luscher, A., E. Lamprea-Burgunder, F. E. Graf, H. P. de Koning and P. Maser (2014) *Trypanosoma brucei* adenine-phosphoribosyltransferases mediate adenine salvage and aminopurinol susceptibility but not adenine toxicity. *Int J Parasitol Drugs Drug Resist*. **4**, 55-63.

Mabbott, N. A., P. S. Coulson, L. E. Smythies, R. A. Wilson and J. M. Sternberg (1998) African trypanosome infections in mice that lack the interferon-gamma receptor

gene: nitric oxide-dependent and -independent suppression of T-cell proliferative responses and the development of anaemia. *Immunology*. **94**, 476-80.

MacLean, L., M. Odiit and J. M. Sternberg (2001) Nitric oxide and cytokine synthesis in human African trypanosomiasis. *J Infect Dis*. **184**, 1086-90.

Machado-Silva, A., S. M. Teixeira, G. R. Franco, A. M. Macedo, S. D. Pena, R. McCulloch and C. R. Machado (2008) Mismatch repair in *Trypanosoma brucei*: heterologous expression of MSH2 from *Trypanosoma cruzi* provides new insights into the response to oxidative damage. *Gene*. **411**, 19-26.

Magez, S., M. Geuskens, A. Beschin, H. del Favero, H. Verschueren, R. Lucas, E. Pays and P. de Baetselier (1997) Specific uptake of tumor necrosis factor-alpha is involved in growth control of *Trypanosoma brucei*. *J Cell Biol*. **137**, 715-27.

Magez, S., M. Radwanska, A. Beschin, K. Sekikawa and P. De Baetselier (1999) Tumor necrosis factor alpha is a key mediator in the regulation of experimental Trypanosoma brucei infections. *Infect Immun*. **67**, 3128-32.

Magez, S., M. Radwanska, M. Drennan, L. Fick, T. N. Baral, F. Brombacher and P. De Baetselier (2006) Interferon-gamma and nitric oxide in combination with antibodies are key protective host immune factors during trypanosoma congolense Tc13 Infections. *J Infect Dis*. **193**, 1575-83.

Magez, S., B. Stijlemans, M. Radwanska, E. Pays, M. A. Ferguson and P. De Baetselier (1998) The glycosyl-inositol-phosphate and dimyristoylglycerol moieties of the glycosylphosphatidylinositol anchor of the trypanosome variant-specific surface glycoprotein are distinct macrophage-activating factors. *J Immunol*. **160**, 1949-56.

Mansfield, J. M. and D. M. Paulnock (2005) Regulation of innate and acquired immunity in African trypanosomiasis. *Parasite Immunol*. **27**, 361-71.

Marinus, M. G. (2012) DNA Mismatch Repair. *EcoSal Plus*. **5**.

Marletta, M. A., P. S. Yoon, R. Iyengar, C. D. Leaf and J. S. Wishnok (1988) Macrophage oxidation of L-arginine to nitrite and nitrate: nitric oxide is an intermediate. *Biochemistry*. **27**, 8706-11.

Martin, L. J. (2008) DNA damage and repair: relevance to mechanisms of neurodegeneration. *J Neuropathol Exp Neurol*. **67**, 377-87.

Masterson, W. J., T. L. Doering, G. W. Hart and P. T. Englund (1989) A novel pathway for glycan assembly: biosynthesis of the glycosyl-phosphatidylinositol anchor of the trypanosome variant surface glycoprotein. *Cell*. **56**, 793-800.

Matthews, K. R. (2005) The developmental cell biology of *Trypanosoma brucei*. *J Cell Sci*. **118**, 283-90.

Mauney, C. H. and T. Hollis (2018) SAMHD1: Recurring roles in cell cycle, viral restriction, cancer, and innate immunity. *Autoimmunity*. **51**, 96-110.

Mauney, C. H., L. C. Rogers, R. S. Harris, L. W. Daniel, N. O. Devarie-Baez, H. Wu, C. M. Furdui, L. B. Poole, F. W. Perrino and T. Hollis (2017) The SAMHD1 dNTP Triphosphohydrolase Is Controlled by a Redox Switch. *Antioxid Redox Signal*. **27**, 1317-1331.

McCulloch, R. and J. D. Barry (1999) A role for RAD51 and homologous recombination in *Trypanosoma brucei* antigenic variation. *Genes Dev*. **13**, 2875-88.

McKean, P. G. (2003) Coordination of cell cycle and cytokinesis in Trypanosoma brucei. *Curr Opin Microbiol*. **6**, 600-7.

McWilliam, H., W. Li, M. Uludag, S. Squizzato, Y. M. Park, N. Buso, A. P. Cowley and R. Lopez (2013) Analysis Tool Web Services from the EMBL-EBI. *Nucleic Acids Res*. **41**, W597-600.

Mesu, V., W. M. Kalonji, C. Bardonneau, O. V. Mordt, S. Blesson, F. Simon, S. Delhomme, S. Bernhard, W. Kuziena, J. F. Lubaki, S. L. Vuvu, P. N. Ngima, H. M. Mbembo, M. Ilunga, A. K. Bonama, J. A. Heradi, J. L. L. Solomo, G. Mandula, L. K. Badibabi, F. R. Dama, P. K. Lukula, D. N. Tete, C. Lumbala, B. Scherrer, N. Strub-Wourgaft and A. Tarral (2018) Oral fexinidazole for late-stage African *Trypanosoma brucei gambiense* trypanosomiasis: a pivotal multicentre, randomised, non-inferiority trial. *Lancet*. **391**, 144-154.

Mi, H., A. Muruganujan, D. Ebert, X. Huang and P. D. Thomas (2019) PANTHER version 14: more genomes, a new PANTHER GO-slim and improvements in enrichment analysis tools. *Nucleic Acids Res*. **47**, D419-D426.

Millar, A. E., J. Sternberg, C. McSharry, X. Q. Wei, F. Y. Liew and C. M. Turner (1999) T-Cell responses during *Trypanosoma brucei* infections in mice deficient in inducible nitric oxide synthase. *Infect Immun*. **67**, 3334-8.

Mishra, A., M. I. Khan, P. K. Jha, A. Kumar, S. Das, P. Das and K. K. Sinha (2018) Oxidative Stress-Mediated Overexpression of Uracil DNA Glycosylase in *Leishmania donovani* Confers Tolerance against Antileishmanial Drugs. *Oxid Med Cell Longev*. **2018**, 4074357.

Misko, T. P., W. M. Moore, T. P. Kasten, G. A. Nickols, J. A. Corbett, R. G. Tilton, M. L. McDaniel, J. R. Williamson and M. G. Currie (1993) Selective inhibition of the inducible nitric oxide synthase by aminoguanidine. *Eur J Pharmacol*. **233**, 119-25.

Mitchell, A. L., T. K. Attwood, P. C. Babbitt, M. Blum, P. Bork, A. Bridge, S. D. Brown, H. Y. Chang, S. El-Gebali, M. I. Fraser, J. Gough, D. R. Haft, H. Huang, I. Letunic, R. Lopez, A. Luciani, F. Madeira, A. Marchler-Bauer, H. Mi, D. A. Natale, M. Necci, G. Nuka, C. Orengo, A. P. Pandurangan, T. Paysan-Lafosse, S. Pesseat, S. C. Potter, M. A. Qureshi, N. D. Rawlings, N. Redaschi, L. J. Richardson, C. Rivoire, G. A. Salazar, A. Sangrador-Vegas, C. J. A. Sigrist, I. Sillitoe, G. G. Sutton, N. Thanki, P. D. Thomas, S. C. E. Tosatto, S. Y. Yong and R. D. Finn (2019) InterPro in 2019: improving coverage, classification and access to protein sequence annotations. *Nucleic Acids Res*. **47**, D351-D360.

Moro-Bulnes, A., V. M. Castillo-Acosta, M. Valente, J. Carrero-Lerida, G. Perez-Moreno, L. M. Ruiz-Perez and D. Gonzalez-Pacanowska (2019) Contribution of Cytidine Deaminase to Thymidylate Biosynthesis in *Trypanosoma brucei:* Intracellular Localization and Properties of the Enzyme. *mSphere*. **4**.

Murata, M., R. Thanan, N. Ma and S. Kawanishi (2012) Role of nitrative and oxidative DNA damage in inflammation-related carcinogenesis. *J Biomed Biotechnol*. **2012**, 623019.

Namangala, B., W. Noel, P. De Baetselier, L. Brys and A. Beschin (2001) Relative contribution of interferon-gamma and interleukin-10 to resistance to murine African trypanosomosis. *J Infect Dis*. **183**, 1794-800.

Nguyen, T., D. Brunson, C. L. Crespi, B. W. Penman, J. S. Wishnok and S. R. Tannenbaum (1992) DNA damage and mutation in human cells exposed to nitric oxide *in vitro*. *Proc Natl Acad Sci U S A*. **89**, 3030-4.

Nilsen, H., I. Rosewell, P. Robins, C. F. Skjelbred, S. Andersen, G. Slupphaug, G. Daly, H. E. Krokan, T. Lindahl and D. E. Barnes (2000) Uracil-DNA glycosylase

(UNG)-deficient mice reveal a primary role of the enzyme during DNA replication. *Mol Cell*. **5**, 1059-65.

Nilsen, H., G. Stamp, S. Andersen, G. Hrivnak, H. E. Krokan, T. Lindahl and D. E. Barnes (2003) Gene-targeted mice lacking the Ung uracil-DNA glycosylase develop B-cell lymphomas. *Oncogene*. **22**, 5381-6.

O'Donovan, G. A. and J. Neuhard (1970) Pyrimidine metabolism in microorganisms. *Bacteriol Rev*. **34**, 278-343.

Ogbadoyi, E., K. Ersfeld, D. Robinson, T. Sherwin and K. Gull (2000) Architecture of the *Trypanosoma brucei* nucleus during interphase and mitosis. *Chromosoma*. **108**, 501-13.

Okomo-Assoumou, M. C., S. Daulouede, J. L. Lemesre, A. N'Zila-Mouanda and P. Vincendeau (1995) Correlation of high serum levels of tumor necrosis factor-alpha with disease severity in human African trypanosomiasis. *Am J Trop Med Hyg*. **53**, 539-43.

Oleson, B. J. and J. A. Corbett (2018) Dual Role of Nitric Oxide in Regulating the Response of beta Cells to DNA Damage. *Antioxid Redox Signal*. **29**, 1432-1445.

Ong, H. B., N. Sienkiewicz, S. Wyllie, S. Patterson and A. H. Fairlamb (2013) *Trypanosoma brucei* (UMP synthase null mutants) are avirulent in mice, but recover virulence upon prolonged culture *in vitro* while retaining pyrimidine auxotrophy. *Mol Microbiol*. **90**, 443-55.

Ortiz, D., M. A. Sanchez, P. Quecke and S. M. Landfear (2009) Two novel nucleobase/pentamidine transporters from *Trypanosoma brucei*. *Mol Biochem Parasitol*. **163**, 67-76.

Overath, P. and M. Engstler (2004) Endocytosis, membrane recycling and sorting of GPI-anchored proteins: *Trypanosoma brucei* as a model system. *Mol Microbiol*. **53**, 735-44.

Pacher, P., J. S. Beckman and L. Liaudet (2007) Nitric oxide and peroxynitrite in health and disease. *Physiol Rev*. **87**, 315-424.

Pai, C. C. and S. E. Kearsey (2017) A Critical Balance: dNTPs and the Maintenance of Genome Stability. *Genes (Basel)*. **8**.

Panaro, M. A., O. Brandonisio, A. Acquafredda, M. Sisto and V. Mitolo (2003) Evidences for iNOS expression and nitric oxide production in the human macrophages. *Curr Drug Targets Immune Endocr Metabol Disord*. **3**, 210-21.

Parkin, D. W. (1996) Purine-specific nucleoside N-ribohydrolase from *Trypanosoma brucei brucei*. Purification, specificity, and kinetic mechanism. *J Biol Chem*. **271**, 21713-9.

Passos-Silva, D. G., M. A. Rajao, P. H. Nascimento de Aguiar, J. P. Vieira-da-Rocha, C. R. Machado and C. Furtado (2010) Overview of DNA Repair in *Trypanosoma cruzi*, *Trypanosoma brucei*, and *Leishmania major*. *J Nucleic Acids*. **2010**, 840768.

Pena-Diaz, P., L. Pelosi, C. Ebikeme, C. Colasante, F. Gao, F. Bringaud and F. Voncken (2012) Functional characterization of TbMCP5, a conserved and essential ADP/ATP carrier present in the mitochondrion of the human pathogen *Trypanosoma brucei*. *J Biol Chem*. **287**, 41861-74.

Phillips, T. A., R. A. VanBogelen and F. C. Neidhardt (1984) lon gene product of *Escherichia coli* is a heat-shock protein. *J Bacteriol*. **159**, 283-7.

Ponte-Sucre, A. (2016) An Overview of *Trypanosoma brucei* Infections: An Intense Host-Parasite Interaction. *Front Microbiol*. **7**, 2126.

Powell, R. D., P. J. Holland, T. Hollis and F. W. Perrino (2011) Aicardi-Goutieres syndrome gene and HIV-1 restriction factor SAMHD1 is a dGTP-regulated deoxynucleotide triphosphohydrolase. *J Biol Chem*. **286**, 43596-600.

Priest, J. W. and S. L. Hajduk (1994) Developmental regulation of mitochondrial biogenesis in *Trypanosoma brucei*. *J Bioenerg Biomembr*. **26**, 179-91.

Qiao, F. and J. U. Bowie (2005) The many faces of SAM. *Sci STKE*. **2005**, re7.

Rada, C., G. T. Williams, H. Nilsen, D. E. Barnes, T. Lindahl and M. S. Neuberger (2002) Immunoglobulin isotype switching is inhibited and somatic hypermutation perturbed in UNG-deficient mice. *Curr Biol*. **12**, 1748-55.

Rainaldi, G., R. Meneveri, L. Mariani, E. Ginelli, A. Moretti and L. Vatteroni (1996) dCTP misincorporation in a Chinese hamster mutator phenotype: the role of GGA genetic context. *Mutagenesis*. **11**, 401-4.

Rampazzo, C., P. Ferraro, G. Pontarin, S. Fabris, P. Reichard and V. Bianchi (2004) Mitochondrial deoxyribonucleotides, pool sizes, synthesis, and regulation. *J Biol Chem*. **279**, 17019-26.

Ranjbarian, F., M. Vodnala, S. M. Vodnala, R. Rofougaran, L. Thelander and A. Hofer (2012) *Trypanosoma brucei* thymidine kinase is tandem protein consisting of two homologous parts, which together enable efficient substrate binding. *J Biol Chem*. **287**, 17628-36.

Rice, G. I., J. Bond, A. Asipu, R. L. Brunette, I. W. Manfield, I. M. Carr, J. C. Fuller, R. M. Jackson, T. Lamb, T. A. Briggs, M. Ali, H. Gornall, L. R. Couthard, A. Aeby, S. P. Attard-Montalto, E. Bertini, C. Bodemer, K. Brockmann, L. A. Brueton, P. C. Corry, I. Desguerre, E. Fazzi, A. G. Cazorla, B. Gener, B. C. Hamel, A. Heiberg, M. Hunter, M. S. van der Knaap, R. Kumar, L. Lagae, P. G. Landrieu, C. M. Lourenco, D. Marom, M. F. McDermott, W. van der Merwe, S.

Orcesi, J. S. Prendiville, M. Rasmussen, S. A. Shalev, D. M. Soler, M. Shinawi, R. Spiegel, T. Y. Tan, A. Vanderver, E. L. Wakeling, E. Wassmer, E. Whittaker, P. Lebon, D. B. Stetson, D. T. Bonthron and Y. J. Crow (2009) Mutations involved in Aicardi-Goutieres syndrome implicate SAMHD1 as regulator of the innate immune response. *Nat Genet*. **41**, 829-32.

Richardson, A. R., K. C. Soliven, M. E. Castor, P. D. Barnes, S. J. Libby and F. C. Fang (2009) The Base Excision Repair system of *Salmonella enterica* serovar typhimurium counteracts DNA damage by host nitric oxide. *PLoS Pathog*. **5**, e1000451.

Robertson, A. B., A. Klungland, T. Rognes and I. Leiros (2009) DNA repair in mammalian cells: Base excision repair: the long and short of it. *Cell Mol Life Sci*. **66**, 981-93.

Robinson, D. R. and K. Gull (1991) Basal body movements as a mechanism for mitochondrial genome segregation in the trypanosome cell cycle. *Nature*. **352**, 731-3.

Rodrigues, V., A. Cordeiro-da-Silva, M. Laforge, A. Ouaissi, K. Akharid, R. Silvestre and J. Estaquier (2014) Impairment of T cell function in parasitic infections. *PLoS Negl Trop Dis*. **8**, e2567.

Rogakou, E. P., D. R. Pilch, A. H. Orr, V. S. Ivanova and W. M. Bonner (1998) DNA double-stranded breaks induce histone H2AX phosphorylation on serine 139. *J Biol Chem*. **273**, 5858-68.

Roldan, E., C. Rodriguez, G. Navas, C. Parra and J. A. Brieva (1992) Cytokine network regulating terminal maturation of human bone marrow B cells capable of spontaneous and high rate Ig secretion *in vitro*. *J Immunol*. **149**, 2367-71.

Rothkamm, K., S. Barnard, J. Moquet, M. Ellender, Z. Rana and S. Burdak-Rothkamm (2015) DNA damage foci: Meaning and significance. *Environ Mol Mutagen*. **56**, 491-504.

Routledge, M. N., D. A. Wink, L. K. Keefer and A. Dipple (1993) Mutations induced by saturated aqueous nitric oxide in the pSP189 supF gene in human Ad293 and *E. coli* MBM7070 cells. *Carcinogenesis*. **14**, 1251-4.

Rudd, S. G., N. C. K. Valerie and T. Helleday (2016) Pathways controlling dNTP pools to maintain genome stability. *DNA Repair (Amst)*. **44**, 193-204.

Ryoo, J., J. Choi, C. Oh, S. Kim, M. Seo, S. Y. Kim, D. Seo, J. Kim, T. E. White, A. Brandariz-Nunez, F. Diaz-Griffero, C. H. Yun, J. A. Hollenbaugh, B. Kim, D. Baek and K. Ahn (2014) The ribonuclease activity of SAMHD1 is required for HIV-1 restriction. *Nat Med*. **20**, 936-41.

Ryoo, J., S. Y. Hwang, J. Choi, C. Oh and K. Ahn (2016) SAMHD1, the Aicardi-Goutieres syndrome gene and retroviral restriction factor, is a phosphorolytic ribonuclease rather than a hydrolytic ribonuclease. *Biochem Biophys Res Commun*. **477**, 977-981.

Sanchez, M. A., S. Drutman, M. van Ampting, K. Matthews and S. M. Landfear (2004) A novel purine nucleoside transporter whose expression is up-regulated in the short stumpy form of the *Trypanosoma brucei* life cycle. *Mol Biochem Parasitol*. **136**, 265-72.

Sanchez, M. A., R. Tryon, J. Green, I. Boor and S. M. Landfear (2002) Six related nucleoside/nucleobase transporters from *Trypanosoma brucei* exhibit distinct biochemical functions. *J Biol Chem*. **277**, 21499-504.

Sanchez, M. A., B. Ullman, S. M. Landfear and N. S. Carter (1999) Cloning and functional expression of a gene encoding a P1 type nucleoside transporter from *Trypanosoma brucei*. *J Biol Chem*. **274**, 30244-9.

Scharer, O. D. (2013) Nucleotide excision repair in eukaryotes. *Cold Spring Harb Perspect Biol*. **5**, a012609.

Schindelin, J., I. Arganda-Carreras, E. Frise, V. Kaynig, M. Longair, T. Pietzsch, S. Preibisch, C. Rueden, S. Saalfeld, B. Schmid, J. Y. Tinevez, D. J. White, V. Hartenstein, K. Eliceiri, P. Tomancak and A. Cardona (2012) Fiji: an open-source platform for biological-image analysis. *Nat Methods*. **9**, 676-82.

Schormann, N., R. Ricciardi and D. Chattopadhyay (2014) Uracil-DNA glycosylases-structural and functional perspectives on an essential family of DNA repair enzymes. *Protein Sci*. **23**, 1667-85.

Schott, K., N. V. Fuchs, R. Derua, B. Mahboubi, E. Schnellbacher, J. Seifried, C. Tondera, H. Schmitz, C. Shepard, A. Brandariz-Nunez, F. Diaz-Griffero, A. Reuter, B. Kim, V. Janssens and R. Konig (2018) Dephosphorylation of the HIV-1 restriction factor SAMHD1 is mediated by PP2A-B55alpha holoenzymes during mitotic exit. *Nat Commun*. **9**, 2227.

Schwede, A., N. Jones, M. Engstler and M. Carrington (2011) The VSG C-terminal domain is inaccessible to antibodies on live trypanosomes. *Mol Biochem Parasitol*. **175**, 201-4.

Seamon, K. J., Z. Sun, L. S. Shlyakhtenko, Y. L. Lyubchenko and J. T. Stivers (2015) SAMHD1 is a single-stranded nucleic acid binding protein with no active site-associated nuclease activity. *Nucleic Acids Res*. **43**, 6486-99.

Sedwick, W. D., O. E. Brown and B. W. Glickman (1986) Deoxyuridine misincorporation causes site-specific mutational lesions in the lacI gene of *Escherichia coli. Mutat Res*. **162**, 7-20.

Selig, L., S. Benichou, M. E. Rogel, L. I. Wu, M. A. Vodicka, J. Sire, R. Benarous and M. Emerman (1997) Uracil DNA glycosylase specifically interacts with Vpr of both human immunodeficiency virus type 1 and simian immunodeficiency virus of sooty mangabeys, but binding does not correlate with cell cycle arrest. *J Virol*. **71**, 4842-6.

Shelton, J., X. Lu, J. A. Hollenbaugh, J. H. Cho, F. Amblard and R. F. Schinazi (2016) Metabolism, Biochemical Actions, and Chemical Synthesis of Anticancer Nucleosides, Nucleotides, and Base Analogs. *Chem Rev*. **116**, 14379-14455.

Sherman, P. A. and J. A. Fyfe (1989) Enzymatic assay for deoxyribonucleoside triphosphates using synthetic oligonucleotides as template primers. *Anal Biochem*. **180**, 222-6.

Shi, M., G. Wei, W. Pan and H. Tabel (2004) *Trypanosoma congolense* infections: antibody-mediated phagocytosis by Kupffer cells. *J Leukoc Biol*. **76**, 399-405.

Sienkiewicz, N., S. Jaroslawski, S. Wyllie and A. H. Fairlamb (2008) Chemical and genetic validation of dihydrofolate reductase-thymidylate synthase as a drug target in African trypanosomes. *Mol Microbiol*. **69**, 520-33.

Sievers, F., A. Wilm, D. Dineen, T. J. Gibson, K. Karplus, W. Li, R. Lopez, H. McWilliam, M. Remmert, J. Soding, J. D. Thompson and D. G. Higgins (2011) Fast, scalable generation of high-quality protein multiple sequence alignments using Clustal Omega. *Mol Syst Biol*. **7**, 539.

Silva-Barrios, S., T. Charpentier and S. Stager (2018) The Deadly Dance of B Cells with Trypanosomatids. *Trends Parasitol*. **34**, 155-171.

Silvester, E., K. R. McWilliam and K. R. Matthews (2017) The Cytological Events and Molecular Control of Life Cycle Development of *Trypanosoma brucei* in the Mammalian Bloodstream. *Pathogens*. **6**.

Smith, T. K., F. Bringaud, D. P. Nolan and L. M. Figueiredo (2017) Metabolic reprogramming during the *Trypanosoma brucei* life cycle. *F1000Res*. **6**.

Sousa, M. M., H. E. Krokan and G. Slupphaug (2007) DNA-uracil and human pathology. *Mol Aspects Med*. **28**, 276-306.

Spinazzola, A., R. Marti, I. Nishino, A. L. Andreu, A. Naini, S. Tadesse, I. Pela, E. Zammarchi, M. A. Donati, J. A. Oliver and M. Hirano (2002) Altered thymidine metabolism due to defects of thymidine phosphorylase. *J Biol Chem*. **277**, 4128-33.

Stamler, J. S., E. J. Toone, S. A. Lipton and N. J. Sucher (1997) (S)NO signals: translocation, regulation, and a consensus motif. *Neuron*. **18**, 691-6.

Steketee, P. C., I. M. Vincent, F. Achcar, F. Giordani, D. H. Kim, D. J. Creek, Y. Freund, R. Jacobs, K. Rattigan, D. Horn, M. C. Field, A. MacLeod and M. P. Barrett (2018) Benzoxaborole treatment perturbs S-adenosyl-L-methionine metabolism in *Trypanosoma brucei*. *PLoS Negl Trop Dis*. **12**, e0006450.

Sternberg, J., N. Mabbott, I. Sutherland and F. Y. Liew (1994) Inhibition of nitric oxide synthesis leads to reduced parasitemia in murine *Trypanosoma brucei* infection. *Infect Immun*. **62**, 2135-7.

Sternberg, J. M., N. Njogu Maina, C. W. Gickhuki and U. J. Ndung (1998) Nitric oxide production in vervet monkeys (*Cercopithecus aethiops*) infected with *Trypanosoma brucei*. *Parasite Immunol*. **20**, 395-7.

Sternberg, M. J. and N. A. Mabbott (1996) Nitric oxide-mediated suppression of T cell responses during *Trypanosoma brucei* infection: soluble trypanosome products

and interferon-gamma are synergistic inducers of nitric oxide synthase. *Eur J Immunol*. **26**, 539-43.

Steverding, D., X. Wang and D. W. Sexton (2009) The trypanocidal effect of NO-releasing agents is not due to inhibition of the major cysteine proteinase in *Trypanosoma brucei*. *Parasitol Res*. **105**, 1333-8.

Stijlemans, B., G. Caljon, J. Van Den Abbeele, J. A. Van Ginderachter, S. Magez and C. De Trez (2016) Immune Evasion Strategies of *Trypanosoma brucei* within the Mammalian Host: Progression to Pathogenicity. *Front Immunol*. **7**, 233.

Stuehr, D. J., H. J. Cho, N. S. Kwon, M. F. Weise and C. F. Nathan (1991) Purification and characterization of the cytokine-induced macrophage nitric oxide synthase: an FAD- and FMN-containing flavoprotein. *Proc Natl Acad Sci U S A*. **88**, 7773-7.

Taketo, M. M. and M. Sonoshita (2002) Phospolipase A2 and apoptosis. *Biochim Biophys Acta*. **1585**, 72-6.

Tanaka, T., A. Kurose, H. D. Halicka, X. Huang, F. Traganos and Z. Darzynkiewicz (2006) Nitrogen oxide-releasing aspirin induces histone H2AX phosphorylation, ATM activation and apoptosis preferentially in S-phase cells: involvement of reactive oxygen species. *Cell Cycle*. **5**, 1669-74.

Tang, C., X. Ji, L. Wu and Y. Xiong (2015) Impaired dNTPase activity of SAMHD1 by phosphomimetic mutation of Thr-592. *J Biol Chem*. **290**, 26352-9.

Teran, D., D. Hockova, M. Cesnek, A. Zikova, L. Naesens, D. T. Keough and L. W. Guddat (2016) Crystal structures and inhibition of *Trypanosoma brucei* hypoxanthine-guanine phosphoribosyltransferase. *Sci Rep*. **6**, 35894.

Tramentozzi, E., P. Ferraro, M. Hossain, B. Stillman, V. Bianchi and G. Pontarin (2018) The dNTP triphosphohydrolase activity of SAMHD1 persists during S-phase when the enzyme is phosphorylated at T592. *Cell Cycle*. **17**, 1102-1114.

Tu, X., P. Kumar, Z. Li and C. C. Wang (2006) An aurora kinase homologue is involved in regulating both mitosis and cytokinesis in *Trypanosoma brucei*. *J Biol Chem*. **281**, 9677-87.

Tu, X. and C. C. Wang (2005) Pairwise knockdowns of cdc2-related kinases (CRKs) in *Trypanosoma brucei* identified the CRKs for G1/S and G2/M transitions and demonstrated distinctive cytokinetic regulations between two developmental stages of the organism. *Eukaryot Cell*. **4**, 755-64.

Valente, M., J. Timm, V. M. Castillo-Acosta, L. M. Ruiz-Perez, T. Balzarini, J. E. Nettleship, L. E. Bird, H. Rada, K. S. Wilson and D. Gonzalez-Pacanowska (2016) Cell cycle regulation and novel structural features of thymidine kinase, an essential enzyme in *Trypanosoma brucei*. *Mol Microbiol*. **102**, 365-385.

Varikuti, S., B. K. Jha, G. Volpedo, N. M. Ryan, G. Halsey, O. M. Hamza, B. S. McGwire and A. R. Satoskar (2018) Host-Directed Drug Therapies for Neglected Tropical Diseases Caused by Protozoan Parasites. *Front Microbiol*. **9**, 2655.

Vasudevan, D. and D. D. Thomas (2014) Insights into the diverse effects of nitric oxide on tumor biology. *Vitam Horm*. **96**, 265-98.

Vickerman, K. (1985) Developmental cycles and biology of pathogenic trypanosomes. *Br Med Bull*. **41**, 105-14.

Vieira-da-Rocha, J. P., D. G. Passos-Silva, I. C. Mendes, E. A. Rocha, D. A. Gomes, C. R. Machado and R. McCulloch (2018) The DNA damage response is

developmentally regulated in the African trypanosome. *DNA Repair (Amst)*. **73**, 78-90.

Vincendeau, P., S. Daulouede, B. Veyret, M. L. Darde, B. Bouteille and J. L. Lemesre (1992) Nitric oxide-mediated cytostatic activity on *Trypanosoma brucei gambiense* and *Trypanosoma brucei brucei*. *Exp Parasitol*. **75**, 353-60.

Vodnala, M., A. Fijolek, R. Rofougaran, M. Mosimann, P. Maser and A. Hofer (2008) Adenosine kinase mediates high affinity adenosine salvage in *Trypanosoma brucei*. *J Biol Chem*. **283**, 5380-8.

Vorontsov, II, G. Minasov, O. Kiryukhina, J. S. Brunzelle, L. Shuvalova and W. F. Anderson (2011) Characterization of the deoxynucleotide triphosphate triphosphohydrolase (dNTPase) activity of the EF1143 protein from *Enterococcus faecalis* and crystal structure of the activator-substrate complex. *J Biol Chem*. **286**, 33158-66.

Wallace, S. S. (2014) Base excision repair: a critical player in many games. *DNA Repair (Amst)*. **19**, 14-26.

Wang, J. L., F. Z. Lu, X. Y. Shen, Y. Wu and L. T. Zhao (2014) SAMHD1 is down regulated in lung cancer by methylation and inhibits tumor cell proliferation. *Biochem Biophys Res Commun*. **455**, 229-33.

Wang, L. (2016) Mitochondrial purine and pyrimidine metabolism and beyond. *Nucleosides Nucleotides Nucleic Acids*. **35**, 578-594.

Wang, Z., M. E. Drew, J. C. Morris and P. T. Englund (2002) Asymmetrical division of the kinetoplast DNA network of the trypanosome. *EMBO J*. **21**, 4998-5005.

Wei, G., H. Bull, X. Zhou and H. Tabel (2011) Intradermal infections of mice by low numbers of african trypanosomes are controlled by innate resistance but enhance susceptibility to reinfection. *J Infect Dis*. **203**, 418-29.

Welbourn, S., S. M. Dutta, O. J. Semmes and K. Strebel (2013) Restriction of virus infection but not catalytic dNTPase activity is regulated by phosphorylation of SAMHD1. *J Virol*. **87**, 11516-24.

White, T. E., A. Brandariz-Nunez, J. C. Valle-Casuso, S. Amie, L. Nguyen, B. Kim, J. Brojatsch and F. Diaz-Griffero (2012) Contribution of SAM and HD domains to retroviral restriction mediated by human SAMHD1. *Virology*. **436**, 81-90.

WHO (2019) Trypanosomiasis, human African (sleeping sickness). *World Health Organization official website*.

Wink, D. A., K. S. Kasprzak, C. M. Maragos, R. K. Elespuru, M. Misra, T. M. Dunams, T. A. Cebula, W. H. Koch, A. W. Andrews, J. S. Allen and et al. (1991) DNA deaminating ability and genotoxicity of nitric oxide and its progenitors. *Science*. **254**, 1001-3.

Wirtz, E., S. Leal, C. Ochatt and G. A. Cross (1999) A tightly regulated inducible expression system for conditional gene knock-outs and dominant-negative genetics in *Trypanosoma brucei*. *Mol Biochem Parasitol*. **99**, 89-101.

Yan, J., S. Kaur, M. DeLucia, C. Hao, J. Mehrens, C. Wang, M. Golczak, K. Palczewski, A. M. Gronenborn, J. Ahn and J. Skowronski (2013) Tetramerization of SAMHD1 is required for biological activity and inhibition of HIV infection. *J Biol Chem*. **288**, 10406-17.

Ye, F. G., C. G. Song, Z. G. Cao, C. Xia, D. N. Chen, L. Chen, S. Li, F. Qiao, H. Ling, L. Yao, X. Hu and Z. M. Shao (2015) Cytidine Deaminase Axis Modulated by miR-484 Differentially Regulates Cell Proliferation and Chemoresistance in Breast Cancer. *Cancer Res*. **75**, 1504-15.

Zeitlin, S. G., B. R. Chapados, N. M. Baker, C. Tai, G. Slupphaug and J. Y. Wang (2011) Uracil DNA N-glycosylase promotes assembly of human centromere protein A. *PLoS One*. **6**, e17151.

Zhang, Y., W. Y. Ye, J. Q. Wang, S. J. Wang, P. Ji, G. Y. Zhou, G. P. Zhao, H. L. Ge and Y. Wang (2013) dCTP pyrophosphohydrase exhibits nucleic accumulation in multiple carcinomas. *Eur J Histochem*. **57**, e29.

Zhou, Q., H. Hu and Z. Li (2014) New insights into the molecular mechanisms of mitosis and cytokinesis in trypanosomes. *Int Rev Cell Mol Biol*. **308**, 127-66.

Zhu, C., W. Gao, K. Zhao, X. Qin, Y. Zhang, X. Peng, L. Zhang, Y. Dong, W. Zhang, P. Li, W. Wei, Y. Gong and X. F. Yu (2013) Structural insight into dGTP-dependent activation of tetrameric SAMHD1 deoxynucleoside triphosphate triphosphohydrolase. *Nat Commun*. **4**, 2722.

Zhu, C. F., W. Wei, X. Peng, Y. H. Dong, Y. Gong and X. F. Yu (2015) The mechanism of substrate-controlled allosteric regulation of SAMHD1 activated by GTP. *Acta Crystallogr D Biol Crystallogr*. **71**, 516-24.